



**UNIVERSITAT
JAUME I**

UNIVERSITAT JAUME I

Departament de Química Inorgànica i Orgànica

Àrea de Química Inorgànica

Design of polytopic ligands for the preparation of multifunctional catalysts

Doctoral Thesis

Sergio Gonell Gómez

PhD. supervisors: Eduardo Peris and Macarena Poyatos

Castelló de la Plana, March 2015

Prof. Dr. Eduardo Peris Fajarnés, Catedràtic de l'àrea de Química Inorgànica i Dra. Macarena Poyatos de Lorenzo, contractada Ramón y Cajal de la mateixa àrea, pertanyents al Departament de Química Inorgànica i Orgànica de la Universitat Jaume I,

Certifiquen: Que la Tesi Doctoral amb el títol 'Design of polytopic ligands for the preparation of multifunctional catalysts' ha sigut desenvolupada sota la seua direcció, en l'àrea de Química Inorgànica del Departament de Química Inorgànica i Orgànica de la Universitat Jaume I, per Sergio Gonell Gómez.

Castelló de la Plana, a

Ft: Prof. Dr. Eduardo Peris Fajarnés

Ft: Dra Macarena Poyatos de Lorenzo

Acknowledgements/Agraïments

Sembla mentida que ja estiga escrivint els agraïments de la meua tesi, com passa el temps, en fi...

En primer lloc m'agradaria agrair profundament als meus directors de tesi, Eduardo Peris i Macarena Poyatos, tota la confiança que m'han donat durant aquests darrers quatre anys, per donar-me l'oportunitat d'incorporar-me a aquest grup tant meravellós i perquè sense vosaltres no seria el químic que sóc ara. Gràcies Eduardo per saber transmetre'm la passió per la química, per tots els bons consells que m'has donat, totes les discussions sobre química i per ensenyar-me el valor de la constància i del treball dur. Maca, amb tu vaig donar les primeres passes al laboratori, tota la mà que tinc al laboratori és gràcies a tu, moltes gràcies també pels bons consells i per les inacabables correccions d'abstracts, pòsters, presentacions i capítols de tesi.

També m'agradaria donar les gràcies a tota la gent que ha passat o que encara hi és al laboratori de Química Organometàl·lica i Catàlisi Homogènia de l'UJI. Jose Mata, moltes gràcies pels teus consells, per refinar les meues estructures al començament de la meua tesi, per l'ajuda que m'has donat per a refinar-me-les jo mateix i perquè sempre és un plaer parlar amb tu. A Goyo, per tota l'ajuda que m'has donat, és una alegria trobar a gent tant involucrada com tu!! A Sara, qui ens anava a dir quan anàvem a la mateixa classe a l'institut que acabaríem fent la tesi al mateix temps en el mateix grup de recerca!! Ha sigut un plaer passar aquests quatre anys compartint tantes coses amb tu. A Hugo, per totes les festes que ens hem pegat (saca las chelas wey!!!), a Carmen per ser un sol i estar sempre disposada a tenir una bona conversació, a Sheila per el bon cor que tens i a Susana per estar sempre al cas de tot. A Roberto perquè després de cinc anys de carrera va ser un plaer gaudir del teu sentit de l'humor i treballar amb tu en el laboratori. Als nouvinguts del grup Victor i David, perquè sou uns cracks i tot vos anirà de categoria.

A aquells amb qui vaig començar al laboratori i que ara ja són doctors, vosaltres em vaau marcar el camí a seguir: Ampa (todo perciozo!!), Arturo (unos tequilitas wey!!) i Cande (ai maree!!!).

A la gent que ha passat per aquest laboratori deixant una empremta inoblidable: Fernando Godoy, Sergio Sanz, André, Alex, Miriam, Elena, Mónica, Alberto, George, Lisa, Marco i Diego. Thanks Prof. Dmitri Gusev for your nice stays here, and for all the DFT calculations of this Thesis.

A Bancaixa per la beca d'investigació que vaig gaudir només acabar la carrera. A la Universitat Jaume I per la beca FPI amb la que vaig començar la meua tesi doctoral i al Ministeri de Ciència i Innovació per la beca FPU que encara estic gaudint en l'actualitat. També vull agrair a l'associació SusChem per el premi que em van concedir.

Gràcies a Zoel, Cristina, Manolo, Angel i Javi, amb els que vaig estudiar el màster i tantes bones estones vam passar junts.

I would like to thank Prof. Michel Etienne for the beautiful four months which I spent in his group, it was a pleasure my stay there. I want to thank all the people that I met there, especially Bianca, Patricia, Pascal and Vincent.

Thanks Prof. Ekkehart Hahn for giving me the opportunity to join his group during four months. Thanks to all people that I knew there (you have a delicious beer!!!). A Fran, Mercedes y Leyre por conoceros durante mi estancia allí y darme tantos buenos recuerdos de ella, y porque esto ya se acaba... quiiiiiiiiiiiiinooooooooo!!!!

I also would like to thank Prof. Dmitri Gusev and Dr. Vicent Cèsar for being the experts of my Thesis. I really appreciate your comments and suggestions that have improved the quality of the text.

A tota la gent de QIO, dels que tants reactius he "gorronejat" i tants consells m'han donat. Gràcies a la secretària M^a José, i a les tècniques de QIO Silvia, Inma i Alicia per tots els favors que m'heu fet.

Als tècnics dels Serveis Centrals d'Instrumentació Científica, perquè ha sigut un plaer anar a portar-vos mostres Cristian, Gabriel i Jose, i parlar de les nostres coses. També a Maru, Laura, Javi i Cristina.

A Purificación Escribano per tots els valors que ens vas transmetre en classe i perquè la vida és injusta. A Bea Julian perquè sempre és un plaer parlar amb tu.

A tots els meus amics, Emboirats i Somarruscos, perquè molts cops penso la sort que tinc en tindre uns amics com vosaltres. Moltes gràcies Isaac per la portada de la tesis tan meravellosa que m'has fet.

I finalment, i més important, a la meua família a la que dec ser com sóc. Als meus germans Mireia i Xisco perquè açò de la química se'ns dóna be i avan!!, al meu oncle

i als meus cunyats Angel i Maria per ser com són. Als meus pares per donar-me la força que molts cop em fa falta per seguir endavant.

Index	i
Nomenclature	vi
List of abbreviations	vi

Chapter 1: General introduction and objectives	1
1.1 General introduction	3
1.1.1 Multimetallic catalysis	3
1.1.2 Multimetallic compounds from geometrically isolated poly-NHCs	8
1.1.2.1 <i>Janus</i> -type bis-NHCs	9
1.1.2.2 Rigid tritopic NHCs	12
1.1.3 Polymeric organometallic materials based on poly-NHCs	13
1.1.4 Luminescent azolium salts	14
1.2 Objectives	16
1.3 References	17

Chapter 2: Homo- and hetero-bimetallic complexes with a Y-shaped tris-NHC ligand	21
2.1 Results and discussion	23
2.1.1 Synthesis of tris-imidazolium salt $[\text{DH}_3](\text{BF}_4)_3$	23
2.1.2 Metal complexes with a Y-shaped tris-NHC ligand	26
2.1.2.1 Monometallic complexes based on DH	28
2.1.2.2 Bimetallic complexes based on a Y-shaped tris-NHC ligand	32
2.1.3 Catalytic properties of the Y-shaped tris-NHC-based complexes	46
2.1.3.1 Hydroarylation of alkynes catalyzed by 1DH , 1D and 2D	47
2.1.3.2 Tandem processes catalyzed by 3D and 4D	49
2.2 Conclusions	56
2.3 References	57

Chapter 3: A new <i>Janus</i>-type pyrene-bis-NHC ligand. Coordination properties and catalytic activity	59
3.1 Results and discussion	61
3.1.1 Synthesis of pyrene-based imidazolium salts	62
3.1.1.1 Synthesis of pyrene-based bis-azolium salts	62
3.1.1.2 Synthesis of the pyrene-based mono-azolium salt [IH](I)	67
3.1.2 Complexes with pyrene-based NHC ligands	68
3.1.2.1 IrCl(COD) and RhCl(COD) complexes	68
3.1.2.2 RuCl ₂ (<i>p</i> -cymene) complexes	72
3.1.3 Luminescence properties of the pyrene-based azolium salts	76
3.1.4 Electronic properties of the bimetallic complexes based on F	78
3.1.4.1 Carbonyl derivatives of complexes 1F	78
3.1.4.2 Electrochemical properties of ligand F	79
3.1.5 Catalytic properties of ruthenium complexes 3F-Me and 1I	81
3.1.5.1 Arylation of arylpyridines	82
3.1.5.2 Hydroarylation of terminal alkenes	84
3.1.5.3 Sequential hydroarylation of alkenes and arylation of arylpyridines	85
3.2 Conclusions	89
3.3 References	90
<hr/>	
Chapter 4: A triphenylene-based tris-NHC ligand. Coordination properties and catalytic activity	93
4.1 Results and discussion	95
4.1.1 Synthesis of tris-imidazolium salts [KH₃](BF₄)₃ and [MH₃](BF₄)₃	96
4.1.2 Synthesis of trimetallic complexes	99
4.1.3 Electronic properties of the trimetallic complexes based on K	110
4.1.3.1 Carbonylation of 1K	110
4.1.3.2 Tolman Electronic Parameter and electronic	112

communication	
4.1.3.3 Electrochemical properties	114
4.1.4 Steric hindrance: percent of buried volume (% V_{Bur})	115
4.1.5 Catalytic properties of palladium and gold complexes	115
4.1.5.1 Palladium catalyzed reactions	116
4.1.5.2 Gold catalyzed reaction	118
4.1.5.3 Discussion of the catalytic results	120
4.1.6 Main-chain organometallic microporous polymers based on triphenylene-tris-NHC gold species	125
4.1.6.1 Synthesis and characterization	126
4.1.6.2 Catalytic properties of 5K and 6K	131
4.2 Conclusions	137
4.3 References	139
<hr/>	
Chapter 5: Experimental section	143
5.1 Analytical techniques	145
5.2. Synthesis and characterization	148
5.2.1 Synthesis and characterization of azolium salts	148
5.2.2 Synthesis and characterization of complexes of Chapter 2	163
5.2.3 Synthesis and characterization of complexes of Chapter 3	171
5.2.4 Synthesis and characterization of complexes of Chapter 4	180
5.3 Catalytic experiments	191
5.3.1 Catalytic experiments described in Chapter 2	191
5.3.2 Catalytic experiments and products described in Chapter 3	192
5.3.3 Catalytic experiments described in Chapter 4	197
5.3.3.1 Post-catalytic experiments	199
5.4 X-Ray Diffraction	204
5.5 References	211

Chapter 6: Diseño de ligandos politópicos para la preparación de catalizadores multifuncionales	213
6.1 Introducción	215
6.2. Objetivos	218
6.3 Discusión de resultados	219
6.3.1 Complejos metálicos basados en un ligando tris-NHC en forma de Y	219
6.3.2 Propiedades catalíticas de los complejos basados en un ligando tris-NHC en forma de Y	221
6.3.2.1 Hidroarilación de alquinos catalizada por 1DH , 1D y 2D	221
6.3.2.2 Procesos tándem catalizados por 3D y 4D	222
6.3.3 Complejos bimetálicos basados en ligandos pireno-bis-imidazolilideno	224
6.3.3.1 Síntesis de sales de imidazolio basadas en pireno	224
6.3.3.2 Síntesis de complejos basados en ligandos pireno-imidazolilideno	226
6.3.4 Propiedades catalíticas de complejos de rutenio basados en ligandos pireno-imidazolilideno	228
6.3.4.1 Arilación de arilpiridinas	229
6.3.4.2 Hidroarilación de alquenos terminales	229
6.3.4.3 Hidroarilación de alquenos terminales y arilación de arilpiridinas secuencial	230
6.3.5 Síntesis de compuestos trimetálicos basados en ligandos tris-NHC	231
6.3.6 Propiedades catalíticas de complejos trimetálicos basados en ligandos tris-NHC	234
6.3.7 Polímeros organometálicos microporosos basados en especies trifenileno-tris-NHC de oro	235
6.3.7.1 Síntesis y caracterización	235

6.3.7.2 Actividad catalítica	237
6.4 Conclusiones	239
6.5 Referencias	241

Nomenclature

The nomenclature employed to name the compounds described in this work is:

Ligands or organic intermediates in the synthesis of imidazolium salts: letters of the alphabet (**A-N**). In the cases where a compound could bear different substituents, their nature (Me, Et...) will be included next to the letter of the alphabet.

Precursor salts of the ligands: the ligand letter with the acidic protons and its counterion. For example, $[\mathbf{KH}_3](\mathbf{BF}_4)_3$ is the precursor salt of the ligand **K** which contains three acidic C-H bonds and three tetrafluoroborates as counter-ions.

Metal complexes with NHC ligands: the number followed by the letter of the coordinated ligand. The complexes have been sorted in order of appearance in the text.

List of abbreviations

Δ	refluxing temperature
η	ligand hapticity
μ	bridging ligand
Φ_f	quantum yield
λ	wavelength
ϵ	molar extinction coefficient
ν	frequency
Ar	aromatic
ATR	Attenuated Total Reflection
BET	Brunauer-Emmett-Teller
BimN <i>t</i> Bu ₂	1,3-di(<i>tert</i> -butyl)benzimidazolylidene
Bn	benzyl
BSE	Back-Scattered Electrons
cat.	catalyst
COD	1,5-cyclooctadiene
COE	cyclooctene
Conv.	conversion
Cp*	1,2,3,4,5-pentamethylcyclopentadienyl

CP/MAS	Cross-Polarization Magnetic Angle Spinning
CTC	Concurrent Tandem Catalysis
CV	Cyclic Voltammetry
DCE	1,2-dichloroethane
DFT	Density Functional Theory
Dipp	2,6-diisopropylphenyl
DG	directing group
DMF	dimethylformamide
DPV	Differential Pulse Voltammetry
DMSO	dimethylsulfoxide
E	potential
EA	elemental analysis
EDS	Energy-Dispersive X-ray Spectroscopy
Et	ethyl
EtOAc	ethyl acetate
EtOH	ethanol
Et ₂ O	diethyl ether
ESI-MS	Electrospray Ionization Mass Spectrometry
ESI-TOF-MS	Electrospray Ionization Time-of-flight Mass Spectrometry
FT-IR	Fourier Transform Infrared
GC	Gas Chromatography
h	hour
HFB	hexafluorobenzene
HRMS	High Resolution Mass Spectrometry
HSQC	Heteronuclear Single Quantum Coherence
I	current intensity
IPr-HCl	1,3-bis(2,6-diisopropylphenyl)imidazolium chloride
<i>i</i> PrOH	<i>iso</i> -propanol
KHMDS	potassium bis(trimethylsilyl)amide
L	ligand
M	metal

Me	methyl
Mes	2,4,6-trimethylphenyl
MeOH	methanol
MeCN	acetonitrile
<i>n</i> Bu	1-butyl
<i>n</i> Dec	1-decyl
NHC	N-heterocyclic carbene
<i>n</i> Hex	1-hexyl
NMP	N-methyl-2-pyrrolidone
NMR	Nuclear Magnetic Resonance
δ	chemical shift
br	broad
d	doublet
<i>J</i>	coupling constant
m	multiplet
ppm	parts per million
s	singlet
sp	septuplet
t	triplet
<i>n</i> Oct	1-octyl
<i>n</i> Pr	1-propyl
OAc	acetate
<i>O</i> tBu	<i>tert</i> -butoxide
<i>p</i> -cymene	1-methyl-4-(<i>isopropyl</i>)benzene
PEPPSI	Pyridine-Enhanced Precatalyst Preparation, Stabilization and Initiation
Ph	phenyl
Py	pyridine
Ra-Ni	Raney Nickel
RT	room temperature
SEM	Scanning Electron Microscopy

t	time
T	temperature
TA	temperatura ambiente
<i>t</i> Am	<i>tert</i> -amyl or 1,1-dimethylpropyl
<i>t</i> Bu	<i>tert</i> -butyl
TEP	Tolman Electronic Parameter
TEM	Transmission Electron Microscopy
TFA	trifluoroacetic acid
TGA	TermoGravimetric Analysis
THF	tetrahydrofuran
TM	transition metal
TMSCN	trimethyl silyl cyanide
UV	ultraviolet
VT	variable temperature
% V_{Bur}	percent of buried volume

Chapter 1

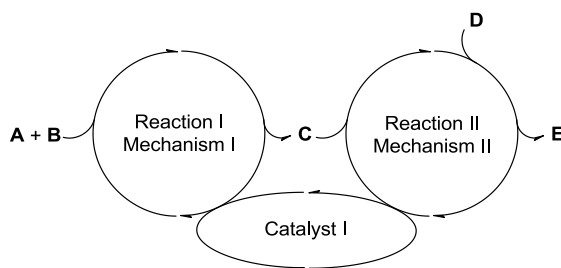
General introduction and objectives

1.1 General introduction

1.1.1 Multimetallic catalysis

In the global context where greener and lower pollutant reactions are pursued, catalytic processes are highly desirable. Reduction of time, energy and waste side-products can be achieved employing appropriate, selective and highly efficient catalysts.¹ The replacement of a multistep process and, in most cases, salt generating chemical synthesis, for efficient catalyzed reactions, increases the atom economy and is more appropriate from the environmental and economic point of view.² Facilitating a complicated catalytic reaction with a simple and effective catalyst, or finding a way for combining several catalytic reactions into a one-pot tandem process, are two of the most important challenges that imply the design of improved catalysts.

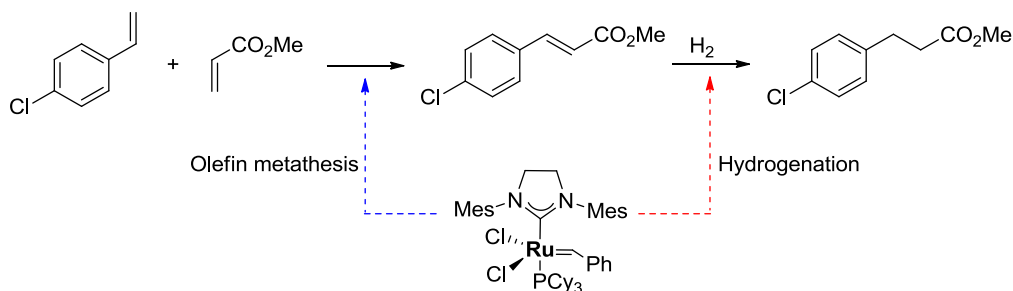
In the search of more efficient ways for preparing complex organic architectures, there has been an increasing effort in finding multifunctional catalysts that may be active for a wide set of organic reactions. The combination of fundamental catalytic steps implying simple and accessible substrates can then lead to sophisticated molecules. In nature, it has been shown that many enzymes contain two metal ions that operate cooperatively.³ Mimicking this natural system in chemical synthesis and performing catalytic cascade reactions in a one-pot manner was intensively investigated over the past decades. One-pot multistep reactions are still not of general applicability in chemocatalysis due to problems with compatibility of reaction conditions.⁷ Several approaches have been envisioned and investigated in this regard.^{2,4-6} The first one and maybe the most straightforward, is using one single catalyst to promote different catalytic reactions in the same reaction vessel (Scheme 1.1).



Scheme 1.1 Auto-tandem catalysis

This approach is the so-called auto-tandem catalysis,^{5,7} and can be divided in two categories: *sequential catalysis* and *concurrent tandem catalysis*.^{2,6} In *sequential*

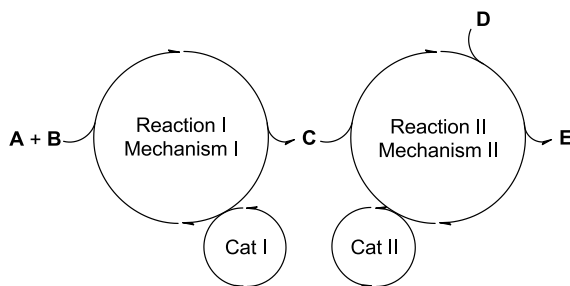
catalysis, one catalyst is used to promote mechanistically different sequential reactions. For instance, two reagents (**A** and **B** in Scheme 1.1) are transformed into a product (**C**) through a catalytic cycle promoted by one catalyst (Reaction I). When this reaction is finished, the product (**C**) is involved in other catalytic reaction (mechanistically different from the first one) promoted by the same catalyst (Reaction II), to produce the final product (**E**). In this kind of catalysis a modification in the reaction conditions or the introduction of another reagent is normally used in order to initiate the second reaction. One of the first examples of sequential catalysis was reported by Grubbs and co-workers.⁸ They demonstrated that either their first- or second-generation catalysts were able to promote first the cross-metathesis of olefins, followed by the hydrogenation of the new double bond formed (Scheme 1.2).



Scheme 1.2 Ruthenium catalyzed sequential cross-metathesis of olefins and hydrogenation

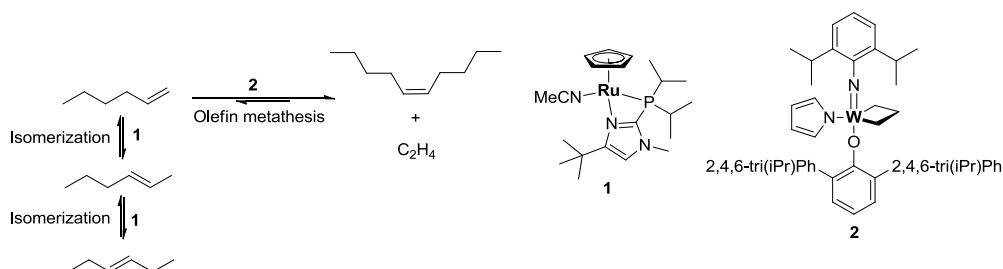
In the *concurrent tandem catalysis* (CTC) two different transformations are simultaneously catalyzed by the same catalyst. For instance, Reaction I and Reaction II in Scheme 1.1 may take place at the same time, and are promoted by the same catalyst. The reagents are added at the beginning of the reaction, and the reaction conditions are not modified during its development. The compatibility of both catalytic cycles with the reaction conditions used is usually the main drawback. Another important problem found in CTC processes is that one single catalyst often has limited scope of reactivity.

In order to increase the versatility of the process, multimetallic catalytic systems have emerged as a very promising tool. In a straightforward approach, two different metal complexes can be combined in the same reaction vessel, aiming that each of the metals facilitates mechanistically independent catalytic cycles (Scheme 1.3).



Scheme 1.3 Orthogonal-tandem catalysis

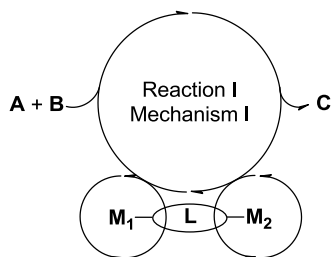
In a typical process, one catalyst will promote the transformation of the reagents (**A** and **B**, in Scheme 1.3) in the first product (**C**). This product reacts with other reagent through another catalytic cycle (different from the first one) promoted by a second catalyst to yield the desired product (**E**). This kind of reactions is called orthogonal-tandem catalysis,^{5,7} although some authors also consider it concurrent tandem catalysis.^{2,7,9} The main drawback of these processes is the compatibility of both catalytic cycles with the reaction conditions and the possibility of negative interactions between the catalysts. A very recent example of this approach was reported by Schrock and Grotjahn.⁹ They combined a ruthenium and a tungsten catalyst for the development of one-pot tandem olefin isomerization/metathesis-coupling (Scheme 1.4). **1** promotes the isomerization of the internal alkene to terminal alkene, and **2** catalyzes the olefin metathesis. The combination of both catalysts allowed achieving good selectivity to the *Z*-internal olefins from a mixture of *E*-olefin isomers.



Scheme 1.4 Tandem olefin isomerization/metathesis-coupling

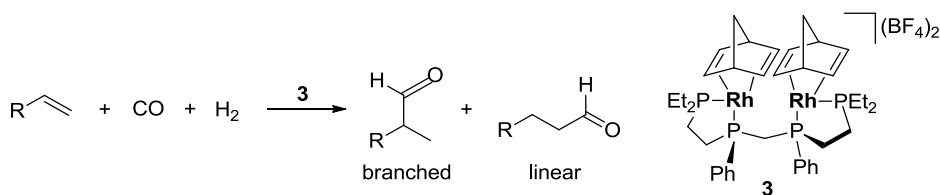
In order to increase the activity of multimetallic systems, the different metal centers involved in a process should be bonded through an appropriate ligand (**L** in Scheme 1.5 and Scheme 1.7). Several active sites in enzymes contain two metals in close proximity, so they can work in a cooperative manner.³ It has been proposed that

bimetallic catalysts bearing the two metals at a close distance (3.5-6 Å), can catalyze a reaction more efficiently compared with the mixture of analogous monometallic catalysts.^{3,10,11} One application of these bimetallic catalytic systems is the promotion of a challenging reaction through the cooperative activity of both metals, for example if the two metals work together to generate a new single bond (Scheme 1.5).^{3,10,11}



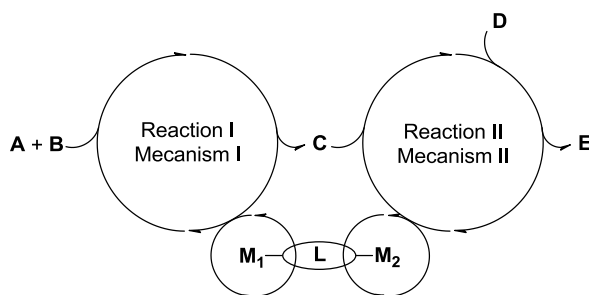
Scheme 1.5

One of the first examples of the cooperative effect using bimetallic catalysts was reported by Stanley and co-workers in 1993,^{12,13} who proved that a bis-rhodium catalyst was highly active in the hydroformylation of α -olefins, and also demonstrated to be very regioselective to the linear product (Scheme 1.6). The short metal-to-metal distance seemed to be decisive in the activity of this catalyst. Similar bis-rhodium catalysts with longer distances between the metals, or the mono-metallic version of **3** provided much lower activities.



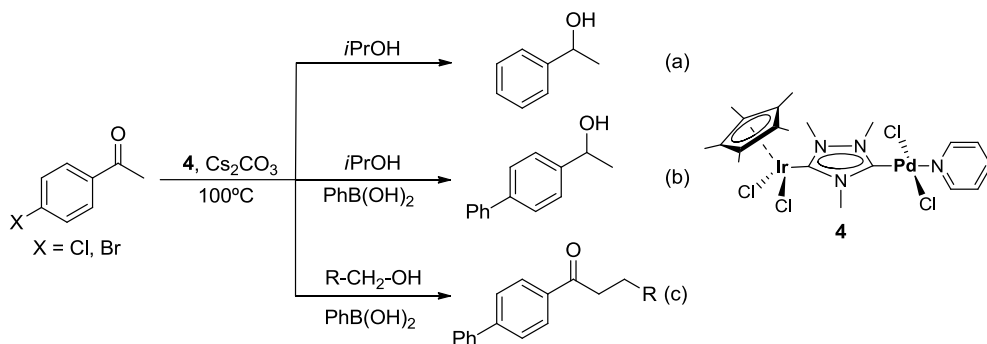
Scheme 1.6 Hydroformylation of α -olefins

The combination of two different metal fragments into a single-frame heterometallic catalyst may constitute an efficient improvement of the efficiency of processes in which two different catalytic cycles are involved (Scheme 1.7), for certain types of orthogonal-tandem catalysis (*vide supra*).



Scheme 1.7

Over the last few years, the Group of Organometallic Chemistry and Homogeneous Catalysis at the Universitat Jaume I (QOMCAT group), reported efficient methods for the preparation of homo- and hetero-bimetallic complexes, mostly based on the 1,2,4-trimethyltriazol-3,5-diylidene ligand with metals of the platinum group, including gold.^{14–17} The preparation of such hetero-bimetallic complexes allowed to study several catalytic processes in which each of the metal centers facilitated mechanistically independent cycles.^{18–21} For instance, compound **4** (Scheme 1.8) is an excellent catalyst for different tandem processes, in which each metal mediated mechanistically distinct reactions: (a) dehalogenation and hydrogen transfer of haloacetophenones, (b) Suzuki-Miyaura C-C coupling and hydrogen transfer of *p*-bromoacetophenone and (c) Suzuki-Miyaura C-C coupling and α -alkylation of *p*-bromoacetophenone (Scheme 1.8). In all cases the activity of this catalyst was higher than the one obtained combining related homo-bimetallic complexes of iridium and palladium,¹⁸ in a clear illustration of a synergistic behavior (or *cooperativity*) between the metals present in the hetero-bimetallic unit.



Scheme 1.8

For this kind of catalytic systems a key feature is the ligand, which needs to simultaneously provide the appropriate stereoelectronic properties to the two different metals, and also facilitate the optimum distance and geometrical arrangement between them. Several polytopic ligands based on different donor atoms were further designed in order to generate multimetallic catalysts, aiming to achieve improved catalytic properties.^{22,23} Designing and preparing suitable ligands for holding effective heterometallic catalysts, is often the key factor that constitutes the most challenging part of the research in this field.

Another interesting class of multimetallic catalysts are dendrimers, which may be decorated with metals. These compounds can have high local catalyst concentrations, which may provide cooperative effects between the metal centers. This phenomenon is called the *dendritic effect*.^{24,25}

1.1.2 Multimetallic compounds from geometrically isolated poly-NHCs

N-heterocyclic carbenes (NHCs)^{26,27} have been recently used for the preparation of a wide variety of multimetallic compounds.²³ NHC-based ligands constitute very attractive scaffolds for the preparation of this type of complexes because they feature a series of properties:

- They have a great coordination versatility, as these ligands have a high affinity for almost all the metals of the periodic table.²⁸
- They often afford stable complexes, as a consequence of the strong M-C bond.
- Their precursors (often azolium salts) are relatively easy to obtain, and therefore access to a wide variety of topologies is basically granted.²⁹

This last attribute allowed synthesizing rigid polytopic NHCs, whose architectures are not available for other kind of ligands.²³ Furthermore, if the NHCs in polytopic ligands are fused to π -extended cores, electronic communication between the different metals may be allowed through the potential interaction between the d_{π} metal orbitals and the π -delocalized system of the NHC *via* M=C π -bonding.^{30,31} This fact may be translated into synergistic or cooperative effects between the metals in multimetallic catalysis.

1.1.2.1 Janus-type bis-NHCs

Janus-type bis-NHCs contain two NHC units in a facially-opposed disposition. This situation avoids chelation over one metal, as typically happens when bis-NHCs with flexible linkers are used.^{32,33} The denomination *Janus* is attributed to its analogy with the representation of the Roman God Janus, who had two faces looking at opposite directions (Figure 1.1, left).

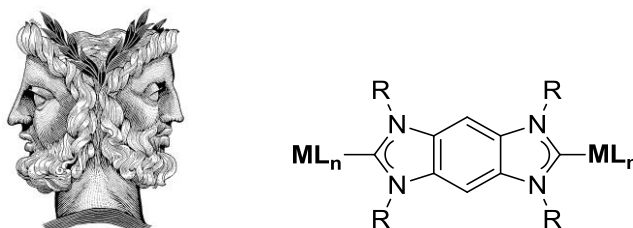


Figure 1.1 Roman God *Janus* (left) and bimetallic complex based on a benzobis(imidazolylidene) ligand (right)

The first example of a *Janus*-type bis-NHC ligand was the benzobis(imidazolylidene) ligand (Figure 1.1, right), reported in a pioneering work by Bielawski and co-workers.^{34–36} The use of this ligand allowed the preparation of homo-bimetallic complexes of Ag(I),³⁵ Rh(I),³⁵ Rh(III),³⁷ Ir(I),³⁸ Ir(III),^{37,38} Fe(II),³⁹ Ru(II),^{39,40} Ni(II),⁴¹ Pt(II),⁴² and Au(I).⁴³ The through-space distance established by the benzobis(imidazolylidene) ligand between two metals is 10.6 Å. Although several works demonstrated that the electronic communication established between the metals bound to this ligand is negligible,^{38,39} Albrecht and co-workers elegantly demonstrated that efficient electronic communication in bis-Ru complexes may be achieved, if additional chelating ligands enforced the appropriate orientation of the carbene and the metal orbitals. In this way the interaction between the d_π orbitals of the metal and the π -system of the ligand is facilitated.⁴⁰ Despite its unique stereoelectronic properties, the benzobis(imidazolylidene) ligand has not been used for the synthesis of hetero-bimetallic complexes, and therefore has not yet been used in heterometallic catalysis.

Another *Janus*-type bis-NHC ligand, which has been widely used in the QOMCAT group for the preparation of bimetallic species, is the 1,2,4-trimethyltriazol-3,5-diylidene ligand (also called “*ditz*”, Chart 1.1). By using this ligand homo-bimetallic compounds based on Rh(I),¹⁴ Ir(I),¹⁴ Ir(III),¹⁵ Ru(II),⁴⁴ Pd(II),^{16,17,45,46} Pt(II)¹⁹ and

Au(I)^{21,47} were described. However, probably more interesting are the different approaches developed in the QOMCAT group, for the preparation of hetero-bimetallic species by combining Ir(I)/Rh(I),¹⁴ Ir(III)/Rh(I),¹⁵ Ir(III)/Pd(II),^{18,48} Ir(III)/Pt(II),¹⁹ Ir(III)/Au(I),²¹ Ir(III)/Ru(II)⁴⁹ and Ru(II)/Pd(II)⁵⁰ centers.

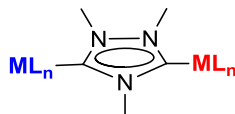
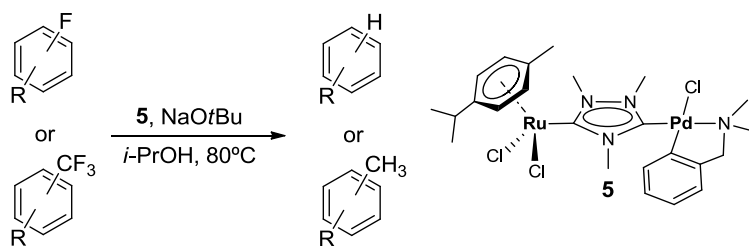


Chart 1.1 Bimetallic complex based on *ditz* ligand

Electrochemical studies of the bis-Ru complex based on *ditz* showed a weak but not negligible interaction between the two ruthenium centers.⁴⁹ More recently, DFT calculations showed that π -interaction apparently plays no significant role in the M-M electronic communication in this and other related bis-NHCs connected by extended polyaromatic systems.³¹

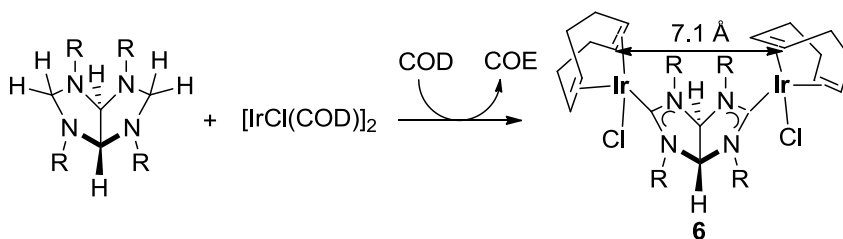
One attractive feature of the *ditz* ligand is that it bears the two metals at a distance of 6 Å, thus enabling the possibility of catalytic cooperativity.³ As a consequence, the catalytic activity of all the hetero-bimetallic species based on *ditz* were tested in several tandem processes, as already described above.

Apart from the tandem processes depicted in Scheme 1.8, another type of application of the heterometallic complexes based on *ditz* implies their application in a much simpler process, although equally challenging, as is the hydrodefluorination of fluoro-organic molecules. In this regard, compound **5** is an excellent catalyst for the hydrodefluorination of different types of carbon-fluorine bonds (Scheme 1.9). The overall process implies the synergistic action of the palladium and the ruthenium centers: the palladium fragment facilitates the C-F activation, while the ruthenium center promotes the transfer hydrogenation from *i*-PrOH/NaOtBu. In this case as in the example showed in Scheme 1.8, the combination of the related homo-bimetallic catalysts containing ruthenium and palladium based on *ditz* provided poor catalytic performances.⁵⁰



Scheme 1.9

Recently, the QOMCAT group developed efficient methods for preparing a large library of *Janus*-type bis-NHC ligands. A very interesting example is the preparation of bis(imidazolinylidene) ligands, which allowed the preparation of homo-bimetallic compounds based on Ir(I)^{51,52} (Scheme 1.10) and Pd(II).⁵² As depicted in Scheme 1.10, the metallation strategy followed to synthesize bis-Ir compounds implies a double C-H bond activation of the corresponding bis(imidazolidine), thus avoiding the use of base,^{51,52} and providing a unique coordination method based on the double activation of geminal C(sp³)-H bonds. The through-space distance between the two metals in these compounds is 7.1 Å (Scheme 1.10). The catalytic activity of the bis-Pd complexes were tested in the acylation of aryl halides.⁵²



Scheme 1.10 Bimetallic complex based on a bis(imidazolinylidene) ligand

Yet other *Janus*-type bis-NHC ligand which was synthesized in our laboratory, in collaboration with Dr. Manuel Alcarazo (*Max Planck Institute für Kohlenforschung, Müllheim an der Ruhr-Germany*), is the pyracenebis(imidazolylidene) shown in Chart 1.2.⁵³ This ligand contains two NHC moieties fused with a polyaromatic core (pyracene). By using it, bimetallic species of Ir(I),⁵³ Rh(I)⁵³ and Pd(II)⁵⁴ were successfully synthesized. The pyracenebis(imidazolylidene) ligand establishes a distance of 14 Å between the two metal centers. The electrochemical measurements on a bis-Ir compound showed that the electronic communication between the metals

is negligible.⁵³ The catalytic activity of bis-Pd compounds were tested in different reactions and provided better catalytic performances than their mono-Pd analogues.⁵⁴

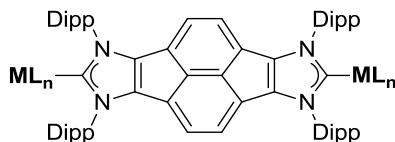


Chart 1.2 Bimetallic complex based on a pyracenebis(imidazolylidene) ligand

1.1.2.2 Rigid tritopic NHCs

The first example of a D_{3h} -symmetric tris-NHC ligand was reported by Bielawski and co-workers in 2010.⁵⁵ The ligand consisted of three NHC units connected by a triptycene core (Chart 1.3). Although the authors reported the generation of the free carbene, they did not coordinate the ligand to any metal, so the properties associated with their metal complexes were not described.

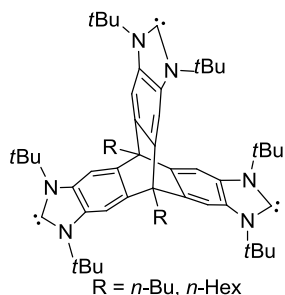


Chart 1.3 Triptycene-tris-imidazolylidene

During the course of the development of this PhD. Thesis, our group described several C_3 -symmetry rigid trimetallic complexes based on tris-NHC ligands.⁵⁶ A very interesting example is the tribenzotriquinacene-tris-imidazolylidene ligand, which was synthesized in our group, in a collaborative work with Prof. Dietmar Kuck (*Bielefeld University-Germany*) (Chart 1.4). This ligand has C_{3v} symmetry due to the presence of a tribenzotriquinacene core, which provides a bowl-shaped topology to the ligand. A tris-Rh(I) complex was obtained and its electronic properties were investigated, concluding that the three rhodium atoms are essentially electronically disconnected.⁵⁷

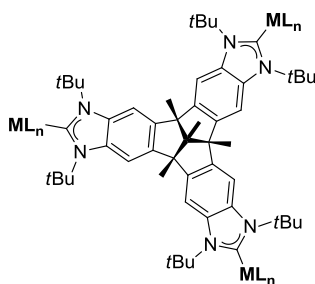
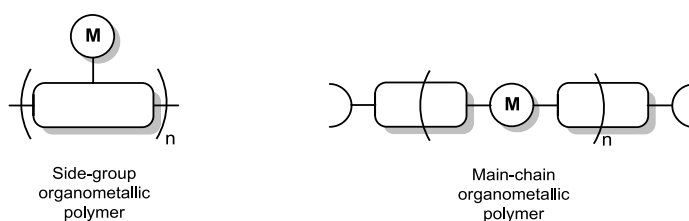


Chart 1.4 Trimetallic complex based on a tribenzotriquinacene-tris-imidazolylidene ligand

1.1.3 Polymeric organometallic materials based on poly-NHCs

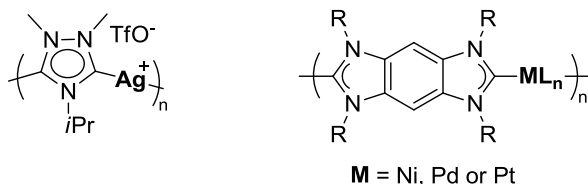
During the last years, organometallic polymer chemistry has emerged as a very important research area in which several efforts to increase the library of compounds have been done.⁵⁸ Organometallic polymers can be divided in two types depending on the position of the metal with respect the primary polymer: if the metal is not situated in the polymer backbone, a side-group organometallic polymer is formed (Scheme 1.11, left). In this type of materials, the metal is bonded in a pendant situation with respect to the core of the polymer, which is mainly organic. The other kind are the main-chain organometallic polymers, in which the metal-ligand bond is necessary for the existence of the polymer, in other words, the metal forms part of the main chain of the polymer (Scheme 1.11, right).⁵⁹



Scheme 1.11 Types of organometallic polymers

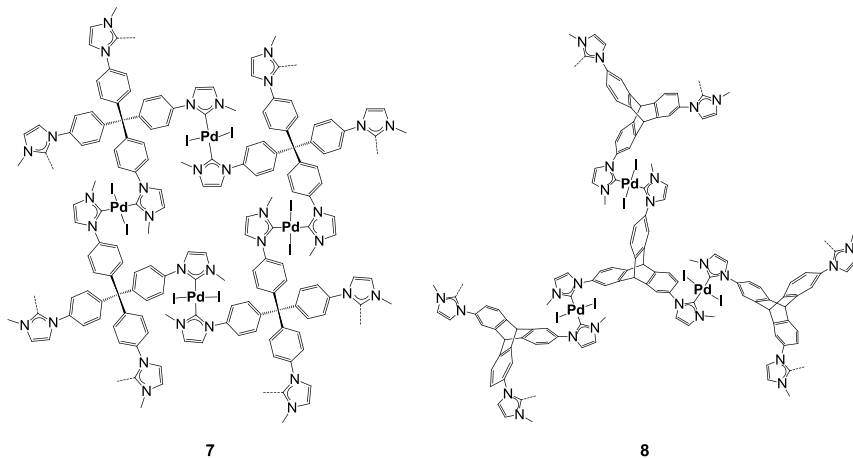
Recently, poly-NHCs have been used as ligands for the synthesis of main-chain organometallic polymers. In fact, the first time that benzobis(imidazolylidenes) and triazoldiylidenes were used as *Janus*-type bis-NHCs, they were acting as building blocks for main-chain organometallic polymers (Scheme 1.12). In a pioneering work, Bertrand and co-workers described the use of *ditz* to obtain one-dimensional main-chain organometallic polymers based on silver (Scheme 1.12, left).^{60,61} Some years later, Bielawski and co-workers synthesized a series of bisazolium salts, which were

employed to synthesize linear main-chain organometallic polymers based on Ni, Pd and Pt (Scheme 1.12, right).^{34,62}



Scheme 1.12 One-dimensional main-chain organometallic polymers based on *Janus*-type bis-NHCs

More recently, tetra- and tris-NHCs were used to obtain two kinds of three-dimensional main-chain organometallic polymers (Scheme 1.13).^{63,64} Both materials showed spherical shapes, although in the case of **7** those spheres were empty (hollow spheres). Polymers **7** and **8** were used as heterogeneous catalysts in different palladium-facilitated reactions.

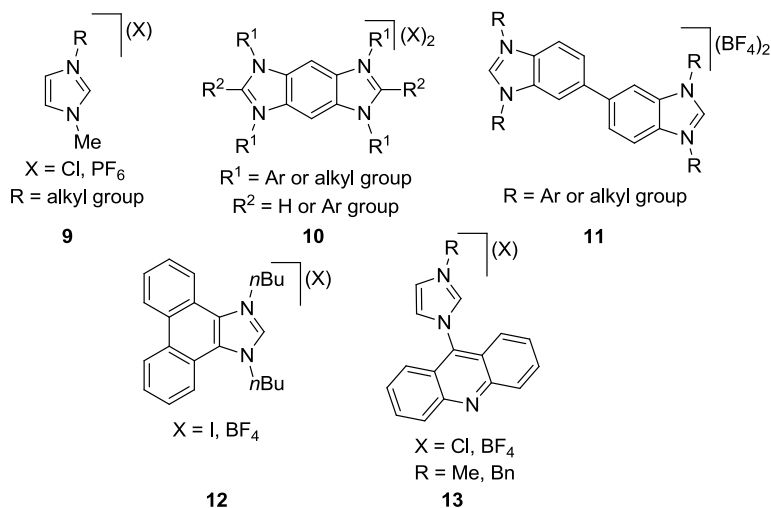


Scheme 1.13 Three-dimensional main-chain organometallic polymers based on poly-NHCs

1.1.4 Luminescent azolium salts

Organic light-emitting compounds have attracted the attention of several research groups, as their synthetic versatility has provided applications in multiple fields.^{65–67} Imidazolium salts have recently proven to be a very interesting class of fluorophores. The first examples in which the luminescent properties of these compounds were

studied were related to their behavior as ionic liquids.^{68–72} These salts usually bear long alkyl chains which could be combined with different counter-ions (**9** in Scheme 1.14). Their emission intensities were very low due to their relatively small chromophores.^{69–72} Bielawski and co-workers introduced two azolium moieties annulated to different aromatic cores (**10** and **11** in Scheme 1.14) providing compounds with high quantum efficiencies,^{73,74} and with remarkable properties as ionic liquid crystals.^{75,76}



Scheme 1.14 Examples of reported fluorescent imidazolium salts

Then, several examples appeared in the literature related to fluorescent imidazolium salts. Most of them contain a polyaromatic group, which can be introduced in the backbone of the azolium or as N-substituents, in order to increase the efficiency of the emission.^{77–82} For instance, Tapu and co-workers synthesized phenanthrene-based azoliums (**12** in Scheme 1.14), which exhibited over 3 times stronger emission than phenanthrene.⁷⁸ Recently, Gimeno and co-workers reported imidazolium salts with acridine groups as one of the N-substituents (**13** in Scheme 1.14). They studied the luminescent properties of these salts and their related silver and gold-based NHC complexes, probing to be intense blue-green emitters in the solid state and blue emitters in solution.⁸¹

1.2 Objectives

During the last years, our group of research has developed new complexes based on N-heterocyclic carbenes. In particular, improved catalytic systems based on multimetallic catalysts were developed. On the grounds of these previous achievements, the general objective of this Ph.D. Thesis is to obtain new multimetallic complexes for the development of improved catalytic processes. This general objective can be divided in the following more specific objectives, which may be taken as the specific research strategies of the work developed in the next few chapters:

- Synthesis of new poly-azoliums with polyaromatic cores, for the generation of rigid and geometrically isolated poly-NHC ligands.
- Coordination of these NHCs to different metals, aiming to obtain multimetallic complexes with fixed distances between the metals.
- Study of the physico-chemical properties of the new compounds obtained (electrochemistry, luminescence, etc).
- Study of the catalytic properties of the new complexes, with special attention to study the existence of any cooperative effect.
- Synthesis of new main-chain organometallic polymers based on the new poly-NHCs synthesized, and evaluation of their catalytic properties.

1.3 References

- (1) Beller, M.; Renken, A.; van Santen, R. A. *Catalysis. From Principles to Applications*; Wiley-VCH, 2012.
- (2) Wasilke, J.-C.; Obrey, S. J.; Baker, R. T.; Bazan, G. C. *Chem. Rev.* **2005**, *105*, 1001.
- (3) Van den Beuken, E. K.; Feringa, B. L. *Tetrahedron* **1998**, *54*, 12985.
- (4) Lee, J. M.; Na, Y.; Han, H.; Chang, S. *Chem. Soc. Rev.* **2004**, *33*, 302.
- (5) Fogg, D. E.; dos Santos, E. N. *Coord. Chem. Rev.* **2004**, *248*, 2365.
- (6) Ajamian, A.; Gleason, J. L. *Angew. Chem. Int. Ed.* **2004**, *43*, 3754.
- (7) Shindoh, N.; Takemoto, Y.; Takasu, K. *Chem. Eur. J.* **2009**, *15*, 12168.
- (8) Louie, J.; Bielawski, C. W.; Grubbs, R. H. *J. Am. Chem. Soc.* **2001**, *123*, 11312.
- (9) Dobreiner, G. E.; Erdogan, G.; Larsen, C. R.; Grotjahn, D. B.; Schrock, R. R. *ACS Catal.* **2014**, *4*, 3069.
- (10) Park, J.; Hong, S. *Chem. Soc. Rev.* **2012**, *41*, 6931.
- (11) Allen, A. E.; Macmillan, D. W. C. *Chem. Sci.* **2012**, 633.
- (12) Broussard, M. E.; Juma, B.; Train, S. G.; Peng, W. J.; Laneman, S. A.; Stanley, G. G. *Science* **1993**, *260*, 1784.
- (13) Peng, W.-J.; Train, S. G.; Howell, D. K.; Fronczek, F. R.; Stanley, G. G. *Chem. Commun.* **1996**, 2607.
- (14) Mas-Marzá, E.; Mata, J. A.; Peris, E. *Angew. Chem. Int. Ed.* **2007**, *46*, 3729.
- (15) Zanardi, A.; Corberán, R.; Mata, J. A.; Peris, E. *Organometallics* **2008**, *27*, 3570.
- (16) Zanardi, A.; Mata, J. A.; Peris, E. *Organometallics* **2009**, *28*, 4335.
- (17) Zanardi, A.; Mata, J. A.; Peris, E. *Organometallics* **2009**, *28*, 1480.
- (18) Zanardi, A.; Mata, J. A.; Peris, E. *J. Am. Chem. Soc.* **2009**, *131*, 14531.
- (19) Zanardi, A.; Mata, J. A.; Peris, E. *Chem. Eur. J.* **2010**, *16*, 13109.
- (20) Zanardi, A.; Mata, J. A.; Peris, E. *Chem. Eur. J.* **2010**, *16*, 10502.
- (21) Sabater, S.; Mata, J. A.; Peris, E. *Chem. Eur. J.* **2012**, *18*, 6380.
- (22) Bratko, I.; Gómez, M. *Dalton Trans.* **2013**, *42*, 10664.
- (23) Mata, J. A.; Hahn, F. E.; Peris, E. *Chem. Sci.* **2014**, *5*, 1723.

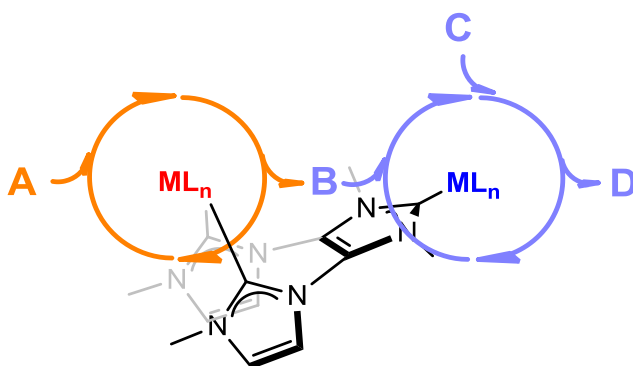
- (24) Helms, B.; Fréchet, J. M. J. *Adv. Synth. Catal.* **2006**, *348*, 1125.
- (25) Reek, J.; Arevalo, S.; Van Heerbeek, R.; Kamer, P.; Van Leeuwen, P. *Adv. Catal.* **2006**, *49*, 71.
- (26) Herrmann, W. A.; Köcher, C. *Angew. Chemie Int. Ed.* **1997**, *36*, 2162.
- (27) Bourissou, D.; Guerret, O.; Gabbai, F. P.; Bertrand, G. *Chem. Rev.* **2000**, *100*, 39.
- (28) Díez-González, S.; Marion, N.; Nolan, S. P. *Chem. Rev.* **2009**, *109*, 3612.
- (29) Benhamou, L.; Chardon, E.; Lavigne, G.; Bellemin-Lapponnaz, S.; César, V. *Chem. Rev.* **2011**, *111*, 2705.
- (30) Schuster, O.; Mercs, L.; Albrecht, M. *Chim. Int. J. Chem.* **2010**, *64*, 184.
- (31) Gusev, D. G.; Peris, E. *Dalton Trans.* **2013**, *42*, 7359.
- (32) Mata, J. A.; Poyatos, M.; Peris, E. *Coord. Chem. Rev.* **2007**, *251*, 841.
- (33) Poyatos, M.; Mata, J. A.; Peris, E. *Chem. Rev.* **2009**, *109*, 3677.
- (34) Boydston, A. J.; Williams, K. A.; Bielawski, C. W. *J. Am. Chem. Soc.* **2005**, *127*, 12496.
- (35) Khramov, D. M.; Boydston, A. J.; Bielawski, C. W. *Angew. Chem. Int. Ed.* **2006**, *45*, 6186.
- (36) Boydston, A. J.; Bielawski, C. W. *Dalton Trans.* **2006**, 4073.
- (37) Schmidtendorf, M.; Schulte to Brinke, C.; Hahn, F. E. *J. Organomet. Chem.* **2014**, *751*, 620.
- (38) Tennyson, A. G.; Rosen, E. L.; Collins, M. S.; Lynch, V. M.; Bielawski, C. W. *Inorg. Chem.* **2009**, *48*, 6924.
- (39) Mercs, L.; Neels, A.; Albrecht, M. *Dalton Trans.* **2008**, 5570.
- (40) Nussbaum, M.; Schuster, O.; Albrecht, M. *Chem. Eur. J.* **2013**, *19*, 17517.
- (41) Hahn, F. E.; Radloff, C.; Pape, T.; Hepp, A. *Organometallics* **2008**, *27*, 6408.
- (42) Radloff, C.; Hahn, F. E.; Pape, T.; Fröhlich, R. *Dalton Trans.* **2009**, 7215.
- (43) Radloff, C.; Weigand, J. J.; Hahn, F. E. *Dalton Trans.* **2009**, 9392.
- (44) Viciano, M.; Sanaú, M.; Peris, E. *Organometallics* **2007**, *26*, 6050.
- (45) Guo, S.; Huynh, H. V. *Organometallics* **2012**, *31*, 4565.
- (46) Guo, S.; Huynh, H. V. *Organometallics* **2014**, *33*, 2004.

- (47) Guo, S.; Sivaram, H.; Yuan, D.; Huynh, H. V. *Organometallics* **2013**, *32*, 3685.
- (48) Sabater, S.; Mata, J. A.; Peris, E. *Eur. J. Inorg. Chem.* **2013**, 4764.
- (49) Sabater, S.; Mata, J. A.; Peris, E. *Organometallics* **2012**, *31*, 6450.
- (50) Sabater, S.; Mata, J. a; Peris, E. *Nat. Commun.* **2013**, *4*, 2553.
- (51) Prades, A.; Poyatos, M.; Mata, J. A.; Peris, E. *Angew. Chem. Int. Ed.* **2011**, *50*, 7666.
- (52) Valdés, H.; Poyatos, M.; Peris, E. *Organometallics* **2013**, *32*, 6445.
- (53) Prades, A.; Peris, E.; Alcarazo, M. *Organometallics* **2012**, *31*, 4623.
- (54) Guisado-Barrios, G.; Hiller, J.; Peris, E. *Chem. Eur. J.* **2013**, *19*, 10405.
- (55) Williams, K. A.; Bielawski, C. W. *Chem. Commun.* **2010**, *46*, 5166.
- (56) Gonell, S.; Poyatos, M.; Peris, E. *Angew. Chem. Int. Ed.* **2013**, *52*, 7009.
- (57) Segarra, C.; Linke, J.; Mas-Marzá, E.; Kuck, D.; Peris, E. *Chem. Commun.* **2013**, *49*, 10572.
- (58) Nguyen, P.; Gómez-Elipe, P.; Manners, I. *Chem. Rev.* **1999**, *99*, 1515.
- (59) Williams, K. A.; Boydston, A. J.; Bielawski, C. W. *Chem. Soc. Rev.* **2007**, *36*, 729.
- (60) Guerret, O.; Solé, S.; Gornitzka, H.; Teichert, M.; Trinquier, G.; Bertrand, G. *J. Am. Chem. Soc.* **1997**, *119*, 6668.
- (61) Guerret, O.; Solé, S.; Gornitzka, H.; Trinquier, G.; Bertrand, G. *J. Organomet. Chem.* **2000**, *600*, 112.
- (62) Boydston, A. J.; Rice, J. D.; Sanderson, M. D.; Dykhno, O. L.; Bielawski, C. W. *Organometallics* **2006**, *25*, 6087.
- (63) Choi, J.; Yang, H. Y.; Kim, H. J.; Son, S. U. *Angew. Chem. Int. Ed.* **2010**, *49*, 7718.
- (64) Zhang, C.; Wang, J.-J.; Liu, Y.; Ma, H.; Yang, X.-L.; Xu, H.-B. *Chem. Eur. J.* **2013**, *19*, 5004.
- (65) Thomas, S. W.; Joly, G. D.; Swager, T. M. *Chem. Rev.* **2007**, *107*, 1339.
- (66) Lo, S.-C.; Burn, P. L. *Chem. Rev.* **2007**, *107*, 1097.
- (67) Santos-Figueroa, L. E.; Moragues, M. E.; Climent, E.; Agostini, A.; Martínez-Máñez, R.; Sancenón, F. *Chem. Soc. Rev.* **2013**, *42*, 3489.
- (68) Binnemans, K. *Chem. Rev.* **2005**, *105*, 4148.

- (69) Billard, I.; Moutiers, G.; Labet, A.; El Azzi, A.; Gaillard, C.; Mariet, C.; Lützenkirchen, K. *Inorg. Chem.* **2003**, *42*, 1726.
- (70) Guillet, E.; Imbert, D.; Scopelliti, R.; Bünzli, J.-C. G. *Chem. Mater.* **2004**, *16*, 4063.
- (71) Paul, A.; Mandal, P. K.; Samanta, A. *J. Phys. Chem. B* **2005**, *109*, 9148.
- (72) Paul, A.; Mandal, P. K.; Samanta, A. *Chem. Phys. Lett.* **2005**, *402*, 375.
- (73) Boydston, A. J.; Vu, P. D.; Dykhno, O. L.; Chang, V.; Wyatt, A. R.; Stockett, A. S.; Ritschdorff, E. T.; Shear, J. B.; Bielawski, C. W. *J. Am. Chem. Soc.* **2008**, *130*, 3143.
- (74) Er, J. A. V.; Tennyson, A. G.; Kamplain, J. W.; Lynch, V. M.; Bielawski, C. W. *Eur. J. Inorg. Chem.* **2009**, 1729.
- (75) Boydston, A. J.; Pecinovsky, C. S.; Chao, S. T.; Bielawski, C. W. *J. Am. Chem. Soc.* **2007**, *129*, 14550.
- (76) Wiggins, K. M.; Kerr, R. L.; Chen, Z.; Bielawski, C. W. *J. Mater. Chem.* **2010**, *20*, 5709.
- (77) Kim, S. K.; Seo, D.; Han, S. J.; Son, G.; Lee, I.-J.; Lee, C.; Lee, K. D.; Yoon, J. *Tetrahedron* **2008**, *64*, 6402.
- (78) Tapu, D.; Owens, C.; VanDerveer, D.; Gwaltney, K. *Organometallics* **2009**, *28*, 270.
- (79) Chow, A. L.-F.; So, M.-H.; Lu, W.; Zhu, N.; Che, C.-M. *Chem. Asian J.* **2011**, *6*, 544.
- (80) Kriechbaum, M.; List, M.; J F Berger, R.; Patzschke, M.; Monkowius, U. *Chem. Eur. J.* **2012**, *18*, 5506.
- (81) Gimeno, M. C.; Laguna, A.; Visbal, R. *Organometallics* **2012**, *31*, 7146.
- (82) Tapu, D.; McCarty, Z.; Hutchinson, L.; Ghattas, C.; Chowdhury, M.; Salerno, J.; VanDerveer, D. *J. Organomet. Chem.* **2014**, *749*, 134.

Chapter 2

Homo- and hetero-bimetallic complexes with a Y-shaped tris-NHC ligand

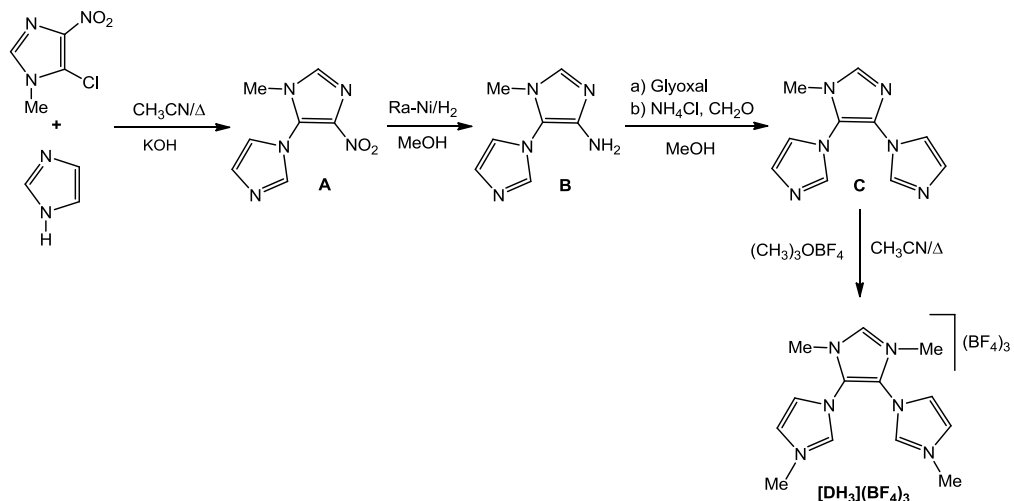


2.1 Results and discussion

As mentioned in Chapter 1, the synthetic versatility of NHCs has allowed the design of ligands with a wide variety of structures, yielding complexes with very sophisticated architectures.¹ We were interested in synthesizing ligands capable to coordinate to two different metals in two different coordination environments, in order to produce bimetallic complexes. These compounds should enable different chemical properties for each metal fragment, regardless that the pair of metals bound to the ligand are the same, or different. For this reason, we envisioned a new tris-NHC ligand, which should be able to bridge two different metal fragments, by simultaneously acting as bis-chelate and monodentate ligand. To accomplish this purpose, we obtained the tris-imidazolium salt $[\text{DH}_3](\text{BF}_4)_3$ (Scheme 2.1). The synthesis of this salt and the coordination strategies used to prepare different kinds of mono- and bimetallic complexes are discussed in this chapter.

2.1.1 Synthesis of tris-imidazolium salt $[\text{DH}_3](\text{BF}_4)_3$

The tris-imidazolium compound $[\text{DH}_3](\text{BF}_4)_3$ was prepared following a four-steps synthetic procedure, as depicted in Scheme 2.1.



Scheme 2.1 Synthesis of $[\text{DH}_3](\text{BF}_4)_3$

The first step involves a nucleophilic aromatic substitution between the deprotonated imidazole and 5-chloro-1-methyl-4-nitroimidazole. The reaction was carried out in refluxing acetonitrile for 2 hours, and afforded compound **A** in 96 % yield after

purification (vacuum sublimation at 120°C). Then, the nitro group of compound **A** was reduced in the presence of Nickel-Raney under hydrogen atmosphere (1 atm), yielding the amine **B**. The amine **B** was reacted with glyoxal, NH₄Cl and formaldehyde, following a modified reported procedure,² yielding the tris-imidazole **C**. Finally, **C** was alkylated in the presence of an excess of (CH₃)₃OBF₄ (Meerwein's salt) in refluxing acetonitrile, affording the tris-imidazolium salt [DH₃](BF₄)₃, as a light brown solid, in 20 % overall yield. This tris-azolium salt has unique topological features that may be useful for the preparation of bimetallic complexes, as will be described in the following sections of this chapter.

Compounds **A**, **B**, **C** and [DH₃](BF₄)₃ were characterized by means of NMR spectroscopy, mass spectrometry and elemental analysis. As an example, the NMR spectroscopic characterization of [DH₃](BF₄)₃ is described below. All the details regarding the characterization of compounds **A**, **B** and **C** can be found in the Experimental Section (Chapter 5).

¹H NMR spectrum of [DH₃](BF₄)₃

Figure 2.1 shows the ¹H NMR spectrum of [DH₃](BF₄)₃. The number of signals and their integration is consistent with the C_{2v} symmetry of the molecule. The signals due to the acidic protons at the NCHN group, *a* and *b*, appear as singlets at 9.66 a 9.41 ppm, respectively. The signals attributed to the protons of the CH groups of the imidazolium units are shown as two singlets between 7.95 and 8.07 ppm (*c*). Finally, the resonances corresponding to the protons of the methyl groups bound to the nitrogen of the imidazole ring are displayed as two singlets at 3.95 and 3.87 ppm (*d*).

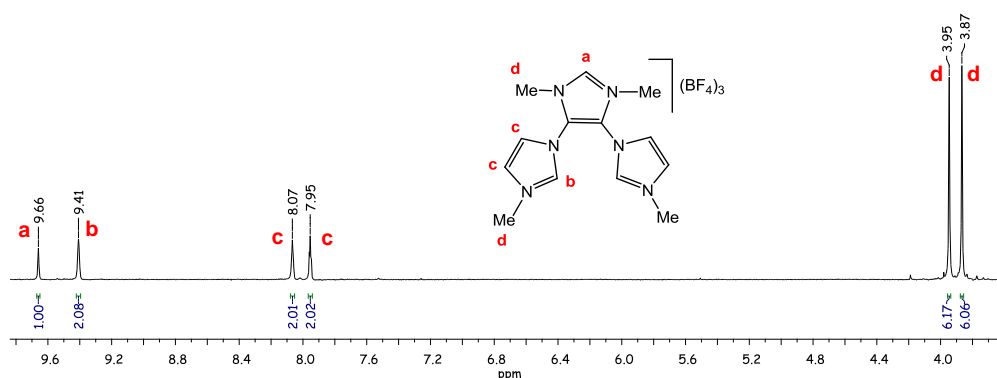


Figure 2.1 ¹H NMR spectrum of [DH₃](BF₄)₃ in DMSO-*d*₆

$^{13}\text{C}\{^1\text{H}\}$ NMR spectrum of $[\text{DH}_3](\text{BF}_4)_3$

Figure 2.2 shows the $^{13}\text{C}\{^1\text{H}\}$ NMR spectrum of $[\text{DH}_3](\text{BF}_4)_3$. Again, the number of signals displayed in the spectrum is consistent with the two-fold symmetry of the compound. The signals attributed to the NCHN carbons, 1 and 2, are displayed at 140.3 and 136.5 ppm, respectively. The resonances corresponding to the carbons of the CH groups of the imidazolium units are observed at 125.4 and 124.0 ppm (3), and the signal due to the $C_{\text{quaternary}}$ is displayed at 121.7 ppm (4). The two signals assigned to the carbons of the methyl groups appear at 36.9 and 34.3 ppm (5).

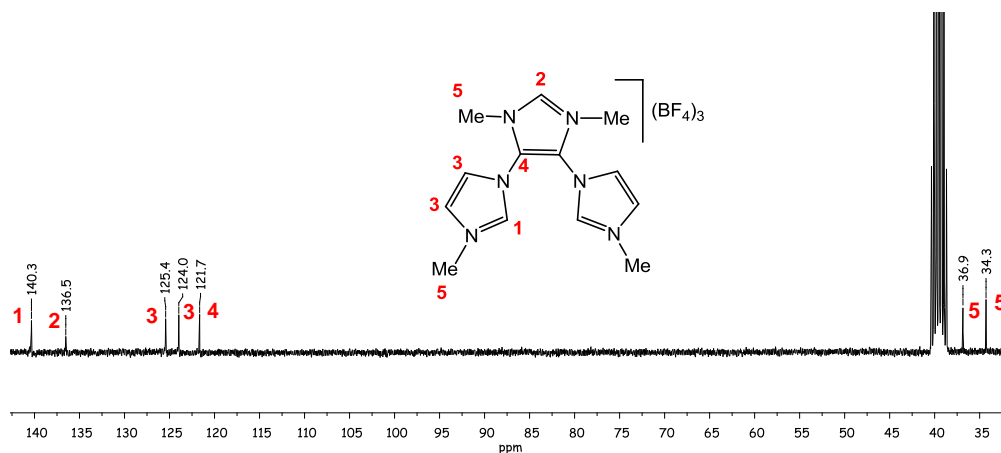
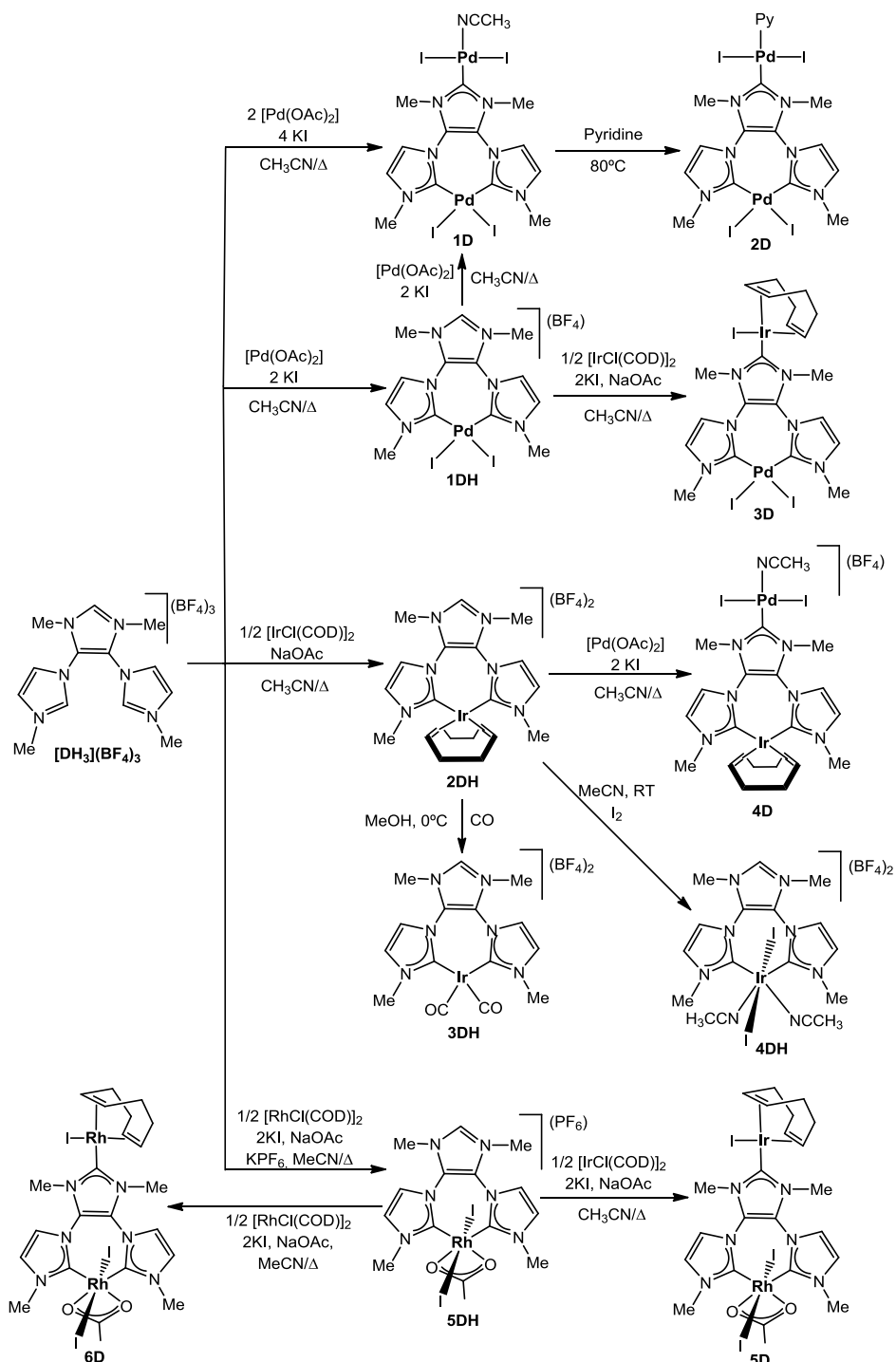


Figure 2.2 $^{13}\text{C}\{^1\text{H}\}$ NMR spectrum of $[\text{DH}_3](\text{BF}_4)_3$ in $\text{DMSO-}d_6$

2.1.2 Metal complexes with a Y-shaped tris-NHC ligand

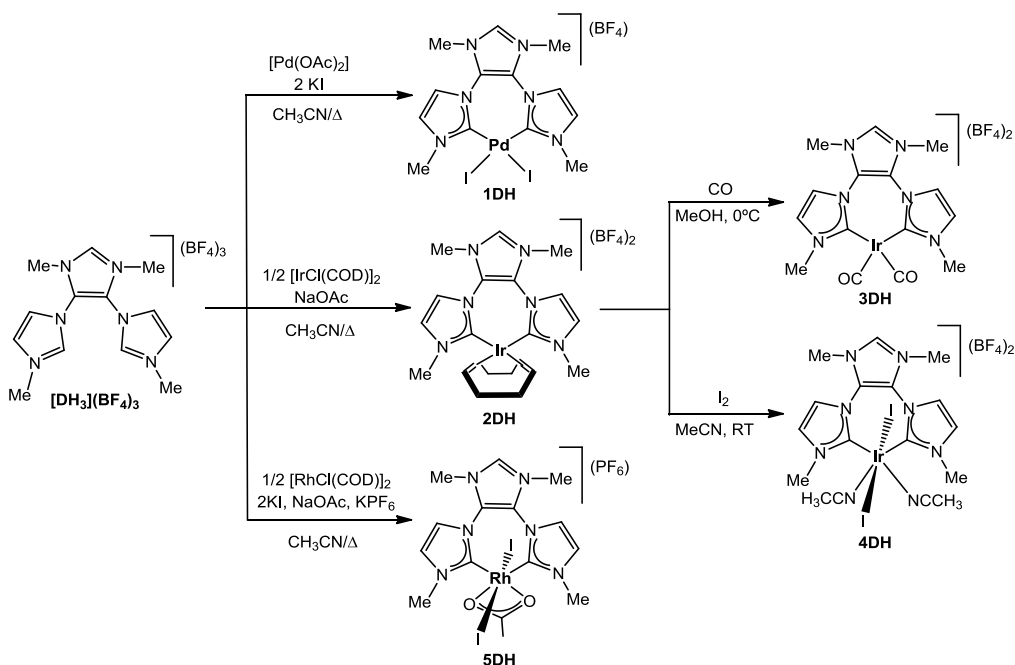
Scheme 2.2 shows the different methodologies employed to prepare mono- and bimetallic NHC complexes using $[\text{DH}_3](\text{BF}_4)_3$. For the labelling of the coordinated ligand we have used **DH** to indicate the formation of the bis-NHC ligand with a remaining imidazolium unit. The tris-NHC ligand, which is the fully deprotonated form of $[\text{DH}_3](\text{BF}_4)_3$, is represented as **D**. Scheme 2.2 illustrates the coordination versatility of the ligand derived from $[\text{DH}_3](\text{BF}_4)_3$. Taking advantage of the chelate effect and controlling the amount of metal precursor introduced in the reaction media, mono- or bimetallic complexes can be obtained selectively. An interesting feature of the coordination of $[\text{DH}_3](\text{BF}_4)_3$, is that the first metal always takes the bis-chelate face of the ligand, as this process is entropically favored.³ This allows the synthesis of monometallic complexes with a chelate bis-NHC and an azolium remaining unit. This azolium can be activated later to produce homo- or hetero-bimetallic complexes, in which the two metals will be bridged by the Y-shaped tris-NHC ligand. In the next sections of this chapter, the different methodologies used to obtain mono- and bimetallic complexes based on the ligand derived from $[\text{DH}_3](\text{BF}_4)_3$ will be described.

Scheme 2.2 Synthesis of complexes **1DH** to **5DH**, and **1D** to **6D**

2.1.2.1 Monometallic complexes based on DH

The reaction of the tris-azolium salt $[\text{DH}_3](\text{BF}_4)_3$ with one equivalent of $[\text{Pd}(\text{OAc})_2]$ or in a 2:1 ratio with $[\text{MCl}(\text{COD})]_2$ ($\text{M} = \text{Ir}$ or Rh), using the reaction conditions displayed in Scheme 2.3, afforded the corresponding monometallic complexes, in which the bis-NHC ligand coordinates in a bis-chelating fashion. Compounds **1DH**, **2DH** and **3DH** are cationic complexes, because they maintain an imidazolium fragment.

Compound **1DH** was obtained in excellent yield (92 %) by treating compound $[\text{DH}_3](\text{BF}_4)_3$, with one equivalent of $[\text{Pd}(\text{OAc})_2]$ in refluxing acetonitrile. In order to complete the coordination sphere about the palladium center, an iodide salt (KI) was also added to the reaction mixture.



Scheme 2.3 Synthesis of complexes **1DH** to **5DH**

The reaction of $[\text{DH}_3](\text{BF}_4)_3$ with $[\text{IrCl}(\text{COD})]_2$ in a 2:1 ratio, in the presence of NaOAc, produced **2DH** as a red, air sensitive solid, in 83 % yield. The COD ligand in **2DH** can be easily substituted by two CO ligands. Bubbling CO through a cold MeOH solution of **2DH** affords complex **3DH** as a yellow solid after the addition of diethyl ether. The IR spectrum of **3DH** displays two CO stretching bands at 2079 and

2017 cm^{-1} , as expected for the C_s symmetry of the molecule. These values suggest a low electron-donating character of the ligand compared to other bis-chelating NHCs,⁴ which is reasonable taking into account the cationic nature of the bis-NHC ligand in compound **3DH**. The Ir(I) atom can be oxidized to Ir(III) using I_2 , yielding compound **4DH**. The reaction was carried out treating **2DH** with I_2 in acetonitrile, at room temperature. This complex was purified by column chromatography, and precipitated from a mixture of acetonitrile and diethyl ether as a yellow, air stable solid in 38 % yield.

The rhodium(III) compound (**5DH**) was synthesized following a previously reported procedure for related bis-chelating complexes.⁵ The reaction of $[\text{DH}_3](\text{BF}_4)_3$ with $[\text{RhCl}(\text{COD})]_2$ in the presence of NaOAc and KI afforded **5DH** in 33 % yield. This low yield is probably due to partial loss of the product in the purification process (column chromatography).

It is worth mentioning the different reactivity observed in the synthesis of complexes **2DH** and **5DH**, depending on the metal precursor used. Compound **2DH** contains an Ir(I) fragment, while **5DH** contains Rh(III). If $[\text{IrCl}(\text{COD})]_2$ (instead of $[\text{RhCl}(\text{COD})]_2$) is reacted under the same reaction conditions employed to obtain **5DH**, the same Ir(I) complex (**2DH**) is isolated. That is, no oxidation to Ir(III) takes place regardless of the reaction conditions. This behavior is remarkable since reactions in which an Ir(III) complex is produced from the reaction of different kinds of bis-imidazolium salts and $[\text{IrCl}(\text{COD})]_2$, are well known, although the mechanism involved is not well understood.^{6,7} If the reaction to obtain **5DH** is carried out in the absence of KI, a mixture of unidentified products is obtained. Although rhodium and iridium belong to the Group 9 of the periodic table, and often show a similar chemical behavior, sometimes they can provide a different pattern of reactivity, as the one shown in this case.⁸

Compounds **1DH** to **5DH** were characterized by means of NMR spectroscopy, mass spectrometry and elemental analysis. The structure of **1DH** was confirmed by X-Ray Diffraction analysis. Due to the similarity of these five complexes, only the spectroscopic characterization of **1DH** is discussed in detail. All the details regarding the characterization of the other four compounds can be found in the Experimental Section (Chapter 5).

¹H NMR spectrum of 1DH

Figure 2.3 shows the ¹H NMR spectrum of **1DH**. The number of signals and the integration is consistent with the two-fold symmetry of the complex. The signal due to the acidic proton of the remaining azolium unit appears as a singlet at 9.55 ppm (a). The signals attributed to the protons of the CH groups of the imidazolylidenes are shown as two doublets at 8.13 and 7.83 ppm (³J_{H-H} = 2.1 Hz) (b). Finally, the resonances assigned to the protons of the methyl groups are displayed as two singlets at 3.99 and 3.91 ppm (c).

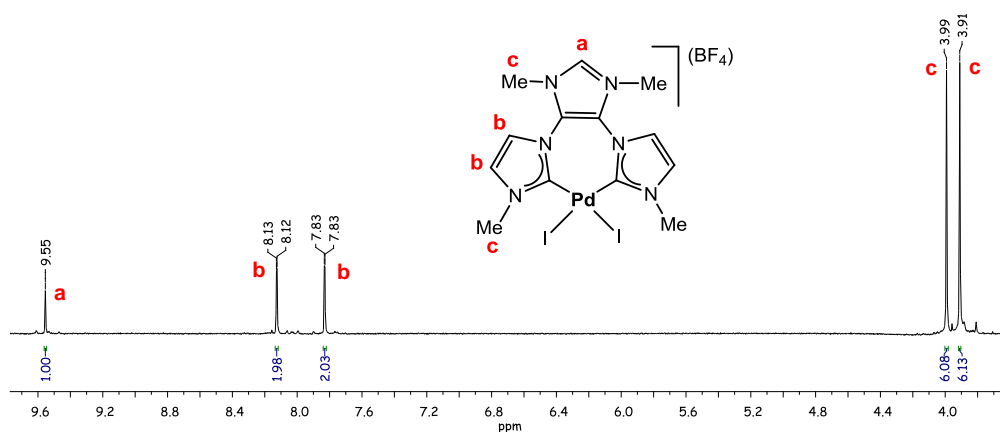


Figure 2.3 ¹H NMR spectrum of **1DH** in DMSO-*d*₆

¹³C{¹H} NMR spectrum of 1DH

Figure 2.4 shows the ¹³C{¹H} NMR spectrum of **1DH**. This spectrum also confirms the two-fold symmetry of the compound. The most characteristic signal is the one attributed to the metallated carbene-carbons at 167.1 ppm (1). The signal corresponding to the carbon of the NCHN at the azolium unit is observed at 135.4 ppm (2). The resonances attributed to the carbons of the CH groups of the imidazolylidenes are observed at 126.7 and 122.2 ppm (3), while the one due to the C_{quaternary} is displayed at 123.1 ppm (4). The signals assigned to the carbons of the methyl groups appear at 34.6 and 30.6 ppm (5).

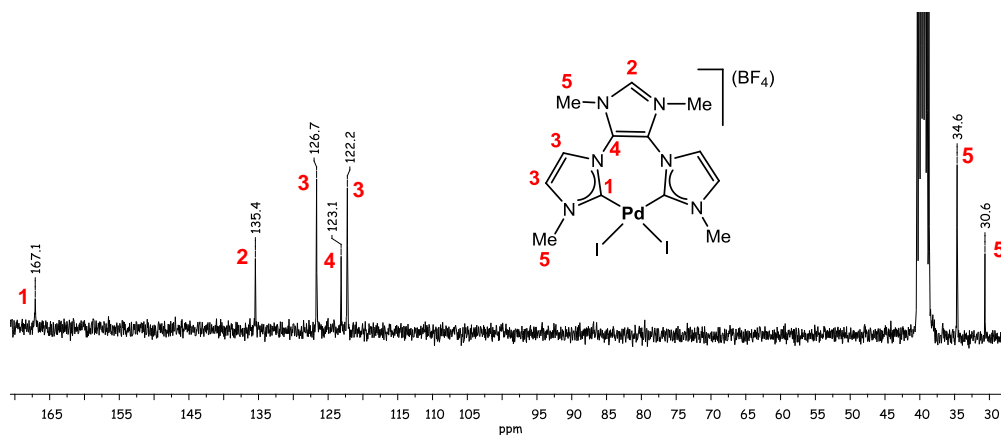


Figure 2.4 $^{13}\text{C}\{^1\text{H}\}$ NMR spectrum of **1DH** in $\text{DMSO-}d_6$

Molecular structure of 1DH

Crystals of **1DH** suitable for X-Ray Diffraction analysis were obtained by slow diffusion of diethyl ether into a concentrated solution of the compound in acetonitrile.

The molecular structure of **1DH**, shown in Figure 2.5, consists of a palladium center with a chelating bis-NHC. Two iodide ligands in a *cis* disposition complete the coordination sphere about the metal. The ionic nature of compound **1DH** is confirmed by the presence of a BF_4^- counter-anion which completes the neutral molecule. Table 2.1 shows the most representative bond distances (\AA) and angles ($^\circ$) of complex **1DH**. The average $\text{Pd-C}_{\text{carbene}}$ distance is $1.993(1) \text{ \AA}$, in the range of other $\text{Pd}(\text{bis-NHC})$ complexes.^{9,10} The two coordinated imidazolylidenes are oriented at an average angle of $65.4(2)^\circ$, relative to the coordination plane. The molecule has a chair conformation, and the “chair angle”, defined as the angle between the plane containing the azolium ring with respect the metal coordination plane, is $97.43(15)^\circ$ (Figure 2.6).

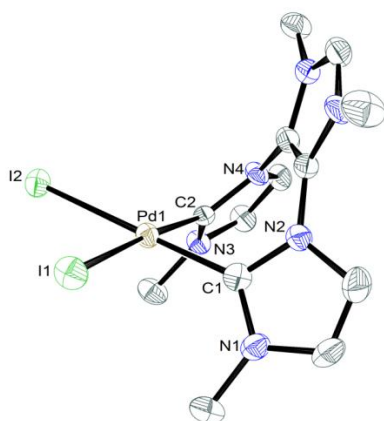


Figure 2.5 Molecular diagram of complex **1DH**. Ellipsoids at 50 % probability. Hydrogen atoms and the counter-ion (BF_4^-) have been omitted for clarity

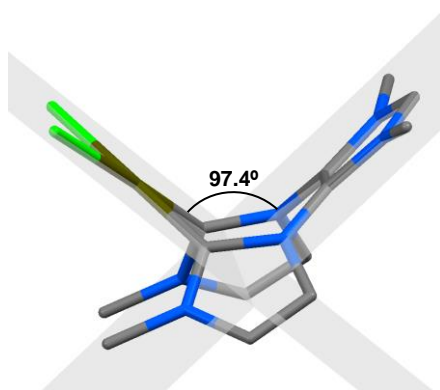


Figure 2.6 Side-on view of complex **1DH** with the “chair angle”

Table 2.1 Selected bond lengths and angles of complex **1DH**

Bond lengths (Å)		Bond angles (°)	
Pd(1)-C(1)	1.993(4)	C(1)-Pd(1)-C(2)	85.17(18)
Pd(1)-C(2)	1.992(5)	I(1)-Pd(1)-I(2)	93.615(14)
Pd(1)-I(1)	2.666(5)	“Chair angle”	97.43(15)
Pd(1)-I(2)	2.642(4)		

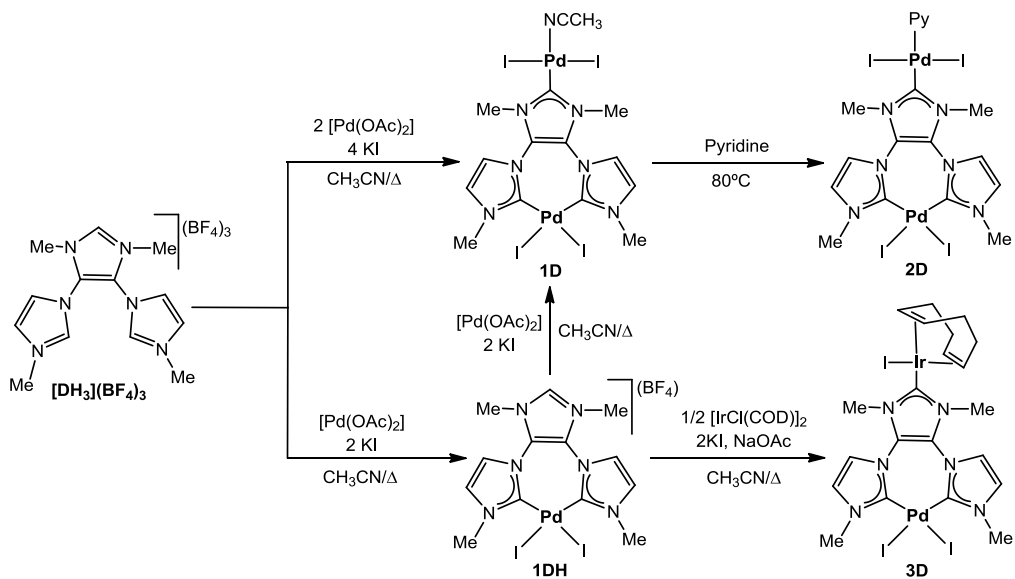
2.1.2.2 Bimetallic complexes based on a Y-shaped tris-NHC ligand

In the following sections of this chapter, the different methodologies employed to obtain bimetallic complexes based on the tris-NHC ligand **D** will be discussed. This section has been divided in two parts, each one containing the description of three

complexes. The separation of these two sections has been made according to the metal that reacts first with the starting tris-azolium, $[\text{DH}_3](\text{BF}_4)_3$. The first section will deal with the complexes obtained when Pd(II) is introduced in the chelate coordination part of the ligands (Pd reacts first), while the second contains Rh or Ir in the chelate part of the ligand (Rh or Ir react first).

a) *Synthesis of 1D, 2D and 3D*

As shown in Scheme 2.4, two methodologies can be used in order to obtain the homo-bimetallic palladium complex **1D**. In the first methodology, compound **1DH** reacts with one equivalent of $[\text{Pd}(\text{OAc})_2]$ in refluxing acetonitrile in the presence of two equivalents of KI. Alternatively, complex **1D** can be directly obtained from the reaction of $[\text{DH}_3](\text{BF}_4)_3$ with two equivalents of $[\text{Pd}(\text{OAc})_2]$ and four equivalents of KI, in refluxing acetonitrile. Compound **1D** was purified by column chromatography and it was precipitated from a mixture of acetonitrile and diethyl ether to give a brown-orange solid in 50 % yield, by either of the two possible synthetic protocols.



Scheme 2.4 Synthesis of complexes **1D** to **3D**

The reaction to obtain compound **2D** from **1D** implies the substitution of a coordinated acetonitrile by pyridine, which is carried out by dissolving **1D** in pyridine, and heating at 80°C for 30 minutes. Compound **2D** precipitated as a yellow solid, and was washed several times with diethyl ether (yield 73 %). The aim of

preparing this pyridine-containing Pd-complex was to favor the PEPPSI effect (Pyridine-Enhanced Precatalysts, Preparation, Stabilization and Initiation),¹¹ which may be relevant in the catalytic studies of this complex (*vide infra*).

The Pd(II)/Ir(I) hetero-bimetallic compound, **3D**, can be obtained treating **1DH** with $[\text{IrCl}(\text{COD})]_2$, NaOAc and KI in refluxing acetonitrile overnight. Alternatively, **3D** can be prepared following a one-pot procedure, without isolating **1DH**, by subsequently adding $[\text{Pd}(\text{OAc})_2]$ and $[\text{IrCl}(\text{COD})]_2$ to a solution of $[\text{DH}_3](\text{BF}_4)_3$ in acetonitrile, and following the reaction conditions depicted in Scheme 2.4. This procedure is a very convenient methodology to prepare hetero-bimetallic complexes, as it simplifies the reaction work-up. In fact, as will be described later, the same one-pot procedure may be also used in the synthesis of the rest of the bimetallic complexes using $[\text{DH}_3](\text{BF}_4)_3$. Compound **3D** was purified by column chromatography, and precipitated from a mixture of acetone and diethyl ether as a yellow solid in 30 % yield. As a consequence of the relative disposition of the iodide ligands of the metal centers (*syn* and *anti*), compound **3D** can adopt two possible conformations (Figure 2.7) that were observed by NMR spectroscopy in a 55:45 molar ratio.

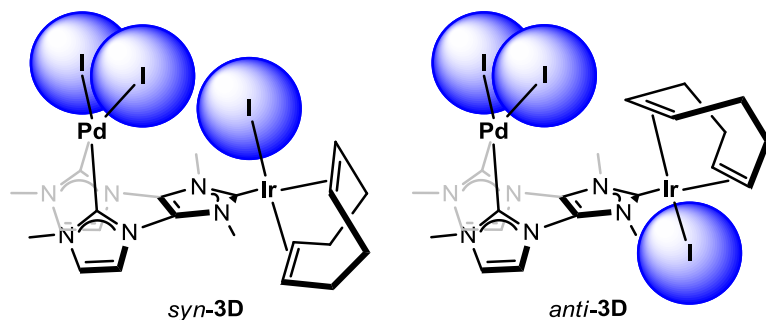


Figure 2.7 Two possible atropisomers of compound **3D**

As shown in Figure 2.7, the two conformations of **3D** imply that the iodide ligand of the iridium fragment is either closer to the iodide ligands of the palladium fragment (*syn-3D*), or at the outer side of the molecule, far from the coordination sphere of the palladium fragment (*anti-3D*). These two atropisomers could not be separated by column chromatography or crystallization, and did not interconvert, even when heating an NMR sample of compound **3D** during several hours. Probably the major atropisomer is *anti-3D*, as the iodide ligands of both metal centers are situated in a more sterically relaxed conformation, pointing to different sides of the molecule.

Complexes **1D**, **2D** and **3D** were characterized by means of NMR spectroscopy, mass spectrometry and elemental analysis. The molecular structures of **2D** and *syn*-**3D** were unambiguously confirmed by X-Ray Diffraction analysis. Due to the similarity between these three compounds, only the spectroscopic characterization of **3D** is discussed below. All the details regarding the characterization of compounds **1D**, and **2D** can be found in the Experimental Section (Chapter 5).

^1H NMR spectrum of **3D**

Figure 2.8 shows the ^1H NMR spectrum of **3D**. The number of signals and their integration are consistent with the presence of two atropisomers in a 55:45 molar ratio. The signals attributed to the protons from the CH groups of the imidazolylidene rings are shown as four singlets at 8.20, 8.11, 7.74 and 7.72 ppm (*a*). The resonances corresponding to the protons of the methyl groups are observed as broad singlets at 3.89 ppm and 3.85 (*b*). The rest of the signals due to the COD protons are conveniently displayed on the spectrum.

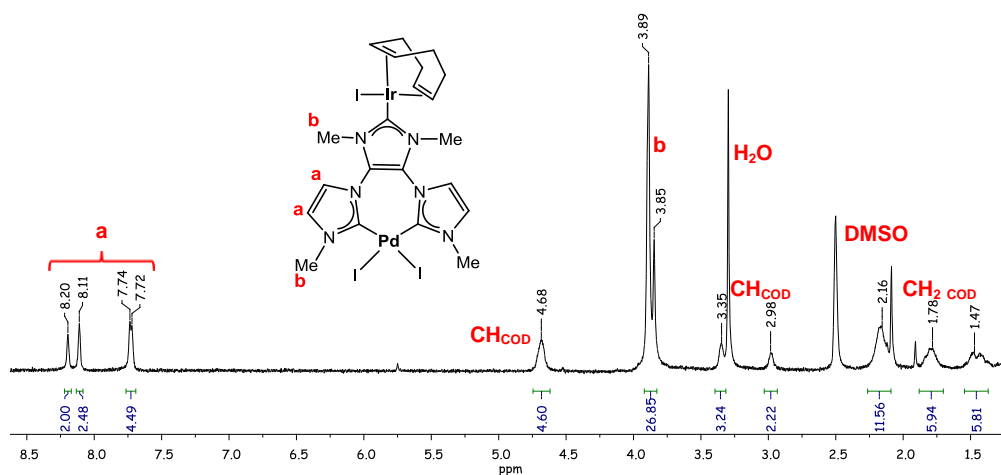


Figure 2.8 ^1H NMR spectrum of **3D** in $\text{DMSO-}d_6$

$^{13}\text{C}\{^1\text{H}\}$ NMR spectrum of **3D**

Figure 2.9 shows the $^{13}\text{C}\{^1\text{H}\}$ NMR spectrum of **3D**. The number of signals present in this spectrum corroborates the presence of the two atropisomers derived from **3D**. The most characteristic signals are those attributed to the metallated carbene-carbons, which are displayed at 178.8 and 178.1 ppm for the iridium coordinated carbon (1), and at 167.5 and 166.0 ppm for the carbons bonded to the palladium atom (2). The

four signals corresponding to the carbons from the CH group of the imidazolylidene rings appear between 126 and 122 ppm (3), while those due to the $C_{\text{quaternary}}$ are displayed around 123 ppm (4). Two of the resonances attributed to the carbons of the methyl groups are overlapped with the residual DMSO- d_6 signal (see Chapter 5 for HSQC spectrum of **3D**), while the other two signals due to these carbons are displayed around 35 ppm (5). The rest of the signals corresponding to the COD carbons are conveniently displayed on the spectrum.

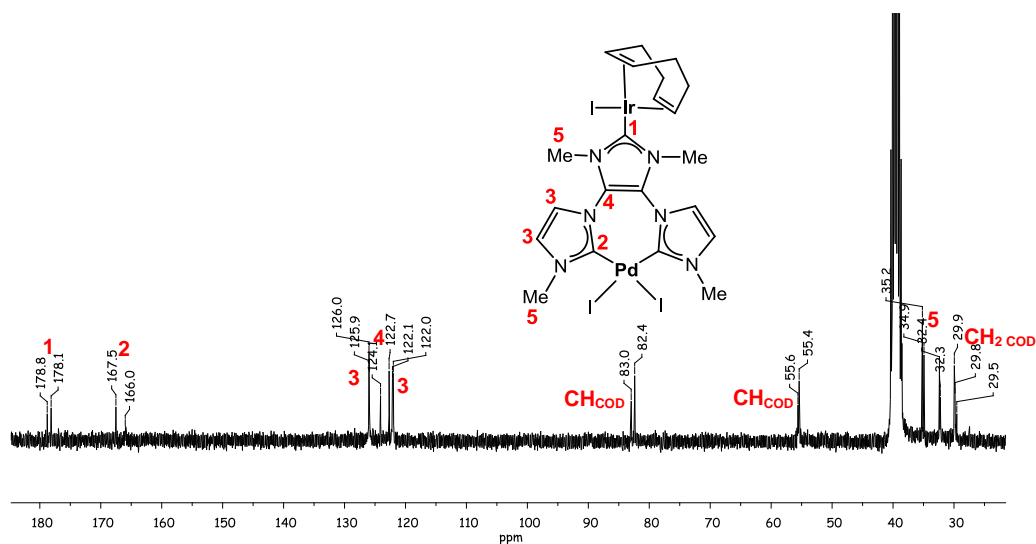


Figure 2.9 $^{13}\text{C}\{^1\text{H}\}$ NMR spectrum of **3D** in $\text{DMSO-}d_6$

Molecular structure of **2D**

Crystals of **2D** suitable for X-Ray Diffraction analysis were obtained by slow diffusion of diethyl ether into a concentrated solution of the compound in acetonitrile.

The molecular structure of **2D**, shown in Figure 2.10, consists of two palladium centers bridged by a Y-shaped tris-NHC, which is acting in a bis-chelate/monodentate way. The monocarbene palladium fragment completes its coordination sphere with a pyridine and two iodide ligands in a relative *trans* configuration. The other palladium fragment contains a chelate bis-NHC ligand, and two iodide ligands in a *cis* disposition complete the coordination sphere about the metal. Table 2.2 shows the most representative bond lengths (\AA) and angles ($^\circ$) of complex **2D**. The Pd- C_{carbene} distance in the mono-NHC fragment is 1.960(7) \AA . The angle between the coordination plane of the monocarbene palladium fragment and the plane of the

coordinated azole ring is $85.5(2)^\circ$, while the two coordination planes of the metals are displaying an angle of $84.59(15)^\circ$. The average Pd-C_{carbene} distance in the bis-chelate palladium fragment is $1.985(18) \text{ \AA}$, similar to the analogue distance shown by **1DH**. The two coordinated imidazolylidenes lie at an average angle of $66.7(3)^\circ$, relative to the coordination plane, and the “chair angle” (defined as the angle between the coordination plane of the chelate fragment and the plane of the monocarbene azole ring) is $88.2(2)^\circ$ (Figure 2.11). This “chair angle” keeps the two palladium atoms at a close through-space distance of $6.722(8) \text{ \AA}$.

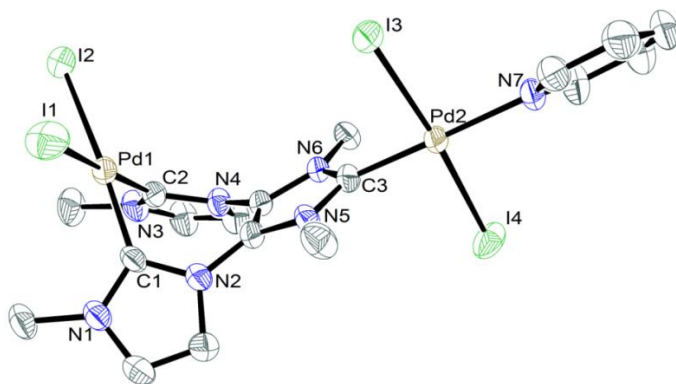


Figure 2.10 Molecular diagram of complex **2D**. Ellipsoids at 50 % probability. Hydrogen atoms and solvent (diethyl ether) have been omitted for clarity

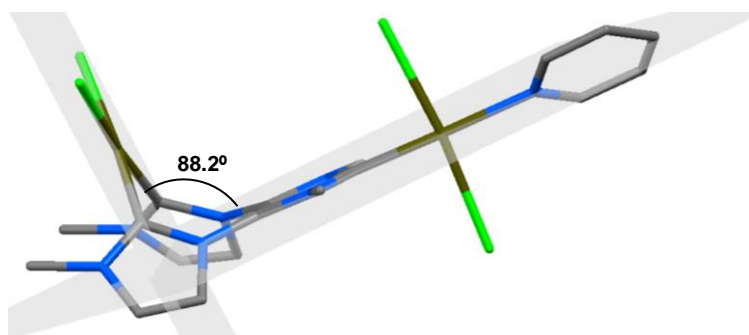


Figure 2.11 Side-on view of complex **2D** with the “chair angle”

Table 2.2 Selected bond lengths and angles of complex **2D**

Bond lengths (Å)		Bond angles (°)	
Pd(1)-C(1)	1.997(9)	C(1)-Pd(1)-C(2)	85.4(3)
Pd(1)-C(2)	1.972(8)	I(1)-Pd(1)-I(2)	92.81(3)
Pd(1)-I(1)	2.650(8)	I(3)-Pd(2)-I(4)	174.32(3)
Pd(1)-I(2)	2.642(8)	C(3)-Pd(2)-N(7)	178.9(3)
Pd(2)-C(3)	1.960(7)	“chair angle”	88.2(2)
Pd(2)-I(3)	2.642(8)		
Pd(2)-I(4)	2.593(8)		
Pd(2)-N(7)	2.106(6)		
Pd(1)-Pd(2)	6.722(8)		

Molecular structure of **3D**

Crystals of **3D** suitable for X-Ray Diffraction analysis were obtained by slow diffusion of diethyl ether into a concentrated solution of the compound in acetonitrile.

The molecular structure of **3D**, shown in Figure 2.12, consists of a tris-NHC ligand bridging a Pd(II) and an Ir(I) center. The ligand is monocoordinated to the Ir(I) fragment, which completes its coordination sphere with a COD and an iodide ligand. The Pd(II) fragment contains a bis-NHC ligand coordinated in a bis-chelating form; two iodide ligands in a relative *cis* configuration complete the coordination sphere. The molecular structure depicted in Figure 2.12 corresponds to the *syn-3D* atropisomer (Figure 2.7), in which the iodide ligand of the Ir(I) center is pointing to coordination sphere of the Pd(II) fragment. Table 2.3 shows the most representative bond lengths (Å) and angles (°). The Ir-C_{carbene} distance is 2.032(9) Å. The angle between the coordination plane containing the monocarbene iridium fragment and the plane of the coordinated azole ring is 86.8(2)°. Interestingly, the coordination planes of both metals are quasiperpendicular (89.0(2)°). The average Pd-C_{carbene} distance is 1.971(6) Å, similar to the analogue distance shown in **1DH** and **2D**. The two coordinated imidazolylidenes lie at an average angle of 52.0(4)°, relative to the coordination plane, and the “chair angle” is 88.4(3)° (Figure 2.13). This “chair angle” provides a through-space distance between the two metal centers of 6.712(1) Å.

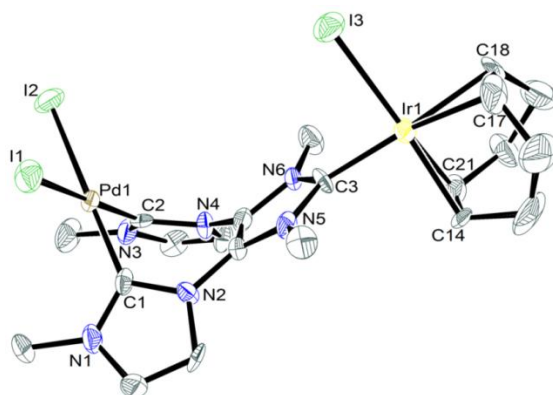


Figure 2.12 Molecular diagram of complex **3D**. Ellipsoids at 50 % probability. Hydrogen atoms and solvent (CH_3CN) have been omitted for clarity

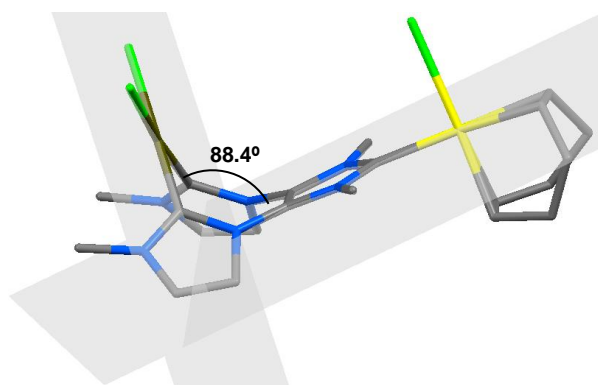


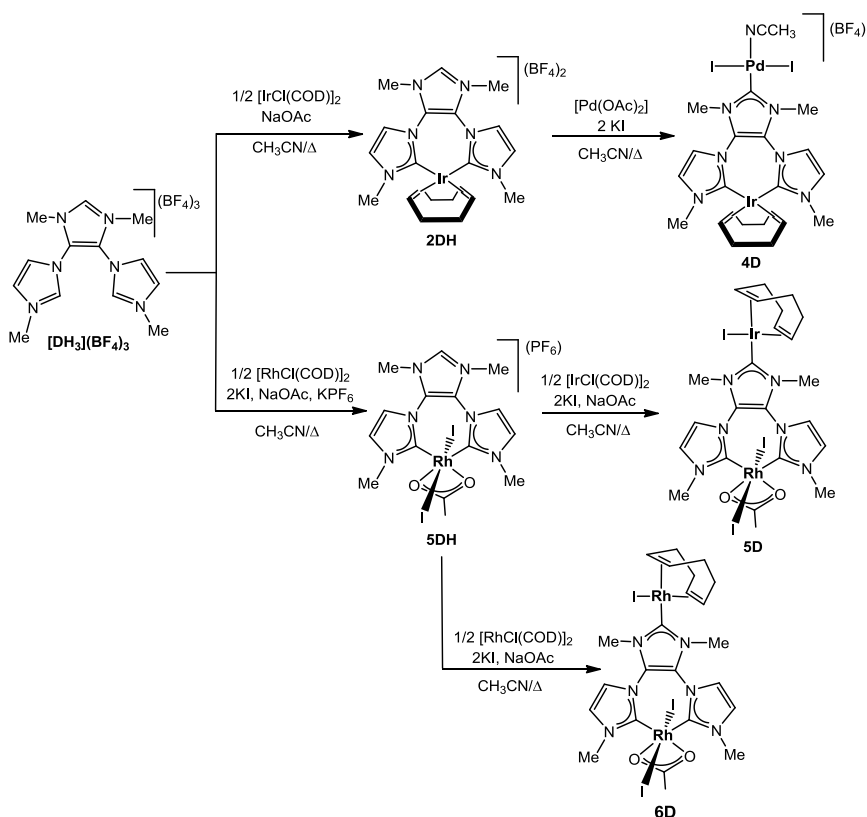
Figure 2.13 Side-on view of complex **3D** with the “chair angle”

Table 2.3 Selected bond lengths and angles of complex **3D**

Bond lengths (Å)		Bond angles (°)	
Pd(1)-C(1)	1.967(8)	C(1)-Pd(1)-C(2)	87.1(3)
Pd(1)-C(2)	1.975(9)	I(1)-Pd(1)-I(2)	95.97(3)
Pd(1)-I(1)	2.6606(9)	C(3)-Ir(1)-I(3)	89.2(2)
Pd(1)-I(2)	2.6347(9)	“chair angle”	88.4(3)
Ir(1)-C(3)	2.032(9)		
Ir(1)-I(3)	2.6664(7)		
Ir(1)-C(14)	2.108(9)		
Ir(1)-C(17)	2.157(10)		
Ir(1)-C(18)	2.191(9)		
Ir(1)-C(21)	2.112(9)		
Pd(1)-Ir(1)	6.712(9)		

b) Synthesis of 4D, 5D and 6D

As we have described above, the first metal treated with $[\text{DH}_3](\text{BF}_4)_3$ is the one that coordinates the tris-NHC from its chelate face. This section describes the complexes that have been obtained by first reacting $[\text{DH}_3](\text{BF}_4)_3$ with Rh and Ir, and thus they contain these metal fragments in the chelate part of the resulting tris-NHC ligand. The synthesis of the Ir(I)/Pd(II) complex **4D** (Scheme 2.5) can be carried out by treating compound **2DH**, in refluxing acetonitrile, with one equivalent of $[\text{Pd}(\text{OAc})_2]$ and two equivalents of KI. Alternatively, **4D** can be prepared following a one-pot procedure, without isolating **2DH**, by subsequently adding $[\text{IrCl}(\text{COD})_2]$ and $[\text{Pd}(\text{OAc})_2]$ to a solution of $[\text{DH}_3](\text{BF}_4)_3$ in acetonitrile, and following the reaction conditions depicted in Scheme 2.5. Compound **4D** was purified by column chromatography, and precipitated from a mixture of acetone and diethyl ether as a brown, air sensitive solid in 45 % yield, by either procedure. It is interesting to point out that compound **4D** contains the same metals, in the same oxidation state, as those contained in compound **3D**. However, the two metals are in the reverse coordination environments: the palladium fragment is coordinated by the monodentate face of the ligand, and the iridium atom is bound by the chelate side.



Scheme 2.5 Synthesis of complexes **4D**, **5D** and **6D**

As shown in Scheme 2.5, compounds **5D** and **6D** can be obtained reacting **5DH** with $[MCl(COD)]_2$ ($M = Ir$ or Rh) in a 2:1 molar ratio, in the presence of NaOAc and KI, in refluxing acetonitrile for 3 hours. This synthesis can also be carried out following a one-pot procedure, adding the appropriate reagents, in the sequence indicated in the reaction scheme. Both complexes were purified by column chromatography and were precipitated from a dichloromethane/hexane mixture. Compound **5D** was obtained as a brown solid in 32 %, while complex **6D** was a yellow solid, isolated in 33 % yield.

Although two conformers are possible for compounds **5D** and **6D** (Figure 2.14), due to the relative disposition of the iodide ligand of the monocarbene $M(I)$ fragment with respect to the chelate $Rh(III)$ fragment, only the *anti*-atropisomer is observed by NMR spectroscopy. The formation of the *syn*-atropisomer is assumed to be highly disfavored due to the steric clash between the bulky iodide ligands of both metal fragments (Figure 2.14, right).

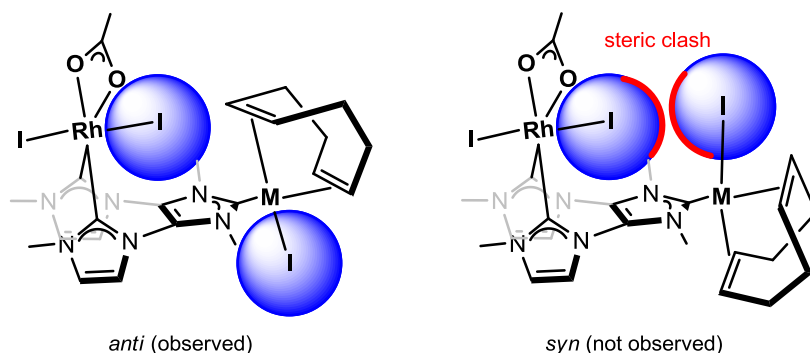


Figure 2.14 Two possible atropisomers of compounds **5D** (M = Ir) and **6D** (M = Rh)

Compounds **4D**, **5D** and **6D** were characterized by means of NMR spectroscopy, mass spectrometry and elemental analysis. The structure of **6D** was unambiguously confirmed by X-Ray Diffraction analysis. As an example, the NMR spectroscopic characterization of **6D** is described below. All the details regarding the characterization of **4D** and **5D** can be found in the Experimental Section (Chapter 5).

¹H NMR spectrum of 6D

Figure 2.15 shows the ¹H NMR spectrum of **6D**. The number of signals and the integration is consistent with the *C_s* symmetry of the compound. The spectrum reveals the formation of only one of the two possible conformers, as described above (Figure 2.14). The signals attributed to the protons of the CH groups of the imidazolylienes are shown as two singlets at 7.36 and 7.18 ppm (*a*). The signals assigned to the protons of the methyl groups are displayed as two singlets at 4.18 and 3.93 ppm (*b*). The resonance due to the protons of the methyl group of the acetate ligand is observed at 1.98 ppm (*c*). The rest of the signals corresponding to the COD protons are conveniently displayed on the spectrum.

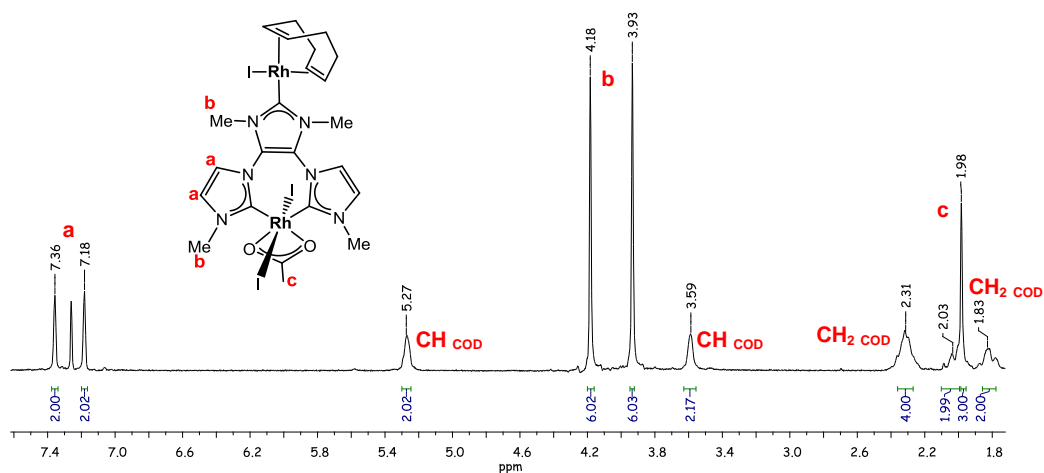


Figure 2.15 ^1H NMR spectrum of **6D** in CDCl_3

$^{13}\text{C}\{^1\text{H}\}$ NMR spectrum of **6D**

Figure 2.16 shows the $^{13}\text{C}\{^1\text{H}\}$ NMR spectrum of **6D**. The number of signals of the spectrum corroborates the two-fold symmetry of the compound and the presence of only one of the two possible atropisomers derived from **6D**. The most characteristic signals are the doublets attributed to the metallated carbene-carbons, as a result of the $\text{Rh-C}_{\text{carbene}}$ coupling. The resonance due to the monodentate carbon is displayed at 185.7 ppm ($^1J_{\text{Rh-C}} = 50.5$ Hz) (2), while the signal assigned to the bis-chelating carbene-carbons is observed at 162.8 ppm ($^1J_{\text{Rh-C}} = 47.4$ Hz) (3). The chemical shift and the coupling constants of these signals are in agreement with those reported for similar rhodium-monocarbene¹² and rhodium-bis-carbene complexes.⁵ The two signals corresponding to the carbons of the CH groups of the imidazolydene rings are displayed at 126.3 and 122.2 ppm (4), while the resonance assigned to the quaternary carbons of the bridging azole appears at 124.9 ppm (5). The signals at 42.9 and 37.3 ppm (6) are assigned to the carbons of the methyl groups. The rest of the resonances corresponding to the carbons of the COD and the acetate ligand are conveniently displayed on the spectrum.

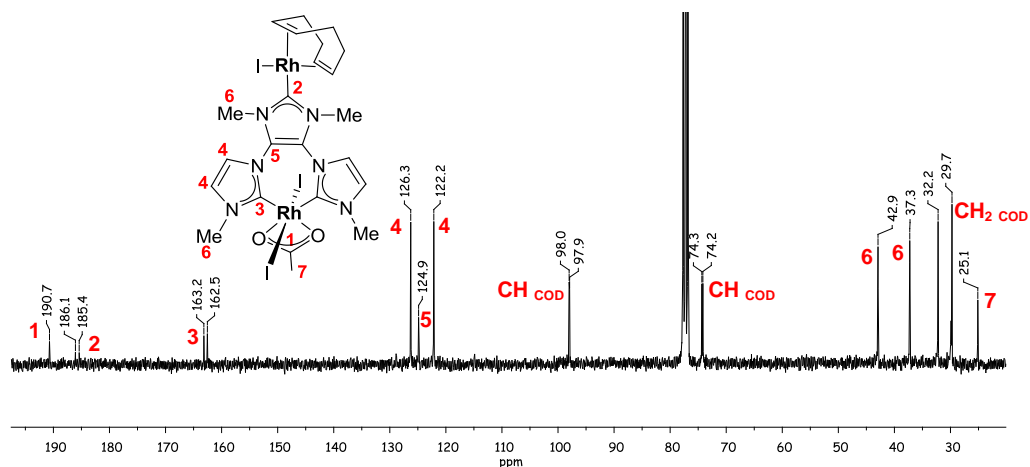


Figure 2.16 $^{13}\text{C}\{^1\text{H}\}$ NMR spectrum of **6D** in CDCl_3

Molecular structure of **6D**

Crystals of **6D** suitable for X-Ray Diffraction analysis were obtained by slow diffusion of diethyl ether into a concentrated solution of the compound in chloroform.

The molecular structure of **6D** (Figure 2.17) consists of a homo-bimetallic complex of Rh(I)/Rh(III), in which the tris-NHC ligand is coordinated in a monodentate way to the Rh(I) atom, while is acting in a chelate fashion on the Rh(III) fragment. The Rh(I) atom completes its coordination sphere with a COD and a iodide ligand, while the chelated-Rh(III) atom contains an acetate and two iodide ligands, affording a pseudo-octahedral coordination. The molecular structure confirms that compound **6D** only exists as the *anti*-atropisomer (Figure 2.14, right), in which the iodide ligand of the Rh(I) center is pointing to the less sterically crowded side of the molecule. Table 2.4 shows the most representative bond lengths (\AA) and angles ($^\circ$) of complex **6D**. The Rh(I)- $\text{C}_{\text{carbene}}$ distance is 2.008(6) \AA , while the Rh(III)- $\text{C}_{\text{carbene}}$ distance is 1.992(4) \AA . The two coordinated imidazolylidenes of the chelate side of the molecule lie at an angle of 32.76(13) $^\circ$, relative to the coordination plane of the Rh(III) atom. This angle is smaller than those shown by compounds **1DH**, **2D** and **3D**, and may be ascribed to the higher steric constrain provided by the two iodide ligands at the Rh(III) octahedral fragment.

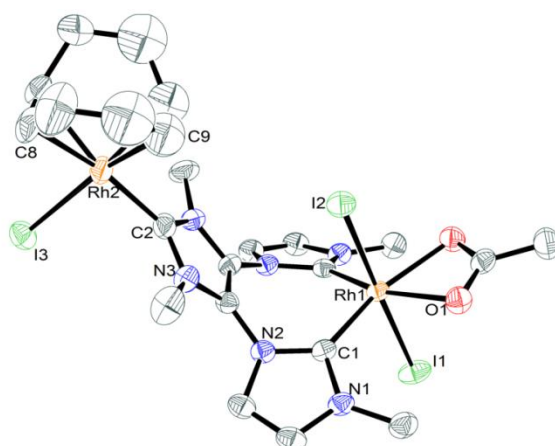


Figure 2.17 Molecular diagram of complex **6D**. Ellipsoids at 50 % probability. Hydrogen atoms have been omitted for clarity

The “chair angle” is $108.2(2)^\circ$ (Figure 2.18), significantly larger than those shown by the other related bimetallic complexes based on **D** ($88.2(2)^\circ$ and $88.4(3)^\circ$, for **2D** and **3D**, respectively), as a consequence of the higher steric hindrance provided by the octahedral Rh(III) fragment. The wide range of ‘chair angles’ found for ligand **D**, reflects the flexibility of the ligand, which is capable to accommodate a variety of coordination spheres. The through-space distance between the two rhodium atoms is $7.003(1) \text{ \AA}$, longer than those observed for compounds **2D** and **3D** (ca. 6.7 \AA , for both).

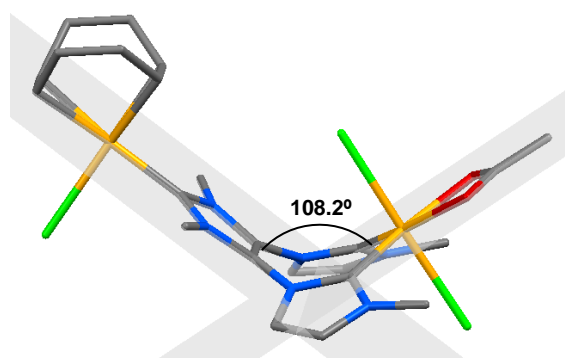


Figure 2.18 Side-on view of complex **6D** with the “chair angle”

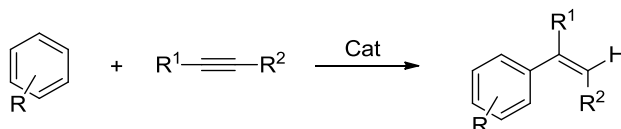
Table 2.4 Selected bond lengths and angles of complex **6D**

Bond lengths (Å)		Bond angles (°)	
Rh(1)-C(1)	1.992(4)	C(1)-Rh(1)-C(1')	95.0(2)
Rh(1)-O(1)	2.163(3)	I(1)-Rh(1)-I(2)	178.86(2)
Rh(1)-I(1)	2.6876(6)	C(2)-Rh(2)-I(3)	86.86(17)
Rh(1)-I(2)	2.6435(6)	“chair angle”	108.2(2)
Rh(2)-C(2)	2.008(6)		
Rh(2)-I(3)	2.6513(6)		
Rh(2)-C(8)	2.209(5)		
Rh(2)-C(9)	2.102(5)		
Rh(1)-Rh(2)	7.0035(7)		

2.1.3 Catalytic properties of the Y-shaped tris-NHC-based complexes

In the following sections, the catalytic properties of the palladium containing complexes (**1DH** and **1D** to **4D**) described above will be discussed.

For the mono-Pd(II) and the bis-Pd(II) complexes (**1DH**, **1D** and **2D**), we chose as benchmark reaction the hydroarylation of alkynes, also known as the Fujiwara reaction (Scheme 2.6).^{13,14} This transformation consists of the addition of an electron-rich aryl group and a hydrogen atom across a C-C acetylenic bond, and produces a vinylarene.

**Scheme 2.6** Hydroarylation of alkynes

The reaction constitutes a high atom-economy C-H activation process, in which several Pd(II)-mono-NHC^{15,16} and Pd(II)-bis-NHC¹⁷⁻²¹ complexes have shown good activity. Based on these precedents, we considered that compounds **1D** and **2D** should be good candidates to facilitate this catalysis, as they combine the presence of mono-coordinated/bis-chelated-(NHC)-Pd(II) fragments. It is thought that the mechanism of this reaction proceeds through an electrophilic aromatic substitution at the alkyne, which first coordinates to the electrophilic palladium fragment and is activated for the

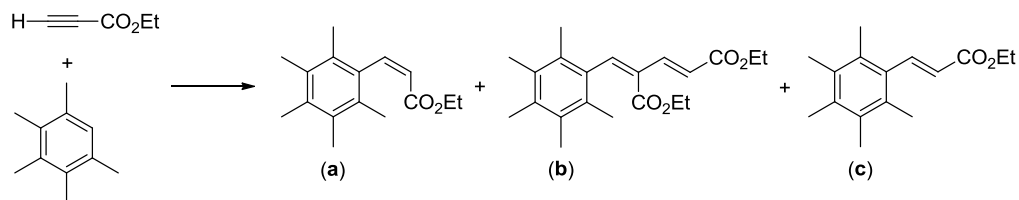
next step of the catalytic cycle. The process is followed by the electrophilic addition of the arene to the activated alkyne, C-H bond cleavage and re-aromatization, to yield the final hydroarylated product.^{22,23}

Because our group pioneered a series of tandem reactions catalyzed by Ir/Pd hetero-bimetallic complexes,²⁴ we also decided to test the Pd(II)/Ir(I) hetero-bimetallic complexes **3D** and **4D** in two tandem catalytic processes, namely the dehalogenation/transfer hydrogenation of *p*-bromoacetophenone, and the Suzuki coupling/transfer hydrogenation of *p*-bromoacetophenone.

2.1.3.1 Hydroarylation of alkynes catalyzed by **1DH**, **1D** and **2D**

We first carried out a catalyst screening by comparing the activity of [Pd(OAc)₂] and our palladium compounds **1DH**, **1D** and **2D**. The reactions were performed treating pentamethylbenzene with ethyl propiolate, using previously reported reaction conditions:¹⁷ 80°C in a mixture of trifluoroacetic acid and dichloroethane (4:1 in volume), with a 0.1 or 0.05 % catalyst loading (Table 2.5). This catalytic reaction can yield the *cis* or *trans* product of hydroarylation (**a** and **c**, respectively), with the *cis*-isomer being the most commonly obtained.^{13,17} Another compound that can be produced, is the product of double alkyne insertion, **b**. The reactions were carried out during 5 hours, in order to avoid any competitive side-reactions, such as alkyne polymerization, hydration by traces of water, or *Z/E* isomerization of the olefin.¹⁹

As can be seen in the data shown in Table 2.5, and by comparing the conversions provided by the different catalysts, compound **1D** provides the best results. However, **2D** is slightly more selective towards the *cis* product, **a**. Among the three new complexes, the mono-Pd(II) compound **1DH** shows the lowest activity and selectivity (compare entries 1, 2 and 3 in Table 2.5). Reducing the catalyst loading to 0.05 %, results in a clear lowering of the conversion produced by **1D** and **2D**, but the selectivity is improved. Catalyst **1D** compares well with the catalytic systems previously reported by Biffis and co-workers,¹⁷ based on bis-NHC-Pd(II)-bis-halide complexes, although the latter was more selective towards the *Z* product (**a**).

Table 2.5 Hydroarylation of pentamethylbenzene with ethyl propiolate^a

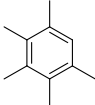
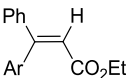
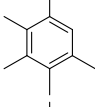
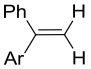
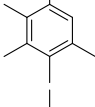
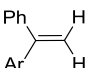
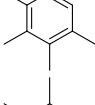
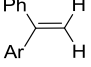
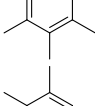
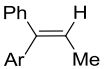
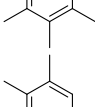
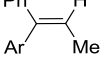
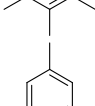
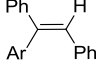
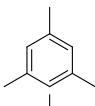
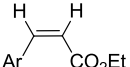
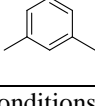
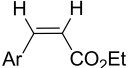
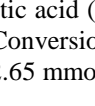
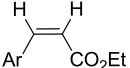
Entry	Cat. (mol %)	Conv. (%) ^b	Yield (%) ^b			Selectivity to a (%)
			a	b	c	
1	1DH (0.1)	48	30	18	-	63
2	1D (0.1)	65	48	17	-	74
3	2D (0.1)	56	45	11	-	80
4	Pd(OAc) ₂ (0.1)	40	35	5	-	88
5	1D (0.05)	33	29	4	-	88
6	2D (0.05)	34	28	6	-	82

^aReaction conditions: 2.65 mmol pentamethylbenzene, 2.65 mmol ethyl propiolate, 4 mL trifluoroacetic acid (TFA), 1 mL 1,2-dichloroethane (DCE) at 80°C, 5 h. ^bConversions and yields determined by ¹H NMR spectroscopy using diethyl phthalate (2.65 mmol) as an internal standard.

In order to broaden the scope of the reaction, catalyst **1D** was used for the coupling of other arenes and acetylenes (Table 2.6), using the same reaction conditions as mentioned above. In general, compound **1D** performs well for all combination of reagents shown in Table 2.6, and in some cases the activity is better than previously reported catalytic systems for the same reactions (in those cases longer reactions times were needed to get similar yields).^{17,19}

Interestingly, complex **1D** is also active at room temperature at the same catalytic loading (entries 3 and 6). The performance of the catalyst at room temperature can be improved by adding a silver salt (AgOAc) to the reaction media to remove the iodide ligands of the coordination sphere about the palladium centers (entries 4 and 10). In these cases, the yields obtained are slightly better than those obtained while heating at 80°C without any silver salt.

Table 2.6 Hydroarylation of arenes with acetylenes using **1D**^a

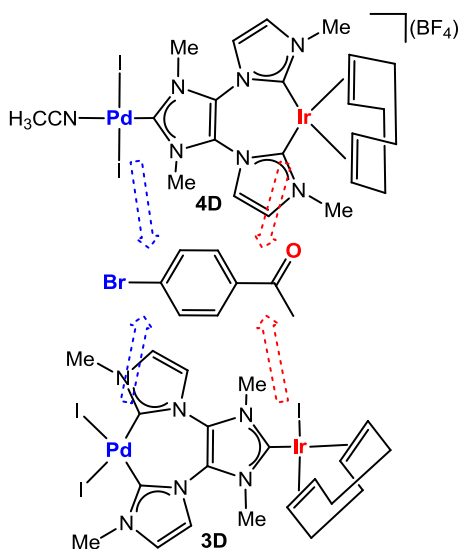
Entry	Arene	Alkyne	T (°C)	Product	Yield (%) ^b
1		Ph—C≡C—CO ₂ Et	80		28
2		Ph—C≡C—H	80		47
3		Ph—C≡C—H	RT		24
4 ^c		Ph—C≡C—H	RT		50
5		Ph—C≡C—Me	80		45
6		Ph—C≡C—Me	RT		43
7		Ph—C≡C—Ph	RT		38
8		H—C≡C—CO ₂ Et	80		43
9		H—C≡C—CO ₂ Et	RT		0
10 ^c		H—C≡C—CO ₂ Et	RT		50

^aReaction conditions: 0.1 mol % catalyst **1D**, 2.65 mmol arene, 2.65 mmol acetylene, 4 mL trifluoroacetic acid (TFA), 1 mL 1,2-dichloroethane (DCE) at the appropriate temperature, for 5 h. ^bConversions and yields determined by ¹H NMR spectroscopy using diethyl phthalate (2.65 mmol) as an internal standard. ^c0.4 mol % of AgOAc was added.

2.1.3.2 Tandem processes catalyzed by **3D** and **4D**

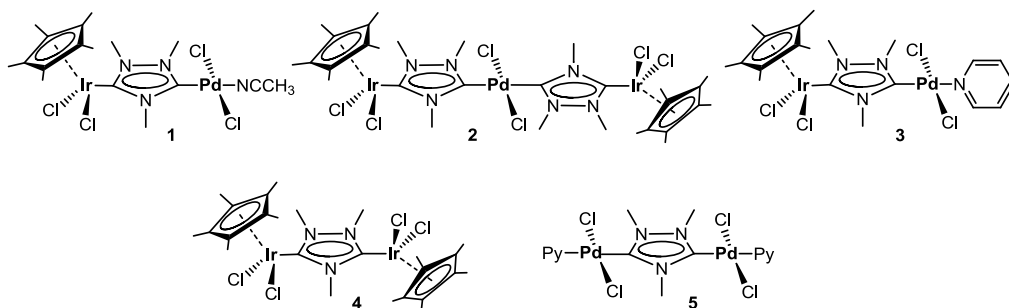
For the study of the catalytic activity of the Pd(II)/Ir(I) compounds **3D** and **4D**, we decided to use as substrate 4-bromoacetophenone as benchmark substrate. This

compound contains two different functionalities that can be involved in very different catalytic cycles: the carbon-bromide bond is typically activated by palladium catalysts,^{25,26} while the carbonyl group may participate in iridium-catalyzed borrowing-hydrogen processes^{27,28} (Scheme 2.7). In fact, the suitability of this substrate to undergo palladium- and iridium-catalyzed processes, was previously described in our group.²⁴ For the study of the catalytic properties of the two complexes, we tested them in the dehalogenation/reduction of 4-bromoacetophenone, and in the Suzuki-Miyaura coupling/reduction of the same substrate. The combination of these two reactions into a tandem process has been widely studied in our laboratory.²⁴



Scheme 2.7

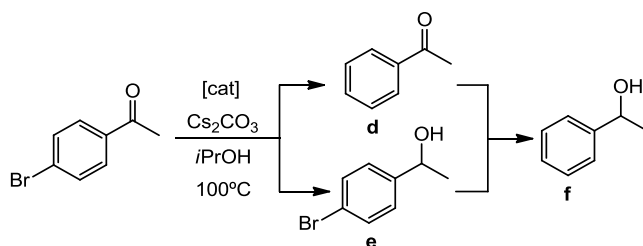
As can be observed in Scheme 2.7, compounds **3D** and **4D** contain the same metal centers, with the same oxidation states, but with different coordination environments. The comparison of the catalytic activities of these two complexes affords a unique opportunity to assess if the activities of the complexes may be attributed to the different coordination modes of the metal fragments in each compound. The activity of these two complexes will be compared with those shown by other Pd/Ir catalysts previously reported in our group (Scheme 2.8).²⁴



Scheme 2.8 Previously reported catalysts based on Pd and Ir

a) Dehalogenation/transfer hydrogenation of *p*-bromoacetophenone

The first tandem process studied was the dehalogenation/transfer hydrogenation of *p*-bromoacetophenone to yield 1-phenylethanol (**f**). The reactions were carried out under previously reported conditions:²⁴ 4-bromoacetophenone with Cs_2CO_3 in 2-propanol at 100°C . The two possible intermediates of this reaction are acetophenone (**d**) and 1-(4-bromophenyl)ethanol (**e**), depending on whether the dehalogenation or the reduction occurs first. As shown in Table 2.7, complex **4D** provides better catalytic activities and selectivities than **3D**. Using a catalyst loading of 2 mol %, complex **4D** is able to fully dehalogenate/hydrogenate 4-bromoacetophenone in 20 hours, to yield 1-phenylethanol. At the same time, and with the same amount of catalyst, complex **3D** only yields 21 % of 1-phenylethanol, being the main product acetophenone (70 %) (compare entries 1 and 5). Even increasing the reaction time to 48 hours, no remarkable improvement in the production of 1-phenylethanol was observed (entry 2). For comparative purposes, the results obtained with previously reported catalysts are also shown in Table 2.7 (entries 8 to 11). Catalyst **4D** shows better activity than **1**, and compares well with the activities shown by the Ir/Pd heterometallic complexes **2** and **3** (compare entries 5, 8, 9 and 10). **4D** also provides better activities than the combination of the two homo-bimetallic catalysts, **4** and **5** (entry 11). Interestingly, **4D** is also a good catalyst at a low catalyst loading of 1 mol %, although longer reaction time was required (48h, entry 7).

Table 2.7 Tandem dehalogenation/transfer hydrogenation of *p*-bromoacetophenone^a

Entry	Catalyst	Cat loading (% mmol)	t (h)	d (%) ^b	e (%) ^b	f (%) ^b
1	3D	2	20	70	9	21
2	3D	2	48	51	8	41
3	3D	1	20	89	5	6
4	3D	1	48	82	5	13
5	4D	2	20	1	0	99
6	4D	1	20	55	3	42
7	4D	1	48	0	0	99
8	1	2	20	22	0	75 ^d
9	2	2	20	0	0	95 ^d
10	3	2	20	0	0	99 ^d
11 ^c	4+5	1 + 1	20	72	0	25 ^d

^aReaction Conditions: 4-bromoacetophenone (0.36 mmol), Cs₂CO₃ (0.43 mmol), catalyst (2 mol%) and 2 mL of 2-propanol. The solution was heated to 100°C under aerobic conditions.

^bYields determined by GC using anisole as internal reference (0.36 mmol). ^c1 mol % of **4** + 1 mol % of **5**. ^dData taken from ref. 24.

The dehalogenation/transfer hydrogenation of 4-bromoacetophenone is a very clean reaction, which proceeds without the generation of side-products apart from **d** and **e**. This gave us the opportunity to study the time-course profile of the reaction, and compare the reaction profiles provided by **3D** and **4D** (Figure 2.19 and Figure 2.20, respectively). Figure 2.19 shows that catalyst **3D** dehalogenates the substrate very fast, but when acetophenone (**d**) is formed in the reaction media, the transfer hydrogenation process to obtain **f** takes place slowly. The reaction profile of **4D** (Figure 2.20) is similar to the one shown by the previously reported hetero-bimetallic complex **3**.²⁴ In this case, the debromination is also faster than the reduction, but the reduction of the resulting acetophenone is faster than the reduction of the former substrate (4-bromoacetophenone), as observed by the increase of the slope of the

time-dependent reaction profile, that indicates the formation of **f** (green line, in Figure 2.20).

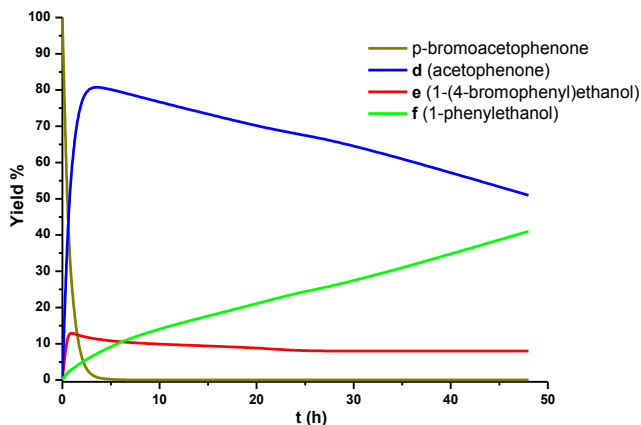


Figure 2.19 Time course of the transformation of *p*-bromoacetophenone using 2 mol % of **3D**

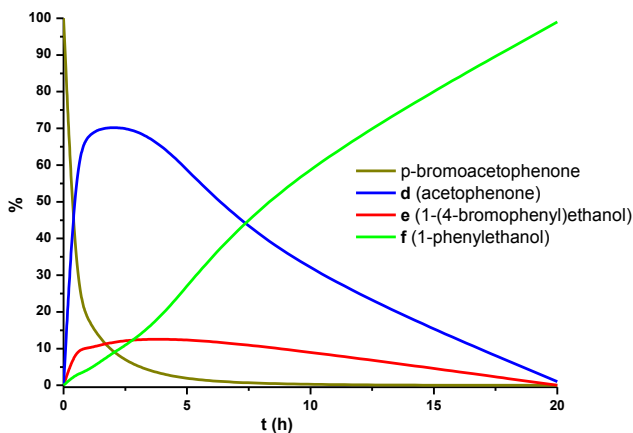


Figure 2.20 Time course of the transformation of *p*-bromoacetophenone using 2 mol % of **4D**

From these reaction profiles, two conclusions can be extracted:

- 1) The Pd(II) fragments of catalysts **3D** and **4D** show good performances in the dehalogenation process, although **4D**, which contains a mono-carbene-Pd(II) fragment, provides better activities than the bis-carbene-Pd(II) of **3D**

(compare the initial rate in the formation of acetophenone in Figure 2.19 and Figure 2.20).

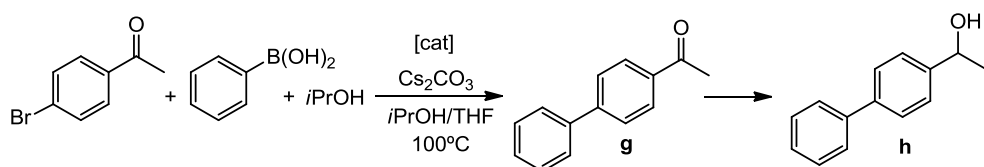
- 2) There is a large difference in the catalytic outcomes provided by the Ir(I) fragments of **3D** and **4D**. The mono-carbene-Ir(I) fragment of **3D** is not able to fully achieve the reduction of the ketone, even at long reaction periods, while the bis-carbene-Ir(I) fragment of **4D** is a good catalyst for this transformation. This fact can be qualitatively explained taking into account that complexes bearing a chelate ligand usually show higher stabilities than their monocoordinated analogues, so the iridium fragment in **4D** can survive in more catalytic cycles. Besides, the Ir(I) atom in **4D** contains a bis-NHC ligand, which can provide more electron-density to the metal than the mono-NHC bonded to Ir(I) in **3D**. This fact probably may explain the higher activity of the Ir(I) fragment in **4D** compared with **3D**.

b) Suzuki coupling/transfer hydrogenation of *p*-bromoacetophenone

Encouraged by the results described above, and taking into account the low activity obtained in transfer hydrogenation by catalyst **3D**, we decided to use catalyst **4D** in other tandem reaction, namely the Suzuki-Miyaura coupling/transfer hydrogenation, which our group also studied previously as a model tandem reaction.²⁴ This transformation has a straightforward application, because the resulting biphenyl substituted ketones are known to behave as non-steroidal inhibitors of 5 α -reductase, the enzyme that catalyzes the conversion of testosterone to dihydrotestosterone.²⁹ Table 2.8 shows the results obtained using **4D** for this transformation, treating 4-bromoacetophenone with phenylboronic acid in a mixture of *i*PrOH/THF (1/1 in volume). This reaction can produce different side-products, as for example those resulting from the dehalogenation of the substrate (**d** and **f**), and also the intermediate ketone resulting from the Suzuki-Miyaura coupling (**g**). For comparative purposes, the results were compared with those given by the previously described catalysts **3**, **4** and **5**.²⁴ As shown in the results depicted in Table 2.8, **4D** is able to produce compound **h** in 72 % yield after 24 hours (entry 5). Interestingly, in 30 minutes the product of the Suzuki-Miyaura coupling is obtained in 85 % yield (entry 1), confirming the high activity of the Pd(II) fragment of **4D**. The debromination process is a serious competitor for this reaction, as can be seen from the formation of acetophenone in a 13 % yield after 30 min (entry 1). Unfortunately, complex **4D**

shows a lower catalytic activity than **3**, which is able to produce the arylated/hydrogenated product **h** in 88 % yield after 7 hours (entry 7) with a very high selectivity. The catalytic performance of **4D** is better than the one observed for the combination of the two homo-bimetallic complexes **4** and **5** (compare entries 2 and 8).

Table 2.8 Tandem Suzuki-Miyaura/transfer hydrogenation of 4-bromoacetophenone^a



Entry	Catalyst	t (h)	d (%) ^b	e (%) ^b	f (%) ^b	g (%) ^b	h (%) ^b
1	4D	0.5	13	2	0	85	0
2	4D	4	10	0	5	52	31
3	4D	7	5	0	10	38	47
4	4D	20	3	0	12	16	69
5	4D	24	2	0	13	13	72
6	3	4	-	-	-	58	28 ^d
7	3	7	-	-	-	2	88 ^d
8^c	4+5	4	-	-	-	55	5 ^d

^aReaction Conditions: 4-bromoacetophenone (0.36 mmol), phenylboronic acid (0.55mmol), Cs₂CO₃ (1.08 mmol), catalyst (2 mol%), 2 mL of *i*PrOH and 2mL of THF. The solution was heated at 100°C. ^bYields determined by GC using anisole as internal reference (0.36 mmol).

^c1 mol % of **4** + 1 mol % of **5**. ^dData taken from ref. 24.

2.2 Conclusions

In this chapter we described the preparation and characterization of a new tris-imidazolium salt $[\text{DH}_3](\text{BF}_4)_3$, through a four-steps synthetic route. This tris-azolium salt is a convenient tris-NHC precursor, which can be coordinated to different metal-fragments, affording mono- (**1DH-5DH**) or bimetallic (**1D-6D**) complexes. The bimetallic complexes contain two metals bridged by the Y-shaped tris-NHC, which simultaneously acts as monodentate over one metal and chelate over the other.

The new complexes were fully characterized by standard spectroscopic techniques. As the addition of the first metal fragment selectively produces the chelate complex, sophisticated hetero-bimetallic complexes can be obtained just by deciding the order in which the metal precursors are introduced in the reaction vessel. The synthesis of the hetero-bimetallic complexes is also allowed by a one-pot procedure without isolating the monometallic intermediate, thus greatly facilitating the reaction work-up.

The catalytic properties of the new complexes were also studied. The palladium complexes (**1DH**, **1D** and **2D**) were tested in the hydroarylation of alkynes. The best catalytic activity was provided by the bimetallic complex **1D**. Complex **1D** is a good catalyst for this transformation at low catalyst loadings, and is active for transforming challenging substrates even at room temperature.

The Pd/Ir hetero-bimetallic complexes **3D** and **4D** were tested in two tandem reactions, namely the dehalogenation/transfer hydrogenation, and the Suzuki-Miyaura coupling/transfer hydrogenation of 4-bromoacetophenone. For both reactions **4D** is the complex that affords higher activity, although lower than the hetero-bimetallic complexes previously described in our group. The main differences in the activity of **3D** and **4D** are ascribed to the transfer hydrogenation step, which is the one facilitated by the Ir(I) fragment. The differences in activity may be due to the lower stability of the Ir(I) fragment in **3D**, which is NHC-monocoordinated, compared to the chelate coordination of the bis-NHC ligand enjoyed by the Ir(I) fragment in **4D**.

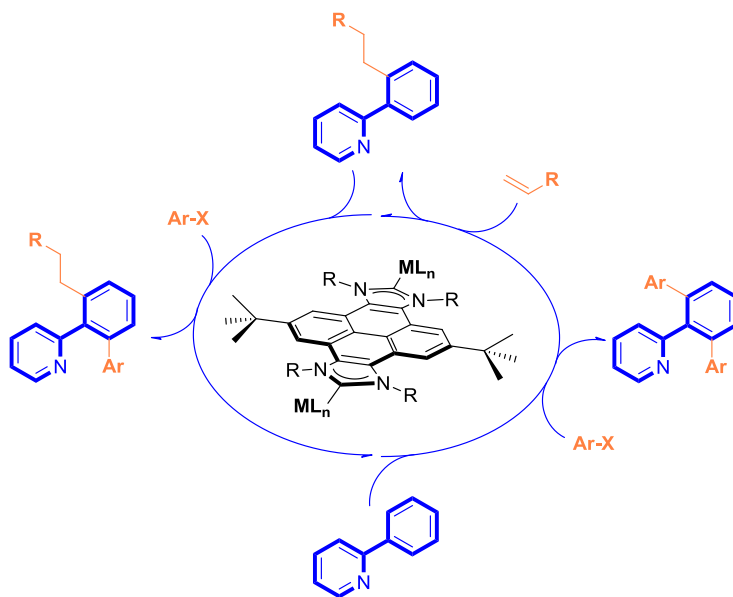
2.3 References

- (1) Poyatos, M.; Mata, J. A.; Peris, E. *Chem. Rev.* **2009**, *109*, 3677.
- (2) Ahrens, S.; Herdtweck, E.; Goutal, S.; Strassner, T. *Eur. J. Inorg. Chem.* **2006**, 1268.
- (3) Ribas Gispert, J. *Coordination Chemistry*; Wiley-VCH Verlag, 2008.
- (4) Viciano, M.; Mas-Marzá, E.; Sanaú, M.; Peris, E. *Organometallics* **2006**, *25*, 3063.
- (5) Albrecht, M.; Crabtree, R. H.; Mata, J.; Peris, E. *Chem. Commun.* **2002**, 32.
- (6) Albrecht, M.; Miecznikowski, J. R.; Samuel, A.; Faller, J. W.; Crabtree, R. H. *Organometallics* **2002**, *21*, 3596.
- (7) Iglesias, M.; Pérez-Nicolás, M.; Sanz Miguel, P. J.; Polo, V.; Fernández-Alvarez, F. J.; Pérez-Torrente, J. J.; Oro, L. A. *Chem. Commun.* **2012**, *48*, 9480.
- (8) Housecroft, C. E.; Sharpe, A. G. *Inorganic Chemistry*; Fourth Edi.; Pearson, 2012.
- (9) Herrmann, W. A.; Elison, M.; Fischer, J.; Köcher, C.; Artus, G. R. J. *Angew. Chem. Int. Ed.* **1995**, *34*, 2371.
- (10) Heckenroth, M.; Neels, A.; Stoeckli-Evans, H.; Albrecht, M. *Inorg. Chim. Acta* **2006**, *359*, 1929.
- (11) O'Brien, C. J.; Kantchev, E. A. B.; Valente, C.; Hadei, N.; Chass, G. A.; Lough, A.; Hopkinson, A. C.; Organ, M. G. *Chem. Eur. J.* **2006**, *12*, 4743.
- (12) Herrmann, W. A.; Schütz, J.; Frey, G. D.; Herdtweck, E. *Organometallics* **2006**, *25*, 2437.
- (13) Jia, C.; Piao, D.; Oyamada, J.; Lu, W.; Kitamura, T.; Fujiwara, Y. *Science* **2000**, *287*, 1992.
- (14) Jia, C.; Lu, W.; Oyamada, J.; Kitamura, T.; Matsuda, K.; Irie, M.; Fujiwara, Y. *J. Am. Chem. Soc.* **2000**, *122*, 7252.
- (15) Viciu, M. S.; Stevens, E. D.; Petersen, J. L.; Nolan, S. P. *Organometallics* **2004**, *23*, 3752.
- (16) Saravanakumar, R.; Ramkumar, V.; Sankararaman, S. *Organometallics* **2011**, *30*, 1689.
- (17) Biffis, A.; Tubaro, C.; Buscemi, G.; Basato, M. *Adv. Synth. Catal.* **2008**, *350*, 189.
- (18) Buscemi, G.; Biffis, A.; Tubaro, C.; Basato, M. *Catal. Today* **2009**, *140*, 84.

- (19) Biffis, A.; Gazzola, L.; Gobbo, P.; Buscemi, G.; Tubaro, C.; Basato, M. *Eur. J. Org. Chem.* **2009**, 3189.
- (20) Buscemi, G.; Biffis, A.; Tubaro, C.; Basato, M.; Graiff, C.; Tiripicchio, A. *Appl. Organomet. Chem.* **2009**, 24, 285.
- (21) Gazzola, L.; Tubaro, C.; Biffis, A.; Basato, M. *New J. Chem.* **2010**, 34, 482.
- (22) Hartwig, J. *Organotransition Metal Chemistry. From Bonding to Catalysis*; University Science Books, 2010.
- (23) Tunge, J. A.; Foresee, L. N. *Organometallics* **2005**, 24, 6440.
- (24) Zanardi, A.; Mata, J. A.; Peris, E. *J. Am. Chem. Soc.* **2009**, 131, 14531.
- (25) Loch, J. A.; Albrecht, M.; Peris, E.; Mata, J.; Faller, J. W.; Crabtree, R. H. *Organometallics* **2002**, 21, 700.
- (26) Godoy, F.; Segarra, C.; Poyatos, M.; Peris, E. *Organometallics* **2011**, 30, 684.
- (27) Corberán, R.; Peris, E. *Organometallics* **2008**, 27, 1954.
- (28) Blanco, M.; Álvarez, P.; Blanco, C.; Jiménez, M. V.; Fernández-Tornos, J.; Pérez-Torrente, J. J.; Oro, L. A.; Menéndez, R. *ACS Catal.* **2013**, 3, 1307.
- (29) Picard, F.; Schulz, T.; Hartmann, R. W. *Bioorg. Med. Chem.* **2002**, 10, 437.

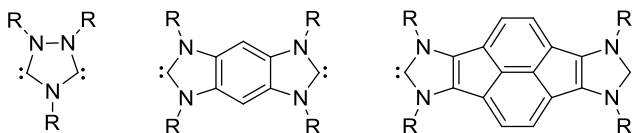
Chapter 3

A new *Janus*-type pyrene-bis-NHC ligand. Coordination properties and catalytic activity



3.1 Results and discussion

As stated in Chapter 1, the rigid nature of NHCs has allowed the design and synthesis of bis-NHCs in which the two carbene moieties are displayed in a fixed facially-opposed disposition (*Janus*-type bis-NHC ligands), preventing chelation over one only metal centers.¹⁻⁵ Although the bimetallic or polymeric complexes based on this kind of ligands have shown applications in several fields,⁶⁻⁹ *Janus*-type bis-NHC ligands are still very little known. The most representative examples of *Janus*-type bis-NHCs are represented in Scheme 3.1. Besides their interest in the formation of metal complexes with unusual chemical properties, some of the bis-imidazolium salts that generate this family of ligands exhibit interesting luminescence properties.¹⁰⁻¹³



Scheme 3.1 Representative examples of *Janus*-type bis-NHCs

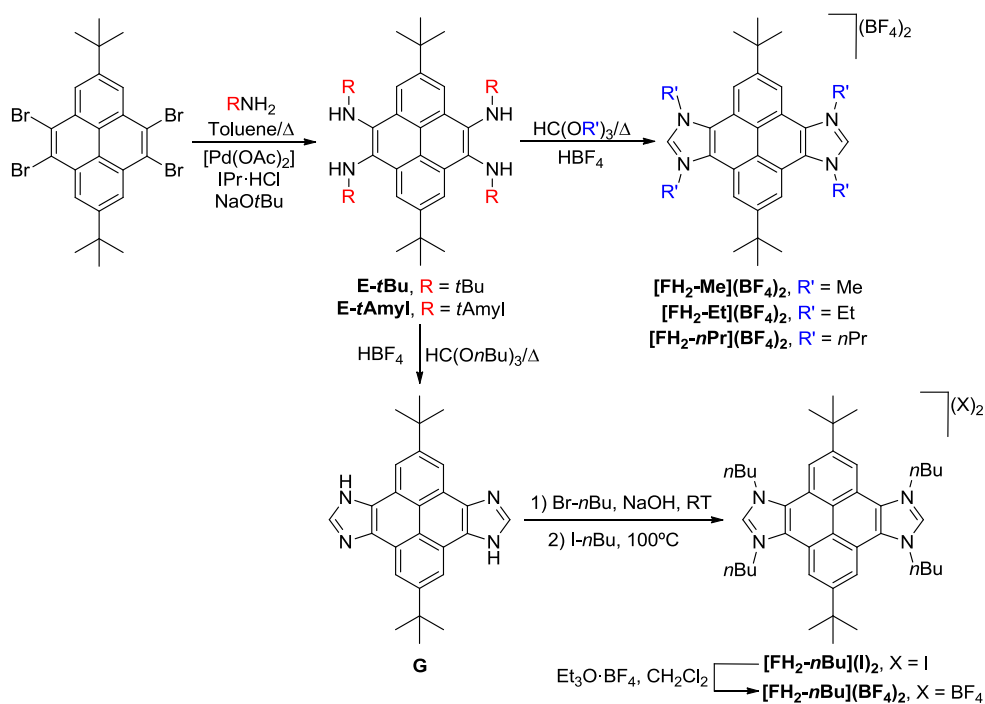
Taking all this into account, we decided to expand the number of *Janus*-type bis-NHCs ligands, by designing and synthesizing a new family of bis-azolium salts based on pyrene. For these new compounds we envisioned interesting photophysical properties, as pyrene is a well-known chromophore in photochemical research.¹⁴ Also, the rigidity of the ligands derived from these salts will provide bimetallic complexes with a fixed distance between the metals, and the high electronic delocalization of the pyrenic core may induce electronic communication between them.

In the next sections of this chapter, the synthesis and characterization of these new bis-imidazolium salts, as well as the description of their photochemical properties will be discussed. Then the synthesis and characterization of the related bimetallic and monometallic complexes, together with the discussion of their electrochemical and catalytic properties will be described in detail.

3.1.1 Synthesis of pyrene-based imidazolium salts

3.1.1.1 Synthesis of pyrene-based bis-azolium salts

With the aim of obtaining our new pyrene-based bis-azoliums, we designed a synthetic route inspired by the methodology developed by Bielawski and co-workers to synthesize benzobis(imidazolium) salts.¹⁵ As shown in Scheme 3.2, 4,5,9,10-tetrabromo-2,7-di-*tert*-butylpyrene was chosen as starting material. The two bulky *tert*-butyl groups were introduced at the 2 and 7 positions of pyrene to avoid the bromination at their adjacent positions.¹⁶ The multifold amination of the tetrabromopyrene was carried out in the presence of a palladium catalyst (generated from the reaction of IPr·HC, [Pd(OAc)₂] and NaOtBu), and an amine (*tert*-butyl amine or *tert*-amyl amine), in refluxing toluene. The reaction affords, almost quantitatively, the corresponding tetra-aminopyrenes, **E-*t*Bu** and **E-*t*Amyl**, as brown-red solids. The next step of the synthesis involves the formylative cyclization of these tetra-amines. The reaction was carried out using a trisalkyl orthoformate as solvent, and in the presence of tetrafluoroboric acid. Unexpectedly, instead of the bis-imidazolium salts containing either the bulky *tert*-butyl or *tert*-amyl groups as N-substituents (from now on *wingtips*), the new salts contained methyl, ethyl or *n*-propyl wingtips (**[FH₂-Me](BF₄)₂**, **[FH₂-Et](BF₄)₂** and **[FH₂-*n*Pr](BF₄)₂**, respectively in Scheme 3.2) depending on the trisalkyl orthoformate used for the cyclization. Thus, the bulky *tert*-butyl or *tert*-amyl groups were removed from the nitrogen along with the cyclization process. These salts were obtained with yields ranging from 64 to 84 % if **E-*t*Bu** was used as starting material or with yields between 43 and 63 % if **E-*t*Amyl** was used.



Scheme 3.2 Synthesis of pyrene-based bis-azoliums

Formally, the *tert*-butyl of *tert*-amyl substituents of compounds **E-*t*Bu** and **E-*t*Amyl**, were replaced by the alkyl group of the cyclization agent (HC(OR')₃). Interestingly, when tris-*n*-butyl orthoformate is used in this reaction, the pyrene-bisimidazole **G** is obtained in good yield. Alkylation of compound **G** following a reported procedure,¹⁷ yields the corresponding pyrene-based bis-imidazolium salt with *n*-butyl substituents, **[FH₂-*n*Bu](I)₂**, in good yield. Anion metathesis of **[FH₂-*n*Bu](I)₂** in the presence of Et₃O·BF₄ affords the tetrafluoroborate salt **[FH₂-*n*Bu](BF₄)₂**.

The reactivity shown for the bis-annulation reaction is unexpected, and we did not find any similar behavior in the literature. The reaction constitutes a highly valuable synthetic transformation, as the multifold amination of brominated compounds is normally restricted to amines without protons at the beta position, (usually *tert*-butyl amines or anilines), to avoid β-elimination in the palladium-catalyzed process. With this methodology, linear alkyl substituents can be introduced to the final bis-azolium, by using the appropriate alkyl orthoformates. Another interesting point that is worth mentioning, is that the use of toxic alkylating agents, which are commonly used to

obtain imidazolium salts with linear alkyl substituents,^{18–20} can be avoided with this procedure.

The formation of **G** suggests that the bulky *tert*-butyl (or *tert*-amyl) groups are lost in the reaction process, probably as a consequence of the steric constraints imposed during the rehybridization of the nitrogen atom from sp^3 to sp^2 (Figure 3.1). It has to be taken into account that in the final products the bulky groups bound to the nitrogen atoms are highly sterically constrained, due to the presence of the protons of the pyrene, as shown in Figure 3.1, so this situation is avoided if the bulky groups are substituted by linear alkyl groups.

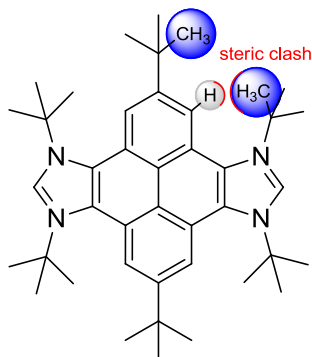


Figure 3.1 Steric clash produced between the *t*-Bu groups and the pyrenic core

We were able to isolate and crystallographically characterize one intermediate of the reaction of **E-*t*Bu** with triethyl orthoformate and tetrafluoroboric acid (Figure 3.2). The product contains a pyrenic core with two *tert*-butyl substituted nitrogen atoms and two primary amines. The presence of two primary amines indicates that the *tert*-butyl (or *tert*-amyl) groups are lost prior to the cyclization process.

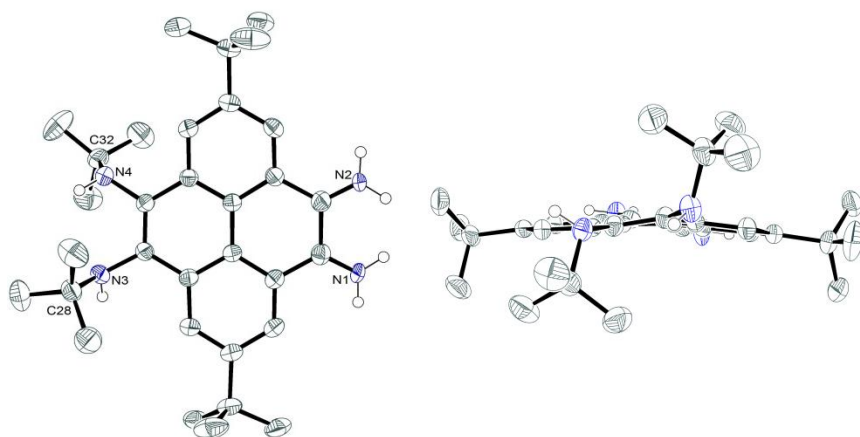


Figure 3.2 Two perspectives of 4,5-di-*tert*-butylamine-9,10-diamine-2,7-di-*tert*-butylpyrene. Hydrogen atoms (except those belonging to the amine groups) have been omitted for clarity. Ellipsoids at 50 % probability

All the new compounds were characterized by means of NMR, mass spectrometry and elemental analysis. The structure of $[\text{FH}_2\text{-Me}](\text{BF}_4)_2$ was unambiguously confirmed by X-Ray diffraction studies. Due to the similarity between all the compounds synthesized in this section, only the NMR spectroscopic characterization of $[\text{FH}_2\text{-Me}](\text{BF}_4)_2$ is described below. All the details regarding the characterization of the other products may be found in the Experimental Section (Chapter 5).

^1H NMR spectrum of $[\text{FH}_2\text{-Me}](\text{BF}_4)_2$

Figure 3.3 shows the ^1H NMR spectrum of $[\text{FH}_2\text{-Me}](\text{BF}_4)_2$. The number of signals and their integration are consistent with the D_{2h} symmetry of the compound. The signal due to the acidic protons of the NCHN (*a*) appears as a singlet at 9.83 ppm. The resonance attributed to the aromatic protons of the pyrene core is shown as a singlet at 9.04 ppm (*b*). The protons corresponding to the methyl groups bound to the nitrogen of the imidazole ring are displayed as a singlet at 4.76 ppm (*c*). Finally, the signal due to the protons of the *t*-butyl groups is observed at 1.68 ppm (*d*).

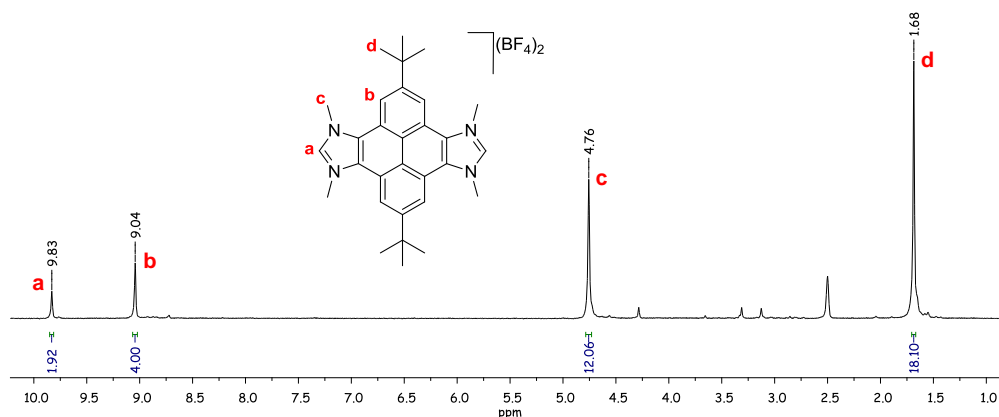


Figure 3.3 ^1H NMR spectrum of $[\text{FH}_2\text{-Me}](\text{BF}_4)_2$ in $\text{DMSO-}d_6$

$^{13}\text{C}\{^1\text{H}\}$ NMR spectrum of $[\text{FH}_2\text{-Me}](\text{BF}_4)_2$

Figure 3.4 shows the $^{13}\text{C}\{^1\text{H}\}$ NMR spectrum of $[\text{FH}_2\text{-Me}](\text{BF}_4)_2$. Again, the number of signals displayed in the spectrum is consistent with the two-fold symmetry of the compound. The signal attributed to the NCHN carbons (1) is displayed at 143.1 ppm. The resonance due to the aromatic CH groups of the pyrene core is shown at 118.4 ppm (2). The carbons corresponding to the methyl groups of the wingtips are observed at 38.3 ppm (3), while the signal attributed to the carbons of the *t*-butyl substituents are observed at 35.7 and 31.2 ppm (4 and 5, respectively). The rest of the signals corresponding to the quaternary carbons of the pyrene core are conveniently displayed on the spectrum.

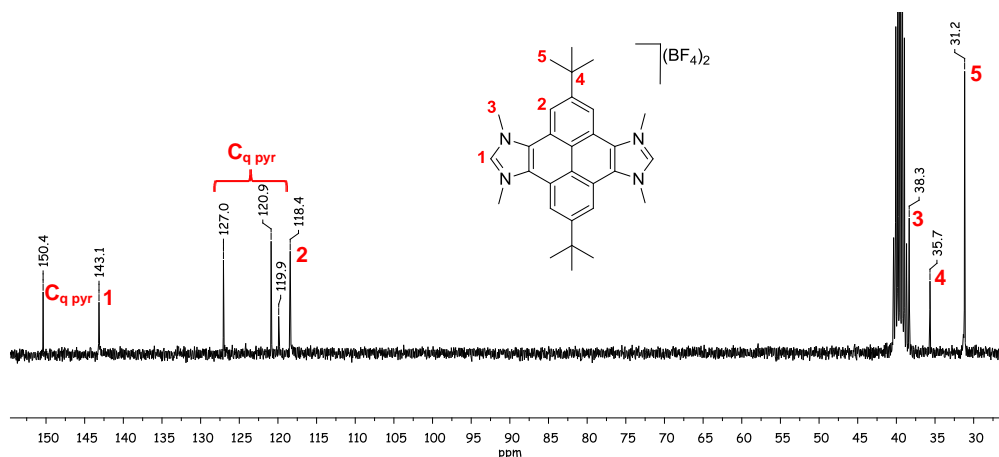


Figure 3.4 $^{13}\text{C}\{^1\text{H}\}$ NMR spectrum of $[\text{FH}_2\text{-Me}](\text{BF}_4)_2$ in $\text{DMSO-}d_6$

Molecular structure of $[\text{FH}_2\text{-Me}](\text{BF}_4)_2$

Crystals of $[\text{FH}_2\text{-Me}](\text{BF}_4)_2$ suitable for X-Ray diffraction analysis were obtained by slow diffusion of diethyl ether into a concentrated solution of the compound in acetonitrile.

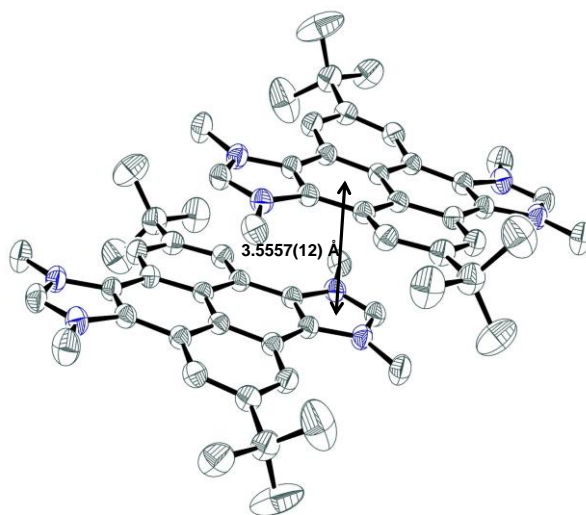
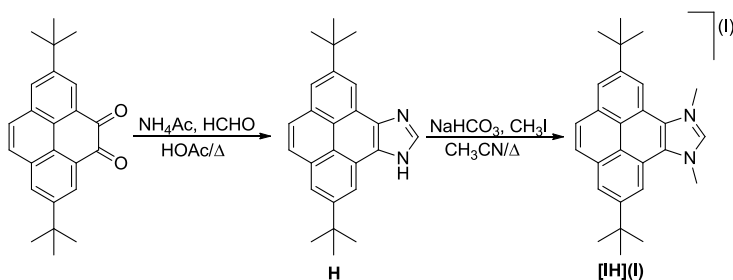


Figure 3.5 Molecular diagram of $[\text{FH}_2\text{-Me}](\text{BF}_4)_2$. Ellipsoids at 50 % probability. Hydrogen atoms, counterions (BF_4^-) and solvent (MeCN) have been omitted for clarity

The molecular structure of $[\text{FH}_2\text{-Me}](\text{BF}_4)_2$, shown in Figure 3.5, confirms that the two imidazolium moieties are connected through a pyrenic core. The structure also shows the presence of methyl wingtips, instead of the expected *tert*-butyl (or *tert*-amyl) substituents. The crystal packing reveals a π -stacking between pairs of bis-azoliums that are located at a distance of 3.5557(12) Å.

3.1.1.2 Synthesis of the pyrene-based mono-azolium salt $[\text{IH}](\text{I})$

For comparative purposes, we decided to synthesize a pyrene-based mono-imidazolium salt. As shown in Scheme 3.3, two steps are necessary for the synthesis of $[\text{IH}](\text{I})$.



Scheme 3.3 Synthesis of pyrene-based monoazolium [IIH](I)

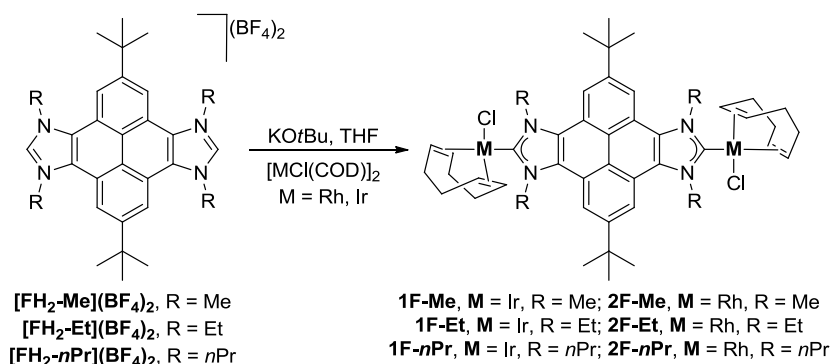
The starting material was 2,7-di-*tert*-butylpyrene-4,5-dione, which was obtained using a previously reported procedure.²¹ The dione was reacted with ammonium acetate and formaldehyde in refluxing acetic acid overnight. After work-up, compound **H** was obtained as a brown solid in almost quantitative yield (97 %). Then, compound **H** was alkylated using iodomethane and sodium bicarbonate in refluxing acetonitrile, to afford the desired mono-azolium [IIH](I), as a yellow solid in a good yield (69 %).

Compounds **H** and [IIH](I) were characterized by means of NMR and UV-visible spectroscopy, mass spectrometry and elemental analysis. All the details regarding the characterization of these compounds can be found in the Experimental Section (Chapter 5).

3.1.2 Complexes with pyrene-based NHC ligands

3.1.2.1 IrCl(COD) and RhCl(COD) complexes

Once the new family of pyrene-based imidazolium salts was prepared, we decided to study their coordination capabilities as NHC precursors. First, we obtained bimetallic complexes using [MCl(COD)]₂ (M = Ir or Rh) as metal sources (Scheme 3.4). The reaction of the corresponding bis-azolium salt with [MCl(COD)]₂ (M = Ir or Rh) in the presence of KO^{*t*}Bu in THF at room temperature, afforded the desired bimetallic complexes. These compounds were isolated in good to moderate yield (40-75 %) after purification by column chromatography and precipitation from a mixture CH₂Cl₂/hexanes.



Scheme 3.4 Synthesis of bis-Ir and bis-Rh complexes based on **F** ligand

As a consequence of the relative configuration of the two metal fragments about the bis-NHC ligand, the complexes can be obtained as a mixture of two atropisomers (Figure 3.6). In the *anti*-atropisomer the two chloride ligands are pointing to different sides of the molecule, while in the *syn*-atropisomer the two chloride ligands are pointing to the same side of the molecule. These atropisomers were observed by NMR spectroscopy in a 1:1 molar relative ratio for all bimetallic complexes synthesized. We were unable to separate both atropisomers by column chromatography or by fractional crystallization, and we did not observe any interconversion between them using VT-NMR experiments or even by heating an NMR sample during several hours.

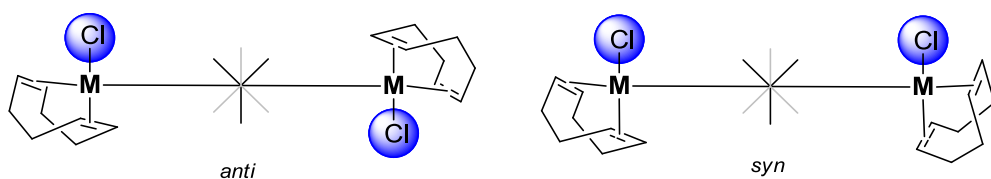


Figure 3.6 Schematic side representation of the two possible atropisomers of the bis-Ir and bis-Rh complexes based on **F** (M = Ir or Rh)

Compounds **1F** and **2F** were characterized by means of NMR spectroscopy, mass spectrometry and elemental analysis. The molecular structure of **1F-Et** was unambiguously confirmed by X-Ray Diffraction studies. Due to the similarity between these compounds only the NMR spectroscopic characterization of **1F-Et** is described below. All the details regarding the characterization of the other complexes may be found in the Experimental Section (Chapter 5).

¹H NMR spectrum of 1F-Et

Figure 3.7 shows the ¹H NMR spectrum of **1F-Et**. The number of signals and their integration are consistent with the two-fold symmetry of the compound. The spectrum also reveals the presence of two atropisomers (*syn* and *anti*) in a 1:1 relative molar ratio, as shown by the splitting of several signals that otherwise should have appeared as singlets (protons of the methyls of the *t*Bu groups, *CH* protons of the pyrene, etc.). The signals due to the *CH* groups of the pyrene core (*a*) appear as two singlets at 8.76 ppm. The two diastereotopic protons of the *CH*₂ groups of the wingtips, display their resonances as two multiplets at 5.91 and 5.36 ppm (*b*). The signals attributed to the methyl groups at the wingtips are displayed as a triplet at 1.81 ppm (*c*), while the resonances due to the protons of the *t*-butyl groups are observed at 1.66 ppm as two singlets (*d*). The rest of the signals corresponding to the protons of the COD ligands are conveniently displayed on the spectrum.

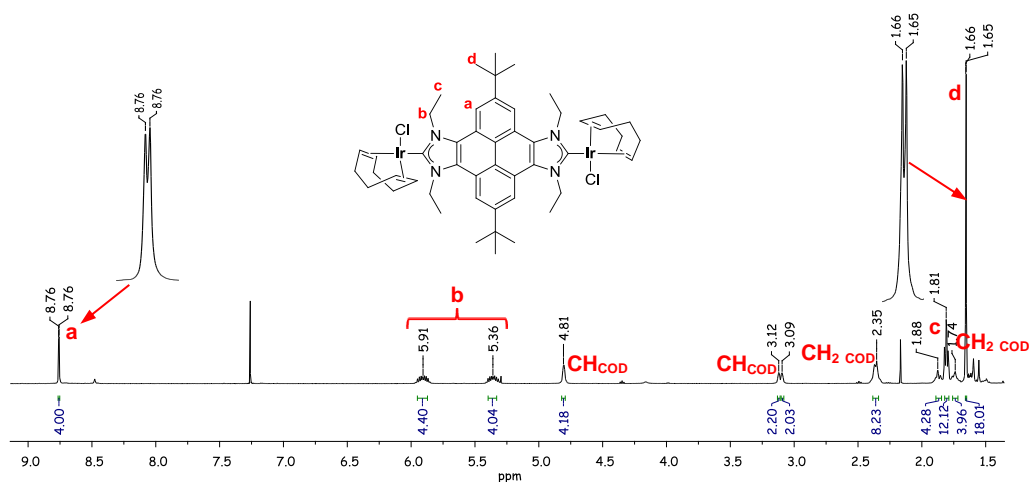


Figure 3.7 ¹H NMR spectrum of **1F-Et** in CDCl₃

¹³C{¹H} NMR spectrum of 1F-Et

Figure 3.8 shows the ¹³C{¹H} NMR spectrum of **1F-Et**. Again, the number of signals displayed in the spectrum is consistent with the two-fold symmetry of the compound, and also confirms the presence of the two atropisomers. The most characteristic signals are those attributed to the metallated carbene-carbons, which are displayed at 188.6 ppm (*1*) (split, as the consequence of the presence of the two isomers, as all other signals in this NMR spectrum). The resonances due to the aromatic *CH* group of the pyrene core are shown at 116.1 ppm (*2*). The signals due to the *CH*₂ groups of the

wingtips are displayed at 47.0 ppm (3). The signals attributed to the carbons of the *t*-butyl groups are observed at 35.9 and 31.6 ppm (4 and 5, respectively), while the resonance due to the methyl groups of the wingtips is observed at 15.6 ppm (6). The rest of the resonances corresponding to the quaternary carbons of the pyrenic core and to the COD ligand are conveniently displayed on the spectrum.

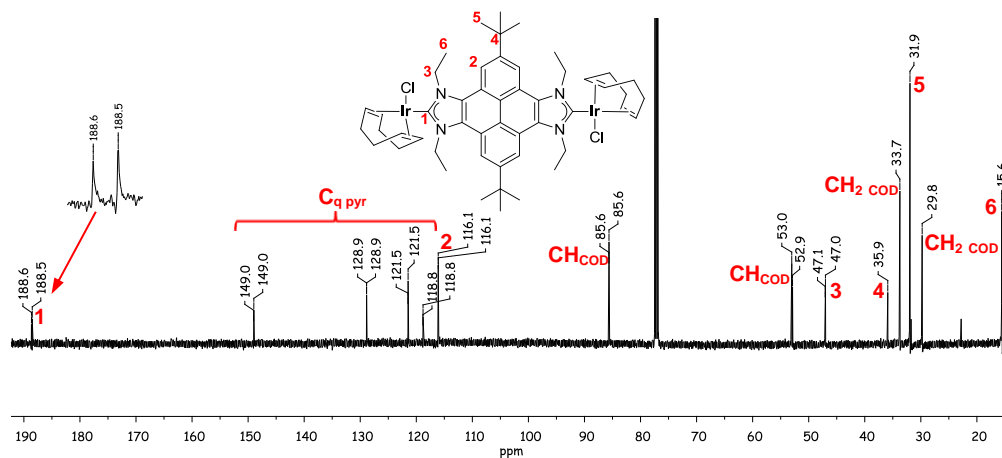


Figure 3.8 $^{13}\text{C}\{^1\text{H}\}$ NMR spectrum of **1F-Et** in CDCl_3

Molecular structure of **1F-Et**

Crystals of **1F-Et** suitable for X-Ray Diffraction analysis were obtained by slow diffusion of hexane into a concentrated solution of the compound in dichloromethane.

The molecular structure of **1F-Et**, shown in Figure 3.9, consists of a pyrene-bis-imidazolydene ligand bridging two iridium atoms which complete their coordination sphere with a COD and a chloride ligands. The molecular structure shown in Figure 3.9 corresponds to the *syn*-atropisomer, in which the two chloride ligands are pointing to same side of the molecule. The pyrenic core of the ligand slightly deviates from planarity, as observed in the side view of the molecule (Figure 3.9, bottom), which reflects a bow-shaped distortion. Table 3.1 shows the most representative bond lengths (\AA) and angles ($^\circ$). The $\text{Ir-C}_{\text{carbene}}$ average distance is 2.031(5) \AA , and the through-space distance between the two metals is 13.141(1) \AA . The average angle between the plane containing the azole ring and the coordination plane of the iridium fragment is 81.7(2) $^\circ$.

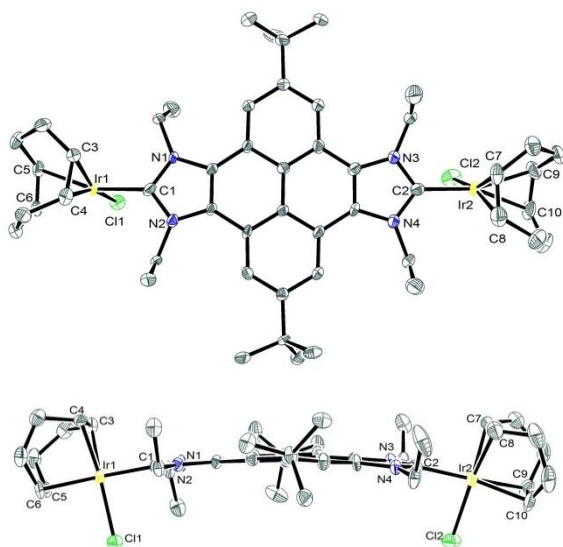


Figure 3.9 Two perspectives of the molecular structure of complex **1F-Et**. Ellipsoids at 50 % probability. Hydrogen atoms have been omitted for clarity

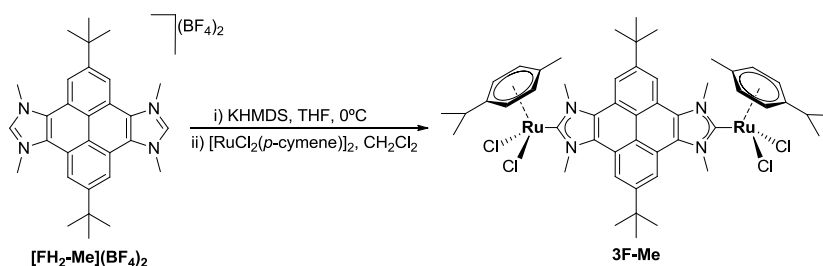
Table 3.1 Selected bond lengths and angles of complex **1F-Et**

Bond lengths (Å)		Bond angles (°)	
Ir(1)-C(1)	2.027(7)	C(1)-Ir(1)-Cl(1)	87.0(2)
Ir(1)-Cl(1)	2.3563(19)	C(2)-Ir(2)-Cl(2)	86.4(2)
Ir(1)-C(3)	2.097(8)		
Ir(1)-C(4)	2.102(7)		
Ir(1)-C(5)	2.180(7)		
Ir(1)-C(6)	2.178(7)		
Ir(2)-C(2)	2.034(7)		
Ir(2)-Cl(2)	2.366(2)		
Ir(2)-C(7)	2.091(7)		
Ir(2)-C(8)	2.112(9)		
Ir(2)-C(9)	2.189(8)		
Ir(2)-C(10)	2.173(8)		
Ir(1)-Ir(2)	13.1406(6)		

3.1.2.2 RuCl₂(*p*-cymene) complexes

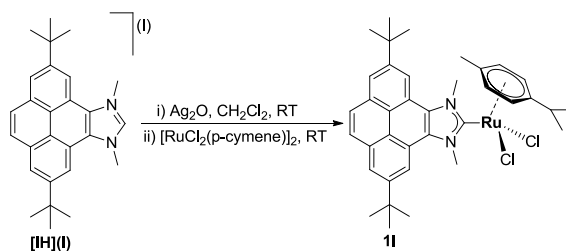
The pyrene-based bis-ruthenium complex **3F-Me**, was obtained following a procedure reported by our group (Scheme 3.5).²² The salt **[FH₂-Me](BF₄)₂** was

treated with potassium bis(trimethylsilyl)amide (KHMDs) at 0°C in THF, in order to generate the free carbene, which was transferred *via* an oven-dried *cannula* to another Schlenk containing a solution of $[\text{RuCl}_2(p\text{-cymene})]_2$ in dichloromethane. The mixture was stirred at 45°C during 1 hour and then was refluxed for 20 minutes. Precipitation from a mixture of acetone/diethyl ether afforded compound **3F-Me** as a brownish solid in good yield (75 %). Compound **3F-Me** may contain the *syn* or *anti* atropisomers, depending on the disposition of the two *p*-cymene ligands relative to the planar bridging ligand (the schematic representation is similar to the one shown in Figure 3.6 but with a *p*-cymene ligand instead of a COD, and two chloride ligands instead of one). However, in this case the lower crowding about the metal may allow the free rotation about the NHC-Ru bond, and therefore no atropisomers may be expected.



Scheme 3.5 Synthesis of the pyrene-based bis-Ru(II) complex **3F-Me**

The synthesis of the pyrene-based mono-ruthenium complex **1I**, was performed through a transmetallation route (Scheme 3.6).²³ The salt **[IH](I)** was treated with Ag_2O in CH_2Cl_2 during two hours under the exclusion of light, in order to generate the silver carbene, which we did not isolate. Then $[\text{RuCl}_2(p\text{-cymene})]_2$ was added, and the reaction was stirred at room temperature during two hours. The suspension was filtered through a pad of Celite. Precipitation from a mixture CH_2Cl_2 /hexane afforded complex **1I** as a brown solid in good yield (73 %).



Scheme 3.6 Synthesis of the pyrene-based mono-Ru(II) complex **1I**

¹H NMR spectrum of 3F-Me

Figure 3.10 shows the ¹H NMR spectrum of **3F-Me**. The number of signals and their integration are consistent with the two-fold symmetry of the compound. The spectrum does not reveal the presence of the two atropisomers, probably because in this case the metal fragment is able to free-rotate about the NHC-Ru bond. This should also explain the relative broadening of the signals, which may indicate rotation on the NMR timescale. The signal due to the CH groups of the pyrene core (*a*) appears as a singlet at 8.99 ppm. The resonance attributed to CH₃ groups of the wingtips (*b*) is shown as a singlet at 4.92 ppm. The singlet corresponding to the protons of the *t*-Bu groups is observed at 1.61 ppm (*c*). The rest of the resonances attributed to the protons of the *p*-cymene ligand are conveniently displayed on the spectrum.

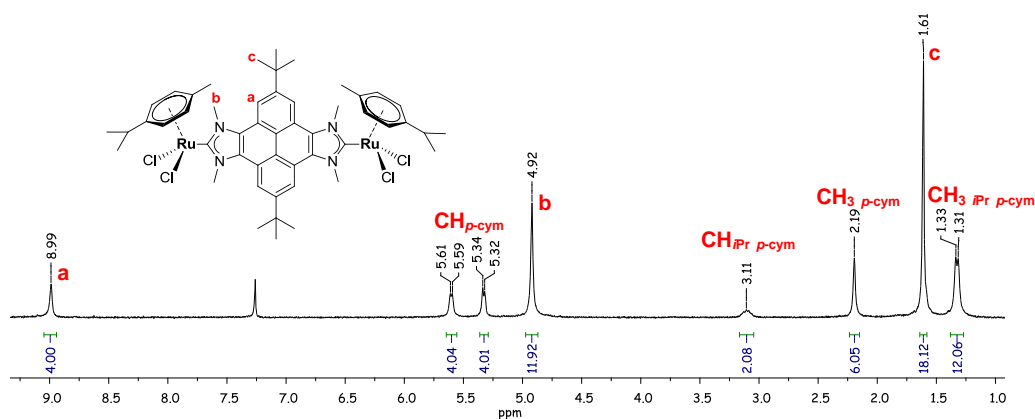


Figure 3.10 ¹H NMR spectrum of **3F-Me** in CDCl₃

¹³C{¹H} NMR spectrum of 3F-Me

Figure 3.11 shows the ¹³C{¹H} NMR spectrum of **3F-Me**. The number of signals displayed in the spectrum is consistent with the two-fold symmetry of the compound. The most characteristic signal is the one attributed to the metallated carbene-carbons, which is displayed at 186.6 ppm (*1*). The resonance corresponding to the aromatic CH groups of the pyrenic core is shown at 116.8 ppm (*2*). The signal due to the methyl groups of the wingtips is displayed around 43.2 ppm (*3*), while those attributed to the carbons of the *t*-butyl groups are observed at 35.8 and 31.8 ppm (*4* and *5*, respectively). The rest of the resonances corresponding to the quaternary carbons of the pyrenic core and to the *p*-cymene ligand are conveniently displayed on the spectrum.

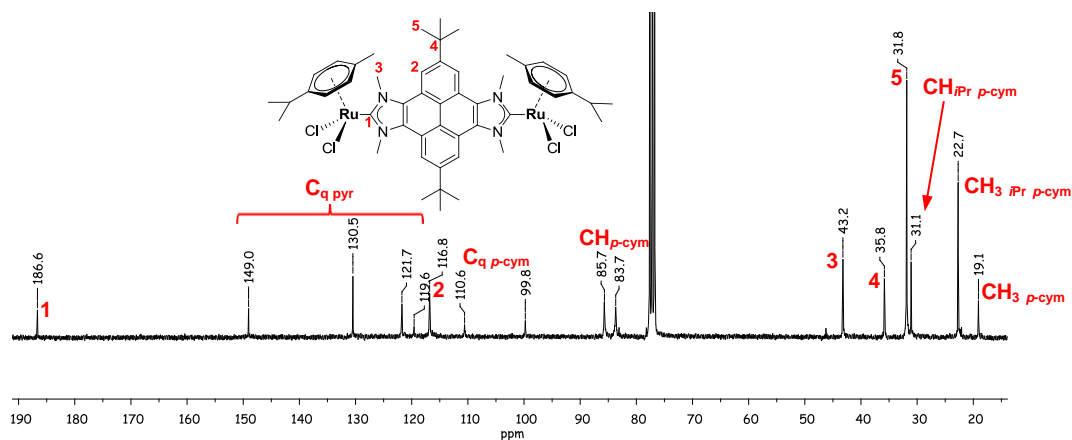


Figure 3.11 $^{13}\text{C}\{^1\text{H}\}$ NMR spectrum of **3F-Me** in CDCl_3

Molecular structure of **3F-Me**

Crystals of **3F-Me** suitable for X-Ray Diffraction analysis were obtained by slow diffusion of hexane into a concentrated solution of the compound in 1,2-dichloroethane.

The molecular structure of **3F-Me** shown in Figure 3.12, consists of a pyrene-bis-imidazolylidene ligand bridging two ruthenium centers, which complete their coordination sphere with a *p*-cymene and two chloride ligands. The molecular structure corresponds to the *anti*-atropisomer in which the *p*-cymene ligands at each ruthenium fragment are pointing to different sides of the molecule. In this case the pyrenic core of the ligand is perfectly planar as observed by the side-view of the molecule (Figure 3.12, bottom). Table 3.2 shows the most representative bond lengths (\AA) and angles ($^\circ$) of the complex. The $\text{Ru-C}_{\text{carbene}}$ distance is 2.097(5) \AA , in the range of other ‘ $\text{Ru}(p\text{-cymene})(\text{NHC})$ ’ complexes.^{24–26} The Ru-Cl and $\text{Ru-C}_{\text{centroid}}$ distances, and the $\text{C}_{\text{carbene}}\text{-Ru-Cl}$ angles lie in the expected range. The through-space distance between the two metals is 13.393(1) \AA , slightly longer than the related Ir-Ir distance observed for **1F-Et**. This is probably because the pyrenic core in **3F-Me** is planar, while the bow-shaped distortion of the ligand in **1F-Et** slightly approaches the metal centers.

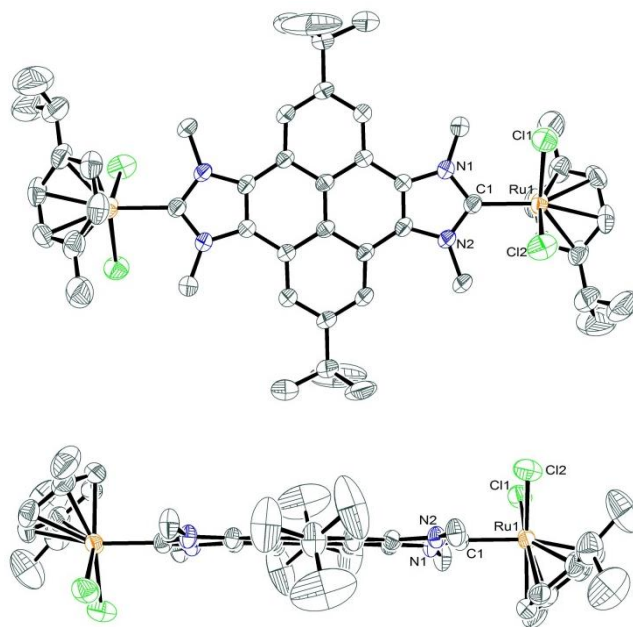


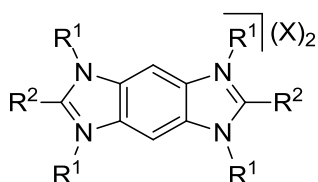
Figure 3.12 Two perspectives of the molecular structure of complex **3F-Me**. Ellipsoids at 50 % probability. Hydrogen atoms and solvent (1,2-dichloroethane) have been omitted for clarity

Table 3.2 Selected bond lengths and angles of complex **3F-Me**

Bond lengths (Å)		Bond angles (°)	
Ru(1)-C(1)	2.097(5)	C(1)-Ru(1)-Cl(1)	91.24(14)
Ru(1)-Cl(1)	2.4378(15)	C(2)-Ru(2)-Cl(2)	88.14(15)
Ru(1)-Cl(2)	2.4231(17)	Cl(1)-Ru(1)-Cl(2)	84.65(6)
Ru(1)-C _{centroid}	1.693(3)		

3.1.3 Luminescence properties of the pyrene-based azolium salts

Janus-type bis-azoliums have proven to be a very useful and robust kind of fluorophores.¹² In particular, Bielawski and co-workers have shown that benzobis(imidazolium) salts (Scheme 3.7) feature high synthetic flexibility that allows the fine-tuning of their physico-chemical properties.^{6,10,11,13,15} They were able to synthesize a wide range of these compounds, whose properties (emission wavelength, quantum yield, melting point...) were systematically modified by varying the substituents of the salts (R^1 , R^2 and the counterion, Scheme 3.7)



Scheme 3.7 Benzobis(imidazolium) salts (R^1 = aromatic or alkyl group, R^2 = H or aromatic group)

The imidazolium salts described in this section contain one or two azolium fragments and a pyrenic core, which is a widely used chromophore in photochemical research,¹⁴ so we decided to study their photochemical properties. Furthermore, it is a good opportunity to study the photophysical changes due to the presence of one or two azolium fragments and the different N-alkyl substituents introduced.

Table 3.3 summarizes the photochemical properties of the different pyrene-based azoliums. The UV-vis and fluorescence spectra of these compounds can be found in the Experimental Section (Chapter 5). The UV-vis spectra of the pyrene-based bis-azolium salts are almost superimposable, having two maxima absorption at 263 and 286 nm with nearly the same molar extinction coefficients. The UV-vis spectrum provided by **[IH]I** shows two maxima absorption which are hypsochromically shifted by 13 and 11 nm with respect those observed for the pyrene-bis-azoliums. This observation suggests that the bis-azolium salts are more electron deficient than the mono-azolium analogue **[IH]I**, and this produces a lowering of the energy of the π - π^* transition.¹²

Table 3.3 Photophysical properties of pyrene-based-azoliums^a

Entry	Compound	$\lambda_{\text{abs max}}$ (nm) ($\log(\epsilon)$) ^a	$\lambda_{\text{em max}}$ (nm) ^b	Φ_f ^b
1	[FH₂-Me](BF₄)₂	263 (4.79), 286 (4.69)	371, 391, 412, 416	0.41
2	[FH₂-Et](BF₄)₂	264 (4.77), 287 (4.67)	372, 392, 413, 437	0.38
3	[FH₂-<i>n</i>Pr](BF₄)₂	264 (4.79), 288 (4.69)	372, 392, 413, 437	0.29
4	[FH₂-<i>n</i>Bu](I)₂	264 (4.79), 288 (4.69)	372, 392, 414, 434	0.33
5	[FH₂-<i>n</i>Bu](BF₄)₂	264 (4.72), 288 (4.72)	372, 392, 414, 438	0.37
6	[IH](I)	251 (4.83), 277 (4.54)	373, 393, 416, 440	0.32

^aMeasurements were performed in MeCN under ambient conditions. Molar extinction coefficients (ϵ , in $M^{-1}cm^{-1}$) were determined from Beer's law plots. ^bEmission quantum yield was measured in degassed MeCN, with recrystallized anthracene in degassed EtOH as standard ($\Phi_f = 0.27$), exciting at 317 nm.

The presence of one or two azolium units, the different nature of N-alkyl substituents and the different counterions have negligible effect on the emission spectra of these compounds. Thus all the salts show nearly superimposable emission spectra with a vibronic-structured band centered at *ca* 390 nm.²⁷ The vibrational progressional spacings are about 20 nm. The emission quantum yields (Φ_f) vary from 0.29 to 0.41, **[FH₂-Me](BF₄)₂** being the most efficient fluorophore. This is reasonable as this salt contains methyl groups (the smallest of the series), which provides to the molecule less non-radiative (vibrational and rotational) deactivations modes from the excited state, compared with the other salts.

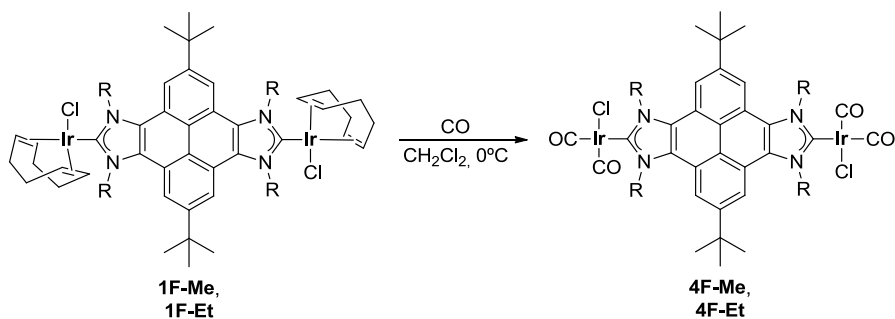
3.1.4 Electronic properties of the bimetallic complexes based on F

For the determination of the electronic properties of the complexes obtained in this section, we decided to use two approaches. The first one is based on the preparation of the carbonyl derivatives of complexes **1F**, and the study of their IR spectra. The second approach involves electrochemical measurements of all monometallic and bimetallic complexes. The next sections describe all the details about these two approaches.

3.1.4.1 Carbonyl derivatives of complexes **1F**

The [IrCl(NHC)(CO)₂] series has become widely used to experimentally compare the electronic donating properties of NHC ligands and estimate the Tolman Electronic Parameter (TEP),²⁸ setting aside the drawbacks of the [LNi(CO)₃] system. Ever since Crabtree²⁹ and Nolan³⁰ proposed the Ir system, many other authors have used it to explore the ligand-donating properties of other NHCs.^{31,32} Then, Wolf and Plenio established a regression formula to correlate the $\nu(\text{CO})$ of [RhCl(NHC)(CO)₂] complexes with the $\nu(\text{CO})$ of [IrCl(NHC)(CO)₂] ones, therefore unifying the Rh and Ir scale for the determination of the electron-donating properties of NHC ligands.³³ Hence, both systems are useful to estimate and compare the donor ability of NHCs.

Compounds **1F-Me** and **1F-Et** can be transformed into their corresponding carbonyl derivatives by bubbling CO through a solution of these complexes in dichloromethane at 0°C (Scheme 3.8). Precipitation from a mixture CH₂Cl₂/hexane afforded the desired carbonylated compounds in excellent yields (93% for **4F-Me**, and 95 % for **4F-Et**).



Scheme 3.8 Synthesis of complexes **4F-Me** and **4F-Et**

The bimetallic complexes **4F-Me** and **4F-Et** were characterized by NMR and IR spectroscopy, mass spectrometry and elemental analysis. The most significant feature of the ^1H NMR spectrum is the disappearance of the signals corresponding to the COD ligand, proving that the substitution of the COD by two carbonyl ligands has taken place. In the $^{13}\text{C}\{^1\text{H}\}$ NMR spectrum, the two resonances corresponding to the carbonyl ligands are displayed around 168 ppm (167.8 ppm for **4F-Me** and 168.3 ppm **4F-Et**). In this case, the two atropisomers (*syn* and *anti*) are only observed for **4F-Et**, probably because in **4F-Me** the rotation about the Ir-C_{carbene} bond is less hindered, as the methyl groups are less bulky than the ethyl ones, and the bulky COD has been replaced by two less sterically-demanding CO ligands.²⁹

The IR spectrum of **4F-Me** displays two CO stretching bands (as expected for the *cis* disposition of the carbonyl ligands) at 2069 and 1988 cm^{-1} , very similar to the values observed for **4F-Et** (2069 and 1987 cm^{-1}). These values allowed us to estimate the Tolman Electronic Parameter (TEP) as 2054 cm^{-1} , by using the well-known correlations.^{29,30,32} This value is very similar to the one calculated for 1,3-diethylbenzimidazolylidene, 2055 cm^{-1} , indicating a similar degree of electron-donating capacity.

3.1.4.2 Electrochemical properties of ligand F

Another technique that has recently been proposed to estimate the electronic properties of NHC ligands is cyclic voltammetry. The initial studies were carried out by Plenio and co-workers with rhodium and iridium NHC complexes.^{34,35} More importantly, this kind of measurements are also a valuable tool to determine the electronic communication in multimetallic systems.^{6,36–38} For these reasons, we

carried out electrochemical experiments with the bimetallic complexes based on the pyrene-bis-imidazolilydene ligand.

We first performed the cyclic voltammetric studies on the bis-Rh and bis-Ir complexes **1F** and **2F**. Almost all these complexes showed irreversible waves, probably due to the small volume of the linear alkylic wingtips of the ligand, which decreases the steric protection of the metal center.¹² Compound **1F-Et** is the only complex that afforded a quasi-reversible one-electron oxidation wave centered at $E_{1/2} = 0.94$ V arising from the Ir^{III} oxidation (Figure 3.13, left). This value correlates well with those shown by other bis-^{5,6} or mono-IrCl(COD)^{34,35} complexes. In fact, this value is higher than the one observed for the previously reported pyracenebis(imidazolylidene)-bis-IrCl(COD) ($E_{1/2} = 0.86$ V),⁵ indicating a lower electron-donating capacity of the pyrenebis(imidazolylidene) ligand, in agreement with the reported IR measurements of the related carbonylated bis-iridium complexes (*vide supra*).

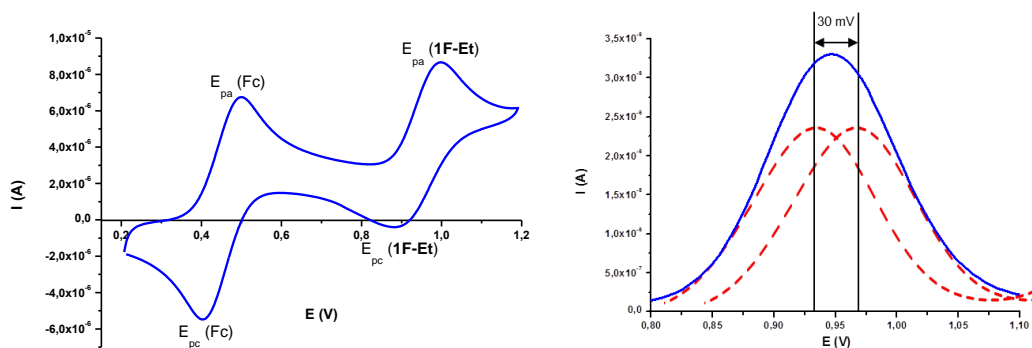


Figure 3.13 Cyclic voltammetry diagram of complex **1F-Et** (left) and relevant section of the differential pulse voltammetry (DPV) (right). The convoluted curves (red discontinuous lines) were obtained from adding two potential-shifted and weighed signals of the monometallic complex [IrCl(1,3-diethylbenzimidazolylidene)(COD)]. Measurements performed on a 1 mM solution of the analyte in dry CH₂Cl₂ with 0.1 M [NBu₄][PF₆] as the supporting electrolyte, 50 mVs⁻¹ scan rate, Fc⁺/Fc used as internal standard with $E_{1/2}$ (Fc⁺/Fc) = 0.446 V vs. SCE.

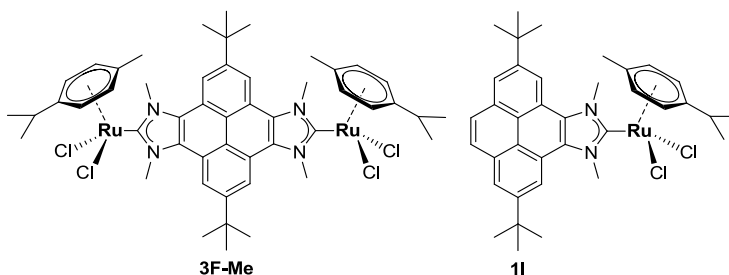
For the study of the electronic coupling between the two iridium centres, differential pulse voltammetry (DPV) analysis of **1F-Et** was performed. For this purpose and, in order to perform the proper comparisons, [IrCl(1,3-diethylbenzimidazolylidene)(COD)] was synthesized, using the same methodology as

the one used to obtain complexes **1F**. DPV experiments of complex **1F-Et** shows a broader signal, compared to the one observed for the iridium monocarbene complex [IrCl(1,3-diethylbenzimidazolylidene)(COD)] (Figure 3.13, right). Taking the DPV signal of this mono-iridium complex as a reference, the deconvolution of the DPV curve for **1F-Et** reveals the presence of two oxidation bands separated by 30 mV. This separation corresponds to an essentially decoupled system,³⁹ especially when compared to other known π -linked bis-NHCs.^{5,6,36,37} This is in agreement with previously suggestions which indicate that electronic communication in bis-NHCs with polyaromatic cores is mainly due to σ -interactions,⁴⁰ unless an appropriate orientation of the orbitals of the metal is achieved by chelating ligands, as recently suggested.⁴¹

These experiments were also performed with the ruthenium complexes **3F-Me** and **1I**, and similar conclusions were extracted. Compound **3F-Me** afforded a quasi-reversible one-electron oxidation wave, centered at $E_{1/2} = 1.336$ V. Complex **1I** displays two oxidation waves corresponding to the oxidation of the ruthenium center ($E_{1/2} = 1.271$ V) and to the oxidation of the pyrene fragment ($E_{1/2} = 1.462$ V), with the first being quasi-reversible and the second irreversible. The deconvolution of the DPV curve of **3F-Me** using **1I** as reference, revealed two bands separated by 40 mV, thus proving that our system is essentially decoupled.

3.1.5 Catalytic properties of ruthenium complexes **3F-Me** and **1I**

In recent years, chelation-assisted reactions have proven to be a highly valuable kind of transformations, as they normally imply a C-H activation/C-C bond formation, and constitute a high atom economy process.⁴² The first approach to this methodology was reported in a pioneering work by Murai and co-workers, in which they introduced the use of heteroatoms as directing groups.⁴³ After that, the number of publications in this field has grown exponentially showing a wide versatility, with ruthenium-based catalysts being the most widely used.⁴⁴⁻⁴⁶ For these reasons, we decided to test our new ruthenium complexes (**3F-Me** and **1I**, Scheme 3.9) in two chelation-assisted transformations, namely the arylation of arylpyridines and the hydroarylation of terminal alkenes. The combination of both processes in a sequential one-pot procedure to produce mixed arylated/alkylated arylpyridines will also be discussed in the next section.



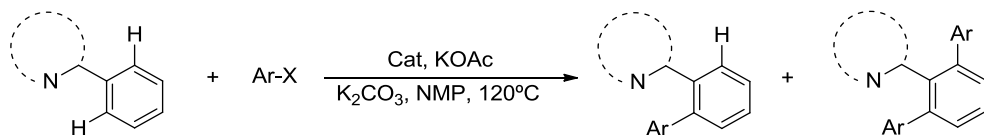
Scheme 3.9 Catalyst tested in chelation-assisted reactions

3.1.5.1 Arylation of arylpyridines

Oi and co-workers reported the first examples of the ruthenium catalyzed arylation of arylpyridines with arylhalides.⁴⁷ Then, several publications appeared, in which the search for efficient catalysts for this challenging transformation was the main objective.^{20,45,48,49} In this reaction, the arylpyridine is selectively arylated at the *ortho* position of the aryl ring, so two products are possible: the mono-arylated and the bis-arylated compound (Table 3.4). Depending on the reaction conditions and the catalyst used, either of the products can be selectively obtained.^{50,51}

In order to test the activity of our mono- and bimetallic complexes of ruthenium **1I** and **3F-Me**, we decided to use the same reaction conditions that were previously employed in our group:²⁰ 120°C in NMP (N-methyl-2-pyrrolidone), with a mixture of KOAc and K₂CO₃ using a 5 % catalyst loading based on metal.

The study of the catalytic activity of these two compounds should give us interesting information about how the bimetallic nature of complex **3F-Me** may have (or may not have) any substantial benefits compared with its monometallic analogue complex, **1I**.

Table 3.4 Arylation of arylpyridines using catalysts **3F-Me** and **1I**^a

Entry	Pyridine	Ar-X	Cat	t(h)	Mono (%) ^b	Bis (%) ^b
1			3F-Me	3	1	98 (85)
2			1I	3	-	98
3			3F-Me	2	-	98
4			3F-Me	5	-	99
5			3F-Me	2	-	99
6			3F-Me	4	-	99
7			3F-Me	1	-	99 (82)
8			1I	1	-	99
9			3F-Me	2	95	-

^aReaction conditions: KOAc (0.05 mmol), 5 % catalyst loading (based on metal), 2 mL of NMP, room temperature for 1 h, then substrate (0.5 mmol), Ar-X (1.25 mmol), K₂CO₃ (1.25 mmol), 120°C. ^bYields determined by GC using anisole (0.5 mmol) as internal standard. Isolated yields in parenthesis.

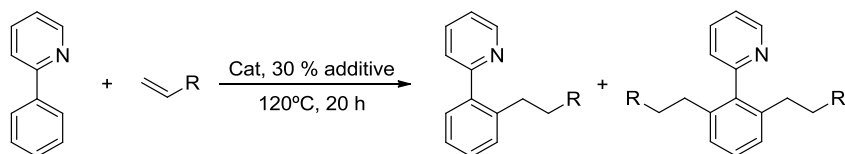
The results are summarized in Table 3.4. For the reaction of 2-phenylpyridine, N-phenylpyrazol and benzo[*h*]quinoline with different arylhalides, catalysts **3F-Me** and **1I** provide good activities, and are selective to the bisarylated products in short reactions times (1-5 h). Interestingly, bromobenzene reacts faster than chlorobenzene (compare entries 1 and 3), therefore showing the opposite tendency than the one observed previously in our group for related (arene)Ru(NHC) complexes.²⁰ Additionally, we observed that the catalytic performances of **3F-Me** and **1I** were very similar (compare entries 1 and 2 and entries 7 and 8), so for this process the presence of two metals in **3F-Me** does not seem to provide any catalytic benefit. In general, the results shown in Table 3.4 improve those obtained with related [RuCl₂(*p*-

cymene)(NHC)] catalysts, for which longer reaction times were needed and proved to be less selective.²⁰

3.1.5.2 Hydroarylation of terminal alkenes

Encouraged by the results obtained in the arylation reaction, we decided to test our new ruthenium catalysts in the hydroarylation of terminal alkenes and study the compatibility of both processes, to evaluate whether we could combine them into a one tandem process. The hydroarylation of terminal alkenes has been known for a long time, and can be also regarded as the alkylation of aromatic rings with alkenes.⁴³ One of the limitations of the process is that it normally requires the use of activated alkenes, such as styrenes and vinylsilanes. However, this drawback was elegantly solved recently by Ackermann and co-workers, by using carboxylate-assisted ruthenium catalysts, which allowed the widening of the scope of the reaction to unactivated terminal alkenes.^{52,53}

Table 3.5 shows the results obtained in the hydroarylation of 2-phenylpyridine with different alkenes. The reactions were performed in the presence of a carboxylate (KOAc or KO₂CMes) and using a 5 % catalyst loading based on metal, at 120°C during 20 hours. First, we were interested in testing the compatibility of this process with the arylation reaction, so NMP and KOAc or KO₂CMes were employed (entries 1 and 2). Unfortunately, low conversions were achieved using these conditions. A dramatic improvement was observed when toluene was used as solvent (entry 3), and almost quantitative yields were obtained when it was combined with KO₂CMes (entry 4). Using these conditions, the monoalkylated products were selectively obtained in good yield when 2-phenylpyridine was reacted with 1-decene, 1-octene or 1-hexene. As for the arylation reaction, almost the same activity was observed for **3F-Me** and **II**. Interestingly, a small amount of the bisalkylated product was obtained when the activated trimethylvinylsilane was used (entry 11). As the reaction was performed during long periods of time and at high temperatures, a drop of mercury was added to the reaction media in order to discard that the reaction would be heterogeneously catalyzed.⁵⁴ In the presence of mercury the catalytic activity **3F-Me** did not decrease (compare entries 4 and 6), thus the heterogeneity of the reaction is very unlikely. The catalytic activity was comparable to the recently reported system based on [RuCl₂(*p*-cymene)]₂.⁵²

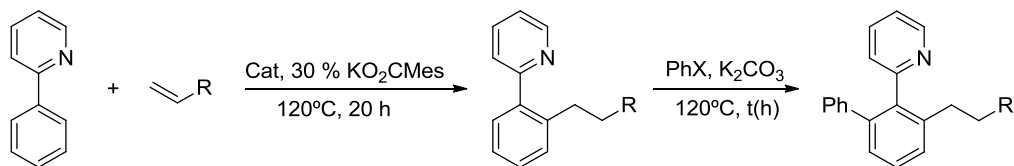
Table 3.5 Hydroarylation of terminal alkenes with 2-phenylpyridine, using catalysts **3F-Me** and **1I**^a

Entry	R	Cat	Additive	Solvent	Mono (%)	Bis(%) ^b
1		3F-Me	KOAc	NMP	6	-
2		3F-Me	KO ₂ CMe _s	NMP	14	-
3	<i>n</i> -octyl	3F-Me	KOAc	Toluene	72	-
4		3F-Me	KO ₂ CMe _s	Toluene	93 (81)	-
5		1I	KO ₂ CMe _s	Toluene	95	-
6 ^c		3F-Me	KO ₂ CMe _s	Toluene	93	-
7	<i>n</i> -hexyl	3F-Me	KO ₂ CMe _s	Toluene	94 (79)	-
8		1I	KO ₂ CMe _s	Toluene	96	-
9	<i>n</i> -butyl	3F-Me	KO ₂ CMe _s	Toluene	94 (80)	-
10		1I	KO ₂ CMe _s	Toluene	97	-
11	trimethylsilyl	3F-Me	KO ₂ CMe _s	Toluene	90 (80)	9 (7)

^aReaction conditions: 0.5 mmol 2-phenylpyridine, 1.5 mmol alkene, 0.15 mmol additive, 5 % catalyst loading (based on metal), 2 mL of solvent, 120°C, 20 h. Mes = 2,4,6-trimethylphenyl. ^bYields determined by GC using anisole (0.5 mmol) as internal standard. Isolated yields in parenthesis. ^cReaction carried out in the presence of a drop of mercury.

3.1.5.3 Sequential hydroarylation of alkenes and arylation of arylpyridines

Given that our new catalysts showed good activity in both chelation-assisted processes discussed above, we decided to test the viability of combining the two reactions in a sequential process, in order to produce unsymmetrically substituted arylpyridines. There are a few examples in the literature in which a catalytic system can promote two sequential chelation-assisted reactions, although in most cases, an extra amount of catalyst has to be added to the reaction media to promote the second catalytic cycle.^{51,55,56}

Table 3.6 Sequential hydroarylation of alkenes and arylation of arylpyridines catalyzed by **3F-Me**, **1I** and $[\text{RuCl}_2(p\text{-cymene})]_2$ ^a

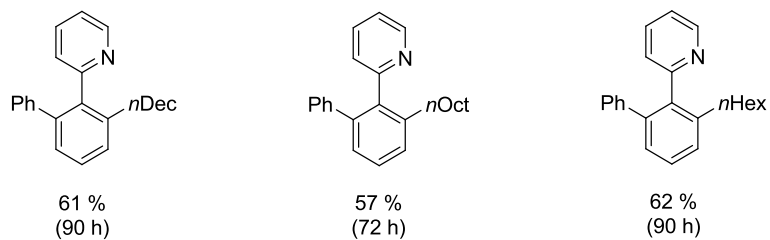
Entry	R	Cat	PhX	t (h)	Yield (%) ^b
1		1I	PhBr	24	38
2		1I	PhBr	72	51
3		3F-Me	PhCl	24	48
4		3F-Me	PhBr	24	52
5 ^c		3F-Me	PhBr	24	3
6 ^d	<i>n</i> -octyl	3F-Me	PhBr	24	15
7		3F-Me	PhBr	72	61
8		3F-Me	PhBr	90	71 (64)
9 ^e		3F-Me	PhBr	24	50
10		$[\text{RuCl}_2(p\text{-cymene})]_2$	PhBr	24	52
11		1I		24	32
12		1I		48	42
13	<i>n</i> -hexyl	3F-Me	PhBr	24	44
14		3F-Me		72	73 (62)
15		$[\text{RuCl}_2(p\text{-cymene})]_2$		24	51
16		1I		24	37
17		1I		48	49
18		3F-Me		24	45
19	<i>n</i> -butyl	3F-Me	PhBr	72	70
20		3F-Me		90	77 (65)
21		$[\text{RuCl}_2(p\text{-cymene})]_2$		24	45
22		$[\text{RuCl}_2(p\text{-cymene})]_2$		48	60

^aReaction conditions: 0.5 mmol 2-phenylpyridine, 1.5 mmol alkene, 0.15 mmol KO_2CMes , 5 % catalyst loading (based on metal), 2 mL of toluene, 120°C, 20 h. Then 1 mmol of PhX and 1 mmol K_2CO_3 , 120°C for the appropriate time. ^bYields determined by GC using anisole (0.5 mmol) as internal standard. Isolated yields in parenthesis. ^c2 mL of H_2O were added in the second step of the reaction. ^d2 mL of NMP were added in the second step of the reaction. ^eThe reaction was carried out in the presence of a drop of mercury.

Because the hydroarylation of alkenes selectively yields the monoalkylated products, we decided to design the sequence by first running the alkylation, and then the subsequent arylation of the remaining *ortho*-C-H bond of the phenyl ring. Toluene was the solvent of choice, because it showed to be the optimum one for the hydroarylation, and proved to be good for the arylation.⁵⁷ The reactions were performed treating 2-phenylpyridine with the appropriate terminal alkene, in toluene, in the presence of KO₂CMe and 5 % of catalyst loading (based on metal), at 120°C during 20 hours. Then, the corresponding arylhalide and K₂CO₃ were added, and the reactions were heated at 120°C for the appropriate time. The results for the sequential process are listed in Table 3.6 where *t* (time) refers to the time for the second step of the reaction (arylation). The catalysts provided moderate yields of the unsymmetrically substituted phenylpyridines after 24 hours (38-52 % GC yield). To improve these results, the reaction time had to be increased up to 90 h, for which good yields were achieved (71-77 % GC yield, entries 8, 14 and 20). This indicates that the catalysts are active even at long reaction periods. In order to reduce the reaction time, water or NMP were added at the beginning of the second step, since these solvents are known to favor the arylation,^{49,50} although we did not observe any improvements (compare entry 4 with entries 5 and 6). Noteworthy, although in the individual steps catalysts **3F-Me** and **1I** showed almost the same activities, in this case the bimetallic complex **3F-Me** performs better than the mono-ruthenium complex **1I**. [RuCl₂(*p*-cymene)]₂ was also used for comparative purposes, showing similar activity to that of **3F-Me**.

Since the reaction implies high temperatures and long reaction periods, a drop of mercury was added to the reaction mixture to discard that the reaction is heterogeneously catalyzed. Under these conditions almost the same yield of the unsymmetrically substituted arylpyridine is obtained (compare entries 4 and 9 in Table 3.6), thus suggesting that the process is homogeneously catalyzed.

It is important to point out that this is the first time that a sequential approach combining alkylation/arylation is carried out for obtaining mixed arylated/alkylated arylpyridines, a fact that is even more remarkable if we take into account that only one catalyst is used. Scheme 3.10 depicts the maximum isolated yields in the production of unsymmetrically substituted arylpyridines using catalyst **3F-Me**.



Scheme 3.10 Maximum isolated yields in the production of unsymmetrically substituted arylpyridines using catalyst **3F-Me**.

3.2 Conclusions

In this section we have prepared and characterized new pyrene-bis-azolium and pyrene-mono-azolium salts. The synthesis of the bis-azoliums occurred through an unexpected reactivity in the bisannulation step, providing bis-azolium salts bearing N-alkyl groups coming from trisalkyl orthoformate employed. We have studied the photochemical properties of these salts that have shown emission in the range of 370-420 nm, and quantum yields ranging from 0.29 to 0.41.

The pyrene-basedazolium salts were used as *Janus*-type bis-NHC precursors. These ligands were coordinated to IrCl(COD) (complexes **1F**), RhCl(COD) (complexes **2F**) and RuCl₂(*p*-cymene) (complex **3F-Me**) fragments yielding homo-bimetallic complexes that were fully characterized by standard spectroscopic techniques. The monometallic analogue of **3F-Me** (**1I**) was also synthesized and characterized.

The electronic properties of the bis-NHC ligands were studied using the carbonyl derivatives **4F**, concluding that their electron-donating power is very similar to the one showed for 1,3-diethylbenzimidazolylidene. Electrochemical measurements of **1F-Et** and **3F-Me** showed that the electronic communication between the metals bridged by these ligands is almost negligible.

The catalytic activity of the two RuCl₂(*p*-cymene) complexes (**3F-Me** and **1I**) was tested in three chelation-assisted reactions: arylation of arylpyridines, hydroarylation of terminal alkenes and in the combination of these two processes to yield mixed arylated/alkylated arylpyridines. Both catalysts provide very similar catalytic performances for the first two processes, while for the combination of the two catalytic reactions the bimetallic catalyst **3F-Me** show higher catalytic activities.

3.3 References

- (1) Guerret, O.; Solé, S.; Gornitzka, H.; Teichert, M.; Trinquier, G.; Bertrand, G. *J. Am. Chem. Soc.* **1997**, *119*, 6668.
- (2) Boydston, A. J.; Williams, K. A.; Bielawski, C. W. *J. Am. Chem. Soc.* **2005**, *127*, 12496.
- (3) Khramov, D. M.; Boydston, A. J.; Bielawski, C. W. *Angew. Chem. Int. Ed.* **2006**, *45*, 6186.
- (4) Prades, A.; Poyatos, M.; Mata, J. A.; Peris, E. *Angew. Chem. Int. Ed.* **2011**, *50*, 7666.
- (5) Prades, A.; Peris, E.; Alcarazo, M. *Organometallics* **2012**, *31*, 4623.
- (6) Tennyson, A. G.; Rosen, E. L.; Collins, M. S.; Lynch, V. M.; Bielawski, C. W. *Inorg. Chem.* **2009**, *48*, 6924.
- (7) Mata, J. A.; Hahn, F. E.; Peris, E. *Chem. Sci.* **2014**, *5*, 1723.
- (8) Karimi, B.; Akhavan, P. F. *Chem. Commun.* **2009**, 3750.
- (9) Guisado-Barrios, G.; Hiller, J.; Peris, E. *Chem. Eur. J.* **2013**, *19*, 10405.
- (10) Boydston, A. J.; Pecinovsky, C. S.; Chao, S. T.; Bielawski, C. W. *J. Am. Chem. Soc.* **2007**, *129*, 14550.
- (11) Boydston, A. J.; Vu, P. D.; Dykhno, O. L.; Chang, V.; Wyatt, A. R.; Stockett, A. S.; Ritschdorff, E. T.; Shear, J. B.; Bielawski, C. W. *J. Am. Chem. Soc.* **2008**, *130*, 3143.
- (12) Er, J. A. V.; Tennyson, A. G.; Kamplain, J. W.; Lynch, V. M.; Bielawski, C. W. *Eur. J. Inorg. Chem.* **2009**, 1729.
- (13) Wiggins, K. M.; Kerr, R. L.; Chen, Z.; Bielawski, C. W. *J. Mater. Chem.* **2010**, *20*, 5709.
- (14) Figueira-Duarte, T. M.; Müllen, K. *Chem. Rev.* **2011**, *111*, 7260.
- (15) Khramov, D. M.; Boydston, A. J.; Bielawski, C. W. *Org. Lett.* **2006**, *8*, 1831.
- (16) Hu, J.; Era, M.; Elsegood, M. R. J.; Yamato, T. *Eur. J. Org. Chem.* **2010**, 72.
- (17) Tapu, D.; Owens, C.; VanDerveer, D.; Gwaltney, K. *Organometallics* **2009**, *28*, 270.
- (18) Corberán, R.; Sanaú, M.; Peris, E. *J. Am. Chem. Soc.* **2006**, *128*, 3974.
- (19) Viciano, M.; Mas-Marzá, E.; Sanaú, M.; Peris, E. *Organometallics* **2006**, *25*, 3063.
- (20) Prades, A.; Poyatos, M.; Peris, E. *Adv. Synth. Catal.* **2010**, *352*, 1155.

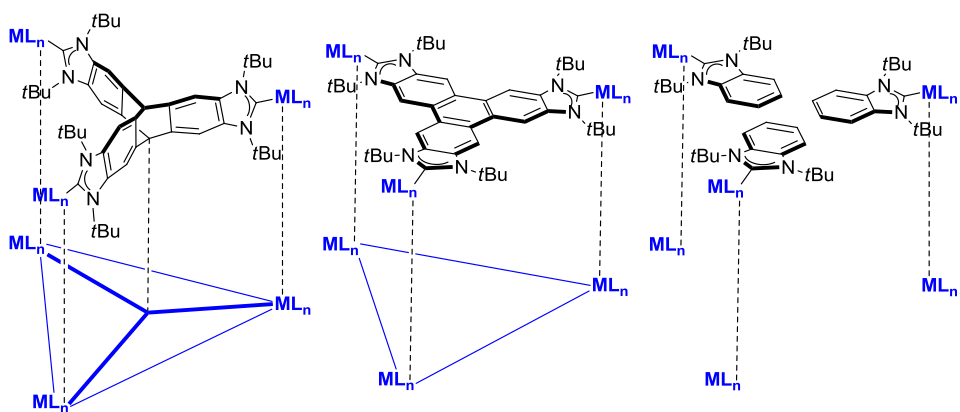
- (21) Hu, J.; Zhang, D.; Harris, F. W. *J. Org. Chem.* **2005**, *70*, 707.
- (22) Viciano, M.; Sanaú, M.; Peris, E. *Organometallics* **2007**, *26*, 6050.
- (23) Wang, H. M. J.; Lin, I. J. B. *Organometallics* **1998**, *17*, 972.
- (24) Poyatos, M.; Mas-Marzá, E.; Sanaú, M.; Peris, E. *Inorg. Chem.* **2004**, *43*, 1793.
- (25) Cariou, R.; Fischmeister, C.; Toupet, L.; Dixneuf, P. H. *Organometallics* **2006**, *25*, 2126.
- (26) Ozdemir, I.; Demir, S.; Cetinkaya, B.; Toupet, L.; Castarlenas, R.; Fischmeister, C.; Dixneuf, P. H. *Eur. J. Inorg. Chem.* **2007**, 2862.
- (27) Valeur, B.; Berberan-Santos, N. M. *Molecular Fluorescence. Principles and Applications*; Second Edi.; Wiley-VCH, 2013.
- (28) Tolman, C. A. *Chem. Rev.* **1977**, *77*, 313.
- (29) Chianese, A. R.; Li, X.; Janzen, M. C.; Faller, J. W.; Crabtree, R. H. *Organometallics* **2003**, *22*, 1663.
- (30) Kelly III, R. A.; Clavier, H.; Giudice, S.; Scott, N. M.; Stevens, E. D.; Bordner, J.; Samardjiev, I.; Hoff, C. D.; Cavallo, L.; Nolan, S. P. *Organometallics* **2008**, *27*, 202.
- (31) Dröge, T.; Glorius, F. *Angew. Chem. Int. Ed.* **2010**, *49*, 6940.
- (32) Nelson, D. J.; Nolan, S. P. *Chem. Soc. Rev.* **2013**, *42*, 6723.
- (33) Wolf, S.; Plenio, H. *J. Organomet. Chem.* **2009**, *694*, 1487.
- (34) Leuthäusser, S.; Schwarz, D.; Plenio, H. *Chem. Eur. J.* **2007**, *13*, 7195.
- (35) Wolf, S.; Plenio, H. *J. Organomet. Chem.* **2010**, *695*, 2418.
- (36) Mercs, L.; Neels, A.; Albrecht, M. *Dalton Trans.* **2008**, 5570.
- (37) Sabater, S.; Mata, J. A.; Peris, E. *Organometallics* **2012**, *31*, 6450.
- (38) Sakamoto, R.; Kambe, T.; Tsukada, S.; Takada, K.; Hoshiko, K.; Kitagawa, Y.; Okumura, M.; Nishihara, H. *Inorg. Chem.* **2013**, *52*, 7411.
- (39) Morris, R. B.; Day, P. *Adv. Inorg. Chem. Radiochem.* **1967**, *10*, 247.
- (40) Gusev, D. G.; Peris, E. *Dalton Trans.* **2013**, *42*, 7359.
- (41) Nussbaum, M.; Schuster, O.; Albrecht, M. *Chem. Eur. J.* **2013**, *19*, 17517.
- (42) Arockiam, P. B.; Bruneau, C.; Dixneuf, P. H. *Chem. Rev.* **2012**, *112*, 5879.

- (43) Murai, S.; Kakiuchi, F.; Sekine, S.; Tanaka, Y.; Kamatani, A.; Sonoda, M.; Chatani, N. *Nature* **1993**, *366*, 529.
- (44) Kakiuchi, F.; Murai, S. *Acc. Chem. Res.* **2002**, *35*, 826.
- (45) Ackermann, L.; Vicente, R.; Kapdi, A. R. *Angew. Chem. Int. Ed.* **2009**, *48*, 9792.
- (46) Ackermann, L. *Chem. Commun.* **2010**, *46*, 4866.
- (47) Oi, S.; Fukita, S.; Hirata, N.; Watanuki, N.; Miyano, S.; Inoue, Y. *Org. Lett.* **2001**, *3*, 2579.
- (48) Ozdemir, I.; Demir, S.; Cetinkaya, B.; Gourlaouen, C.; Maseras, F.; Bruneau, C.; Dixneuf, P. H. *J. Am. Chem. Soc.* **2008**, *130*, 1156.
- (49) Požgan, F.; Dixneuf, P. H. *Adv. Synth. Catal.* **2009**, *351*, 1737.
- (50) Arockiam, P. B.; Fischmeister, C.; Bruneau, C.; Dixneuf, P. H. *Angew. Chem. Int. Ed.* **2010**, *49*, 6629.
- (51) Arockiam, P. B.; Fischmeister, C.; Bruneau, C.; Dixneuf, P. H. *Green Chem.* **2013**, *15*, 67.
- (52) Schinkel, M.; Marek, I.; Ackermann, L. *Angew. Chem. Int. Ed.* **2013**, *52*, 3977.
- (53) Schinkel, M.; Wallbaum, J.; Kozhushkov, S. I.; Marek, I.; Ackermann, L. *Org. Lett.* **2013**, *15*, 4482.
- (54) Crabtree, R. H. *Chem. Rev.* **2012**, *112*, 1536.
- (55) Ackermann, L.; Born, R.; Alvarez-Bercedo, P. *Angew. Chem. Int. Ed.* **2007**, *46*, 6364.
- (56) Li, B.; Bheeter, C. B.; Darcel, C.; Dixneuf, P. H. *ACS Catal.* **2011**, *1*, 1221.
- (57) Ackermann, L.; Vicente, R.; Althammer, A. *Org. Lett.* **2008**, *10*, 2299.

Chapter 4

A triphenylene-based tris-NHC ligand.

Coordination properties and catalytic activity



4.1 Results and discussion

As discussed in Chapter 3, and in the general introduction provided in Chapter 1, bimetallic and polymeric complexes based on *Janus*-type bis-NHC ligands have shown very attractive properties in several fields.¹⁻⁴ Despite the extraordinary synthetic versatility of NHCs, there are only a few examples of rigid tritopic NHC ligands that could maintain a fixed distance between three metal centers. In fact, the only example before this PhD work, was the one reported by Bielawski and co-workers (Chart 4.1),⁵ which consisted of a D_{3h} -symmetric tris-NHC connected by a triptycene core. In this example, the electronic communication between the three carbene units is disrupted due to the presence of the saturated core. Although this tris-NHC possesses a great potential as a ligand for multimetallic complexes, the authors only reported the free carbene, thus not affording any information about its coordination capabilities.

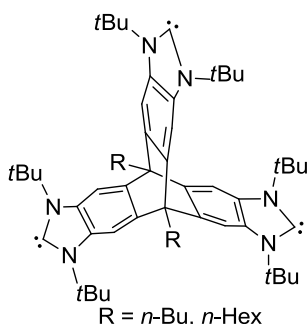


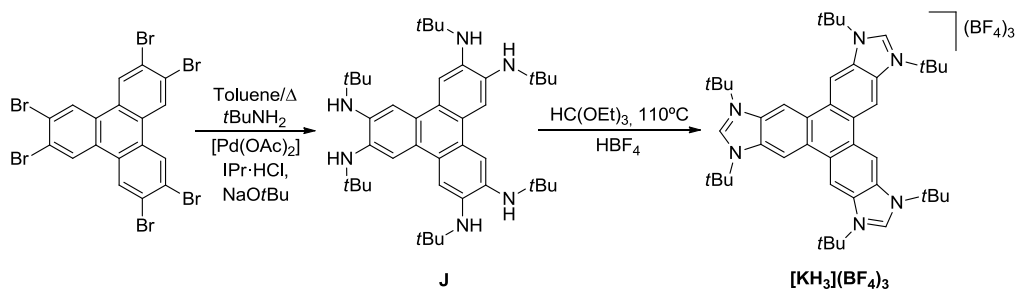
Chart 4.1

We were interested in building ligands that provided the maximum electronic communication between metals, for which we thought that a rigid and planar polyaromatic system should satisfy our needs. In this context, we envisioned the great potential of a tris-NHC ligand with a rigid structure based on triphenylene. This ligand should be able to bear three metal fragments at a fixed distance, and could potentially provide electronic communication between them due to the presence of the extended π -delocalized system. In the next sections, the synthesis and characterization of a triphenylene-based tris-imidazolium salt and the related tris-NHC-based complexes will be discussed. The synthesis and characterization of main-chain microporous organometallic polymers based on triphenylene-tris-NHC gold

species will also be described. The electrochemical and catalytic properties of these compounds will be studied as well.

4.1.1 Synthesis of tris-imidazolium salts $[\text{KH}_3](\text{BF}_4)_3$ and $[\text{MH}_3](\text{BF}_4)_3$

Scheme 4.1 shows the synthetic route used to obtain the tris-imidazolium salt $[\text{KH}_3](\text{BF}_4)_3$. The starting material was 2,3,6,7,10,11-hexabromotriphenylene, which was synthesized following a previously reported procedure.⁶ The first step consists of a multifold amination using the same reaction conditions employed earlier for the preparation of the tetra-aminopyrene compounds (**E-tBu** and **E-tAmyl**) in Chapter 3, and similar to those described by Bielawski and co-workers.^{5,7} The reaction was carried out in the presence of a palladium catalyst (generated from the reaction of IPr·HCl, $[\text{Pd}(\text{OAc})_2]$ and NaOtBu), 2,3,6,7,10,11-hexabromotriphenylene and *t*-butylamine in refluxing toluene. The reaction afforded the desired hexa-amino-triphenylene **J**, in quasi-quantitative yield (98 %) as a dark red, sun-light sensitive solid.

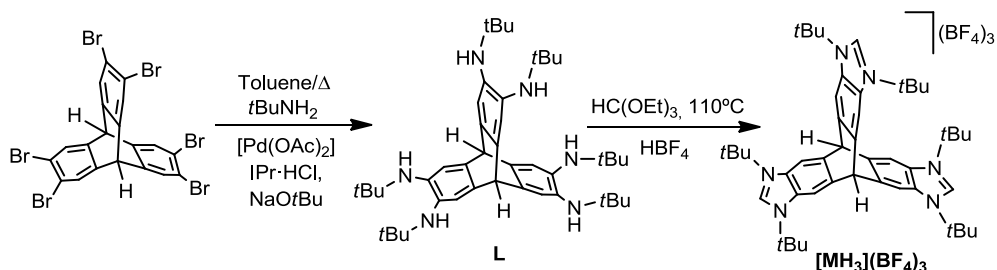


Scheme 4.1 Synthesis of $[\text{KH}_3](\text{BF}_4)_3$

The second step of the synthesis involves the formylative cyclization of **J** in the presence of triethyl orthoformate and tetrafluoroboric acid. The reaction yields the expected tris-imidazolium salt $[\text{KH}_3](\text{BF}_4)_3$ as an off-white solid in excellent yield (96 %) after precipitation from a mixture CH_3CN /diethyl ether.

For comparative purposes, a triptycene-containing tris-imidazolium salt was synthesized. The synthetic route to this compound is based on that described earlier by Bielawski and co-workers.⁵ Scheme 4.2 shows the two-steps procedure followed to obtain $[\text{MH}_3](\text{BF}_4)_3$ starting from 2,3,6,7,12,13-hexabromotriptycene.⁸ The multifold amination of this compound employing identical conditions as those used to

obtain compound **J**, quantitatively yielded the hexa-aminotriptycene **L**, as a brown solid. Tris-annulation of **L** with triethyl orthoformate and tetrafluoroboric acid affords the tris-imidazolium salt $[\text{MH}_3](\text{BF}_4)_3$, which was obtained as an off-white tan solid in excellent yield (96 %), after precipitation with diethyl ether.



Scheme 4.2 Synthesis of $[\text{MH}_3](\text{BF}_4)_3$

Compounds **J**, $[\text{KH}_3](\text{BF}_4)_3$, **L** and $[\text{MH}_3](\text{BF}_4)_3$ were characterized by means of NMR spectroscopy and mass spectrometry. As an example, the NMR spectroscopic characterization of $[\text{KH}_3](\text{BF}_4)_3$ is described below. All the details regarding the characterization of the other compounds can be found in the Experimental Section (Chapter 5).

¹H NMR spectrum of $[\text{KH}_3](\text{BF}_4)_3$

Figure 4.1 shows the ¹H NMR spectrum of $[\text{KH}_3](\text{BF}_4)_3$. The number of signals and their integration are consistent with the D_{3h} symmetry of the compound. The resonance attributed to the aromatic protons of the triphenylene core is shown as a singlet at 9.20 ppm (*a*). The singlet due the acidic protons of the NCHN (*b*) appears at 9.17 ppm. The signal assigned to the protons of the *t*-butyl groups bonded to the nitrogen of the imidazole ring is displayed as a singlet at 2.04 ppm (*c*).

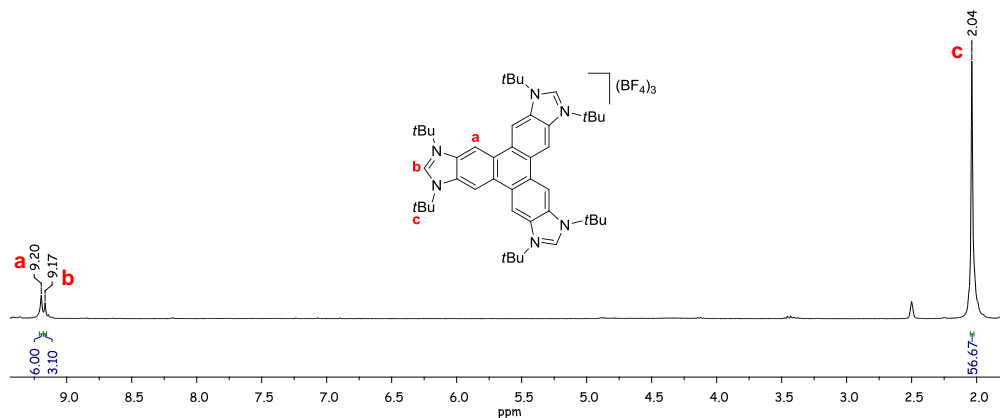


Figure 4.1 ^1H NMR spectrum of $[\text{KH}_3](\text{BF}_4)_3$ in $\text{DMSO-}d_6$

$^{13}\text{C}\{^1\text{H}\}$ NMR spectrum of $[\text{KH}_3](\text{BF}_4)_3$

Figure 4.2 shows the $^{13}\text{C}\{^1\text{H}\}$ NMR spectrum of $[\text{KH}_3](\text{BF}_4)_3$. The number of signals displayed in the spectrum is consistent with the three-fold symmetry of the compound. The signal attributed to the NCHN carbons (1) is displayed at 142.6 ppm. The resonances due to the aromatic $\text{C}_{\text{quaternary}}$ and CH groups of the triphenylene core are shown at 131.3, 126.7 (2) and 112.0 ppm (3), respectively. The signal assigned to the carbons of the *t*-butyl substituents are observed at 61.9 and 28.5 ppm (4 and 5 respectively).

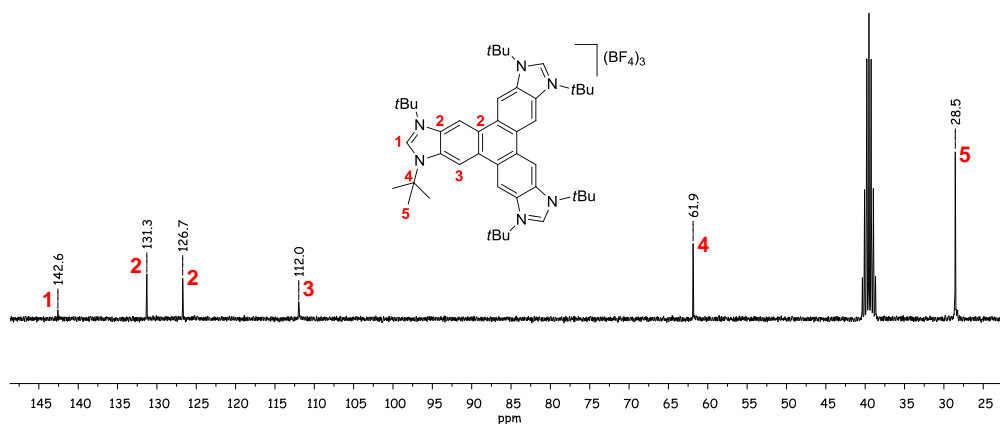
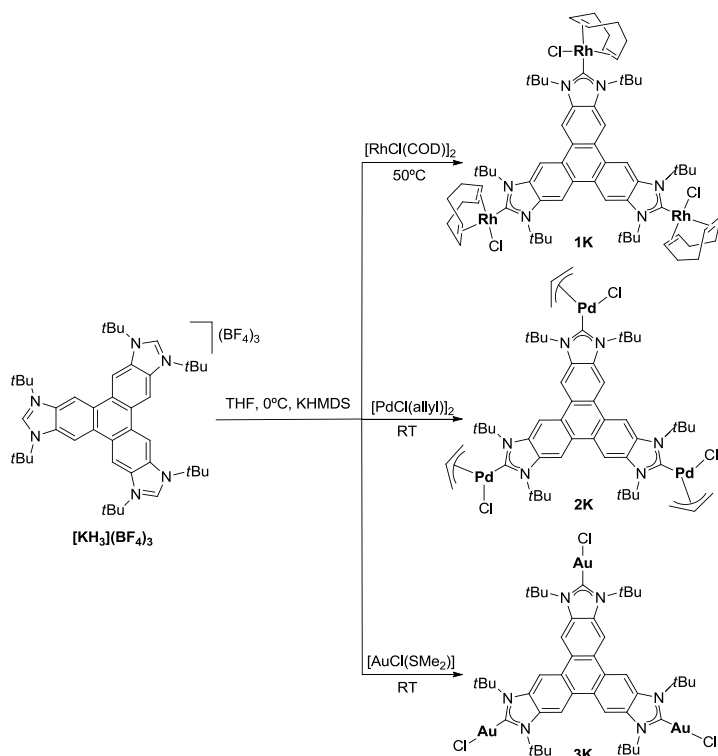


Figure 4.2 $^{13}\text{C}\{^1\text{H}\}$ NMR spectrum of $[\text{KH}_3](\text{BF}_4)_3$ in $\text{DMSO-}d_6$

4.1.2 Synthesis of trimetallic complexes

Scheme 4.3 depicts the methodology employed to obtain the trimetallic complexes **1K** to **3K**. In the first step of the reaction, $[\text{KH}_3](\text{BF}_4)_3$ was treated with potassium bis(trimethylsilyl)amide (KHMSD) at 0°C in THF, in order to generate the free carbene, which was used *in situ* for the reaction with the corresponding metal precursor ($[\text{RhCl}(\text{COD})]_2$, $[\text{PdCl}(\text{allyl})]_2$ or $[\text{AuCl}(\text{SMe}_2)]$).

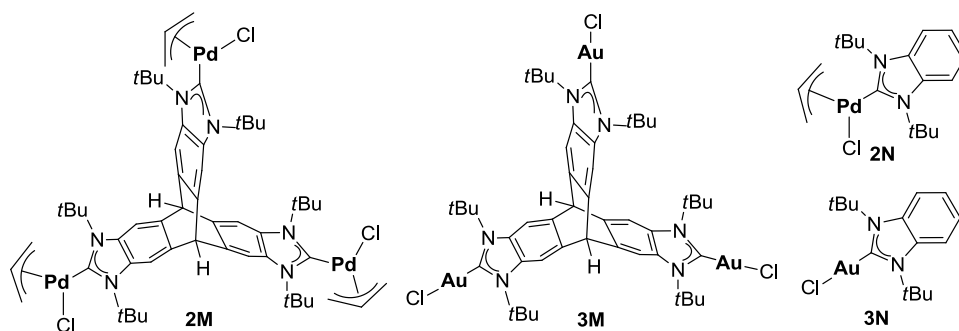


Scheme 4.3 Synthesis of trimetallic complexes **1K** to **3K**

While **2K** and **3K** were prepared at room temperature, the isolation of **1K** in good yield required higher temperatures (50°C). Compounds **1K** and **2K** were obtained as yellow solids in moderate yields (42 and 40 %, respectively) after purification by column chromatography and precipitation from a mixture dichloromethane/hexanes. Compound **3K** was obtained as a yellow solid after precipitation from a mixture dichloromethane/pentane (yield 62 %).

For comparative purposes, the tri-palladium and tri-gold complexes (**2M** and **3M**, respectively in Scheme 4.4) based on a triptycene tris-NHC were obtained using the

same synthetic protocol shown in Scheme 4.3. Unfortunately, efforts to obtain the tris-rhodium complex based on this ligand were unfruitful regardless of the reaction conditions employed. The monometallic complexes **2N** and **3N** based on a 1,3-bis(*tert*-butyl)benzimidazolylidene ligand, were also obtained using the methodology depicted in Scheme 4.3. It is worth mentioning that the monometallic complexes (**2N** and **3N**) can be regarded as exactly one third of the trimetallic complexes (**2K** and **3K**, respectively).



Scheme 4.4

Due to the relative disposition of the chloride ligands in compounds **1K** and **2K**, two atropisomers are possible (Figure 4.3). In the *syn*-atropisomer all the chloride ligands are pointing to the same side of the molecule, while in the *anti*-atropisomer two chlorides are pointing to one side of the molecule and the third to the opposite side. The ^1H NMR spectrum of **2K** is complicated because, apart from the possible atropisomers depicted in Figure 4.3, the three η^3 -allyl ligands can present η^3 - η^1 - η^3 isomerization,⁹ breaking the symmetry of the compound. VT-NMR experiments did not provide any simplification of the ^1H NMR spectra, either at low or high temperatures. On the other hand, complex **1K** shows only the *syn*-atropisomer by NMR spectroscopy. The VT-NMR experiments did not allow to detect any interconversion between the *syn*- and *anti*-atropisomers, probably due to the restricted rotation about the C-Rh bond due to the steric bulk of the *t*-butyl substituents of the wingtips.¹⁰

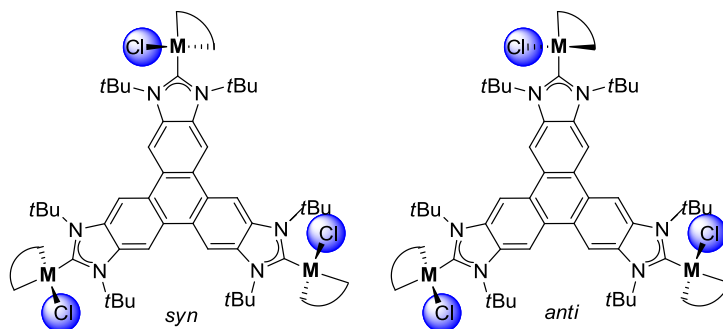


Figure 4.3 Possible *syn* and *anti*-atropisomers of compounds **1K** (M = Rh(COD)) and **2K** (M = Pd(η^3 -allyl))

All compounds described in this section were characterized by means of NMR spectroscopy, mass spectrometry and elemental analysis. The molecular structures of **1K**, **3K**, **3M** and **3N** were unambiguously confirmed by X-Ray Diffraction studies. Due to the similarity between all these compounds, only the NMR spectroscopic characterization of **1K** is described below. All the details regarding the characterization of the other complexes can be found in the Experimental Section (Chapter 5).

¹H NMR spectrum of 1K

Figure 4.4 shows the ¹H NMR spectrum of **1K**. The number of signals and their integration are consistent with the three-fold symmetry of the compound and with the presence of only the *syn*-atropisomer. The resonance attributed to the aromatic protons of the triphenylene core is shown as a singlet at 8.74 ppm (*a*). The resonance corresponding to the protons of the *t*-butyl groups of the wingtips are displayed as a singlet at 2.58 ppm (*b*). The rest of the resonances corresponding to the protons of the COD ligands are conveniently displayed on the spectrum.

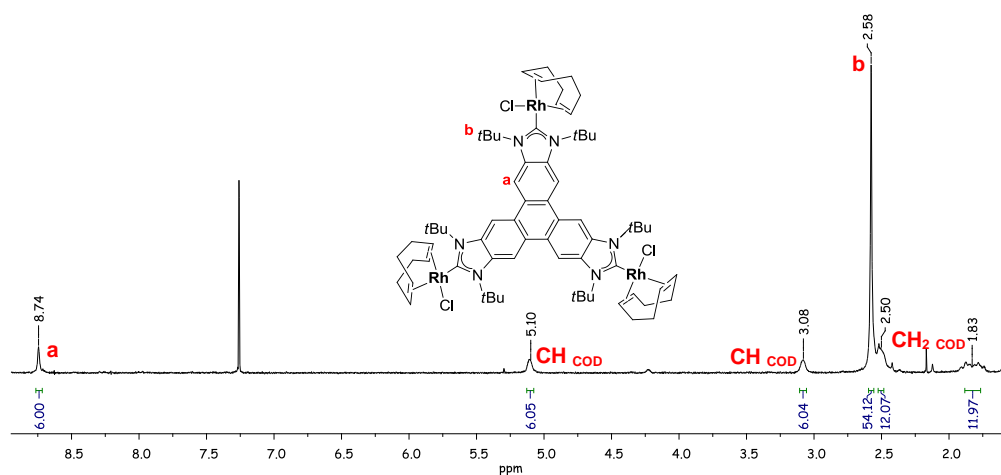


Figure 4.4 ^1H NMR spectrum of **1K** in CDCl_3

$^{13}\text{C}\{^1\text{H}\}$ NMR spectrum of **1K**

Figure 4.5 shows the $^{13}\text{C}\{^1\text{H}\}$ NMR spectrum of **1K**. Again, the number of signals displayed in the spectrum is consistent with the three-fold symmetry of the compound, and with the presence of only the *syn*-atropisomer. The most characteristic signal is the doublet attributed to the magnetically equivalent metallated carbene-carbons at 200.9 ppm ($^1J_{\text{Rh-C}} = 49.1$ Hz) (*I*). The resonances due to the aromatic $\text{C}_{\text{quaternary}}$ and CH groups of the triphenylene core are shown at 135.5, 124.0 (*2*) and 107.9 ppm (*3*), respectively. The signals assigned to the carbons of the *t*-butyl substituents are observed at 60.9 and 32.6 ppm (*4* and *5*, respectively). The rest of the resonances corresponding to the carbons of the COD ligands are conveniently displayed on the spectrum.

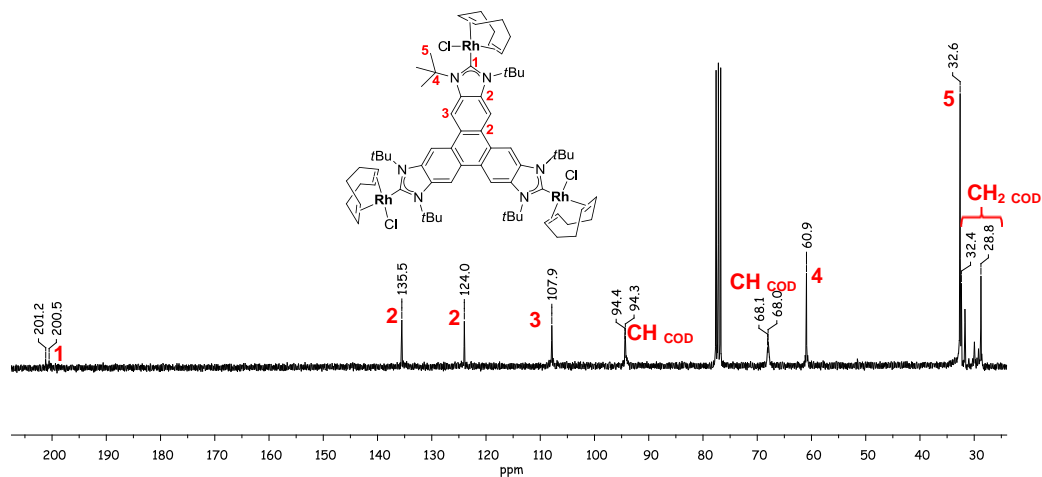


Figure 4.5 $^{13}\text{C}\{^1\text{H}\}$ NMR spectrum of **1K** in CDCl_3

Molecular structure of **1K**

Crystals of **1K** suitable for X-Ray Diffraction analysis were obtained by slow diffusion of diethyl ether into a concentrated solution of the compound in acetonitrile.

The molecular structure of **1K** (Figure 4.6) consists of a triphenylene-based tris-imidazolylidene ligand connecting three rhodium atoms, which complete their coordination sphere with a COD and a chloride ligands. The molecular structure shown in Figure 4.6 confirms the presence of only the *syn*-atropisomer in which the three chloride ligands are pointing toward the same side of the molecule.

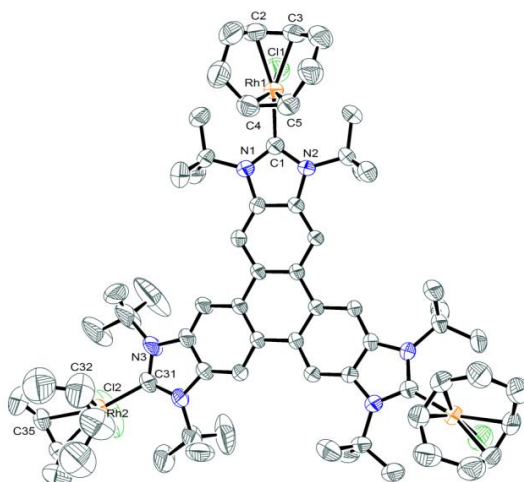


Figure 4.6 Molecular diagram of complex **1K**. Ellipsoids at 50 % probability. Hydrogen atoms and solvent (MeCN) have been omitted for clarity

Interestingly, the triphenylenic core provides a slightly twisted structure (Figure 4.7). Table 4.1 shows the most representative bond lengths (Å) and angles (°) of complex **1K**. The Rh-C_{carbene} average distance is 2.065(8) Å, and the through-space distance between the metals is 13.4085(10) Å. The average angle between the plane containing theazole ring and the coordination plane of the rhodium fragment is 89.01(18)°.

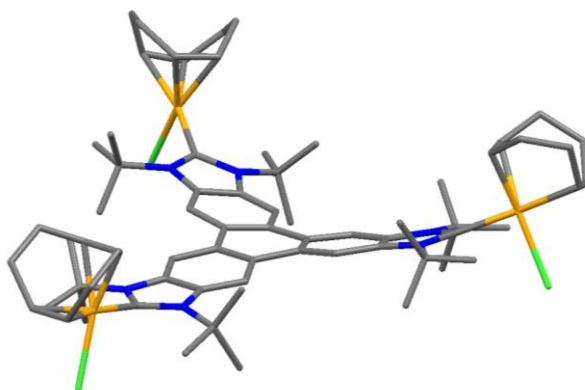


Figure 4.7 Side-on view of **1K**

Table 4.1 Selected bond lengths and angles of complex **1K**

Bond lengths (Å)		Bond angles (°)	
Rh(1)-C(1)	2.060(6)	C(1)-Rh(1)-Cl(1)	91.28(18)
Rh(1)-Cl(1)	2.413(2)	C(31)-Rh(2)-Cl(2)	94.5(4)
Rh(1)-C(2)	2.223(7)		
Rh(1)-C(3)	2.194(6)		
Rh(1)-C(4)	2.098(7)		
Rh(1)-C(5)	2.121(7)		
Rh(2)-C(31)	2.073(9)		
Rh(2)-C(32)	2.071(11)		
Rh(2)-Cl(2)	2.380(5)		
Rh-Rh	13.4085(10)		

Molecular structure of 3K

Crystals of **3K** suitable for X-Ray Diffraction analysis were obtained by slow diffusion of hexane into a concentrated solution of the compound in chloroform.

The molecular structure of **3K** (Figure 4.8) consists of a triphenylene-based tris-imidazolylidene ligand connecting three gold atoms, which complete their coordination sphere with a chloride ligand. In this case, the triphenylenic core also deviates from planarity, as observed in Figure 4.9.

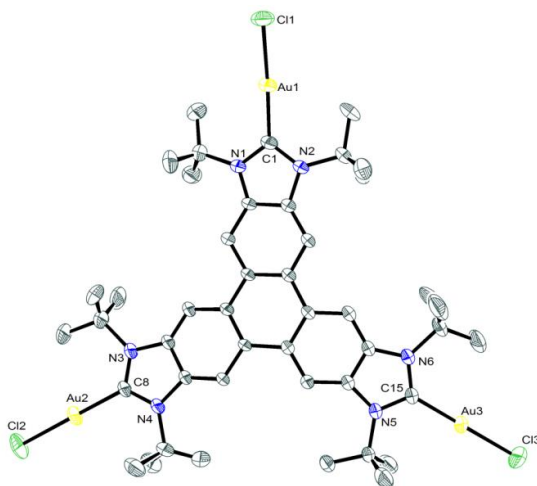


Figure 4.8 Molecular diagram of complex **3K**. Ellipsoids at 50 % probability. Hydrogen atoms have been omitted for clarity

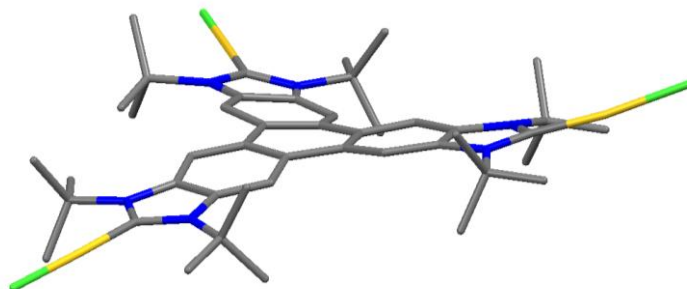


Figure 4.9 Side-on view of **3K**

Table 4.2 shows the most representative bond lengths (Å) and angles (°) of complex **3K**. The Au-C_{carbene} average distance is 1.997(14) Å, and the through-space distance between the metals is 13.4854(19) Å. The average of the C-Au-Cl angle is 178.0(5)°.

Table 4.2 Selected bond lengths and angles of complex **3K**

Bond lengths (Å)		Bond angles (°)	
Au(1)-C(1)	1.997(12)	C(1)-Au(1)-Cl(1)	175.4(3)
Au(1)-Cl(1)	2.297(4)	C(8)-Au(2)-Cl(2)	179.5(4)
Au(2)-C(8)	2.011(11)	C(15)-Au(3)-Cl(3)	179.1(5)
Au(2)-Cl(2)	2.282(4)		
Au(3)-C(15)	1.984(12)		
Au(3)-Cl(3)	2.269(5)		
Au-Au	13.4854(19)		

Molecular structure of 3M

Crystals of **3M** suitable for X-Ray Diffraction analysis were obtained by slow diffusion of diethyl ether into a concentrated solution of the compound in chloroform.

The molecular structure of **3M** (Figure 4.10) consists of a triptycene-based tris-imidazolylidene ligand connecting three gold atoms, which complete their coordination sphere with a chloride ligand. Table 4.3 shows the most representative bond lengths (Å) and angles (°) of complex **3M**. The average of the C-Au-Cl angle is 179.8(11)°, therefore illustrating the perfect linear arrangement of the ligand about the metal. The Au-C_{carbene} average distance is 2.08(4) Å, and the through-space distance between the metals is 13.642(3) Å. It is worth mentioning that the latter distance is very similar to those observed in the triphenylene-based trimetallic complexes **1K** and **3K** (*vide supra*).

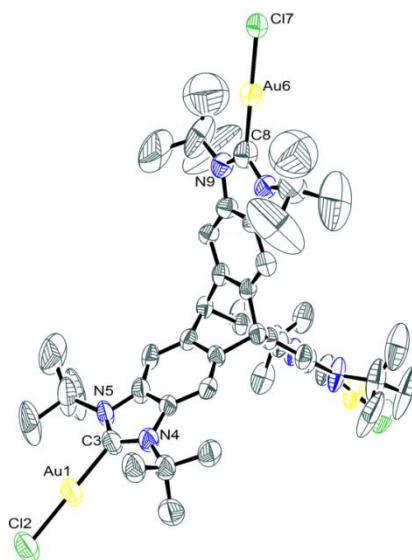


Figure 4.10 Molecular diagram of complex **3M**. Ellipsoids at 30 % probability. Hydrogen atoms and solvent (diethyl ether) have been omitted for clarity

Table 4.3 Selected bond lengths and angles of complex **3M**

Bond lengths (Å)		Bond angles (°)	
Au(1)-C(3)	2.10(2)	C(3)-Au(1)-Cl(2)	179.7(11)
Au(1)-Cl(2)	2.263(8)	C(8)-Au(6)-Cl(7)	180.000(3)
Au(6)-C(8)	2.03(4)		
Au(6)-Cl(7)	2.268(7)		
Au-Au	13.642(3)		

Molecular structure of 3N

Suitable crystals of **3N** for X-Ray Diffraction analysis were obtained by slow diffusion of hexane into a concentrated solution of the compound in chloroform.

The molecular structure of **3N** (Figure 4.11) consists of a 1,3-di(*tert*-butyl)benzimidazolyliene ligand coordinated to a gold atom, which completes its coordination sphere with a chloride ligand. Table 4.4 shows the most representative bond lengths (Å) and angles (°) of complex **3N**. The Au-C_{carbene} distance is 1.989(3) Å, and the C-Au-Cl angle is 176.37(8)°

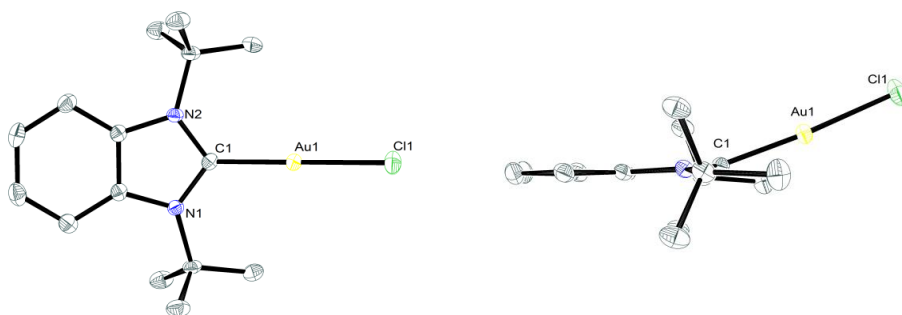


Figure 4.11 Two perspectives of the molecular structure of complex **3N**. Ellipsoids at 50 % probability. Hydrogen atoms have been omitted for clarity

Table 4.4 Selected bond lengths and angles of complex **3N**

Bond lengths (Å)		Bond angles (°)	
Au(1)-C(1)	1.989(3)	C(1)-Au(1)-Cl(1)	176.37(8)
Au(1)-Cl(1)	2.2779(8)		

From the side-on view of the molecular structure of **3N** (Figure 4.11, right), it can be observed that the gold atom is 0.59 Å above the plane defined by the azole ring. This unusual feature is also observed in the other structures discussed above, for complexes **1K**, **3K** and **3M**. The average deviation distances of the metals in these compounds are shown in Table 4.5.

Table 4.5 Deviation distance of the metal atom from the azole plane in compounds **1K**, **3K**, **3M** and **3N**

Compound	Deviation Distance (Å)
1K	0.48
3K	0.23
3M	0.16
3N	0.59

Bielawski and co-workers also observed this deviation of the metal center from the azole plane in their benzo(bisimidazolylidene) ligand bearing bulky adamantyl groups, when it was coordinated to RhCl(COD) fragments. In this case, the metal is 0.75 Å above the plane defined by the benzimidazolylidene.¹¹ In our case the

deviations are smaller, probably due to the lower bulkiness provided by the *t*-Bu groups compared with the adamantyl substituents.

To study the dynamics of this phenomenon, DFT calculations were carried out taking compound **3N** as a model. Figure 4.12 depicts the energy diagram of **3N** taking into account the Au-Cl bond bending and the *t*-Bu rotation separately. This DFT analysis was performed by Prof. Dmitri Gusev, from the Wilfrid Laurier University.

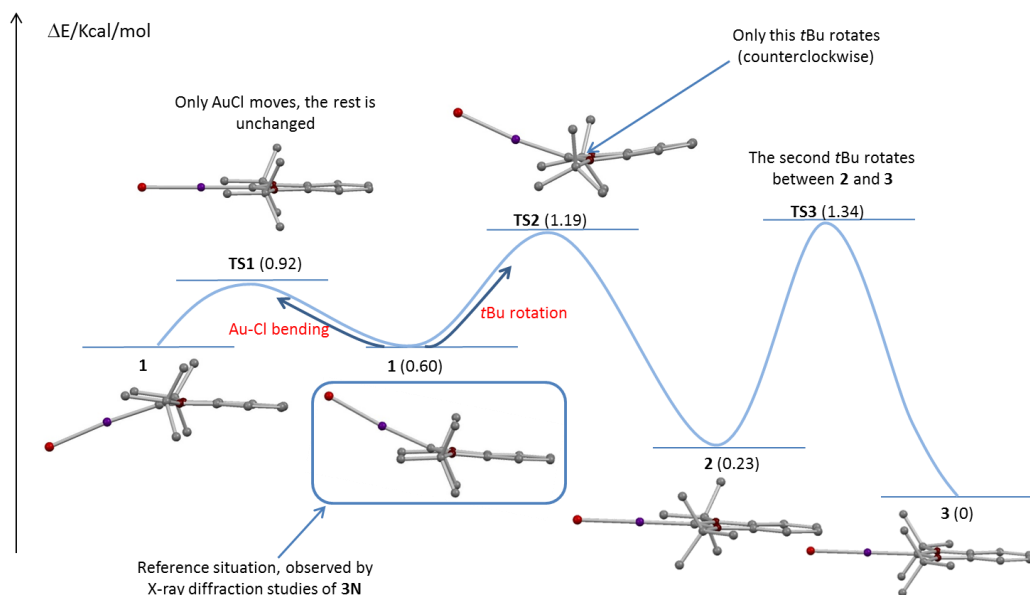


Figure 4.12 DFT energy variation profile of **3N**

In the conformation of minimum energy (**3** in Figure 4.12), the Au-Cl bond is contained in the plane defined by the azole ring, and both *t*-Bu substituents are situated in the position of minimum repulsion with respect to the gold center. The conformation observed by X-Ray diffraction analysis of **3N** (**1** in Figure 4.12), is just 0.6 Kcal/mol less stable than **3**. This situation implies that the metal fragment is out of the azole plane to avoid the repulsion with the methyls of the *t*Bu groups, which are pointing forward. Taking this conformation as starting point, and bending the Au-Cl fragment to the plane of the azole, leads to a situation in which the methyl groups are pointing to the metal affording a maximum repulsion (**TS1**, 0.32 Kcal/mol with respect to **1**). The low energy required for the Au-Cl bond bending suggests that this

process happens at room temperature. We can also consider the effect of the rotation of wingtips in the energy profile. If we start again from conformer **1**, and maintain the Au-Cl fragment in the azole plane, allowing the sequential rotation of the *t*-Bu groups (**1**→**TS2**→**2** followed by **2**→**TS3**→**3**), we reach to a maximum energy in **TS3** (1.34 Kcal/mol less stable than **3**), indicating that the rotation of the wingtips is also available at room temperature.

In summary, in solution there is equilibrium between the conformers **1**, **2** and **3**, as the energy necessary for their interconversion (Au-Cl bending and *t*-Bu rotation) is very low. Thus, the deviation of the metal atom with respect to the plane defined by the azole ring, observed in the different molecular structures obtained, will probably depend on packing parameters of the crystal.

4.1.3 Electronic properties of the trimetallic complexes based on **K**

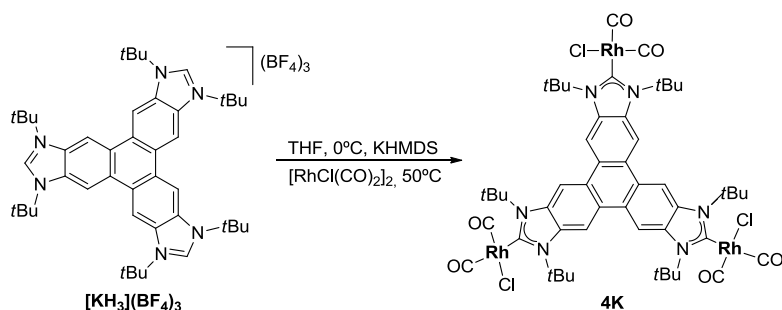
The study of the electronic properties of the trimetallic complexes with the triphenylene-tris-imidazolylidene ligand will be discussed in detail in this section. For this purpose, three approaches will be used.

- 1) Preparation of the carbonyl derivative of **1K**, for the estimation of the electron-donating properties of the ligand, based on the C-O IR-stretching frequencies.
- 2) Study of the through-ligand electronic communication. For this, two methodologies will be carried out. Firstly, the modification of the electron-donating ability of the ligand depending on the number of metal fragments (Ni(CO)₃) introduced will be estimated through the DFT-calculated TEP values. All the TEP values discussed in this section were determined by Prof. Gusev (Wilfrid Laurier University, Ontario, Canada), who carried out the appropriate calculations. Secondly, the electrochemical measurements of **1K** will be discussed.

4.1.3.1 Carbonylation of **1K**

Efforts to transform compound **1K** in its carbonyl derivative following the standard reactions conditions (bubbling CO at 0°C through a dichloromethane solution) were

unfruitful. This is probably due to the high steric shielding that the bulky *t*-butyl groups are providing around the metal, which prevents substitution of the COD ligands, as suggested for related monometallic complexes.¹² Fortunately, the deprotonation of $[\text{KH}_3](\text{BF}_4)_3$ with KHMDS and subsequent reaction of the free carbene with $[\text{RhCl}(\text{CO})_2]_2$ (Scheme 4.5), afforded the desired carbonylated rhodium complex **4K** as a yellow solid in 26 % yield, after precipitation from a dichloromethane/hexane mixture.



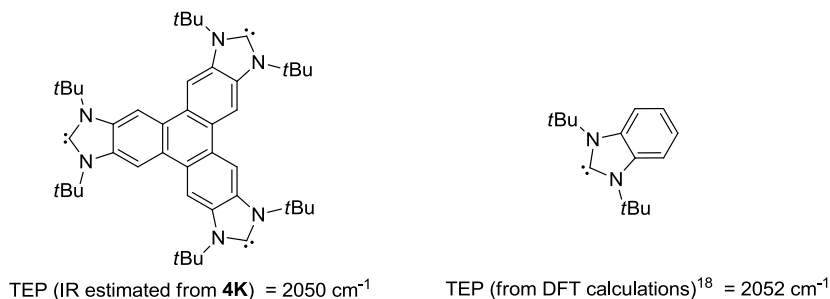
Scheme 4.5 Synthesis of carbonyl compound **4K**

The trimetallic compound **4K** was characterized by NMR and IR spectroscopy, and mass spectrometry. In the $^{13}\text{C}\{^1\text{H}\}$ NMR spectrum, the two resonances corresponding to the carbonyl ligands are displayed at 185.8 ppm ($^1J_{\text{Rh-C}} = 75.7$ Hz) and 182.7 ppm ($^1J_{\text{Rh-C}} = 57.2$ Hz). In this case, also only the *syn*-atropisomer is observed by NMR spectroscopy, as illustrated by the appearance of just one resonance due to the carbene carbon at 187.5 ppm ($^1J_{\text{Rh-C}} = 42.4$ Hz). The VT-NMR experiments did not provide any evidences about any interconversion between the *syn*- and the *anti*-atropisomers, probably due to the restricted rotation about the Rh-C_{carbene} bond, produced by the bulky *t*-butyl substituents of the ligand.¹⁰ The IR spectrum of **4K** displays two CO stretching bands (as expected for the *cis* disposition of the carbonyl ligands) at 2078 and 1999 cm^{-1} . These values allowed us to estimate the Tolman Electronic Parameter (TEP) as 2050 cm^{-1} , by using well-known correlations.^{10,13,14}

For comparative purposes, we also tried to synthesize the related mono-rhodium carbonyl complex based on the 1,3-di(*tert*-butyl)benzimidazolylidene ligand ($\text{BimN}t\text{Bu}_2$), $[\text{RhCl}(\text{BimN}t\text{Bu}_2)(\text{CO})_2]$. Unfortunately, efforts to obtain this compound starting from $[\text{RhCl}(\text{BimN}t\text{Bu}_2)(\text{COD})]$,¹² or by reacting the free carbene with $[\text{RhCl}(\text{CO})_2]_2$ were unfruitful. This can be due to the high tendency of the benzimidazol-2-ylidenes ligands to dimerize^{15,16} or to the low stability of the carbonyl

derivatives.¹⁷ Therefore, we were not able to do a direct comparison of the experimental $\nu(\text{CO})$ values of the trimetallic complex with its monometallic counterpart.

Prof. Gusev recently proposed DFT calculations as valuable tools to obtain the TEP values of a wide set of NHCs, with very good concordance with the experimental values.¹⁸ In fact, Prof. Gusev used this approach for the determination of the TEP value of $\text{BimN}t\text{Bu}_2$, which was estimated to be 2052 cm^{-1} . This value is very similar to that provided for the tris-NHC **K** (2050 cm^{-1}), indicating an almost identical donor ability of both ligands (Scheme 4.6).



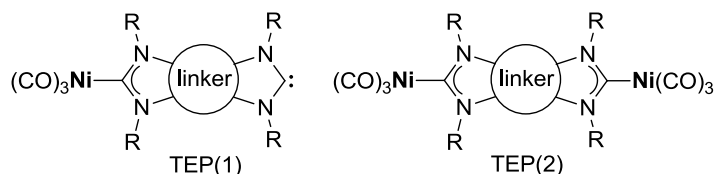
Scheme 4.6

Attempts to obtain the triptycene-based tris- $\text{Rh}(\text{CO})_2\text{Cl}$ complex were unsuccessful, so the direct comparison of the donor ability of this ligand could not be done. However, as the triptycenic core disturbs the possible π -communication between the three carbenic fragments, it can be assumed that the electronic properties of this ligand should be similar to those observed for $\text{BimN}t\text{Bu}_2$.

4.1.3.2 Tolman Electronic Parameter (TEP) and electronic communication

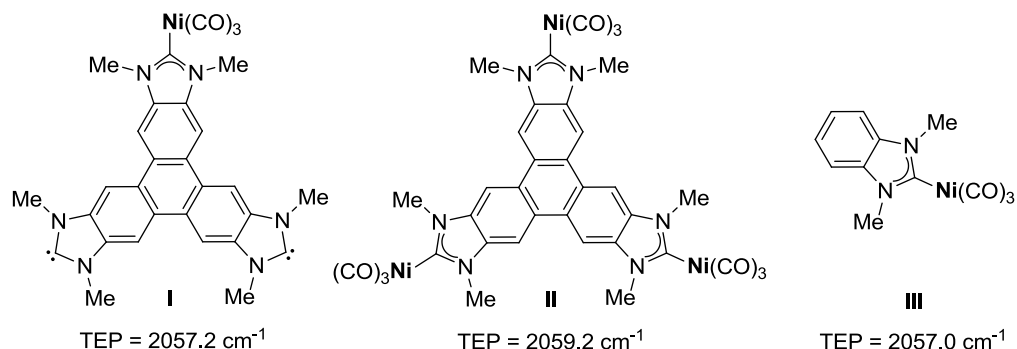
In order to study whether there is any kind of electronic communication between the three metal fragments connected by the triphenylene-based tris-imidazolyliene, we first followed a recently reported procedure by Gusev and Peris based on DFT calculations.¹⁹ In this approach, it was suggested that variations in the TEP values associated to the coordination of different fragments can be an effective way to determine if there is electronic communication between metals bridged by rigid bis-NHCs. Thus, the authors estimated the TEP value of the ligands when they were coordinated to a single $\text{Ni}(\text{CO})_3$ fragment and the other edge of the ligand contained

the lone pair of the free NHC (TEP(1) in Scheme 4.7). Then, the TEP value of the related bimetallic complex based on $\text{Ni}(\text{CO})_3$ was calculated (TEP(2) in Scheme 4.7). It is expected that the difference in the values of TEP(1) and TEP(2) is related to the through-ligand electronic communication.



Scheme 4.7

We thought that the same argument could be used for the determination of the electronic communication in our triphenylene-based tris-NHC ligand. First we calculated the TEP value for the compound in which the ligand is coordinated to only one $\text{Ni}(\text{CO})_3$ fragment, bearing the other two carbene units in their free form (**I** in Scheme 4.8). In order to simplify the calculations, N-methyl groups were used instead of N-*t*-Bu. The TEP found for this system was 2057.2 cm^{-1} , a value very similar to that previously obtained for the 1,3-dimethylbenzimidazolylidene **III** (2057.0 cm^{-1}),¹⁸ indicating a similar donor capacity.



Scheme 4.8

When two additional $\text{Ni}(\text{CO})_3$ fragments were added to the system, the TEP value increased up to 2059.2 cm^{-1} (**II** in Scheme 4.8). This increase in the TEP value is due to the inductive effect provided by the $\text{Ni}(\text{CO})_3$ fragments, which are withdrawing electron-density from the ligand, and reduce the overall electron-donating power of the tris-NHC ligand. The slight difference in the TEP values of **I** and **II** indicates that

the three metals bridged by the tris-NHC are basically disconnected, despite having an apparently effective π -delocalized system.

4.1.3.3 Electrochemical properties

As stated earlier, we also performed electrochemical measurements in order to confirm our previous observations on the lack of electronic communication between the metals in the triphenylene-based trimetallic system.

The cyclic voltammetry of the tri-rhodium complex **1K** displays a reversible one-electron oxidation wave, centered at $E_{1/2} = 0.61$ V arising from the $\text{Rh}^{\text{I/II}}$ oxidation (Figure 4.13, left). This potential is slightly higher than the one reported for the related monometallic complex $[\text{RhCl}(\text{BimNtBu}_2)(\text{COD})]$ (0.56 V)¹² indicating a lower donating capacity of the tris-NHC compared to the BimNtBu_2 ligand,^{20,21} in agreement with the results obtained before (*vide supra*).

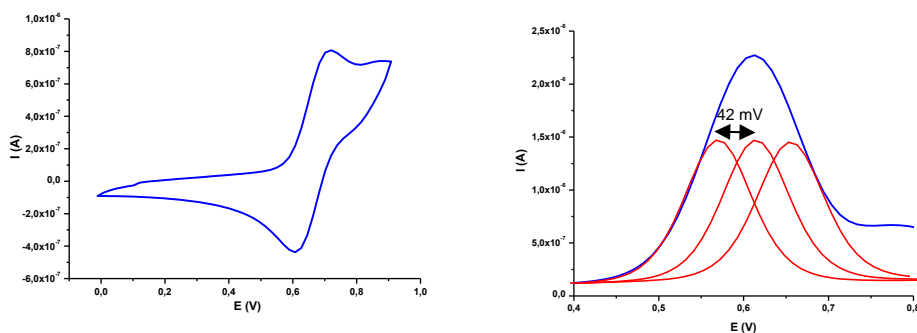


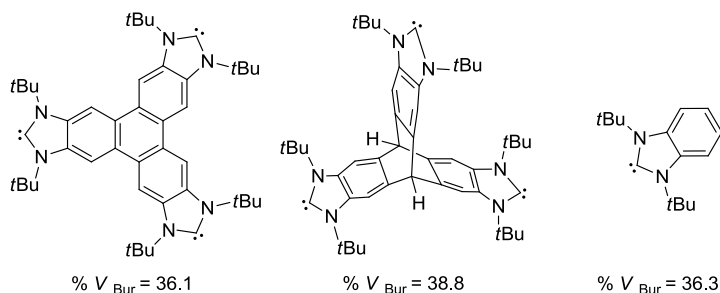
Figure 4.13 Cyclic voltammetry diagram of complex **1K** (left) and relevant section of the differential pulse voltammetry (DPV) (right). The convoluted curves (red lines) were obtained from adding three potential-shifted and weighed signals of the monometallic complex $[\text{RhCl}(1,3\text{-di}(\text{tert-butyl})\text{benzimidazolyli-dene})(\text{COD})]$. Measurements performed on a 1 mM solution of the analyte in dry CH_2Cl_2 with 0.1 M $[\text{NBu}_4][\text{PF}_6]$ as the supporting electrolyte, 100 mVs^{-1} scan rate, Fc^+/Fc used as internal standard with $E_{1/2}(\text{Fc}^+/\text{Fc}) = 0.446$ V vs. SCE.

The differential pulse voltammetry (DPV) of complex **1K** showed a broader signal, compared to that observed for the rhodium monocarbene complex $[\text{RhCl}(1,3\text{-di}(\text{tert-butyl})\text{benzimidazolyli-dene})(\text{COD})]$ (Figure 4.13, right). Taking the DPV signal of this monocarbene-rhodium complex as a reference, the deconvolution of the DPV curve for **1K** reveals the presence of three oxidation bands separated by 42 mV. This separation corresponds to an essentially decoupled system,²² especially when

compared to other known π -linked bis-NHCs.^{1,23–26} This is in agreement with the results observed for the homo-bimetallic complexes based on a pyrene-bis-imidazolyliene, discussed in Chapter 3.

4.1.4 Steric hindrance: percent of buried volume (% V_{Bur})

Once the electronic properties of the triphenylene-tris-imidazolyliene and the benzimidazolyliene ligands were studied, we decided to estimate the steric bulk of the ligands used in this chapter. The most common parameter employed for measuring the sterics of NHC ligands is the percent of buried volume (% V_{Bur}). This parameter was introduced by Nolan and Cavallo,²⁷ and is defined as the percent of the total volume occupied by the ligand of a sphere centered in the metal.²⁸ We estimated the % V_{Bur} for our ligands, by using the SambVca software developed by Cavallo and co-workers²⁹ from the corresponding crystallographic data described above. The % V_{Bur} obtained are indicated in Scheme 4.9. Interestingly, the steric bulk of the triphenylene-tris-imidazolyliene ligand and the benzimidazolyliene (36.1 and 36.3, respectively) are almost identical. The % V_{Bur} of the triptycene-tris-imidazolyliene ligand (% V_{Bur} = 38.8) is slightly higher than those obtained for the other ligands.



Scheme 4.9 % V_{Bur} of **K**, **M** and **N**

In summary, from the last sections it can be concluded that the stereoelectronic properties of the three ligands employed in this chapter are very similar, although the triptycene-tris-imidazolyliene (**M**) seems to have slightly higher steric bulk than the other two ligands (**K** and **N**).

4.1.5 Catalytic properties of palladium and gold complexes

In the following sections, the catalytic properties of the palladium (**2K**, **2M** and **2N**) and gold (**3K**, **3M** and **3N**) containing complexes described above will be discussed. The study and comparison of the catalytic activity provided by these compounds

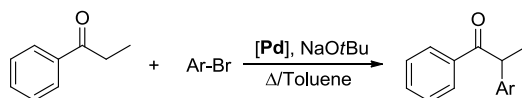
should give us interesting information about how the trimetallic nature of the catalyst (**2K**, **2M**, **3K** and **3M**) may have (or may not have) any benefit compared to their monometallic analogues (**2N** and **3N**).

For the palladium-based catalysts we studied the α -arylation of ketones and the Suzuki-Miyaura coupling, reactions for which several NHC-palladium-based complexes have proven to be very active.^{30,31} For the gold-catalysts we studied the hydroamination of alkynes to test their catalytic activity. This reaction is a 100% atom efficient transformation, and some gold-NHCs have shown good catalytic performances.³²⁻³⁵

4.1.5.1 Palladium catalyzed reactions

In order to test the catalytic activity of the tris-Pd (**2K** and **2M**) and mono-Pd (**2N**) complexes, we first studied the α -arylation of ketones. This reaction was concurrently reported by Miura³⁶, Buchwald³⁷ and Hartwig³⁸ in 1997, and consists of the reaction of an alkyl-ketone with an aryl halide to produce the corresponding α -arylated ketone. For our study, we decided to use propiophenone and different *para*-substituted aryl bromides. The reaction conditions employed were similar to other previously reported ones:³⁹ 120°C in toluene, in the presence of NaOtBu and using 1 mol % catalyst loading, based on the amount of metal. Table 4.6 summarizes the results obtained in this reaction. It is important to note that in this table (entries 7 to 9) and in the next ones, the catalytic results obtained using some additives are also shown. The interpretation of these results will be discussed in the following sections.

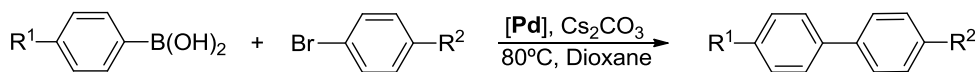
The trimetallic complexes (**2K** and **2M**) clearly provide better catalytic performances than their monometallic analogue (**2N**). For all the substrates employed the best catalyst was **2K**. This accounts for all kind of aryl bromides, including unsubstituted aryl bromides (entries 1-3), aryl bromides with electron-donating groups (entries 4-6 and 13-15) and with electron-withdrawing groups (entries 10-12).

Table 4.6 α -Arylation of propiophenone with aryl bromides^a

Entry	Ar-Br	Cat.	Yield(%) ^b
1		2K	99
2		2M	97
3		2N	75
4		2K	99
5		2M	89
6		2N	60
7 ^c		2K	90
8 ^c		2M	87
9 ^c		2N	65
10		2K	99
11		2M	86
12		2N	69
13		2K	99
14		2M	85
15		2N	65

^aReaction conditions: 1 mol % catalyst loading (based on metal), 0.5 mmol propiophenone, 0.55 mmol arylbromide, 0.65 mmol NaOtBu, 2 mL toluene, T = 120°C, 1 h. ^bYields determined by GC using anisole (0.5 mmol) as internal standard. ^cReaction carried out in the presence 0.05 mmol of pyrene.

In order to confirm that the catalytic benefits provided by **2K** were not restricted to the α -arylation of ketones, the Suzuki-Miyaura C-C coupling was investigated employing the same three catalysts. The results obtained are displayed in Table 4.7. Again, complex **2K** was found to be the best catalyst. Interestingly, the mono-Pd compound **2N** shows higher catalytic activity than the tri-Pd complex **2M** for all the substrates that were investigated.

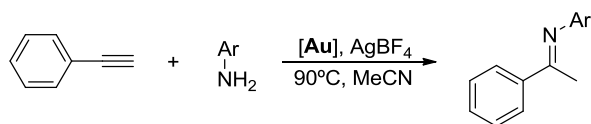
Table 4.7 Suzuki-Miyaura reaction^a

Entry	R ¹	R ²	Cat.	Yield(%) ^b
1			2K	90
2			2M	78
3			2N	81
4 ^c			2K	95
5 ^c	H	H	2M	66
6 ^c			2N	71
7 ^d			2K	73
8 ^d			2M	66
9 ^d			2N	67
10			2K	81
11	H	OMe	2M	62
12			2N	69
13			2K	71
14	Me	H	2M	55
15			2N	61
16			2K	66
17	Me	OMe	2M	36
18			2N	46

^aReaction conditions: 2 mol % catalyst loading (based on metal), 0.5 mmol arylbromide, 0.6 mmol arylboronic acid, 1 mmol Cs₂CO₃, 2 mL 1,4-dioxane, T = 80°C, 2 h. ^bYields determined by GC using anisole (0.5 mmol) as internal standard. ^cReaction carried out in the presence 0.5 mmol of hexafluorobenzene. ^dReaction carried out in the presence 0.05 mmol of pyrene.

4.1.5.2 Gold catalyzed reaction

In order to confirm that the enhanced catalytic performance shown by complex **2K**, compared to those of **2M** and **2N**, was not limited to palladium-promoted reactions, the hydroamination of alkynes, in the presence of the gold-based catalysts (**3K**, **3M** and **3N**), was investigated. This reaction consists of the addition of an amine to an alkyne to produce the corresponding imine.

Table 4.8 Hydroamination of phenylacetylene^a

Entry	Ar-NH ₂	Cat.	Yield(%) ^b
1		3K	94
2		3M	87
3		3N	89
4		3K	95
5		3M	54
6		3N	82
7		3K	95
8		3M	82
9		3N	91
10		3K	99
11		3M	86
12		3N	85
13 ^c		3K	96
14 ^c		3M	81
15 ^c		3N	83
16 ^d		3K	87
17 ^d		3M	62
18 ^d		3N	85
19		3K	91
20		3M	60
21		3N	70

^aReaction conditions: 1 mol % catalyst loading (based on metal), 0.5 mmol phenylacetylene, 0.55 mmol amine, 2 % mol AgBF₄, 1 mL MeCN, T = 90°C, 6 h. ^bYields determined by GC using anisole (0.5 mmol) as internal standard. ^cReaction carried out in the presence 0.5 mmol of hexafluorobenzene. ^dReaction carried out in the presence 2 mmol of hexafluorobenzene.

We focused our attention on the reaction of phenylacetylene with anilines with different substitution patterns. It is important to note that for all the substrates that

were studied, the product obtained was always the result of the Markovnikov addition of the aniline. Table 4.8 shows the results obtained in this reaction using catalysts **3K**, **3M** and **3N**.

Again, the best catalytic performances are provided by the catalyst based on the triphenylene-tris-imidazolylidene ligand, **3K**. In general, compound **3N** shows better catalytic activity than **3M**, except when 2-methylaniline is used, for which both catalysts show similar catalytic activity.

4.1.5.3 Discussion of the catalytic results

From the results obtained in all the three catalytic reactions described in this section, it can be concluded that the trimetallic complexes based on the triphenylene-tris-imidazolylidene ligand (**2K** and **3K**) show higher catalytic activity than the related complexes based on a triptycene-tris-imidazolylidene (**2M** and **3M**) and a benzimidazolylidene (**2N** and **3N**). In principle, the differences in the catalytic activities may be ascribed to the following reasons:

- a) Differences in the stereoelectronic properties of the ligands used
- b) Different stabilities of the catalysts
- c) Higher nano-local concentration provided by the trimetallic complexes
- d) π -Stacking between the substrates and the rigid π -extended polyaromatic ligand

In the next few paragraphs we will approach these possibilities individually.

a) Stereoelectronic properties of the ligands used

The observed differences in the catalytic activities cannot be ascribed to differences in the stereoelectronic properties of the ligands, since we proved that they are quasi-identical (see Section 4.1.3 and Section 4.1.4).

b) Stability of the complexes

In order to study this point, we carried out stability tests to all three complexes used in this study. For that purpose, the compounds were refluxed in CD_3CN in the presence of an internal standard and their decomposition was monitored by ^1H NMR spectroscopy. The triptycene-based complexes **2M** and **3M** fully decomposed after 3 hours, while the triphenylene-based and the benzimidazolylidene-based catalysts

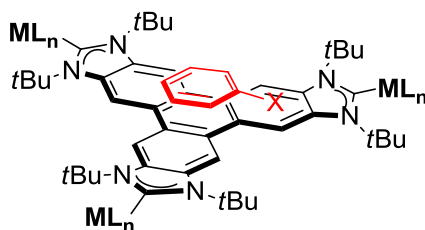
showed higher stabilities (the degree of decomposition was below 50 %). This result suggests that the lowest catalytic activities of **2M** and **3M** in the Suzuki-Miyaura reaction and in the hydroamination of phenylacetylene may be due to their faster decomposition under the reaction conditions.

c) Effect of the higher nano-local concentration in trimetallic complexes

The trimetallic nature of the catalysts containing the triphenylene-based tris-NHC could be the reason of the improved catalytic performances of them. The ligand is fixing the distance between the metals, allowing a high and constant nano-local concentration of catalytic active sites, which cannot be achieved with the monometallic analogues. This effect is also known as the *dendrimer effect*.^{40,41} However, this should be also true for the catalysts containing the triptycene-based tris-NHC, as the distance between the metals bonded to this ligand is almost the same as the one observed for the ligand based on triphenylene (see Section 4.1.2), thus providing the same nano-local concentration of catalytic active sites. As can be seen from the catalytic results given above, the activity of the triphenylene-based catalysts is always higher than that shown by the triptycene-based catalysts, and therefore the effect of the nano-concentration may not be critical. However, taking into account the low thermal stability of catalysts **2M** and **3N**, it is difficult to fully attribute the differences of activity to only one of these reasons.

d) π -Stacking effect of additives

The polyaromatic nature of the ligand in catalysts **2K** and **3K** could be attracting the substrates through π -stacking interactions, facilitating their interaction with the metal centers, thus improving the catalytic activity of the system (Scheme 4.10).



Scheme 4.10

In order to shed some light on this point, we decided to carry out the catalytic tests in the presence of additives that are known to be good π -stacking agents. The selected

additives were hexafluorobenzene (HFB) and pyrene, because they are assumed to be inert under the reaction conditions used. For the α -arylation of propiophenone, the addition of catalytic amounts of pyrene (10 % mol) partially inhibited the catalytic activity of **2K**, while the activity of **2N** and **2M** was mostly unaffected (compare entries 4-6 with entries 7-9, in Table 4.6). When HFB was used as additive for this reaction, we observed its disappearance by GC analysis and the generation of other unidentified side-products. This is probably because in the presence of a strong base as NaOtBu, HFB can suffer nucleophilic aromatic substitution reactions.⁴²

The addition of 0.5 mmol of HFB to the Suzuki-Miyaura reaction slightly increased the catalytic activity of **2K** while the catalyst performances of **2N** and **2M** were reduced (compare entries 1-3 with entries 4-6 in Table 4.7). However, when a catalytic amount of pyrene (10 % mol) is added to the reaction media, the yield obtained for the bisarylated compound is almost the same using the three palladium-based catalysts (compare entries 1-3 with entries 7-9 in Table 4.7, Figure 4.14).

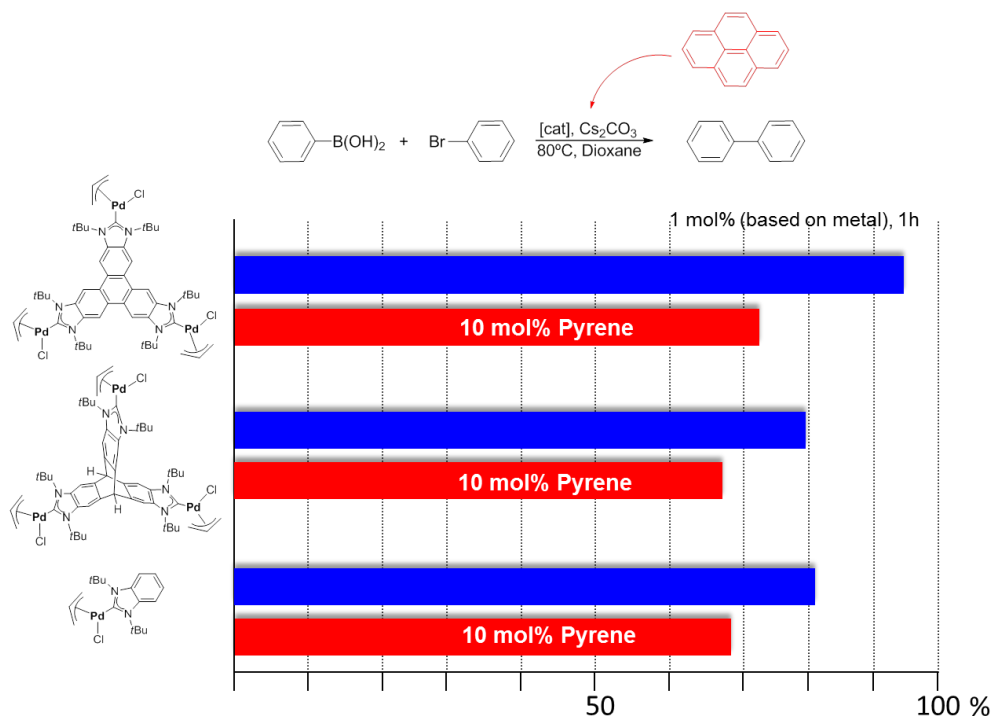


Figure 4.14 Blue bars: catalytic activity of the catalysts without additives. Red bars: catalytic activity of the catalyst in the presence of 10 % mol of pyrene

The limited solubility of pyrene in acetonitrile prevented its use as additive in the hydroamination of phenylacetylene. Addition of 1 equivalent of HFB to the reaction media has a small effect on the catalytic activity of the three gold-based catalysts (compare entries 10-12 with entries 13-15 in Table 4.8). With four equivalents of HFB as additive, the catalytic activity of **3K** is partially inhibited (compare entries 10 and 16 in Table 4.8), while no effect is observed in the catalytic performance of **3N** (compare entries 12 and 18 in Table 4.8). A high decrease in the catalytic activity of **3M** was observed in the presence of an excess of HFB, probably due to the decomposition of the catalyst in the reaction media.

The results discussed above suggest that the addition of a good π -stacking agent to the reaction media has a certain effect in the catalytic activity of all the catalysts used, but the magnitude of this effect is higher for the triphenylene-based catalysts (**2K** and **3K**).

Titration experiments

In order to experimentally confirm the π -stacking between some additives and the triphenylene ligand in **3K**, ^1H NMR titration experiments were carried out in polar deuterated solvents.⁴³⁻⁴⁵ Pyrene was gradually added to a $\text{CD}_3\text{OD}/\text{CD}_2\text{Cl}_2$ solution of **3K**. A gradual effect over the signal corresponding to the protons of the polyaromatic core was observed (Figure 4.15). The signal affected by the addition of pyrene is shifted to lower frequencies, suggesting that a non-covalent interaction is produced between the polyaromatic core of the complexes and the added pyrene.⁴³⁻⁴⁵

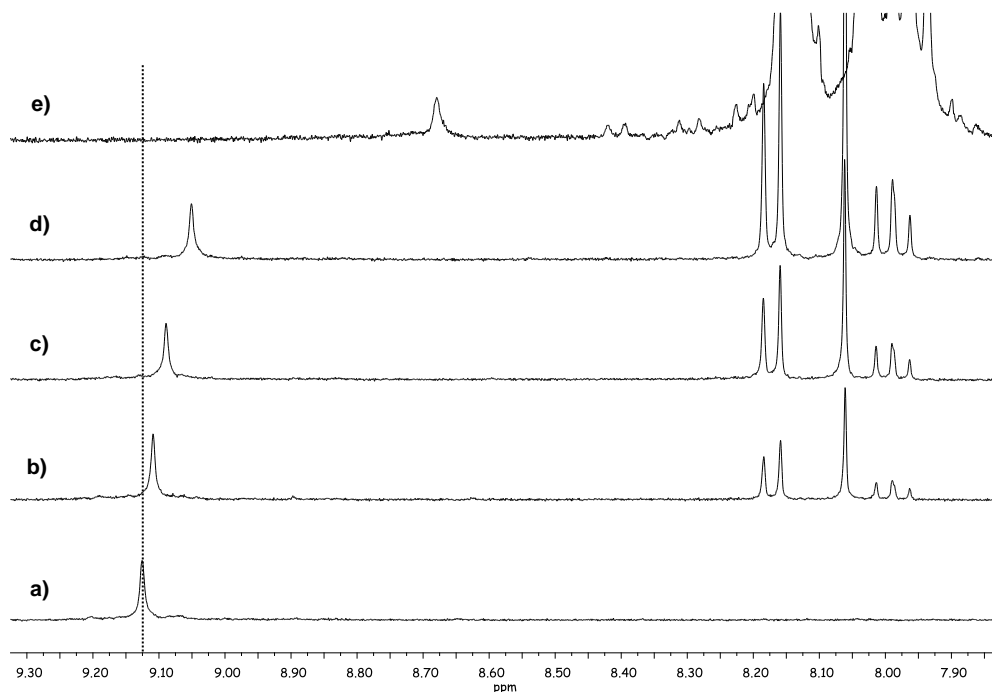
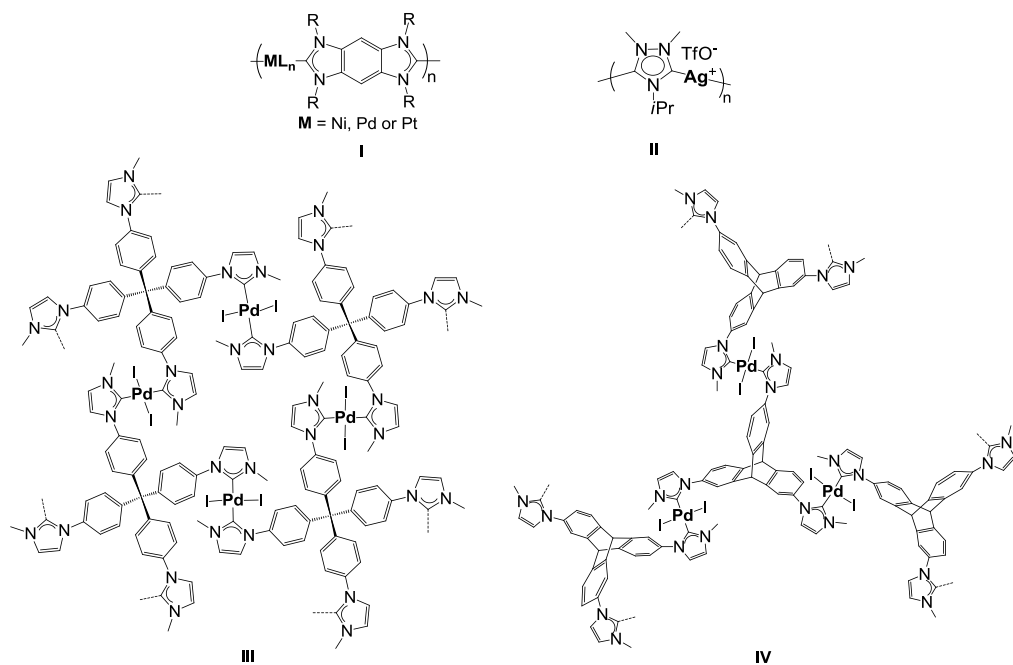


Figure 4.15 ^1H NMR spectrum (300 MHz, $\text{CD}_3\text{OD}/\text{CD}_2\text{Cl}_2$, 298 K) of a) complex **3K**; b) **3K** + 0.8 equiv pyrene; c) **3K** + 2 equiv pyrene; d) **3K** + 3 equiv pyrene; e) **3K** + excess pyrene.

From the results described above, we may conclude that the higher catalytic activity provided by the complexes with the triphenylene-based tris-NHC ligand, may be ascribed to the π -stacking of the substrates and the ligand, which may facilitate the interaction between the substrate and the catalytically active metal fragment. At this point it is important to mention, that the higher catalytic performance of the complexes containing the triphenylene-based-tris-NHC may also be ascribed to the higher nano-local concentration provided by this tritopic ligand. Unfortunately, although the catalytic experiments with the complexes containing the triptycene-based-tris-NHC ligand -which affords exactly the same nano-local concentration of metal- indicate the lower activity of these ones, the lower stability of the complexes **2M** and **3M**, suggest that their lower catalytic performances may be ascribed to thermodynamic reasons rather than kinetic ones. All in all, our experiments with π -stacking additives indicate that π -stacking has a strong influence in the catalytic outcome of the reactions, and we believe that it should play an important role that must be taken into account in the design of future catalytic processes.

4.1.6 Main-chain organometallic microporous polymers based on triphenylene-tris-NHC gold species

As stated in Chapter 1, poly-NHCs have proven to be good ligands for the synthesis of main-chain organometallic polymers⁴⁶ forming one- (**I** and **II** in Scheme 4.11)^{47–49} or three-dimensional architectures (**III** and **IV** in Scheme 4.11).^{50–52} One of the main differences between these kinds of polymers is that the mono-dimensional ones tend to be soluble, while the three-dimensional ones use to be highly insoluble and show microporosity. The main application of these materials is related with heterogeneously^{3,50–53} or homogeneously⁵⁴ catalyzed reactions.



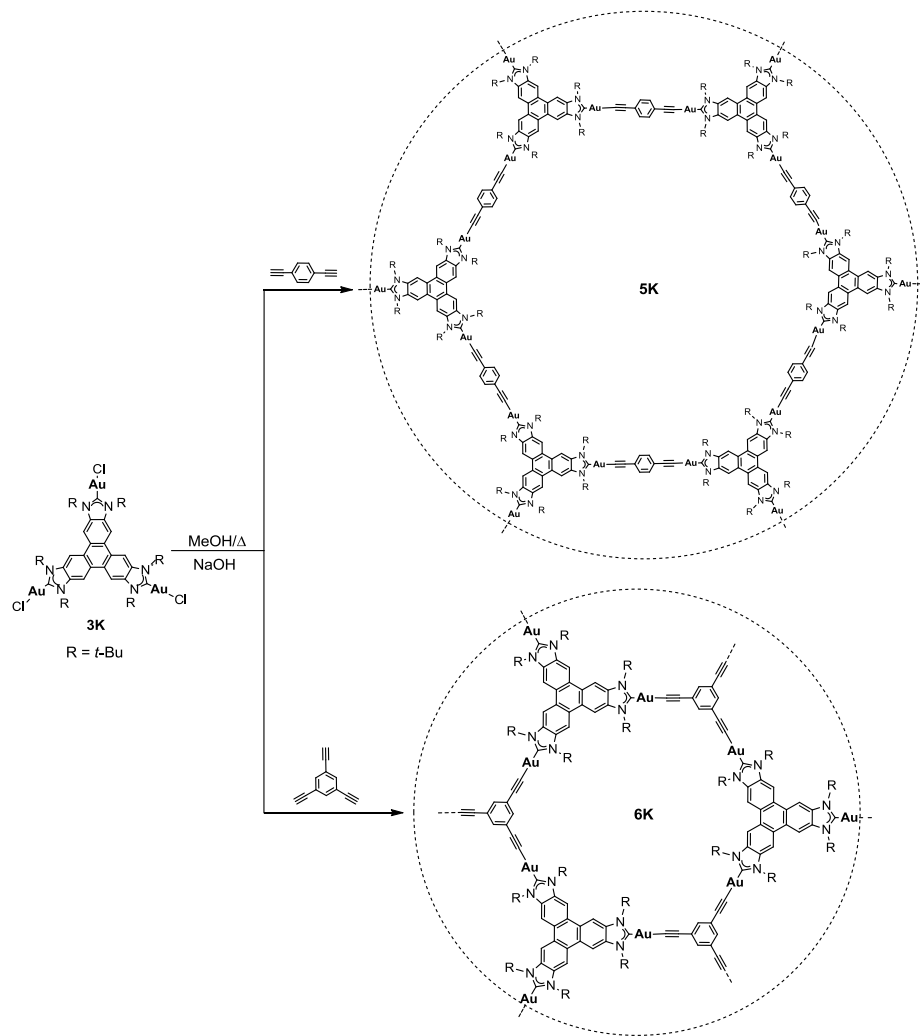
Scheme 4.11 Previously reported main-chain organometallic polymers based on poly-NHCs

We decided to take profit of the particular topology of the triphenylene-tris-imidazolylidene ligand to obtain two- or three-dimensional organometallic networks. Our triphenylene-based ligand may potentially provide the resulting materials with attractive physicochemical properties. In the following sections of this chapter, the synthesis and characterization of two new main-chain microporous organometallic polymers based on triphenylene-tris-NHC gold species will be discussed, as well as their catalytic activity in two heterogeneously-catalyzed reactions.

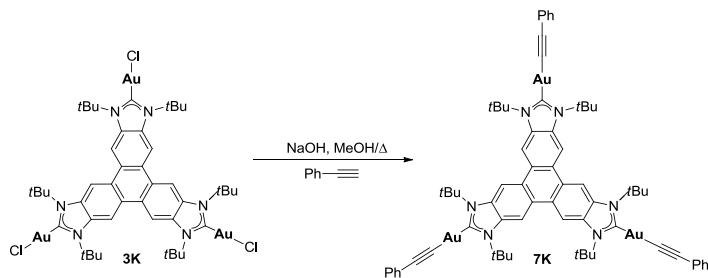
4.1.6.1 Synthesis and characterization

We decided to take advantage of the high affinity of acetylides to coordinate to gold⁵⁵⁻⁶⁰ to obtain new triphenylene-based organometallic polymers. For the coordination of phenyl-acetylide, we followed a previously reported work.⁵⁹ The tris-NHC gold complex **3K** was treated under basic conditions with 1,4-diethynylbenzene or 1,3,5-triethynylbenzene in refluxing methanol, to generate **5K** (68 % yield) or **6K** (90 % yield), respectively (Scheme 4.12). Both compounds were obtained as brownish, highly insoluble solids. For comparative purposes, the molecular analogue of **5K** and **6K** was synthesized. The reaction of **3K** in the presence of NaOH and phenylacetylene in refluxing methanol yields the desired tri-metallic complex **7K** in excellent yield (91 %) as a white solid, after precipitation from a mixture of dichloromethane/hexanes.

Compounds **5K** and **6K** were characterized by means of solid state ¹³C NMR spectroscopy (using Cross-Polarization Magic-Angle Spinning (CP/MAS) NMR), Scanning Electron Microscopy (SEM), Transmission Electron Microscopy (TEM), X-Ray powder diffraction, ThermoGravimetric Analysis (TGA), FT-IR spectroscopy, elemental analysis and N₂ adsorption-desorption experiments. Compound **7K** was characterized by means of NMR spectroscopy, mass spectrometry and elemental analysis. The NMR spectra of the three compounds and the SEM images of the polymeric materials are described below. All the other details regarding the characterization of the materials can be found in the Experimental Section (Chapter 5).



Scheme 4.12 Synthesis of 5K and 6K



Scheme 4.13 Synthesis of 7K

¹H NMR spectrum of 7K

Figure 4.16 shows the ¹H NMR spectrum of **7K**. The number of signals and their integration are consistent with the *D*_{3h} symmetry of the compound. The resonance attributed to the aromatic protons of the triphenylene core is shown as a singlet at 9.01 ppm (*a*). The signal due to the protons of the *t*-butyl groups bonded to the nitrogen of the imidazole ring is displayed as a singlet at 2.39 ppm (*b*). The rest of the resonances assigned to the protons of the acetylide ligands are conveniently displayed on the spectrum.

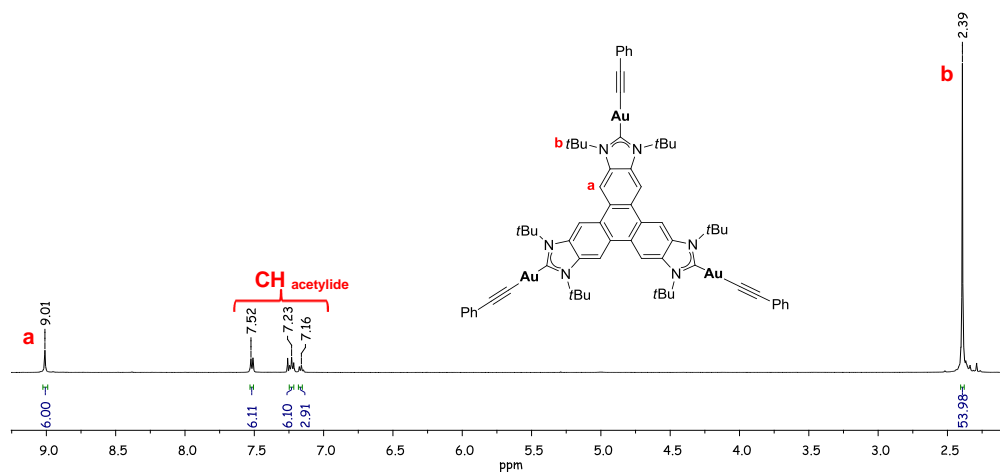


Figure 4.16 ¹H NMR spectrum of **7K** in CDCl₃

¹³C NMR spectrum of 5K, 6K and 7K

The ¹³C CP/MAS NMR spectrum of **5K** and **6K**, and the ¹³C{¹H} NMR spectrum of **7K** are displayed in Figure 4.17 (spectrum a, b) and c), respectively). The number of signals displayed in the spectrum corresponding to **7K** (Figure 4.17c) is consistent with the three-fold symmetry of the compound. The most characteristic signal is the one attributed to the metallated carbene-carbons, which is displayed at 199.6 ppm (*1*). The resonances due to the aromatic C_{quaternary} and CH groups of the triphenylene core are shown at 134.7, 125.5 (*2*) and 109.3 ppm (*3*), respectively. The signals assigned to the carbons of the *tert*-butyl substituents are observed at 62.6 and 33.5 ppm (*4* and *5*, respectively). The rest of the resonances corresponding to the carbons of the acetylide ligands are conveniently displayed on the spectrum.

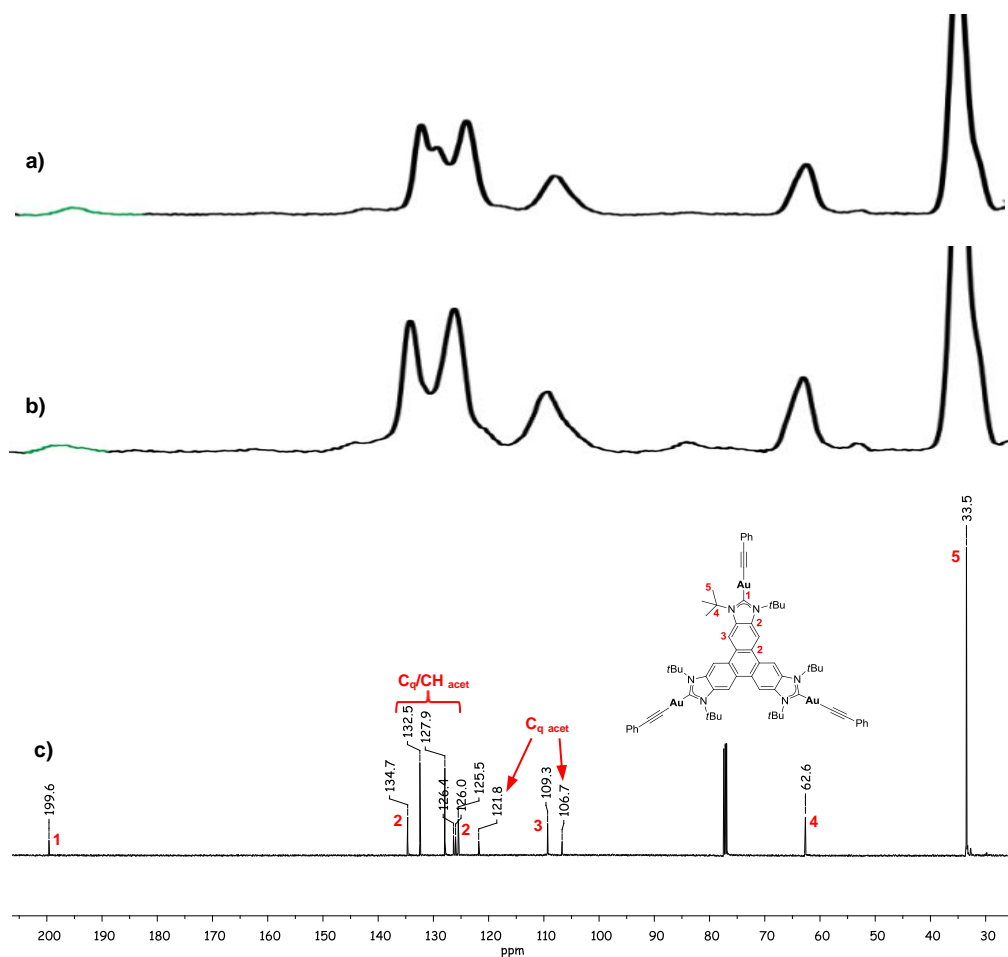


Figure 4.17 a) ^{13}C CP/MAS NMR spectrum of **5K**. b) ^{13}C CP/MAS NMR spectrum of **6K**. c) $^{13}\text{C}\{^1\text{H}\}$ NMR spectrum of **7K** in CDCl_3

The ^{13}C CP/MAS NMR spectra of **5K** and **6K** (Figure 4.17, a) and b), respectively, show good correlation with the $^{13}\text{C}\{^1\text{H}\}$ NMR spectrum of **7K**. For both materials the signal due to the $\text{C}_{\text{carbene}}$ is observed at 200 ppm, very close to the one observed for the metallated carbene carbons in complex **7K** (199.6 ppm). The signals attributed to the aromatic carbons are observed in two groups, as well as the signals corresponding to the carbons of the *t*Bu groups of the wingtips, with chemical shifts that perfectly match with those exhibited by **7K**.

SEM images of **6K** and **7K**

Figure 4.18 shows the SEM images of compounds **5K** and **6K**. Both materials adopt a spherical morphology. The size of the spheres depends on the alkyne used to synthesize each polymer. For **5K** the diameter of the spheres range from 100 to 600 nm [Figure 4.18, a) and b)], while for **6K** the diameter is in the range of 50 to 100 nm [Figure 4.18, c) and d)].

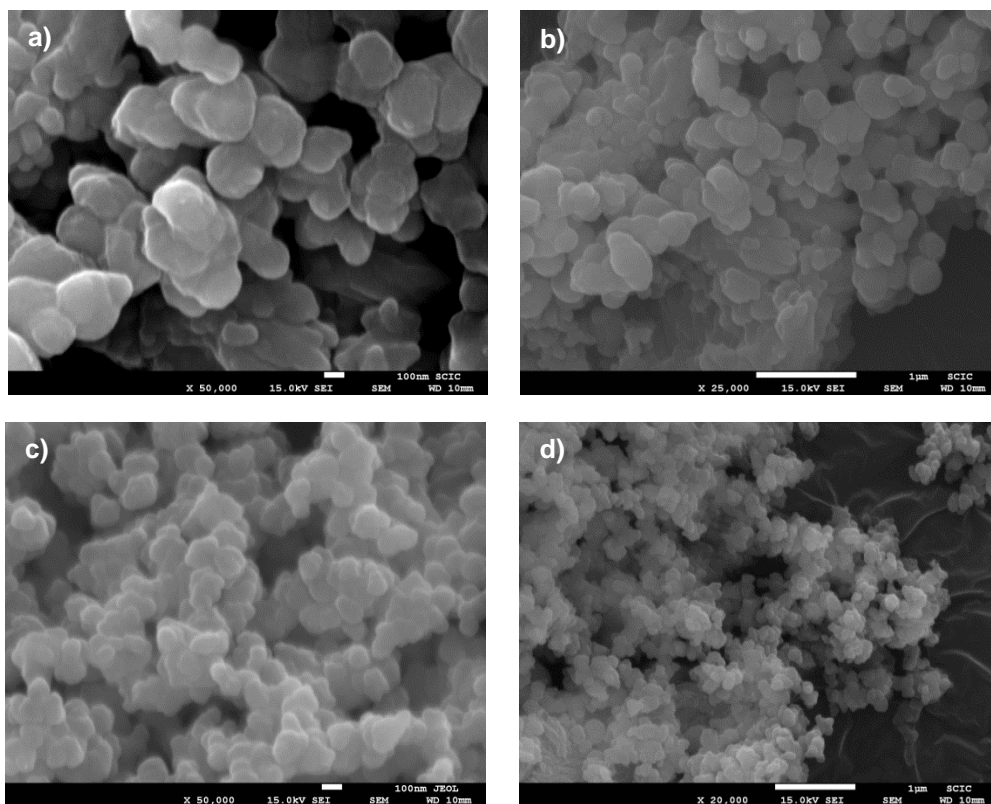


Figure 4.18 SEM micrographs at different magnifications of **5K** (images a) and b)) and **6K** (images c) and d))

The BET surface area for each material was estimated by nitrogen-sorption analysis at 77 K. For **5K** the BET surface area is 43 m²/g, while for **6K** is 222 m²/g, as expected for the different sizes of the spheres formed by both materials (in principle, it is expected that larger spheres produce lower BET surface areas).

Both materials have an amorphous character, as shown by their X-ray diffraction patterns. Elemental mapping by energy-dispersive X-ray spectroscopy (EDS) analysis performed by means of TEM was carried out to confirm the homogeneous elemental distribution of gold and carbon in the materials (Figure 4.19 and Figure 4.20 for **5K** and **6K**, respectively).

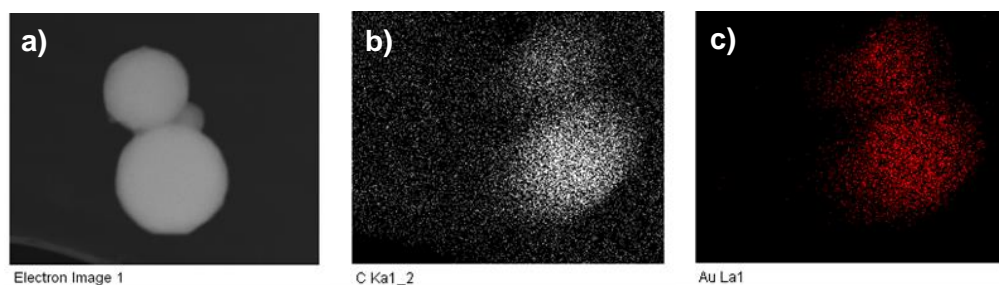


Figure 4.19 a) STEM image of **5K**. b) and c) EDS elemental-mapping images collected by TEM of **5K** showing the homogeneous distribution of carbon (b)) and gold (c)).

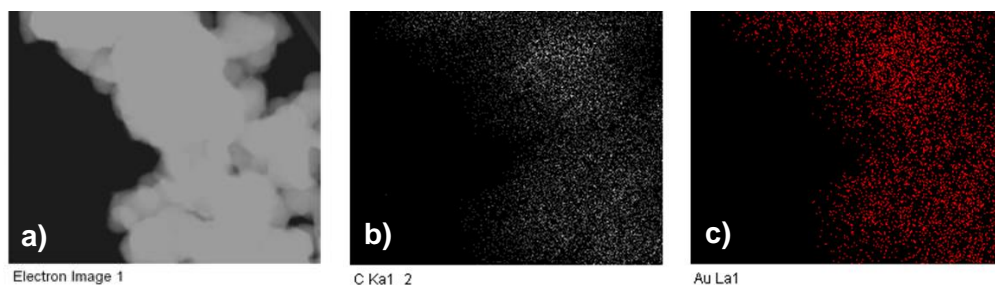


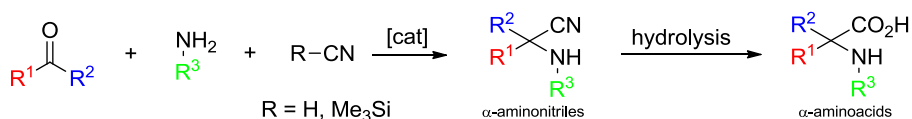
Figure 4.20 a) STEM image of **6K**. b) and c) EDS elemental-mapping images collected by TEM of **6K** showing the homogeneous distribution of carbon (b)) and gold (c)).

4.1.6.2 Catalytic properties of **5K** and **6K**

In the following sections, the catalytic properties of the polymeric compounds (**5K** and **6K**) described above will be discussed. The highly insoluble nature of the materials prompted us to choose heterogeneously catalyzed reactions.

The first reaction tested was the reduction of nitroarenes to the corresponding anilines. This transformation has recently received much attention,^{61–64} because functionalized anilines are important intermediates in the synthesis of pharmaceuticals and fine chemicals. Besides, gold-based catalysts have shown good performances in this catalytic process.^{65–68}

Secondly, the three-component Strecker reaction was tested. This transformation was first reported in 1850,⁶⁹ but even nowadays is a very attractive reaction, especially in its asymmetric version.⁷⁰ In this reaction, α -aminonitriles are obtained from the reaction of very cheap and available reagents: ketones or aldehydes, amines and a cyanide source (typically cyanhydric acid or trimethylsilyl cyanide (TMSCN)) (Scheme 4.14). The α -aminonitriles obtained in this way can be easily converted, by hydrolysis, in the corresponding α -aminoacids, which are valuable compounds in biological fields.⁷¹

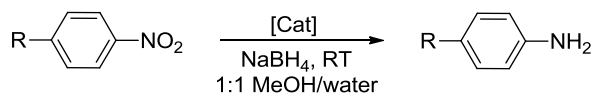


Scheme 4.14 Three-component Strecker reaction

Several catalytic systems based on metals have proven to be effective for this reaction.^{72–76} Recently, catalysts based on palladium-NHCs have shown good activities under homogenous⁷⁷ and heterogeneous⁵⁰ conditions. Because the Strecker reaction is an acid promoted transformation, we thought that our polymeric materials would be good candidates for this reaction, as the Au centers could facilitate the Lewis acidic function necessary for the activation of the substrates.

Reduction of nitroarenes

Table 4.9 shows the results obtained in the reduction of nitroarenes catalyzed by **5K** and **6K**. The reaction was carried out using an excess of NaBH_4 , with a 0.5 % mol catalyst loading (based on metal), at room temperature in a 1:1 mixture $\text{MeOH}/\text{H}_2\text{O}$ during 5 hours. Both catalysts show high activities for the reduction of 4-methoxynitrobenzene (entries 1 and 2) and moderate activity for the hydrogenation of 4-nitrotoluene and 4-bromonitrobenzene (entries 3 to 6).

Table 4.9 Reduction of nitroarenes^a

Entry	R	Cat	Yield(%) ^b
1	OMe	5K	> 95 (92)
2		6K	> 95 (90)
3	Me	5K	65
4		6K	45
5	Br	5K	84
6		6K	65

^aReaction Conditions: 1.078 mmol of nitroarene and 50 mmol of NaBH₄ were stirred in 10 mL of a 1:1 mixture of Milli-Q water and MeOH for 15 min. Then 2.5 mg of **5K** or **6K** were added and the resulting mixture was stirred for 5h. ^bYields determined by ¹H NMR spectroscopy. Isolated yields in parenthesis.

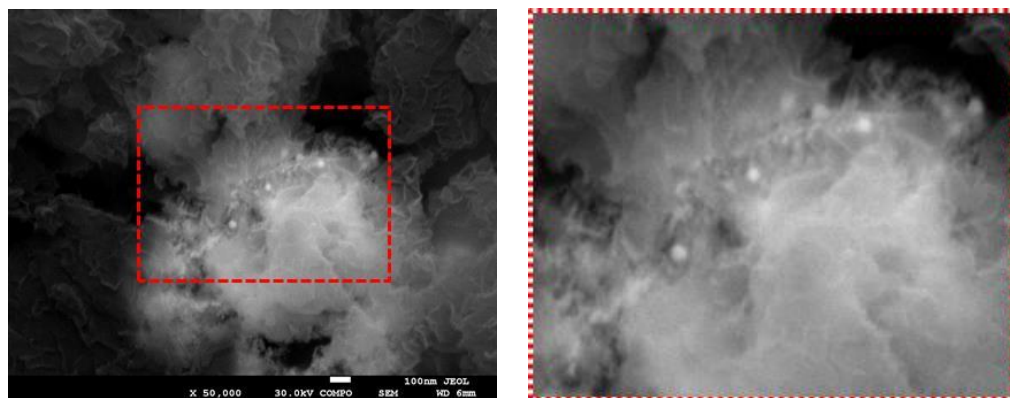


Figure 4.21 SEM micrograph of **6K** after the reduction of nitroarenes. The image was taken using the back-scattered electrons (BSE) signal of the SEM.

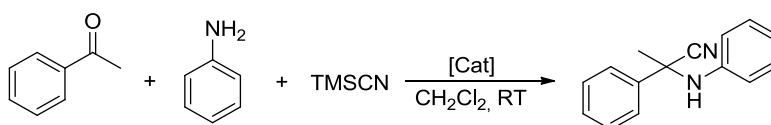
In general, the activity observed for catalyst **5K** was higher than the one observed for **6K**. This is just the opposite tendency that we were expecting, since the surface area observed for **6K** is much higher than the area of **5K**. During the reaction process we observed that the color of the catalyst changed from brown to dark gray. We analyzed the catalyst after the reaction using the back-scattered SEM signal and we observed the formation of gold nanoparticles (Figure 4.21). These nanoparticles are probably

formed during the reaction process due to the use of a strong reductant as NaBH_4 , so we cannot discard that the true catalytic species for this reaction are the nanoparticles rather than the polymeric compounds.

Three-component Strecker reaction

The three-component Strecker reaction was performed in the presence of 4 mol % of catalyst (based on amount of metal), in dichloromethane at room temperature for 12 hours. Recyclability tests were carried out with compounds **5K** and **6K** (Table 4.10). Both catalysts show high activities in the first run (entries 1 and 4). Unfortunately, their activity decreases in successive runs, although catalyst **6K** maintains good performances compared to **5K** (compare entries 2 and 3 with 5 and 6).

Table 4.10 Recycle test in the three-component Strecker reaction^a



Entry	Run	Cat	Yield(%) ^b
1	1		95
2	2	5K	59
3	3		29
4	1		98
5	2	6K	70
6	3		61

^aReaction conditions: 0.5 mmol ketone, 0.55 mmol aniline, 1 mmol TMSCN, 4 mol % catalyst loading (based on Au), 2 mL of CH_2Cl_2 , 12 h at room temperature. ^bYields determined by GC using anisole (0.5 mmol) as internal standard.

After the three runs, **5K** and **6K** were analyzed by SEM (Figure 4.22). The morphology of both catalysts has changed substantially, but we did not detect the formation of gold nanoparticles. The surface area of both materials after the catalytic experiments has also changed ($18 \text{ m}^2/\text{g}$ for **5K** and $26 \text{ m}^2/\text{g}$ for **6K**), but the composition of the polymers did not change much, as confirmed by elemental analysis, FT-IR spectroscopy and TGA. These results suggest that the decrease in the activities of **5K** and **6K** is mainly due to morphological changes of the material. It is

worth mentioning that the amount of the two catalysts used in this reaction is around 10 mg, a very low catalyst loading compared to those typically used in heterogeneous systems.^{65,68}

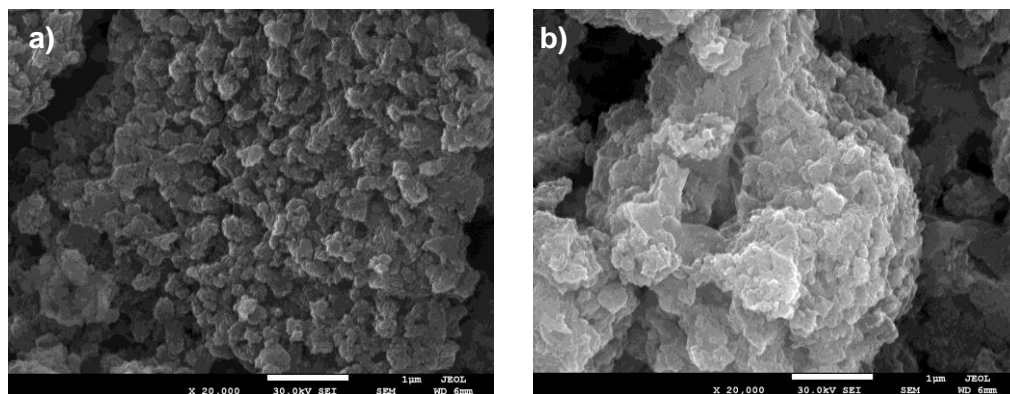
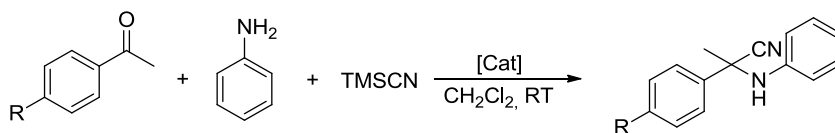


Figure 4.22 SEM micrographs of **5K** (image a)) and **6K** (image b)) after three runs of the Strecker reaction.

In order to broaden the scope of our catalysts in the Strecker reaction, we decided to perform the reaction using other substituted ketones (Table 4.11).

Table 4.11 Three-component Strecker reaction of ketones^a



Entry	R	Cat	Yield(%) ^b
1	Br	5K	85
2	Br	6K	88
3	MeO	5K	76
4	MeO	6K	92
5	NO ₂	5K	20
6	NO ₂	6K	13

^aReaction conditions: 0.5 mmol ketone, 0.55 mmol aniline, 1 mmol TMSCN, 4 mol % catalyst loading (based on Au), 2 mL of CH₂Cl₂, 12 h at room temperature. ^bYields determined by GC using anisole (0.5 mmol) as internal standard.

Both catalysts showed good catalytic performances when 4-bromoacetophenone was used (entries 1 and 2). The methoxy group was also well tolerated by the catalysts

(entries 3 and 4). However, when 4-nitroacetophenone was employed, poor yields were achieved (entries 5 and 6), confirming the inertness of this substrate toward this reaction.^{50,77}

4.2 Conclusions

In this section we described the preparation and characterization of a new triphenylene-tris-imidazolium salt $[\mathbf{KH}_3](\mathbf{BF}_4)_3$, through a two-steps high-yielding synthetic procedure. This salt is the precursor of a tris-NHC with D_{3h} symmetry, in which the three carbene moieties are connected by a polyaromatic core.

Homo-trimetallic complexes based on triphenylene **1K-4K** and **7K** were synthesized and fully characterized by standard spectroscopic techniques. For comparative purposes, the triptycene-based homo-trimetallic compounds **2M** and **3M**, and the monometallic analogues (**2N** and **3N**) were also obtained and characterized. Two new polymeric organometallic materials based on triphenylene-tris-NHC gold species **5K** and **6K**, were synthesized and characterized as well.

The stereoelectronic properties of **K**, **M** and **N** were studied, concluding that they are similar for the three ligands. The electronic communication through ligand **K** is almost negligible, as confirmed by DFT calculations of the TEP and electrochemical measurements of **1K**.

The catalytic properties of the new palladium and gold-based catalysts were studied. The palladium complexes were tested in the α -arylation of propiophenone and in the Suzuki-Miyaura C-C coupling. The catalytic activity of the gold compounds was studied in the hydroamination of phenylacetylene. In all cases the best catalytic performances were achieved by the triphenylene-based complexes (**2K** and **3K**). We suggest that this superior catalytic activity is due to the presence of an aromatic core, because π -stacking interactions between the ligand and the substrates are probably playing a very important role in the catalytic system, as concluded from different kind of experiments carried out.

The catalytic activity of the two polymeric materials **5K** and **6K**, was tested in the reduction of nitroarenes and in the three-component Strecker reaction. For the hydrogenation of nitroarenes, good to moderate catalytic activities were obtained, depending on the substrates used. However, the formation of gold nanoparticles during the reaction process made us think that the real catalysts for this transformation are these nanoparticles rather than the polymeric materials. Both catalysts provided excellent catalytic performances in the three-component Strecker reaction, being the first time in that a gold catalyst has been used in this reaction. The

activity of the materials in the Strecker reaction may be due to the Lewis acidic activation of the ketone or imine upon coordination to Au.

4.3 References

- (1) Tennyson, A. G.; Rosen, E. L.; Collins, M. S.; Lynch, V. M.; Bielawski, C. W. *Inorg. Chem.* **2009**, *48*, 6924.
- (2) Mata, J. A.; Hahn, F. E.; Peris, E. *Chem. Sci.* **2014**, *5*, 1723.
- (3) Karimi, B.; Akhavan, P. F. *Chem. Commun.* **2009**, 3750.
- (4) Guisado-Barrios, G.; Hiller, J.; Peris, E. *Chem. Eur. J.* **2013**, *19*, 10405.
- (5) Williams, K. A.; Bielawski, C. W. *Chem. Commun.* **2010**, *46*, 5166.
- (6) Yatabe, T.; Harbison, M. A.; Brand, J. D.; Wagner, M.; Müllen, K.; Samorí, P.; Rabe, J. P. *J. Mater. Chem.* **2000**, *10*, 1519.
- (7) Khramov, D. M.; Boydston, A. J.; Bielawski, C. W. *Org. Lett.* **2006**, *8*, 1831.
- (8) Hilton, C. L.; Jamison, C. R.; Zane, H. K.; King, B. T. *J. Org. Chem.* **2009**, *74*, 405.
- (9) Dastgir, S.; Coleman, K. S.; Cowley, A. R.; Green, M. L. H. *Organometallics* **2010**, *29*, 4858.
- (10) Chianese, A. R.; Li, X.; Janzen, M. C.; Faller, J. W.; Crabtree, R. H. *Organometallics* **2003**, *22*, 1663.
- (11) Khramov, D. M.; Boydston, A. J.; Bielawski, C. W. *Angew. Chem. Int. Ed.* **2006**, *45*, 6186.
- (12) Er, J. A. V.; Tennyson, A. G.; Kamplain, J. W.; Lynch, V. M.; Bielawski, C. W. *Eur. J. Inorg. Chem.* **2009**, 1729.
- (13) Kelly III, R. A.; Clavier, H.; Giudice, S.; Scott, N. M.; Stevens, E. D.; Bordner, J.; Samardjiev, I.; Hoff, C. D.; Cavallo, L.; Nolan, S. P. *Organometallics* **2008**, *27*, 202.
- (14) Nelson, D. J.; Nolan, S. P. *Chem. Soc. Rev.* **2013**, *42*, 6723.
- (15) Hahn, F.; Wittenbecher, L.; Boese, R.; Blaser, D. *Chem. Eur. J.* **1999**, *5*, 1931.
- (16) Hahn, F.; Wittenbecher, L.; Le Van D; Fröhlich, R. *Angew. Chem. Int. Ed.* **2000**, *39*, 541.
- (17) Bittermann, A.; Herdtweck, E.; Härter, P.; Herrmann, W. A. *Organometallics* **2009**, *28*, 6963.
- (18) Gusev, D. G. *Organometallics* **2009**, *28*, 6458.
- (19) Gusev, D. G.; Peris, E. *Dalton Trans.* **2013**, *42*, 7359.

- (20) Leuthäusser, S.; Schwarz, D.; Plenio, H. *Chem. Eur. J.* **2007**, *13*, 7195.
- (21) Wolf, S.; Plenio, H. *J. Organomet. Chem.* **2010**, *695*, 2418.
- (22) Morris, R. B.; Day, P. *Adv. Inorg. Chem. Radiochem.* **1967**, *10*, 247.
- (23) Mercs, L.; Neels, A.; Albrecht, M. *Dalton Trans.* **2008**, 5570.
- (24) Sabater, S.; Mata, J. A.; Peris, E. *Organometallics* **2012**, *31*, 6450.
- (25) Prades, A.; Peris, E.; Alcarazo, M. *Organometallics* **2012**, *31*, 4623.
- (26) Nussbaum, M.; Schuster, O.; Albrecht, M. *Chem. Eur. J.* **2013**, *19*, 17517.
- (27) Hillier, A. C.; Sommer, W. J.; Yong, B. S.; Petersen, J. L.; Cavallo, L.; Nolan, S. P. *Organometallics* **2003**, *22*, 4322.
- (28) Clavier, H.; Nolan, S. P. *Chem. Commun.* **2010**, *46*, 841.
- (29) Poater, A.; Cosenza, B.; Correa, A.; Giudice, S.; Ragone, F.; Scarano, V.; Cavallo, L. *Eur. J. Inorg. Chem.* **2009**, 1759.
- (30) Johansson, C. C. C.; Colacot, T. J. *Angew. Chem. Int. Ed.* **2010**, *49*, 676.
- (31) Valente, C.; Calimsiz, S.; Hoi, K. H.; Mallik, D.; Sayah, M.; Organ, M. G. *Angew. Chem. Int. Ed.* **2012**, *51*, 3314.
- (32) Zeng, X.; Frey, G. D.; Kinjo, R.; Donnadiou, B.; Bertrand, G. *J. Am. Chem. Soc.* **2009**, *131*, 8690.
- (33) Dash, C.; Shaikh, M. M.; Butcher, R. J.; Ghosh, P. *Inorg. Chem.* **2010**, *49*, 4972.
- (34) Katari, M.; Rao, M. N.; Rajaraman, G.; Ghosh, P. *Inorg. Chem.* **2012**, *51*, 5593.
- (35) Alvarado, E.; Badaj, A. C.; Larocque, T. G.; Lavoie, G. G. *Chem. Eur. J.* **2012**, *18*, 12112.
- (36) Satoh, T.; Kawamura, Y.; Miura, M.; Nomura, M. *Angew. Chemie* **1997**, *109*, 1820.
- (37) Palucki, M.; Buchwald, S. L. *J. Am. Chem. Soc.* **1997**, *119*, 11108.
- (38) Hamann, B. C.; Hartwig, J. F. *J. Am. Chem. Soc.* **1997**, *119*, 12382.
- (39) Viciu, M. S.; Germaneau, R. F.; Nolan, S. P. *Org. Lett.* **2002**, *4*, 4053.
- (40) Helms, B.; Fréchet, J. M. J. *Adv. Synth. Catal.* **2006**, *348*, 1125.
- (41) Reek, J.; Arevalo, S.; Van Heerbeek, R.; Kamer, P.; Van Leeuwen, P. *Adv. Catal.* **2006**, *49*, 71.

- (42) Santa María, M. D.; Cornago, P.; Claramunt, R. M.; Elguero, J.; Fernández-Castaño, C.; Foces-Foces, C. *J. Mol. Struct.* **1999**, *478*, 285.
- (43) Zhang, W.-Y.; Han, Y.-F.; Weng, L.-H.; Jin, G.-X. *Organometallics* **2014**, *33*, 3091.
- (44) Ruiz-Botella, S.; Peris, E. *Organometallics* **2014**, *33*, 5509.
- (45) Valdés, H.; Poyatos, M.; Ujaque, G.; Peris, E. *Chem. Eur. J.* **2015**, *21*, 1578.
- (46) Williams, K. A.; Boydston, A. J.; Bielawski, C. W. *Chem. Soc. Rev.* **2007**, *36*, 729.
- (47) Boydston, A. J.; Williams, K. A.; Bielawski, C. W. *J. Am. Chem. Soc.* **2005**, *127*, 12496.
- (48) Boydston, A. J.; Rice, J. D.; Sanderson, M. D.; Dykhno, O. L.; Bielawski, C. W. *Organometallics* **2006**, *25*, 6087.
- (49) Guerret, O.; Solé, S.; Gornitzka, H.; Teichert, M.; Trinquier, G.; Bertrand, G. *J. Am. Chem. Soc.* **1997**, *119*, 6668.
- (50) Choi, J.; Yang, H. Y.; Kim, H. J.; Son, S. U. *Angew. Chem. Int. Ed.* **2010**, *49*, 7718.
- (51) Zhang, C.; Wang, J.-J.; Liu, Y.; Ma, H.; Yang, X.-L.; Xu, H.-B. *Chem. Eur. J.* **2013**, *19*, 5004.
- (52) Lin, M.; Wang, S.; Zhang, J.; Luo, W.; Liu, H.; Wang, W.; Su, C.-Y. *J. Mol. Catal. A Chem.* **2014**, *394*, 33.
- (53) Karimi, B.; Akhavan, P. F. *Inorg. Chem.* **2011**, *50*, 6063.
- (54) Karimi, B.; Fadavi Akhavan, P. *Chem. Commun.* **2011**, *47*, 7686.
- (55) Wang, H. M. J.; Chen, C. Y. L.; Lin, I. J. B. *Organometallics* **1999**, *18*, 1216.
- (56) Gao, L.; Partyka, D. V.; Updegraff, J. B.; Deligonul, N.; Gray, T. G. *Eur. J. Inorg. Chem.* **2009**, 2711.
- (57) Fortman, G. C.; Poater, A.; Levell, J. W.; Gaillard, S.; Slawin, A. M. Z.; Samuel, I. D. W.; Cavallo, L.; Nolan, S. P. *Dalton Trans.* **2010**, *39*, 10382.
- (58) Konkolewicz, D.; Gaillard, S.; West, A. G.; Cheng, Y. Y.; Gray-Weale, A.; Schmidt, T. W.; Nolan, S. P.; Perrier, S. *Organometallics* **2011**, *30*, 1315.
- (59) Garg, J. A.; Blacque, O.; Heier, J.; Venkatesan, K. *Eur. J. Inorg. Chem.* **2012**, 1750.
- (60) Zhou, Y.-P.; Liu, E.-B.; Wang, J.; Chao, H.-Y. *Inorg. Chem.* **2013**, *52*, 8629.
- (61) Wienhöfer, G.; Sorribes, I.; Boddien, A.; Westerhaus, F.; Junge, K.; Junge, H.; Llusar, R.; Beller, M. *J. Am. Chem. Soc.* **2011**, *133*, 12875.

- (62) Sorribes, I.; Wienhöfer, G.; Vicent, C.; Junge, K.; Llusar, R.; Beller, M. *Angew. Chem. Int. Ed.* **2012**, *51*, 7794.
- (63) Verma, P. K.; Bala, M.; Thakur, K.; Sharma, U.; Kumar, N.; Singh, B. *Catal. Letters* **2014**, *144*, 1258.
- (64) Feng, Y.-S.; Ma, J.-J.; Kang, Y.-M.; Xu, H.-J. *Tetrahedron* **2014**, *70*, 6100.
- (65) Corma, A.; Serna, P. *Science* **2006**, *313*, 332.
- (66) Lou, X.-B.; He, L.; Qian, Y.; Liu, Y.-M.; Cao, Y.; Fan, K.-N. *Adv. Synth. Catal.* **2011**, *353*, 281.
- (67) Choi, Y.; Bae, H. S.; Seo, E.; Jang, S.; Park, K. H.; Kim, B.-S. *J. Mater. Chem.* **2011**, *21*, 15431.
- (68) Layek, K.; Kantam, M. L.; Shirai, M.; Nishio-Hamane, D.; Sasaki, T.; Maheswaran, H. *Green Chem.* **2012**, *14*, 3164.
- (69) Strecker, A. *Ann. Chem. Pharm* **1850**, 75.
- (70) Gröger, H. *Chem. Rev.* **2003**, *103*, 2795.
- (71) Williams, R. M.; Hendrix, J. A. *Chem. Rev.* **1992**, *92*, 889.
- (72) Ishitani, H.; Komiyama, S.; Hasegawa, Y.; Kobayashi, S. *J. Am. Chem. Soc.* **2000**, *122*, 762.
- (73) Josephsohn, N. S.; Kuntz, K. W.; Snapper, M. L.; Hoveyda, A. H. *J. Am. Chem. Soc.* **2001**, *123*, 11594.
- (74) Huguenot, F.; Brigaud, T. *J. Org. Chem.* **2006**, *71*, 7075.
- (75) Kazemeini, A.; Azizi, N.; Saidi, M. R. *Russ. J. Org. Chem.* **2006**, *42*, 48.
- (76) Khan, N. H.; Agrawal, S.; Kureshy, R. I.; Abdi, S. H. R.; Singh, S.; Suresh, E.; Jasra, R. V. *Tetrahedron Lett.* **2008**, *49*, 640.
- (77) Jarusiewicz, J.; Choe, Y.; Yoo, K. S.; Park, C. P.; Jung, K. W. *J. Org. Chem.* **2009**, *74*, 2873.

Chapter 5

Experimental section

5.1 Analytical techniques

Liquid Nuclear Magnetic Resonance (NMR)

^1H and ^{13}C NMR spectra were recorded on the following spectrometers at 298 K:

- Varian Innova 300 MHz (^1H 300 MHz, ^{13}C 75 MHz)
- Varian Innova 500MHz (^1H 500 MHz, ^{13}C 125 MHz)

Chemical shifts are given in ppm (δ), referred to the residual peak of the deuterated solvent (CDCl_3 , CD_2Cl_2 , CD_3CN , acetone- d_6 , CD_3OD and $\text{DMSO-}d_6$) and reported downfield of SiMe_4 .

Solid state NMR

Solid state NMR spectra were recorded on Bruker Advance spectrometers (300 MHz and 400 MHz) equipped with 4 mm single and double resonance NMR probes.

Electrospray Mass Spectra (ESI-MS)

Electrospray Mass Spectra (ESI-MS) were recorded on a Micromass Quatro LC instrument; CH_3OH or CH_3CN were used as mobile phase and nitrogen was employed as the drying and nebulizing gas. High Resolution Mass Spectra (HR MS) were recorded on a Q-TOF Premier instrument.

Elemental Analysis

Elemental analyses were carried out on a TruSpec Micro Series.

Gas Chromatography (GC)

GC analyses were obtained on a Shimadzu GC-2010 apparatus equipped with a FID and a Teknokroma (TRB-5MS, 30 m x 0.25 mm x 0.25 μm) column was used.

Infrared Spectroscopy (IR)

Infrared spectra (FT-IR) were performed on a Bruker EQUINOX 55 spectrometer with a spectral window of 4000-600 cm^{-1} . Liquid samples were placed between KBr windows.

Electrochemical measurements

Electrochemical studies were carried out by using an Autolab Potentiostat (Model PGSTAT101) using a three-electrode cell. The cell was equipped with platinum

working and counter electrodes, as well as a silver wire reference electrode. In all experiments CH_2Cl_2 was used as solvent and $[\text{NBu}_4][\text{PF}_6]$ was used as the supporting electrolyte. All redox potentials were referenced to the Fc^+/Fc couple as internal standard with $E_{1/2}(\text{Fc}/\text{Fc}^+)$ vs. SCE = +0.446 V.

UV-vis spectroscopy

UV-visible absorption spectra were recorded on a Varian Cary 300 BIO spectrophotometer using CH_3CN under ambient conditions. Extinction coefficients (ϵ) were determined from Beer's law measurements using 10, 20, 30 and 40 μM concentrations of the analyte.

Fluorescence spectroscopy

Emission spectra were recorded on a modular Horiba FluoroLog®-3 spectrofluorometer employing degassed CH_3CN . Quantum yields were determined relative to recrystallized anthracene in degassed EtOH as standard ($\Phi_f = 0.27$), exciting at 317 nm.¹

Scanning electron microscopy (SEM)

Scanning electron micrographs of the samples were taken with a field emission gun scanning electron microscope (FEG-SEM) model JEOL 7001F, equipped with a spectrometer of energy dispersion of X-ray (EDX) from Oxford instruments by using the following operational parameters: acceleration voltage 20 KV, measuring time 305 s, working distance 10 mm, counting rate 1.2 kcps. The samples for microstructural and microanalysis determinations were covered with a Pt film.

Transmission electron microscopy (TEM)

A Jem-2100 LaB6 (Jeol) microscope, at an accelerating voltage of 200 KV, coupled with an INCA Energy TEM 200 (Oxford) energy dispersive X-ray spectrometer (EDX) was used for transmission electron microscopy, electron diffraction and microanalysis. Samples were prepared by drying a droplet of the EtOH dispersion on a carbon-coated copper grid.

N_2 sorption experiments

N_2 adsorption–desorption isotherms were collected on a Micromeritics Gemini V gas adsorption analyzer at 77 K, after degassing the samples at 150°C overnight in a

Micromeritics Flow prep 060 system with nitrogen flux gas. The BET surface areas were calculated from the adsorption branch of the isotherm by the BJH method.

X-Ray powder diffraction (XRD)

XRD patterns were recorded on a D4 Endeavor, Bruker-AXS diffractometer with a Cu-K radiation with a wavelength of 0.1542 nm.

Termogravimetric analysis (TGA)

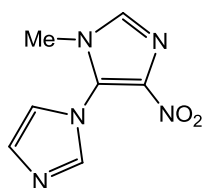
TGA curves were obtained on a TG-STDA Mettler Toledo model TGA/SDTA851e/LF/1600.

5.2 Synthesis and characterization

All the reactions were carried out by using standard Schlenk tube techniques under nitrogen atmosphere unless otherwise stated. Anhydrous solvents were dried using a solvent purification system (SPS M BRAUN) or purchased and degassed prior to use by purging with nitrogen and kept over molecular sieves. All other reagents were used as received from commercial suppliers. Column chromatography was performed on silica gel Merck 60, 62-200 μm unless otherwise stated, using the mixture of solvents indicated. $[\text{IrCl}(\text{COD})]_2$,² $[\text{RhCl}(\text{COD})]_2$,³ $[\text{RhCl}(\text{CO})_2]_2$,⁴ $[\text{AuCl}(\text{SMe}_2)]$,⁵ $[\text{RuCl}_2(p\text{-cymene})]_2$,⁶ 1,3-bis(2,6-diisopropylphenyl)imidazolium chloride (IPr·HCl),⁷ 4,5,9,10-tetrabromo-2,7-di-*tert*-butylpyrene,⁸ 1,3-diethylbenzimidazolium tetrafluoroborate,⁹ 2,7-di-*tert*-butylpyrene-4,5-dione,¹⁰ 2,3,6,7,10,11-hexabromotriphenylene,¹¹ 2,3,6,7,12,13-hexabromotriptycene,¹² KO_2CMes ,¹³ 1,3-di(*tert*-butyl)benzimidazolium chloride,¹⁴ $[\text{RhCl}(1,3\text{-di}(\textit{tert}\text{-butyl})\text{benzimidazolylidene})(\text{COD})]_2$ ⁹ were prepared according to literature procedures.

5.2.1 Synthesis and characterization of azolium salts

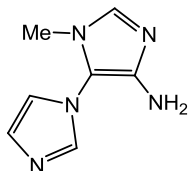
Synthesis of A



Under aerobic conditions 5-chloro-1-methyl-4-nitroimidazole (5 g, 30.35 mmol) and imidazole (1.74 g, 25.3 mmol) were dissolved in 75 mL of acetonitrile, and then KOH (3.2 g, 50.6 mmol) was added. The resulting mixture was refluxed for 2 hours.

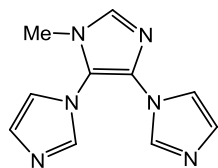
Afterwards, the reaction was filtered and the solvent was removed under vacuum giving a dark brown solid. Compound **1** was obtained as a brown solid after purification by sublimation in vacuum at 120°C. Yield 4.7 g, 96 %. ¹H NMR (500 MHz, MeOD-*d*₄): δ 8.01 (s, 1H, CH_{imid}), 7.86 (s, 1H, CH_{imid}), 7.45 (s, 1H, CH_{imid}), 7.27 (s, 1H, CH_{imid}), 3.58 (s, 3H, NCH_3). ¹³C NMR (75 MHz, MeOD-*d*₄): δ 140.3 (CH_{imid}), 136.4 (CH_{imid}), 130.5 (CH_{imid}), 125.4 (C_q), 122.4 (CH_{imid}), 122.2 (C_q), 32.3 (NCH_3). Anal. Calc. for $\text{C}_7\text{H}_7\text{N}_3\text{O}_2$ (811.95): C, 17.75; H, 1.99; N, 20.70. Found: C, 17.80; H, 2.05; N, 21.10. Electrospray MS (20 V, *m/z*): 191.1 $[\text{M}+\text{H}]^+$.

Synthesis of B



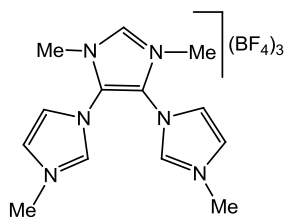
A mixture of compound **A** (1 g, 5.18 mmol) and Raney Nickel (2 mL, activated catalyst 50 % slurry in water) in methanol (50 mL) was stirred at room temperature under H₂ atmosphere (1 atm) for 4 hours. Afterwards, the suspension was filtered through a pad of Celite and the solvent was removed under vacuum, giving the desired product as a brownish oil. The oil so isolated was used in the next step without further purification. Yield 804 mg, 95 %. ¹H NMR (300 MHz, MeOD-*d*₄): δ 7.79 (s, 1H, CH_{imid}), 7.35 (s, 1H, CH_{imid}), 7.24 (s, 1H, CH_{imid}), 7.19 (s, 1H, CH_{imid}), 3.35 (s, 3H, NCH₃). ¹³C NMR (75 MHz, MeOD-*d*₄): δ 141.4 (CH_{imid}), 136.5 (C_q), 133.8 (CH_{imid}), 130.0 (CH_{imid}), 128.2 (C_q), 123.8 (CH_{imid}), 31.1 (NCH₃). Electrospray MS (20 V, *m/z*): 164.2 [M+Na]⁺.

Synthesis of C



Under aerobic conditions, the amine **B** (804 mg, 4.93 mmol) in methanol (10 mL) was treated with 40% aq. glyoxal (0.6 mL, 5.2 mmol) for 16 h at room temperature. NH₄Cl (560 mg, 10.4 mmol) was added, followed by 37% aq. formaldehyde (0.8 mL, 10.2 mol). The mixture was diluted with methanol (50 mL) and the resulting mixture refluxed for 1 h. After this time, H₃PO₄ was added until pH 2. The resulting mixture was then stirred at reflux for additional 8 hours. After removal of the solvent, the dark residue was poured into ice (150 g) and treated with an aq. 40% KOH solution until pH 9. The resulting mixture was extracted with dichloromethane (5×50 mL). The organic phases were combined, dried over Na₂SO₄ and the solvent was removed under vacuum giving compound **C** as a brown solid. The solid so obtained was used in the next step without further purification. Yield 448 mg, 46 %. ¹H NMR (500 MHz, MeOD-*d*₄): δ 7.94 (s, 1H, CH_{imid}), 7.80 (s, 1H, CH_{imid}), 7.74 (s, 1H, CH_{imid}), 7.41 (s, 1H, CH_{imid}), 7.27 (s, 1H, CH_{imid}), 7.08 (s, 1H, CH_{imid}), 7.04 (s, 1H, CH_{imid}), 3.54 (s, 3H, NCH₃). ¹³C NMR (75 MHz, MeOD-*d*₄): δ 141.0 (CH_{imid}), 137.1 (C_q), 136.4 (CH_{imid}), 132.1 (CH_{imid}), 131.0 (CH_{imid}), 130.4 (C_q), 129.9 (CH_{imid}), 129.6 (CH_{imid}), 123.4 (CH_{imid}), 31.6 (NCH₃). Electrospray MS (20 V, *m/z*): 214.9 [M+H]⁺.

Synthesis of $[\text{DH}_3](\text{BF}_4)_3$



A mixture of **C** (484 mg, 2.26 mmol) and $(\text{CH}_3)_3\text{OBF}_4$ (1.4 g, 9.5 mmol) was refluxed in degassed acetonitrile overnight. During this time, the desired product precipitated as a light brown solid. The product was collected by filtration and washed with cold acetonitrile and diethyl ether. Yield 550 mg, 47 %. ^1H NMR (300 MHz, $\text{DMSO-}d_6$): δ 9.66 (s, 1H, NCHN), 9.41 (s, 2H, NCHN), 8.07 (s, 2H, CH_{imid}), 7.95 (s, 2H, CH_{imid}), 3.95 (s, 6H, NCH_3), 3.87 (s, 6H, NCH_3). ^{13}C NMR (75 MHz, $\text{DMSO-}d_6$): δ 140.3 (NCHN), 136.5 (NCHN), 125.4 (CH_{imid}), 124.0 (CH_{imid}), 121.7 (C_q), 36.9 (NCH_3), 34.3 (NCH_3). Electrospray MS (15 V, m/z): 129.1 $[\text{M-H}^+]^{2+}$.

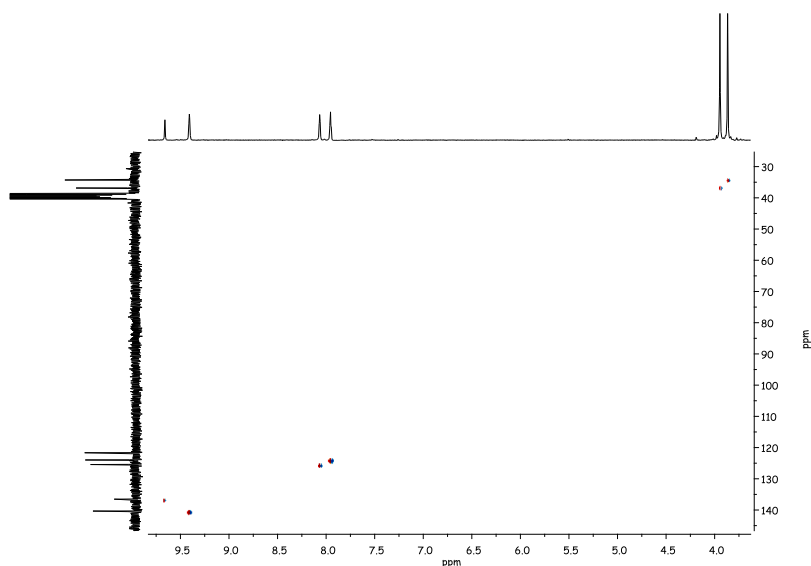
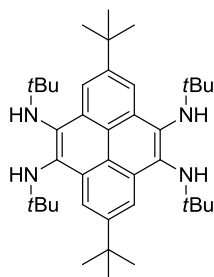


Figure 5.1 HSQC spectrum of $[\text{DH}_3](\text{BF}_4)_3$ in $\text{DMSO-}d_6$ ($J_{\text{H-C}} = 190$ Hz)

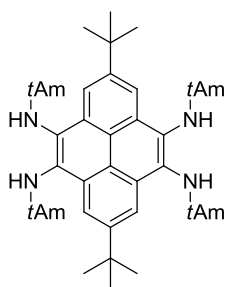
Synthesis of E-*t*Bu



In a Schlenk tube, 4,5,9,10-tetrabromo-2,7-di-*tert*-butylpyrene (800 mg, 1.27 mmol) and NaOtBu (587 mg, 6.1 mmol) were suspended in toluene (20 mL). In another Schlenk tube, a mixture of $[\text{Pd}(\text{OAc})_2]$ (20 mg, 0.089 mmol), $\text{IPr}\cdot\text{HCl}$ (76 mg, 0.178 mmol), NaOtBu (26 mg, 0.267 mmol) and toluene (10 mL) was stirred for 10 min at room temperature. After this time, the latter

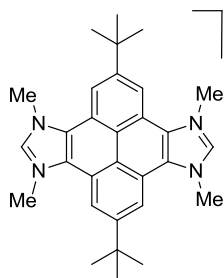
solution was added *via* oven dried cannula over the first one. Then, *tert*-butylamine (654 μL , 6.1 mmol) was added and the resulting mixture was refluxed overnight. The cooled reaction mixture was filtered over Celite and then concentrated under reduced pressure, yielding the desired product as a dark red solid. Yield: 760 mg, >99 %. ^1H NMR (300 MHz, CDCl_3): δ 8.48 (s, 4H, CH_{pyr}), 4.17 (s, 4H, NH), 1.60 (s, 18H, $\text{C}(\text{CH}_3)_3$), 1.28 (s, 36H, $\text{C}(\text{CH}_3)_3$). ^{13}C NMR (75 MHz, CDCl_3): δ 145.9 ($\text{C}_{\text{q pyr}}$), 136.4 ($\text{C}_{\text{q pyr}}$), 131.2 ($\text{C}_{\text{q pyr}}$), 120.2 ($\text{C}_{\text{q pyr}}$), 119.1 (CH_{pyr}), 56.1 ($\text{C}(\text{CH}_3)_3$), 35.8 ($\text{C}(\text{CH}_3)_3$), 32.2 ($\text{C}(\text{CH}_3)_3$), 31.8 ($\text{C}(\text{CH}_3)_3$). Electrospray MS (20 V, m/z): 599.5 $[\text{M}+\text{H}]^+$. HRMS ESI-TOF-MS (positive mode): $[\text{M}+\text{H}]^+$ monoisotopic peak 599.5053, calcd. 599.5054, $\epsilon_r = 0.2$ ppm. Anal. Calcd. for $\text{C}_{40}\text{H}_{62}\text{N}_4$ (598.95): C, 80.21; H, 10.43; N, 9.36. Found: C, 80.60; H, 10.11; N, 8.97.

Synthesis of E-*t*Amyl



In a Schlenk tube, 4,5,9,10-tetrabromo-2,7-di-*tert*-butylpyrene (500 mg, 0.79 mmol) and NaOtBu (365 mg, 3.8 mmol) were suspended in toluene (20 mL). In another Schlenk tube, a mixture of $[\text{Pd}(\text{OAc})_2]$ (12.6 mg, 0.056 mmol), 1,3-bis(2,6-diisopropylphenyl)imidazolium chloride ($\text{IPr}\cdot\text{HCl}$, 47.5 mg, 0.112 mmol), NaOtBu (16.2 mg, 0.168 mmol) and toluene (10 mL) was stirred for 10 min at room temperature. After this time, the latter solution was added *via* oven dried cannula over the first one. Then, *tert*-amylamine (455 μL , 3.8 mmol) was added and the resulting mixture was refluxed overnight. The cooled reaction mixture was filtered over Celite and then concentrated under reduced pressure, yielding the desired product as a dark red solid. Yield: 515 mg, >99 %. ^1H NMR (500 MHz, CDCl_3): δ 8.47 (s, 4H, CH_{pyr}), 4.08 (s, 4H, NH), 1.76 (q, $^3J_{\text{H-H}} = 7.5$ Hz, 8H, $\text{NC}(\text{CH}_2\text{CH}_3)(\text{CH}_3)_2$), 1.60 (s, 18H, $\text{C}(\text{CH}_3)_3$), 1.13 (t, $^3J_{\text{H-H}} = 7.5$ Hz, 12H, $\text{NC}(\text{CH}_2\text{CH}_3)(\text{CH}_3)_2$), 1.11 (s, 24H, $\text{NC}(\text{CH}_2\text{CH}_3)(\text{CH}_3)_2$). ^{13}C NMR (126 MHz, CDCl_3): δ 145.7 ($\text{C}_{\text{q pyr}}$), 136.3 ($\text{C}_{\text{q pyr}}$), 131.5 ($\text{C}_{\text{q pyr}}$), 120.0 ($\text{C}_{\text{q pyr}}$), 118.9 (CH_{pyr}), 58.6 ($\text{NC}(\text{CH}_2\text{CH}_3)(\text{CH}_3)_2$), 37.8 ($\text{NC}(\text{CH}_2\text{CH}_3)(\text{CH}_3)_2$), 35.8 ($\text{C}(\text{CH}_3)_3$), 32.2 ($\text{C}(\text{CH}_3)_3$), 28.2 ($\text{NC}(\text{CH}_2\text{CH}_3)(\text{CH}_3)_2$), 9.4 ($\text{NC}(\text{CH}_2\text{CH}_3)(\text{CH}_3)_2$). Electrospray MS (10 V, m/z): 655.7 $[\text{M}+\text{H}]^+$. HRMS ESI-TOF-MS (positive mode): $[\text{M}+\text{H}]^+$ monoisotopic peak 655.5681, calcd 655.5679, $\epsilon_r = 0.3$ ppm. Satisfactory elemental analysis could not be obtained due to the light sensitive nature of the compound.

Synthesis of $[\text{FH}_2\text{-Me}](\text{BF}_4)_2$



A mixture of compound **E-*t*Bu** (400 mg, 0.67 mmol, 1 equiv.), $\text{HBF}_4 \cdot \text{Et}_2\text{O}$ (202 μL , 1.47 mmol, 2.2 equiv.) and trimethyl orthoformate (20 mL) was refluxed for 16 h under aerobic conditions. After cooling at room temperature, Et_2O was added to the reaction mixture and the precipitated solid was collected by filtration. Compound $[\text{FH}_2\text{-Me}](\text{BF}_4)_2$ was isolated as a reddish solid. Yield: 350 mg, 84 %.

Compound $[\text{FH}_2\text{-Me}](\text{BF}_4)_2$ can also be obtained following the same procedure, but starting from compound **E-*t*Amyl**. In this case the yield of the synthesis is 43 %. ^1H NMR (300 MHz, $\text{DMSO-}d_6$): δ 9.83 (s, 2H, NCHN), 9.04 (s, 4H, CH_{pyr}), 4.76 (s, 12H, NCH₃), 1.68 (s, 18H, $\text{C}(\text{CH}_3)_3$). ^{13}C NMR (75 MHz, $\text{DMSO-}d_6$): δ 150.4 ($\text{C}_{\text{q pyr}}$), 143.2 (NCHN), 127.1 ($\text{C}_{\text{q pyr}}$), 120.9 ($\text{C}_{\text{q pyr}}$), 119.9 ($\text{C}_{\text{q pyr}}$), 118.4 (CH_{pyr}), 38.3 (NCH₃), 35.7 ($\text{C}(\text{CH}_3)_3$), 31.2 ($\text{C}(\text{CH}_3)_3$). Electrospray MS (20 V, m/z): 226.4 $[\text{M}]^{2+}$. Anal. Calcd. for $\text{C}_{30}\text{H}_{36}\text{B}_2\text{F}_8\text{N}_4$ (626.30): C, 57.53; H, 5.79; N, 8.95. Found: C, 57.15; H, 5.70; N, 8.80.

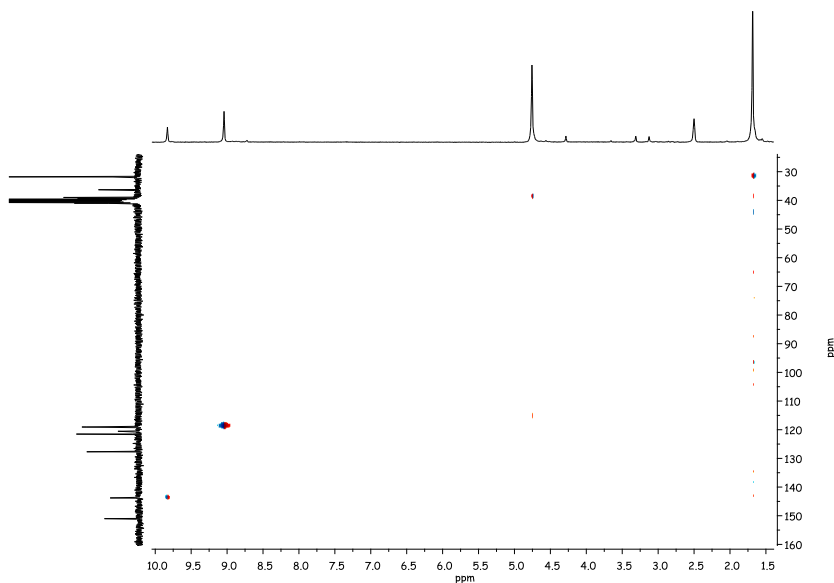
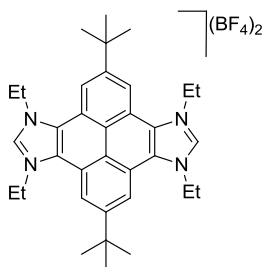


Figure 5.2 HSQC spectrum of $[\text{FH}_2\text{-Me}](\text{BF}_4)_2$ in $\text{DMSO-}d_6$ ($^1J_{\text{H-C}} = 190$ Hz)

Synthesis of $[\text{FH}_2\text{-Et}](\text{BF}_4)_2$

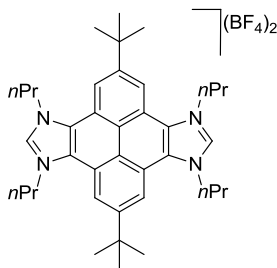


A mixture of compound **E-*t*Bu** (400 mg, 0.67 mmol, 1 equiv.), $\text{HBF}_4 \cdot \text{Et}_2\text{O}$ (202 μL , 1.47 mmol, 2.2 equiv.) and triethyl orthoformate (20 mL) was refluxed for 16 h under aerobic conditions. After cooling at room temperature, Et_2O was added to the reaction mixture and the precipitated solid was collected by filtration. Compound **7-Et** was precipitated in a mixture of $\text{CH}_3\text{CN}/\text{Et}_2\text{O}$ as a beige solid. Yield: 320 mg,

70 %. Compound $[\text{FH}_2\text{-Et}](\text{BF}_4)_2$ can also be obtained following the same procedure, but starting from compound **E-*t*Amyl**. In this case the yield of the synthesis is 63 %.

^1H NMR (300 MHz, $\text{DMSO-}d_6$): δ 9.93 (s, 2H, NCHN), 8.93 (s, 4H, CH_{pyr}), 5.20 (q, $^3J_{\text{H-H}} = 7.0$ Hz, 8H, NCH_2CH_3), 1.82 (t, $^3J_{\text{H-H}} = 7.0$ Hz, 12 H, NCH_2CH_3), 1.69 (s, 18H, $\text{C}(\text{CH}_3)_3$). ^{13}C NMR (75 MHz, $\text{DMSO-}d_6$): δ 150.6 ($\text{C}_{\text{q pyr}}$), 141.9 (NCHN), 126.7 ($\text{C}_{\text{q pyr}}$), 120.6 ($\text{C}_{\text{q pyr}}$), 120.0 ($\text{C}_{\text{q pyr}}$), 118.6 (CH_{pyr}), 46.2 (NCH_2CH_3), 35.7 ($\text{C}(\text{CH}_3)_3$), 31.1 ($\text{C}(\text{CH}_3)_3$), 14.3 (NCH_2CH_3). Electrospray MS (20V, m/z): 254.3 $[\text{M}]^{2+}$. Anal. Calcd. for $\text{C}_{34}\text{H}_{44}\text{B}_2\text{F}_8\text{N}_4$ (682.35): C, 59.84; H, 6.50; N, 8.21. Found: C, 59.55; H, 6.75; N, 7.85.

Synthesis of $[\text{FH}_2\text{-}n\text{Pr}](\text{BF}_4)_2$

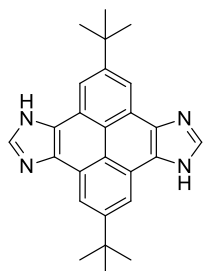


Under aerobic conditions, a mixture of compound **E-*t*Bu** (500 mg, 0.84 mmol, 1 equiv.), 15 mL of tripropyl orthoformate and $\text{HBF}_4 \cdot \text{Et}_2\text{O}$ (253 μL , 1.84 mmol, 2.2 equiv.) was heated in a thick-walled Schlenk tube fitted with a Teflon cap at 150°C for 24h. After cooling at room temperature, Et_2O was added to the reaction mixture and the precipitated solid was collected by filtration. Compound

$[\text{FH}_2\text{-}n\text{Pr}](\text{BF}_4)_2$ was precipitated in a mixture of $\text{CH}_3\text{CN}/\text{Et}_2\text{O}$ as a brown solid. Yield: 396 mg, 64 %. Compound $[\text{FH}_2\text{-}n\text{Pr}](\text{BF}_4)_2$ can also be obtained following the same procedure but starting from compound **E-*t*Amyl**. In this case the yield of the synthesis is 59 %. ^1H NMR (500 MHz, CD_3CN): δ 9.22 (s, 2H, NCHN), 8.89 (s, 4H, CH_{pyr}), 5.03 (t, $^3J_{\text{H-H}} = 7.4$ Hz, 8H, $\text{NCH}_2\text{CH}_2\text{CH}_3$), 2.28 (m, 8H, $\text{NCH}_2\text{CH}_2\text{CH}_3$), 1.70 (s, 18H, $\text{C}(\text{CH}_3)_3$), 1.20 (t, $^3J_{\text{H-H}} = 7.4$ Hz, 8H, $\text{NCH}_2\text{CH}_2\text{CH}_3$). ^{13}C NMR (126 MHz, CD_3CN): δ 152.2 ($\text{C}_{\text{q pyr}}$), 142.5 (NCHN), 128.6 ($\text{C}_{\text{q pyr}}$), 122.1 ($\text{C}_{\text{q pyr}}$), 122.0 ($\text{C}_{\text{q pyr}}$), 119.9 (CH_{pyr}), 53.7 ($\text{NCH}_2\text{CH}_2\text{CH}_3$), 36.7 ($\text{C}(\text{CH}_3)_3$), 31.7 ($\text{C}(\text{CH}_3)_3$), 23.3

(NCH₂CH₂CH₃),, 10.9 (NCH₂CH₂CH₃). Anal. Calcd. for C₃₈H₅₂B₂F₈N₄ (738.45): C, 61.8; H, 7.1; N, 7.59. Found: C, 61.75; H, 7.30; N, 7.40.

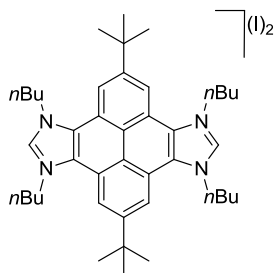
Synthesis of **G**



Under aerobic conditions, a mixture of compound **5-*t*Bu** (500 mg, 0.84 mmol, 1 equiv.), 5 mL of tributyl orthoformate and HBF₄·Et₂O (253 μL, 1.84 mmol, 2.2 equiv.) was heated in a thick-walled Schlenk tube fitted with a Teflon cap at 150°C for 24h. After cooling at room temperature, Et₂O was added to the reaction mixture and the precipitated solid was collected by filtration.

Compound **G** was precipitated in a mixture of CH₃CN/Et₂O as a brown solid. Yield: 326 mg, 98 %. Compound **G** can also be obtained following the same procedure, but starting from compound **E-*t*Amyl**. In this case the yield of the synthesis is also 98 %. ¹H NMR (300 MHz, DMSO-*d*₆): δ 9.78 (s, 2H, NCHN), 9.01 (s, 4H, CH_{pyr}), 1.64 (C(CH₃)₃). ¹³C NMR (75 MHz, DMSO-*d*₆): δ 151.0 (C_{q pyr}), 138.4 (NCHN), 126.6 (C_{q pyr}), 120.7 (C_{q pyr}), 119.1 (C_{q pyr}), 118.0 (CH_{pyr}), 35.8 (C(CH₃)₃), 31.5 (C(CH₃)₃). Electrospray MS (20 V, *m/z*): 395.5 [M+H]⁺. HRMS ESI-TOF-MS (positive mode): [M+H]⁺ monoisotopic peak 395.2232, calcd 395.2236, ε_r = 1 ppm. Satisfactory elemental analysis could not be obtained due to the hygroscopic nature of the compound.

Synthesis of [FH₂-*n*Bu](**I**)₂

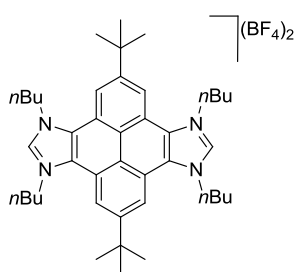


Under aerobic conditions, compound **G** (200 mg, 0.51 mmol) and NaOH (44.9 mg, 1.12 mmol) were dissolved in DMSO (3 mL). The reaction mixture was stirred at room temperature for 2 h. *n*-Butyl bromide (111 μL, 1.02 mmol) was then added and the mixture was stirred at room temperature for 30 min and after that at 37°C overnight.

After this time, the solvent was removed under vacuum. The residue was dissolved in CH₂Cl₂ and filtered through a pad of Celite to remove insoluble salts. The solvent was removed under vacuum and the isolated brown solid was placed in a thick-walled tube together with *n*-butyl iodide (2.4 mL, 21.2 mmol). The mixture was stirred at 100°C for 24 h. Then the solvent was removed under reduced pressure. The solid was suspended and washed with diethyl ether to provide the desired product as a brown solid that was collected by filtration. Yield: 262 mg,

59 %. ^1H NMR (300 MHz, CD_3CN): δ 9.70 (s, 2H, NCHN), 8.88 (s, 4H, CH_{pyr}), 5.10 (t, $^3J_{\text{H-H}} = 7.4$ Hz, 8H, $\text{NCH}_2\text{CH}_2\text{CH}_2\text{CH}_3$), 2.24 (m, 8H, $\text{NCH}_2\text{CH}_2\text{CH}_2\text{CH}_3$), 1.69 (s, 18H, $\text{C}(\text{CH}_3)_3$), 1.66 (m, $\text{NCH}_2\text{CH}_2\text{CH}_2\text{CH}_3$, 8H), 1.06 (t, $^3J_{\text{H-H}} = 7.3$ Hz, $\text{NCH}_2\text{CH}_2\text{CH}_2\text{CH}_3$, 12H). ^{13}C NMR (75 MHz, CD_3CN): δ 152.1 ($\text{C}_{\text{q pyr}}$), 142.3 (NCHN), 128.6 ($\text{C}_{\text{q pyr}}$), 122.1 ($\text{C}_{\text{q pyr}}$), 122.1 ($\text{C}_{\text{q pyr}}$), 119.9 (CH_{pyr}), 52.2 ($\text{NCH}_2\text{CH}_2\text{CH}_2\text{CH}_3$), 36.7 ($\text{C}(\text{CH}_3)_3$), 31.9 ($\text{C}(\text{CH}_3)_3$), 31.8 ($\text{NCH}_2\text{CH}_2\text{CH}_2\text{CH}_3$), 20.4 ($\text{NCH}_2\text{CH}_2\text{CH}_2\text{CH}_3$), 13.9 ($\text{NCH}_2\text{CH}_2\text{CH}_2\text{CH}_3$). Electrospray MS (10 V, m/z): 310.5 $[\text{M}]^{2+}$. HRMS ESI-TOF-MS (positive mode): $[\text{M}]^{2+}$ monoisotopic peak 310.2403, calcd 310.2409, $\varepsilon_{\text{r}} = 0.3$ ppm. Anal. Calcd. for $\text{C}_{42}\text{H}_{60}\text{I}_2\text{N}_4$ (874.74): C, 57.67; H, 6.91; N, 6.41. Found: C, 57.10; H, 6.69; N, 6.57.

Synthesis of $[\text{FH}_2\text{-}n\text{Bu}](\text{BF}_4)_2$



Anion metathesis of the iodide salt $[\text{FH}_2\text{-}n\text{Bu}](\text{I})_2$ was achieved by treating it with $\text{Et}_3\text{O}\cdot\text{BF}_4$ as reported earlier by Bielawski and co-workers.¹⁵ Compound $[\text{FH}_2\text{-}n\text{Bu}](\text{I})_2$ (60 mg, 0.069 mmol) was placed in a Schlenk tube. The tube was evacuated and filled with nitrogen three times. Afterward, 10 mL of CH_2Cl_2 and $\text{Et}_3\text{O}\cdot\text{BF}_4$ (26.1 mg, 0.137 mmol) were subsequently added. The mixture was stirred at room temperature for 30 min. Then, the solution was concentrated under reduced pressure. After the addition of diethyl ether, the desired product precipitated as a brown solid that was collected by filtration and washed with diethyl ether. Yield: 45 mg, 83 %. ^1H NMR (500 MHz, CD_3CN): δ 9.18 (s, 2H, NCHN), 8.88 (s, 4H, CH_{pyr}), 5.04 (t, $^3J_{\text{H-H}} = 7.5$ Hz, 8H, $\text{NCH}_2\text{CH}_2\text{CH}_2\text{CH}_3$), 2.21 (m, 8H, $\text{NCH}_2\text{CH}_2\text{CH}_2\text{CH}_3$), 1.69 (s, 18H, $\text{C}(\text{CH}_3)_3$), 1.64 (m, $\text{NCH}_2\text{CH}_2\text{CH}_2\text{CH}_3$, 8H), 1.06 (t, $^3J_{\text{H-H}} = 7.4$ Hz, $\text{NCH}_2\text{CH}_2\text{CH}_2\text{CH}_3$, 12H). ^{13}C NMR (126 MHz, CD_3CN): δ 152.2 ($\text{C}_{\text{q pyr}}$), 142.2 (NCHN), 128.6 ($\text{C}_{\text{q pyr}}$), 122.1 ($\text{C}_{\text{q pyr}}$), 122.0 ($\text{C}_{\text{q pyr}}$), 119.9 (CH_{pyr}), 52.2 ($\text{NCH}_2\text{CH}_2\text{CH}_2\text{CH}_3$), 36.7 ($\text{C}(\text{CH}_3)_3$), 31.9 ($\text{C}(\text{CH}_3)_3$), 31.7 ($\text{NCH}_2\text{CH}_2\text{CH}_2\text{CH}_3$), 20.4 ($\text{NCH}_2\text{CH}_2\text{CH}_2\text{CH}_3$), 13.8 ($\text{NCH}_2\text{CH}_2\text{CH}_2\text{CH}_3$). Electrospray MS (10 V, m/z): 310.4 $[\text{M}]^{2+}$. Anal. Calcd. for $\text{C}_{42}\text{H}_{60}\text{B}_2\text{F}_8\text{N}_4$ (794.56): C, 63.48; H, 7.61; N, 7.05. Found: C, 63.10; H, 7.24; N, 6.80.

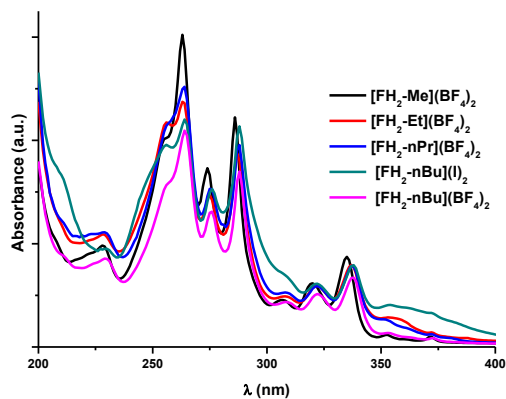


Figure 5.3 UV-vis spectra of pyrene-based bisazolium salts, recorded in MeCN at a concentration of 40 μM , under aerobic conditions

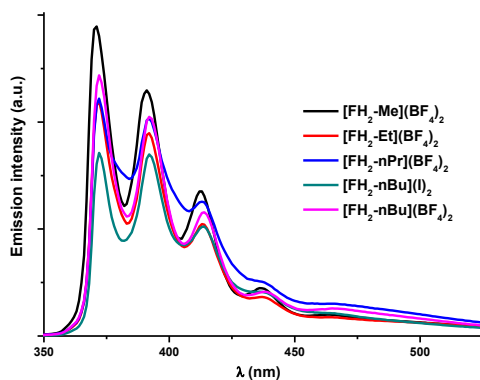
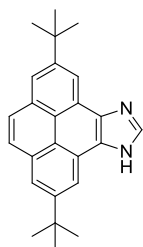


Figure 5.4 Emission spectra of pyrene-based bisazolium salts, at 317 nm in MeCN (40 μM under aerobic conditions).

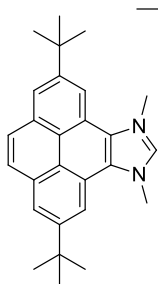
Synthesis of H



A mixture of 2,7-di-*tert*-butylpyrene-4,5-dione (500 mg, 1.45 mmol), NH_4Ac (2.4 g, 30.5 mmol), formaldehyde (136 μL of a 37 % aqueous solution, 1.8 mmol) and glacial acetic acid (15 mL) was refluxed overnight under aerobic conditions. After cooling to room temperature, 40 mL of distilled water were added and the mixture was neutralized with aqueous ammonia (28-30 %). The brown precipitate formed was

collected by filtration, washed with water and subsequently dried with air and under vacuum. Yield: 496 mg, 97 %. ^1H NMR (500 MHz, $\text{DMSO-}d_6$): δ 8.76 (s, 2H, CH_{pyr}), 8.41 (s, 1H, NCHN), 8.21 (s, 2H, CH_{pyr}), 8.11 (s, 2H, CH_{pyr}), 1.57 (s, 18H, $\text{C}(\text{CH}_3)_3$). ^{13}C NMR (126 MHz, $\text{DMSO-}d_6$): δ 171.9 (C_q), 148.5 (C_q), 139.0 (NCHN), 131.1 (C_q), 127.6 (CH_{pyr}), 120.6 (CH_{pyr}), 119.9 (C_q), 115.8 (CH_{pyr}), 114.4 (C_q), 35.1 ($\text{C}(\text{CH}_3)_3$), 31.7 ($\text{C}(\text{CH}_3)_3$). Electrospray MS (20V, m/z): 355.0 $[\text{M-H}]^+$. Electrospray MS (20V, m/z): 355.0 $[\text{M+H}]^+$. Anal. Calcd. for $\text{C}_{25}\text{H}_{26}\text{N}_2(\text{H}_2\text{O})$ (372.22): C, 80.61; H, 7.58; N, 7.52. Found: C, 80.93; H, 7.29; N, 7.42.

Synthesis of **[IH](I)**



(1) A thick-walled Schlenk tube fitted with a Teflon cap was charged with compound **H** (300 mg, 0.85 mmol), NaHCO_3 (146 mg, 1.74 mmol) and acetonitrile (5 mL). The mixture was stirred at 90°C during 1 h. After that, CH_3I (321 mL, 5.1 mmol) was added at room temperature and the mixture was further heated at 90°C overnight. The solvent was removed under vacuum. The brownish solid residue was suspended in CH_2Cl_2 and filtered to remove insoluble inorganic salts. Precipitation of the filtrate with a mixture CH_2Cl_2 /diethyl ether afforded compound **[IH](I)** as a yellow solid. Yield: 301 mg, 69 %. ^1H NMR (500 MHz, $\text{DMSO-}d_6$): δ 9.77 (s, 1H, NCHN), 8.84 (s, 2H, CH_{pyr}), 8.55 (s, 2H, CH_{pyr}), 8.29 (s, 2H, CH_{pyr}), 4.70 (s, 6H, NCH $_3$), 1.62 (s, 18H, $\text{C}(\text{CH}_3)_3$). ^{13}C NMR (126 MHz, $\text{DMSO-}d_6$): δ 149.4 (NCHN), 141.7 (C_q pyr), 131.3 (C_q pyr), 128.3 (CH_{pyr}), 127.0 (C_q pyr), 124.2 (CH_{pyr}), 120.9 (C_q pyr), 119.7 (C_q pyr), 116.9 (CH_{pyr}), 38.0 (NCH $_3$), 35.3 ($\text{C}(\text{CH}_3)_3$), 31.4 ($\text{C}(\text{CH}_3)_3$). Electrospray MS (20V, m/z): 383.0 $[\text{M}]^+$. Anal. Calcd. for $\text{C}_{27}\text{H}_{31}\text{N}_2\text{I}(\text{H}_2\text{O})$ (546.17): C, 61.36; H, 6.29; N, 5.30. Found: C, 60.98; H, 5.95; N, 5.21.

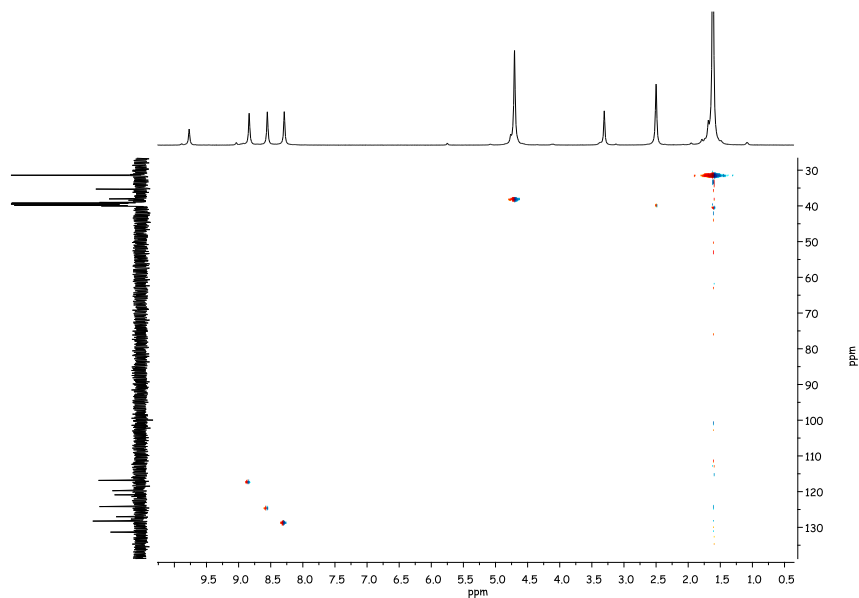


Figure 5.5 HSQC spectrum of **[IH](I)** in DMSO- d_6 ($^1J_{\text{H-C}} = 145$ Hz)

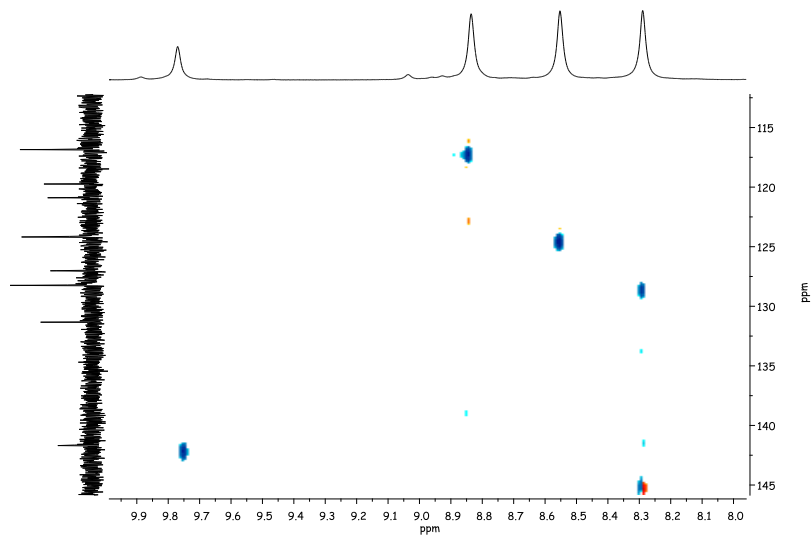


Figure 5.6 HSQC spectrum of **[IH](I)** in DMSO- d_6 ($^1J_{\text{H-C}} = 200$ Hz)

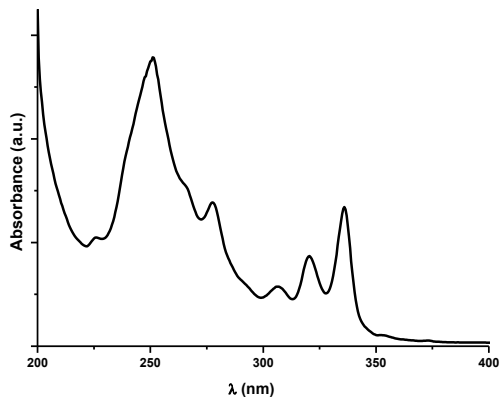


Figure 5.7 UV-vis spectrum of **[HI](I)**, recorded in MeCN at a concentration of 40 μM , under aerobic conditions

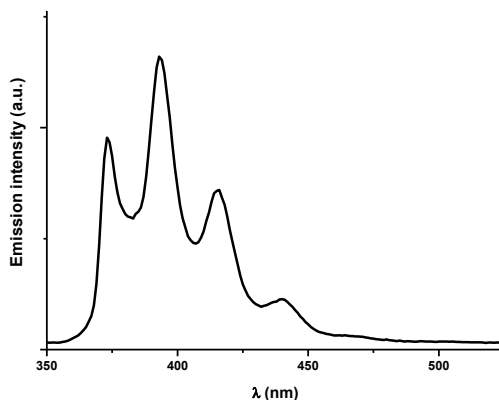
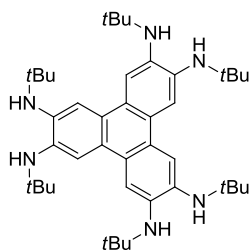


Figure 5.8 Emission spectrum of **[HI](I)**, at 317 nm in MeCN (40 μM under aerobic conditions).

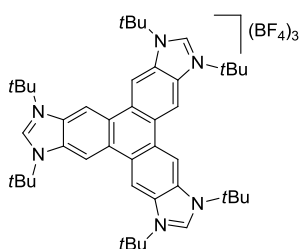
Synthesis of J



In a Schlenk tube, 2,3,6,7,10,11-hexabromotriphenylene (1 g, 1.43 mmol) and NaOtBu (991 mg, 10.3 mol) were suspended in toluene (20 mL). In another Schlenk tube, a mixture of $[\text{Pd}(\text{OAc})_2]$ (24 mg, 0.107 mmol), 1,3-bis(2,6-diisopropylphenyl)imidazolium chloride ($\text{IPr}\cdot\text{HCl}$, 91 mg, 0.214 mmol), NaOtBu (31 mg, 0.321 mmol) and toluene (10

mL) was stirred for 10 min at room temperature. After this time, the latter solution was added *via* oven dried cannula over the first one. Then, *tert*-butylamine (1.1 mL, 10.3 mmol) was added and the resulting mixture was refluxed for 16 h. The cooled reaction mixture was filtered over Celite and then concentrated under reduced pressure, yielding the desired product as a dark red solid. Yield: 920 mg (98 %). ^1H NMR (300 MHz, CDCl_3): δ 7.85 (s, 6H, CH_{arom}), 3.83 (s, 6H, NH), 1.39 (s, 54 H, $\text{C}(\text{CH}_3)_3$). ^{13}C NMR (75 MHz, CDCl_3): δ 137.8 ($\text{C}_{\text{q arom}}$), 123.6 ($\text{C}_{\text{q arom}}$), 113.5 (CH_{arom}), 52.2 ($\text{C}(\text{CH}_3)_3$), 30.0 ($\text{C}(\text{CH}_3)_3$). Electrospray MS (20 V, m/z): 655.4 $[\text{M}+\text{H}]^+$. HRMS ESI-TOF-MS (positive mode): $[\text{M}+\text{H}]^+$ monoisotopic peak 655.5430, calcd 655.5427, $\epsilon_r = 0.5$ ppm. Satisfactory elemental analysis could not be obtained due to the light sensitive nature of the compound.

Synthesis of $[\text{KH}_3](\text{BF}_4)_3$



A mixture of compound **J** (920 mg, 1.4 mmol), $\text{HBF}_4 \cdot \text{Et}_2\text{O}$ (0.64 mL, 4.62 mmol, 3.3 equiv) and triethyl orthoformate (40 mL) was heated at 110°C for 16 h under aerobic conditions. After cooling to room temperature, Et_2O was added to the reaction mixture and the precipitated solid was collected by filtration. Compound $[\text{KH}_3](\text{BF}_4)_3$ was precipitated in a mixture of acetonitrile/diethyl ether as a light tan solid. Yield: 1.27 g (96 %). ^1H NMR (300 MHz, $\text{DMSO}-d_6$): δ 9.20 (s, 6H, CH_{arom}), 9.17 (s, 3H, NCHN), 2.04 (s, 54 H, $\text{C}(\text{CH}_3)_3$). ^{13}C NMR (75 MHz, $\text{DMSO}-d_6$): δ 142.6 (NCHN), 131.3 ($\text{C}_{\text{q arom}}$), 126.7 ($\text{C}_{\text{q arom}}$), 112.0 (CH_{arom}), 61.9 ($\text{C}(\text{CH}_3)_3$), 28.6 ($\text{C}(\text{CH}_3)_3$). Electrospray MS (20 V, m/z): 387.5 $[\text{M}+\text{BF}_4]^{2+}$, 229.4 $[\text{M}]^{3+}$. Anal. Calcd. for $\text{C}_{45}\text{H}_{63}\text{B}_3\text{F}_{12}\text{N}_6(\text{H}_2\text{O})_3$ (1002.55): C, 53.91; H, 6.94; N, 8.39. Found: C, 54.30; H, 7.25; N, 8.28.

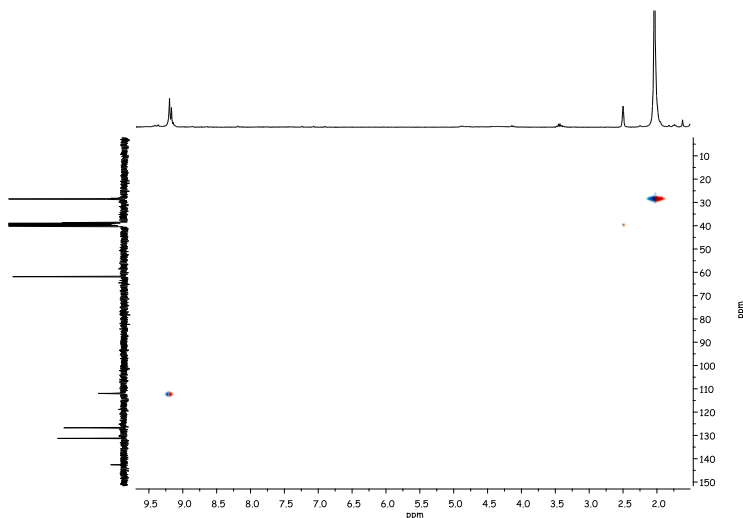


Figure 5.9 HSQC spectrum of $[\text{KH}_3](\text{BF}_4)_3$ in $\text{DMSO-}d_6$ ($^1J_{\text{H-C}} = 146$ Hz)

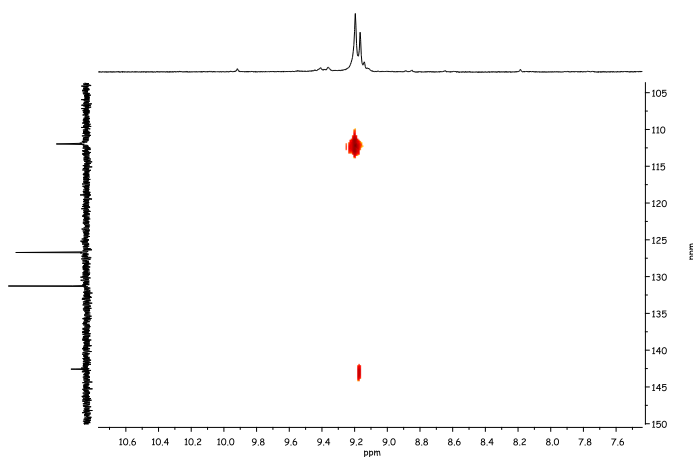
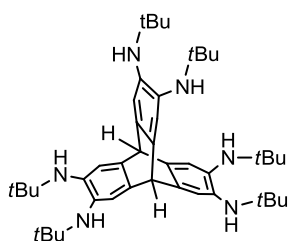


Figure 5.10 HSQC spectrum of $[\text{KH}_3](\text{BF}_4)_3$ in $\text{DMSO-}d_6$ ($^1J_{\text{H-C}} = 190$ Hz)

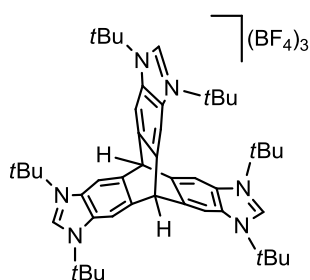
Synthesis of L



Compound **L** was prepared starting from 2,3,6,7,12,13-hexabromotriptycene, in a similar manner as that described by Bielawski and co-workers.¹⁶ In a Schlenk tube, 2,3,6,7,12,13-hexabromotriptycene (1 g, 1.37 mmol) and NaOtBu (952.3 mg, 9.9 mmol) were suspended in toluene (20 mL). The coupling catalyst was prepared by charging

another Schlenk tube with $[\text{Pd}(\text{OAc})_2]$ (22 mg, 0.1 mmol), $\text{IPr}\cdot\text{HCl}$, 85 mg, 0.2 mmol), NaOtBu (29 mg, 0.3 mmol) and toluene (10 mL). After stirring this mixture at room temperature for 10 min, the catalyst solution was added to the first one. Afterward, *tert*-butylamine (1.06 mL, 9.9 mmol) was added and the resulting mixture was stirred at 110°C for 16 h. The reaction was cooled to room temperature, filtered through Celite and concentrated to dryness to afford the desired product as a brown solid. Yield: 921 mg (99 %). ^1H NMR (300 MHz, CDCl_3): δ 6.88 (s, 6H, CH_{arom}), 4.86 (s, 2H, $\text{CH}_{\text{tritycene}}$), 3.48 (s, 6H, NH), 1.23 (s, 54H, $\text{C}(\text{CH}_3)_3$). ^{13}C NMR (75 MHz, CDCl_3): δ 139.2 ($\text{C}_{\text{q arom}}$), 134.6 ($\text{C}_{\text{q arom}}$), 116.7 (CH_{arom}), 53.5 ($\text{CH}_{\text{tritycene}}$), 52.0 ($\text{C}(\text{CH}_3)_3$), 30.3 ($\text{C}(\text{CH}_3)_3$). Electrospray MS (20 V, m/z): 681.7 $[\text{M}+\text{H}]^+$. HRMS ESI-TOF-MS (positive mode): $[\text{M}+\text{H}]^+$ monoisotopic peak 681.5582, calcd 681.5584, $\varepsilon_{\text{r}}=0.3$ ppm. Satisfactory elemental analysis could not be obtained due to the light sensitive nature of the compound.

Synthesis of $[\text{MH}_3](\text{BF}_4)_3$



A mixture of **L** (921 mg, 1.35 mmol), $\text{HBF}_4\cdot\text{Et}_2\text{O}$ (0.61 mL, 4.45 mmol, 3.3 equiv) and triethyl orthoformate (40 mL) was heated at 110°C for 16 h under aerobic conditions. After cooling to room temperature, diethyl ether was added to the reaction mixture and the precipitated tan solid collected by filtration. Yield: 1.26 g (96%). ^1H NMR (300 MHz, $\text{DMSO}-d_6$): δ 8.80 (s, 3H, NCHN), 8.36 (s, 6H, CH_{arom}), 6.38 (s, 2H, $\text{CH}_{\text{tritycene}}$), 1.79 (s, 54H, $\text{C}(\text{CH}_3)_3$). ^{13}C NMR (75 MHz, $\text{DMSO}-d_6$): δ 141.6 (NCHN), 138.8 ($\text{C}_{\text{q arom}}$), 128.8 ($\text{C}_{\text{q arom}}$), 112.5 (CH_{arom}), 60.8 ($\text{C}(\text{CH}_3)_3$), 51.8 ($\text{CH}_{\text{tritycene}}$), 28.1 ($\text{C}(\text{CH}_3)_3$). Electrospray MS (20 V, m/z): 400.4 $[\text{M}+\text{BF}_4]^{2+}$, 238.0 $[\text{M}]^{3+}$. Anal. Calcd. for $\text{C}_{47}\text{H}_{65}\text{B}_3\text{F}_{12}\text{N}_6(\text{H}_2\text{O})_3$ (1028.57): C, 54.88; H, 6.96; N, 8.17. Found: C, 55.27; H, 7.22; N, 8.17.

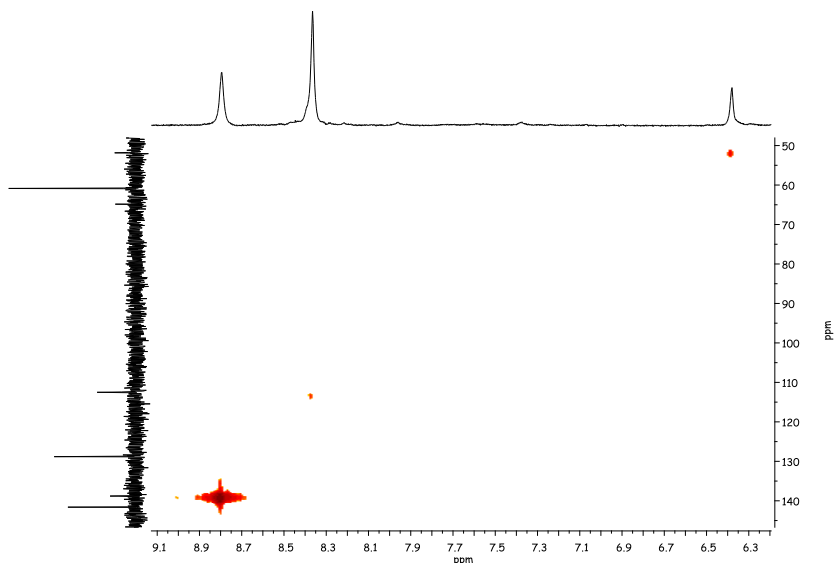
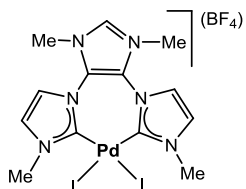


Figure 5.11 HSQC spectrum of $[\text{MH}_3](\text{BF}_4)_3$ in $\text{DMSO-}d_6$ ($^1J_{\text{H-C}} = 190 \text{ Hz}$)

5.2.2 Synthesis and characterization of complexes of Chapter 2

Synthesis of 1DH



A mixture of $\text{Pd}(\text{OAc})_2$ (50 mg, 0.223 mmol), $[\text{DH}_3](\text{BF}_4)_3$ (115.7 mg, 0.223 mmol) and KI (74.7 mg, 0.446 mmol) in acetonitrile (20 mL), was refluxed for 3 h. Afterwards, the mixture was filtered through a pad of Celite and the solvent was removed under vacuum. The resulting orange residue was redissolved in acetone and the insoluble salts were removed by filtration. Finally, the solvent was removed under vacuum, yielding compound **1DH** as an orange solid. Yield: 145 mg, 92 %. $^1\text{H NMR}$ (300 MHz, $\text{DMSO-}d_6$): δ 9.55 (s, 1H, NCHN), 8.13 (d, $^3J_{\text{H-H}} = 2.1 \text{ Hz}$, 2H, CH_{imid}), 7.83 (d, $^3J_{\text{H-H}} = 2.1 \text{ Hz}$, 2H, CH_{imid}), 3.99 (s, 6H, NCH_3), 3.91 (s, 6H, NCH_3). $^{13}\text{C NMR}$ (75 MHz, $\text{DMSO-}d_6$): δ 167.0 ($\text{Pd-C}_{\text{carbene}}$), 135.5 (NCHN), 126.7 (CH_{imid}), 123.1 (C_q), 122.4 (CH_{imid}), 34.6 (NCH_3), 30.6 (NCH_3). Anal. Calc. for $\text{C}_{13}\text{H}_{17}\text{BF}_4\text{I}_2\text{N}_6\text{Pd}$ (704.34): C, 22.17; H, 2.43; N, 11.93. Found: C, 22.20; H, 2.52; N, 11.84. Electrospray MS (20 V, m/z): 616.8 $[\text{M}]^+$.

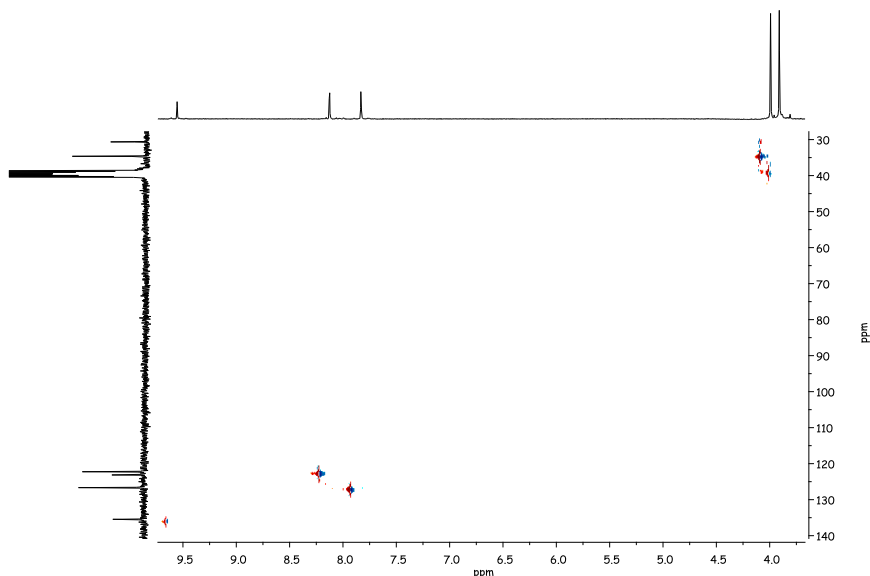
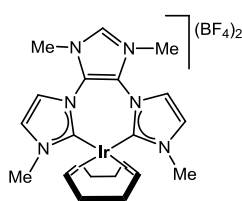


Figure 5.12 HSQC spectrum of **1DH** in DMSO- d_6 ($^1J_{\text{H-C}} = 190$ Hz)

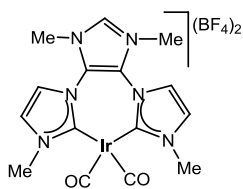
Synthesis of **2DH**



A mixture of compound **[DH₃](BF₄)₃** (78 mg, 0.149 mmol), **[IrCl(COD)]₂** (50 mg, 0.0745 mmol) and NaOAc (49.2 mg, 0.6 mmol) in acetonitrile (15 mL) was refluxed for one hour. The mixture was then filtered at 0°C. Removal of the volatiles afforded **2DH** as a red, air sensitive solid. Yield: 90 mg, 83%.

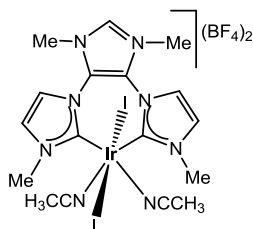
^1H NMR (300 MHz, DMSO- d_6): δ 9.44 (s, 1H, NCHN), 8.00 (d, $^3J_{\text{H-H}} = 2.2$ Hz, 2H, CH_{imid}), 7.73 (d, $^3J_{\text{H-H}} = 2.2$ Hz, 2H, CH_{imid}), 4.34 (m, 2H, CH_{COD}), 4.07 (m, 2H, CH_{COD}), 4.00 (s, 6H, NCH₃), 3.82 (s, 6H, NCH₃), 2.31 (m, 4H, CH_2 COD), 1.75 (m, 4H, CH_2 COD). ^{13}C NMR (75 MHz, DMSO- d_6): δ 181.2 (Ir- $\text{C}_{\text{carbene}}$), 134.2 (C_{q}), 125.8 (NCHN), 123.9 (CH_{imid}), 121.7 (CH_{imid}), 80.3 (CH_{COD}), 75.8 (CH_{COD}), 37.4 (NCH₃), 34.1 (NCH₃), 30.6 (CH_2 COD), 30.5 (CH_2 COD). Satisfactory elemental analysis could not be obtained due to the low stability of the compound. Electrospray MS (15 V, m/z): 645.4 [$\text{M}+\text{BF}_4$]⁺, 279.1 [M]²⁺. Electrospray HR-MS (15 V, m/z): 645.2126 [$\text{M}+\text{BF}_4$]⁺, 279.1038 [M]²⁺.

Synthesis of 3DH



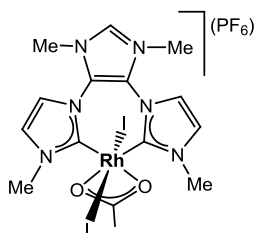
CO gas (1 atm, 10 mL/min) was passed through a solution of complex **2DH** (90 mg, 0.123 mmol) in methanol (15 mL) for 15 minutes at 0°C. After this time, the solution was concentrated under reduced pressure. After addition of diethyl ether, a yellow solid precipitated, that was collected by filtration. Yield: 77 mg, 92%. ¹H NMR (300 MHz, MeCN-*d*₃): δ 8.66 (s, 1H, NCHN), 7.60 (d, ³J_{H-H} = 2.1 Hz, 2H, CH_{imid}), 7.48 (d, ³J_{H-H} = 2.2 Hz, 2H, CH_{imid}), 3.90 (s, 6H, NCH₃), 3.89 (s, 6H, NCH₃). ¹³C NMR (75 MHz, DMSO-*d*₆): δ 172.0 (Ir-C_{carbene}), 171.4 (Ir-CO), 135.5 (NCHN), 126.5 (CH_{imid}), 122.9 (CH_{imid}), 122.3 (C_q), 34.6 (NCH₃), 21.0 (NCH₃). Satisfactory elemental analysis could not be obtained due to the low stability of the compound. IR(KBr): 2079 (ν_{C=O}), 2017 (ν_{C=O}) cm⁻¹. Electrospray MS (20 V, *m/z*): 593.0 [M+BF₄]⁺, 252.9 [M]²⁺. Electrospray HR-MS (20 V, *m/z*): 593.1091 [M+BF₄]⁺, 253.0516 [M]²⁺.

Synthesis of 4DH



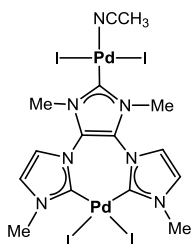
A mixture of compound [DH₃](BF₄)₃ (78 mg, 0.149 mmol), [IrCl(COD)]₂ (50 mg, 0.0745 mmol) and NaOAc (49.2 mg, 0.6 mmol) in acetonitrile (15 mL) was refluxed for one hour. Once at room temperature, I₂ (50.8 mg, 0.2 mmol) was added and the mixture was stirred for 3 h. The solution was then filtered and the volatiles were removed under vacuum. The crude solid was purified by column chromatography. Elution with a 1:1 mixture of dichloromethane/acetonitrile afforded the separation of a yellow band that contained compound **4DH**. Precipitation with a mixture acetonitrile/diethyl ether gave the desired product as a yellow solid. Yield: 49 mg, 38%. ¹H NMR (300 MHz, MeCN-*d*₃): δ 8.69 (s, 1H, NCHN), 7.64 (d, ³J_{H-H} = 2.3 Hz, 2H, CH_{imid}), 7.45 (d, ³J_{H-H} = 2.3 Hz, 2H, CH_{imid}), 4.18 (s, 6H, NCH₃), 3.75 (s, 6H, NCH₃), 2.70 (s, 6H, CH₃CN). ¹³C NMR (75 MHz, DMSO-*d*₆): δ 135.1 (Ir-C_{carbene}), 128.6 (C_q), 127.8 (NCHN), 124.4 (CH_{imid}), 122.7 (CH_{imid}), 118.0 (CH₃CN), 43.5 (NCH₃), 34.9 (NCH₃), 1.1 (CH₃CN). Anal. Calc. for IrI₂N₈C₁₇H₂₃B₂F₈(Et₂O)₂ (1107.31): C, 27.12; H, 3.91; N, 10.12. Found: C, 26.91; H, 4.23; N, 9.91. Electrospray MS (20 V, *m/z*): 393.1 [M]²⁺, 352.0 [M-2MeCN]²⁺.

Synthesis of 5DH



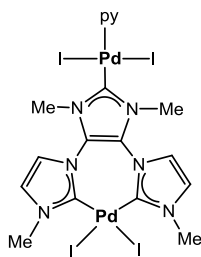
A mixture of compound **[DH₃](BF₄)₃** (105.4 mg, 0.203 mmol), **[RhCl(COD)]₂** (50 mg, 0.1015 mmol), NaOAc (66.54 mg, 0.812 mmol) and KI (136.16 mg, 0.812 mmol) in acetonitrile (20 mL), was refluxed overnight. Afterwards, the solvent was removed under vacuum. The crude solid was purified by column chromatography. Elution with a mixture acetone/KPF₆ afforded the desired compound as an orange solid. Yield: 55 mg, 33%. ¹H NMR (300 MHz, acetone-*d*₆): δ 9.32 (s, 1H, NCHN), 8.17 (d, ³J_{H-H} = 2.2 Hz, 2H, CH_{imid}), 7.84 (d, ³J_{H-H} = 2.2 Hz, 2H, CH_{imid}), 4.21 (s, 6H, NCH₃), 4.04 (s, 6H, NCH₃), 1.87 (s, 3H, COOCH₃). ¹³C NMR (75 MHz, MeCN-*d*₃): δ 191.3 (COOCH₃), 163.0 (d, ¹J_{Rh-C} = 47.2 Hz, Rh-C_{carbene}), 136.3 (NCHN), 129.3 (CH_{imid}), 126.4 (C_q), 124.2 (CH_{imid}), 43.4 (NCH₃), 36.9 (NCH₃), 30.2 (COOCH₃). Anal. Calc. for RhI₂O₂N₆C₁₅H₂₀PF₆(H₂O)₃ (872.1): C, 20.66; H, 3.01; N, 9.64. Found: C, 20.77; H, 3.51; N, 9.23. Electrospray MS (20 V, *m/z*): 672.8 [M]⁺.

Synthesis of 1D



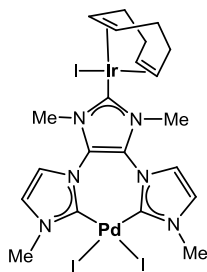
A mixture of Pd(OAc)₂ (100 mg, 0.446 mmol), **[DH₃](BF₄)₃** (115.7 mg, 0.223 mmol) and KI (150 mg, 0.87 mmol) in acetonitrile (20 mL), was refluxed overnight under inert atmosphere. Afterwards, the mixture was filtered through a pad of Celite and the solvent was removed under vacuum. The crude solid was purified by column chromatography. Elution with a 7:3 mixture of dichloromethane/acetone afforded the separation of an orange band that contained compound **1D**. Removal of the volatiles afforded **1D** as a brown-orange solid. Yield: 114 mg, 50 %. Complex **1D** can also be obtained from **1DH**. A mixture of Pd(OAc)₂ (50 mg, 0.223 mmol), **1DH** (157 mg, 0.223 mmol) and KI (74 mg, 0.446 mmol) in acetonitrile (20 mL), was refluxed overnight. After removal of the volatiles, the crude solid was purified as described above. Yield: 112 mg, 50 %. ¹H NMR (300 MHz, DMSO-*d*₆): δ 8.17 (s, 2H, CH_{imid}), 7.75 (s, 2H, CH_{imid}), 3.88 (s, 6H, NCH₃), 3.87 (s, 6H, NCH₃). ¹³C NMR (75 MHz, DMSO-*d*₆): δ 179.4 (NC), 166.9 (Pd-C_{carbene}), 142.3 (Pd-C_{carbene}), 126.2 (CH_{imid}), 123.9 (CH_{imid}), 122.3 (C_q), 40.1 (NCH₃), 36.7 (NCH₃), 30.7 (NCH₃). Electrospray MS (20 V, *m/z*): 932.6 [M-I+CH₃CN]⁺.

Synthesis of 2D



Compound **1D** (50.4 mg, 0.05 mmol) was dissolved in 0.5 mL of pyridine. The mixture was heated for 30 minutes at 80°C. During this time, the desired product precipitated as a yellow solid. The excess of pyridine was removed under vacuum, and the yellow solid was washed several times with diethyl ether and dried under vacuum. Yield: 38 mg, 73 %. ^1H NMR (500 MHz, DMSO- d_6): δ 8.97 (d, $^3J_{\text{H-H}} = 4.4$ Hz, 2H, Py), 8.20 (s, 2H, CH_{imid}), 7.98 (t, $^3J_{\text{H-H}} = 6.9$ Hz, 1H, Py), 7.76 (s, 2H, CH_{imid}), 7.57 (d, $^3J_{\text{H-H}} = 7.0$ Hz, 2H, Py), 4.00 (s, 6H, NCH_3), 3.89 (s, 6H, NCH_3). ^{13}C NMR (75 MHz, DMSO- d_6): δ 167.0 (Pd- $\text{C}_{\text{carbene}}$), 153.2, 124.9 (Py), 122.3 (Py), 148.6 (Pd- $\text{C}_{\text{carbene}}$), 136.6 (C_q), 126.1 (CH_{imid}), 123.4 (CH_{imid}), 40.0 (NCH_3), 36.7 (NCH_3). Anal. Calc. for $\text{C}_{18}\text{H}_{21}\text{I}_4\text{N}_7\text{Pd}_2(1055.86) \cdot 0.5\text{Et}_2\text{O}$: C, 20.48; H, 2.00; N, 9.29. Found: C, 20.62; H, 2.32; N, 10.06. Electrospray MS (20 V, m/z): 1079.5 [$\text{M}+\text{Na}$] $^+$.

Synthesis of 3D



A mixture of $[\text{Pd}(\text{OAc})_2]$ (50 mg, 0.223 mmol), $[\text{DH}_3](\text{BF}_4)_3$ (115.7 mg, 0.223 mmol) and KI (74.7 mg, 0.446 mmol) in acetonitrile was refluxed for 2 h. $[\text{IrCl}(\text{COD})]_2$ (74 mg, 0.11 mmol), NaOAc (24.6 mg, 0.3 mmol) and KI (74 mg, 0.446 mmol) were then added and the resulting mixture was refluxed overnight. The solvent was removed under vacuum and the crude solid was purified by column chromatography. Elution with a 9:1 mixture of dichloromethane/acetone afforded the separation of a yellow band that contained compound **3D**. Precipitation with a mixture acetone/diethyl ether gave the desired product as a yellow solid. Yield: 70 mg, 30%. ^1H NMR (300 MHz, DMSO- d_6): for the minor isomer (45%): δ 8.20 (s, 2H, CH_{imid}), 7.72 (s, 2H, CH_{imid}), 4.68 (m, 2H, CH_{COD}), 3.85 (s, 12H, NCH_3), 2.98 (m, 2H, CH_{COD}), 2.16 (m, 4H, CH_2_{COD}), 1.47 (m, 4H, CH_2_{COD}); for the major isomer (55%): δ 8.11 (s, 2H, CH_{imid}), 7.74 (s, 2H, CH_{imid}), 4.68 (m, 2H, CH_{COD}), 3.89 (s, 12H, NCH_3), 3.35 (m, 2H, CH_{COD}), 2.16 (m, 4H, CH_2_{COD}), 1.78 (m, 4H, CH_2_{COD}). ^{13}C NMR (75 MHz, DMSO- d_6): for the minor isomer: δ 178.8 (Ir- $\text{C}_{\text{carbene}}$), 166.0 (Pd- $\text{C}_{\text{carbene}}$), 126.0 (CH_{imid}), 124.1 (C_q), 122.0 (CH_{imid}), 83.0 (CH_{COD}), 55.6 (CH_{COD}), 39.5 (NCH_3), 34.9 (NCH_3), 32.3 (CH_2_{COD}), 29.8 (CH_2_{COD}); for the major isomer: δ 178.1 (Ir- $\text{C}_{\text{carbene}}$), 167.5 (Pd- $\text{C}_{\text{carbene}}$), 126.0 (CH_{imid}), 122.7

(CH_{imid}), 122.1 (C_q), 82.4 (CH_{CO_D}), 55.4 (CH_{CO_D}), 39.7 (NCH₃), 35.2 (NCH₃), 32.4 (CH₂CO_D), 29.9 (CH₂CO_D). Anal. Calc. for PdIrI₃N₆C₂₁H₂₈(2H₂O) (1079.85): C, 23.36; H, 3.00; N, 7.78. Found: C, 23.00; H, 3.27; N, 7.61. Electrospray MS (20 V, *m/z*): 958.2 [M-I+MeCN]⁺, 917.2 [M-I]⁺.

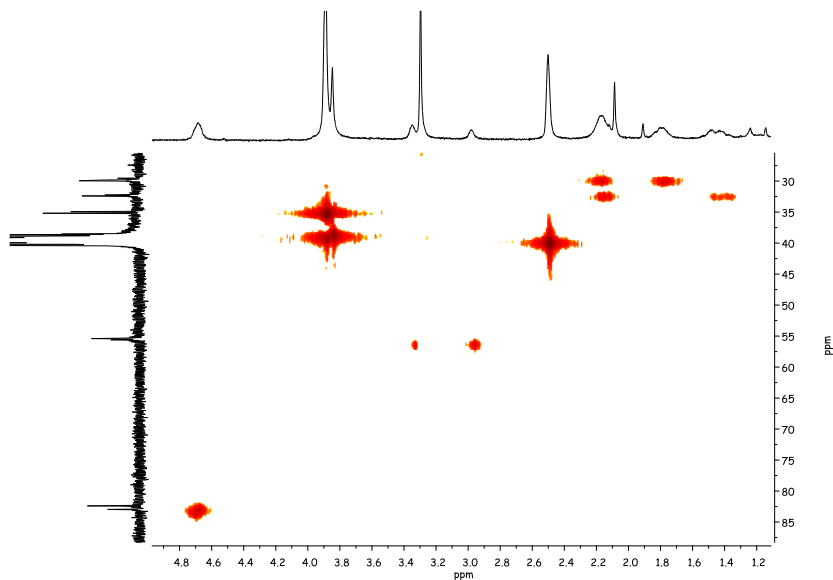


Figure 5.13 HSQC spectrum of **3D** in DMSO-*d*₆ ($J_{\text{H-C}} = 146$ Hz)

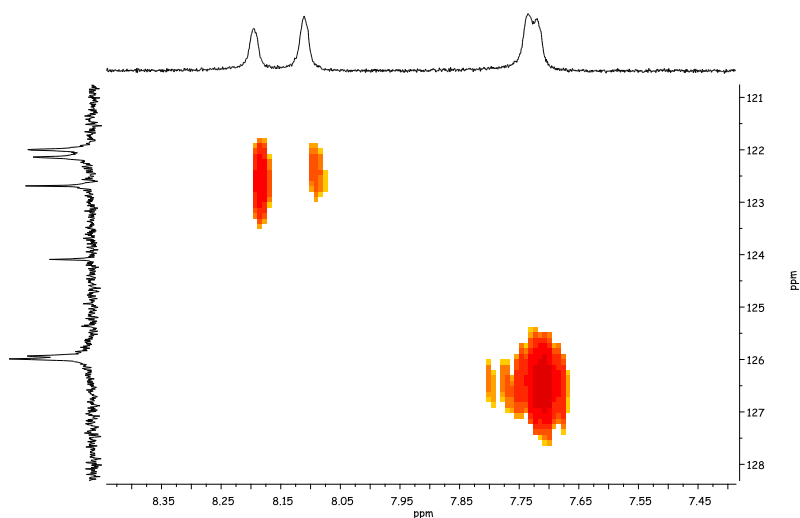
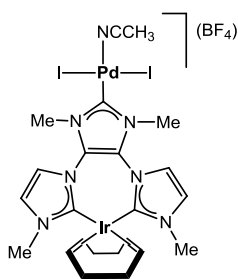


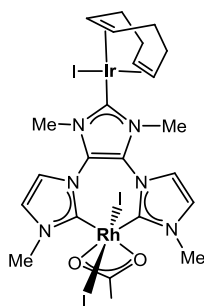
Figure 5.14 HSQC spectrum of **3D** in DMSO-*d*₆ ($J_{\text{H-C}} = 170$ Hz)

Synthesis of 4D



A mixture of compound $[\text{DH}_3](\text{BF}_4)_3$ (78 mg, 0.149 mmol), $[\text{IrCl}(\text{COD})]_2$ (50 mg, 0.0745 mmol) and NaOAc (49.2 mg, 0.6 mmol) in acetonitrile (15 mL) was refluxed for one hour. $[\text{Pd}(\text{OAc})_2]$ (33.7 mg, 0.149 mmol) and KI (100.6 mg, 0.6 mmol) were then added, and the reaction was refluxed for one additional hour. The mixture was filtered through a pad of Celite and the solvent was removed under vacuum. The crude solid was purified by column chromatography. Elution with a 7:3 mixture of dichloromethane/acetone afforded the separation of an orange band that contained compound **4D**. Precipitation with a mixture acetone/diethyl ether gave the desired product as a brown, air sensitive solid. Yield: 70 mg, 45%. ^1H NMR (300 MHz, $\text{DMSO}-d_6$): δ 8.07 (s, 2H, CH_{imid}), 7.67 (s, 2H, CH_{imid}), 4.27 (m, 2H, CH_{COD}), 3.93 (m, 2H, CH_{COD}), 3.88 (s, 6H, NCH_3), 3.80 (s, 6H, NCH_3), 2.30 (m, 2H, CH_2_{COD}), 2.09 (s, 3H, CH_3CN), 2.04 (m, 4H, CH_2_{COD}), 1.66 (m, 2H, CH_2_{COD}). ^{13}C NMR (75 MHz, $\text{DMSO}-d_6$): δ 180.7 (Ir- $\text{C}_{\text{carbene}}$), 163.6 (Pd- $\text{C}_{\text{carbene}}$), 125.4 (CH_{imid}), 124.3 (C_q), 122.0 (CH_{imid}), 79.3 (CH_{COD}), 75.1 (CH_{COD}), 37.2 (NCH_3), 36.2 (NCH_3), 30.7 (CH_2_{COD}), 30.4 (CH_2_{COD}), CH_3CN not observed. Satisfactory elemental analysis could not be obtained due to the low stability of the compound. Electrospray MS (20 V, m/z): 958.1 $[\text{M}]^+$, 917.1 $[\text{M}-\text{MeCN}]^+$. Electrospray HR-MS (20 V, m/z): 957.9382 $[\text{M}]^+$.

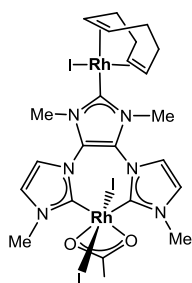
Synthesis of 5D



A mixture of compound $[\text{DH}_3](\text{BF}_4)_3$ (105.4 mg, 0.203 mmol), $[\text{RhCl}(\text{COD})]_2$ (50 mg, 0.101 mmol), NaOAc (66.54 mg, 0.812 mmol) and KI (136.16 mg, 0.812 mmol) in acetonitrile (20 mL) was refluxed overnight. Once at room temperature, $[\text{IrCl}(\text{COD})]_2$ (68.14 mg, 0.101 mmol), NaOAc (25 mg, 0.3 mmol) and KI (68.1 mg, 0.406 mmol) were added, and the resulting mixture was refluxed for 3 additional hours. The solution was then filtered and the solvent was removed under vacuum. The crude solid was purified by column chromatography. Elution with a 95:5 mixture of dichloromethane/acetone afforded the separation of an orange band that contained compound **5D**. Precipitation with a mixture dichloromethane/hexane gave the desired product as a brown solid. Yield: 72 mg, 32%. ^1H NMR (300 MHz, CDCl_3): δ 7.36 (d,

$^3J_{\text{H-H}} = 2.2$ Hz, 2H, CH_{imid}), 7.19 (d, $^3J_{\text{H-H}} = 2.2$ Hz, 2H, CH_{imid}), 4.86 (m, 2H, CH_{COD}), 4.19 (s, 6H, NCH_3), 3.82 (s, 6H, NCH_3), 3.10 (m, 2H, CH_{COD}), 2.14 (m, 4H, CH_2 COD), 1.99 (s, 3H, COOCH_3), 1.82 (m, 4H, CH_2 COD). ^{13}C NMR (75 MHz, CDCl_3): δ 190.7 (COOCH_3), 182.3 (Ir- $\text{C}_{\text{carbene}}$), 163.1 (d, $^1J_{\text{Rh-C}} = 47.5$ Hz, Rh- $\text{C}_{\text{carbene}}$), 126.3 (CH_{imid}), 124.8 (C_q), 122.1 (CH_{imid}), 84.9 (CH_{COD}), 57.5 (CH_{COD}), 42.9 (NCH_3), 36.7 (NCH_3), 32.7 (CH_2 COD), 31.1 (COOCH_3), 30.5 (CH_2 COD). Anal. Calc. for $\text{RhIrI}_3\text{O}_2\text{N}_6\text{C}_{23}\text{H}_{31}(\text{CH}_2\text{Cl}_2)_2$ (1269.22): C, 23.66; H, 2.78; N, 6.62. Found: C, 23.57; H, 2.53; N, 6.55. Electrospray MS (20 V, m/z): 1014 $[\text{M-I}+\text{MeCN}]^+$, 973.1 $[\text{M-I}]^+$.

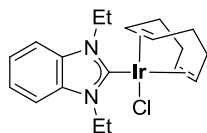
Synthesis of 6D



A mixture of compound $[\text{DH}_3](\text{BF}_4)_3$ (105.4 mg, 0.203 mmol), $[\text{RhCl}(\text{COD})]_2$ (50 mg, 0.101 mmol), NaOAc (66.54 mg, 0.812 mmol) and KI (136.16 mg, 0.812 mmol) in acetonitrile (20 mL) was refluxed overnight. Once at room temperature, $[\text{RhCl}(\text{COD})]_2$ (50 mg, 0.101 mmol), NaOAc (33.3 mg, 0.406 mmol) and KI (68.1 mg, 0.406 mmol) were added, and the resulting mixture was refluxed for 3 additional hours. The solution was then filtered and the solvent was removed under vacuum. The crude solid was purified by column chromatography. Elution with a 95:5 mixture of dichloromethane/acetone afforded the separation of a band that contained the desired product. After removal of the volatiles, **6D** was isolated as a yellow solid. Yield: 68 mg, 33%. ^1H NMR (300 MHz, CDCl_3): δ 7.35 (s, 2H, CH_{imid}), 7.18 (d, 2H, CH_{imid}), 5.27 (m, 2H, CH_{COD}), 4.19 (s, 6H, NCH_3), 3.94 (s, 6H, NCH_3), 3.59 (m, 2H, CH_{COD}), 2.31 (m, 4H, CH_2 COD), 1.99 (s, 3H, COOCH_3), 1.84 (m, 4H, CH_2 COD). ^{13}C NMR (75 MHz, CDCl_3): δ 190.7 (COOCH_3), 185.7 (d, $^1J_{\text{Rh-C}} = 50.5$ Hz, Rh- $\text{C}_{\text{carbene}}$), 162.7 (d, $^1J_{\text{Rh-C}} = 47.4$ Hz, Rh- $\text{C}_{\text{carbene}}$), 126.3 (CH_{imid}), 124.9 (C_q), 122.1 (CH_{imid}), 98.0 (d, $^1J_{\text{Rh-C}} = 6.7$ Hz, Rh- CH_{COD}), 74.3 (d, $^1J_{\text{Rh-C}} = 13.9$ Hz, Rh- CH_{COD}), 42.9 (NCH_3), 37.3 (NCH_3), 32.2 (CH_2 COD), 29.7 (CH_2 COD), 25.1 (COOCH_3). Anal. Calc. for $\text{Rh}_2\text{I}_3\text{O}_2\text{N}_6\text{C}_{23}\text{H}_{31}$ (1010.06): C, 27.35; H, 3.09; N, 8.32. Found: C, 27.51; H, 3.21; N, 8.59. Electrospray MS (20 V, m/z): 923.9 $[\text{M-I}+\text{MeCN}]^+$, 882.9 $[\text{M-I}]^+$.

5.2.3 Synthesis and characterization of complexes of Chapter 3

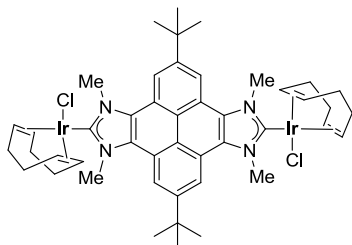
Synthesis of [IrCl(1,3-diethylbenzimidazol-2-ylidene)(COD)]



1,3-Diethylbenzimidazolium tetrafluoroborate (58.4 mg, 0.223 mmol), [IrCl(COD)]₂ (75 mg, 0.112 mmol) and KO^tBu (31.6 mg, 0.245 mmol) were placed together in a Schlenk tube. The tube was evacuated and filled with nitrogen three times. The solids were suspended in THF (5 mL) and the resulting mixture stirred at room temperature overnight. The mixture was filtered over Celite and the filtrate concentrated under reduced pressure. The desired product was isolated as a yellow solid after crystallization from a CH₂Cl₂/hexane mixture. Yield: 80 mg, 70 %. ¹H NMR (300 MHz, CDCl₃): δ 7.33-7.23 (m, 4H, CH_{arom}), 4.91-4.87 (m, 2H, NCH₂CH₃), 4.72 (br s, 2H, CH_{COD}), 4.72-4.66 (m, 2H, NCH₂CH₃), 2.97 (br s, 2H, CH_{COD}), 2.29-2.27 (m, 4H, CH₂_{COD}), 1.85-1.80 (m, 4H, CH₂_{COD}), 1.72-1.66 (m, 4H, CH₂_{COD}), 1.56 (t, ³J_{H-H} = 7.5 Hz, 6H, NCH₂CH₃). ¹³C NMR (300 MHz, CDCl₃): δ 191.3 (Ir-C_{carbene}), 134.7 (C_q_{arom}), 122.4 (CH_{arom}), 110.2 (CH_{arom}), 86.5 (CH_{COD}), 52.5 (CH_{COD}), 43.3 (NCH₂CH₃), 33.7 (CH₂_{COD}), 29.5 (CH₂_{COD}), 15.1 (NCH₂CH₃). Electrospray MS (20V, *m/z*): 516.2 [M-Cl+MeCN]⁺. Anal. Calcd. for C₁₉H₂₆ClIrN₂ (510.09): C, 44.74; H, 5.14; N, 5.49. Found: C, 44.90; H, 5.60; N, 5.80.

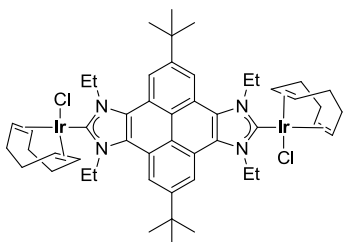
General procedure for the synthesis of complexes 1F and 2F: The corresponding bis-imidazolium salt (1 equiv.), the metal precursor (1 equiv.) and KO^tBu (2.2 equiv.) were placed together in a Schlenk tube. The tube was evacuated and filled with nitrogen three times. Afterward, 10 mL of THF were added and the mixture stirred at room temperature overnight. The mixture was filtered through Celite, and the solution was concentrated under reduced pressure. The solid was dissolved in CH₂Cl₂ and purified by gradient column chromatography using silica gel. Elution with a 95:5 mixture of CH₂Cl₂/acetone afforded the separation of a yellow band that contained the desired metal complex. Metal complexes **1F** and **2F** were isolated as yellow solids after precipitation in a mixture of CH₂Cl₂/hexanes.

Synthesis of 1F-Me



The reaction was carried out using bis-imidazolium salt $[\text{FH}_2\text{-Me}](\text{BF}_4)_2$ (93 mg, 0.15 mmol), $[\text{IrCl}(\text{COD})]_2$ (100 mg, 0.15 mmol) and $\text{KO}t\text{Bu}$ (39 mg, 0.35 mmol). The reaction yielded a mixture of two atropisomers in a 1:1 ratio, which could not be separated. Yield: 65 mg, 40 %. ^1H NMR (300 MHz, CDCl_3): δ 8.88 (s, 2H, CH_{pyr}), 8.87 (s, H, CH_{pyr}), 5.00 (s, 12H, NCH_3), 4.81 (br s, 4H, CH_{COD}), 3.14 (br s, 4H, CH_{COD}), 2.37-2.36 (m, 8H, CH_2COD), 1.91-1.85 (m, 4H, CH_2COD), 1.76-1.70 (m, 4H, CH_2COD), 1.63 (s, 9H, $\text{C}(\text{CH}_3)_3$), 1.62 (s, 9H, $\text{C}(\text{CH}_3)_3$). ^{13}C NMR (75 MHz, CDCl_3): δ 188.4 (Ir- $\text{C}_{\text{carbene}}$), 188.3 (Ir- $\text{C}_{\text{carbene}}$), 149.1 (C_qpyr), 129.5 (C_qpyr), 122.1 (C_qpyr), 118.9 (C_qpyr), 115.7 (CH_{pyr}), 86.1 (CH_{COD}), 52.6 (CH_{COD}), 52.4 (CH_{COD}), 40.4 (NCH_3), 35.8 ($\text{C}(\text{CH}_3)_3$), 33.8 (CH_2COD), 31.9 ($\text{C}(\text{CH}_3)_3$), 29.8 (CH_2COD). Electrospray MS (20V, m/z): 1128.1 $[\text{M}-\text{Cl}+\text{CH}_3\text{CN}]^+$. Anal. Calcd. for $\text{C}_{46}\text{H}_{58}\text{Cl}_2\text{N}_4\text{Ir}_2$ (1122.30): C, 49.23; H, 5.21; N, 4.99. Found: C, 49.30; H, 5.60; N, 4.90.

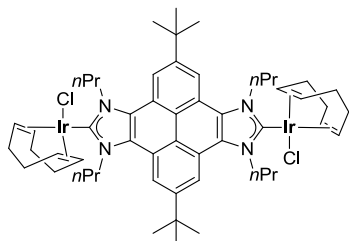
Synthesis of 1F-Et



The reaction was carried out using bis-imidazolium salt $[\text{FH}_2\text{-Et}](\text{BF}_4)_2$ (50.8 mg, 0.07 mmol), $[\text{IrCl}(\text{COD})]_2$ (50 mg, 0.07 mmol) and $\text{KO}t\text{Bu}$ (19 mg, 0.16 mmol). The reaction yielded a mixture of two atropisomers in a 1:1 ratio, which could not be separated. Yield: 40 mg, 46 %. ^1H NMR (500 MHz, CDCl_3): δ 8.76 (s, 2H, CH_{pyr}), 8.75 (s, 2H, CH_{pyr}), 5.95-5.87 (m, 4H, NCH_2CH_3), 5.39-5.32 (m, 4H, NCH_2CH_3), 4.81-4.80 (m, 4H, CH_{COD}), 3.12 (br s, 2H, CH_{COD}), 3.09 (br s, 2H, CH_{COD}), 2.38-2.36 (m, 8H, CH_2COD), 1.88-1.86 (m, 4H, CH_2COD), 1.82 (m, 12H, NCH_2CH_3), 1.77-1.75 (m, 4H, CH_2COD), 1.66 (s, 9H, $\text{C}(\text{CH}_3)_3$), 1.65 (s, 9H, $\text{C}(\text{CH}_3)_3$). ^{13}C NMR (125 MHz, CDCl_3): δ 188.7 (Ir- $\text{C}_{\text{carbene}}$), 188.5 (Ir- $\text{C}_{\text{carbene}}$), 149.00 (C_qpyr), 148.98 (C_qpyr), 128.87 (C_qpyr), 128.86 (C_qpyr), 121.48 (C_qpyr), 121.46 (C_qpyr), 118.81 (C_qpyr), 118.80 (C_qpyr), 116.09 (CH_{pyr}), 116.07 (CH_{pyr}), 85.64 (CH_{COD}), 85.63 (CH_{COD}), 53.0 (CH_{COD}), 52.9 (CH_{COD}), 47.1 (NCH_2CH_3), 47.0 (NCH_2CH_3), 35.9 ($\text{C}(\text{CH}_3)_3$), 33.7 (CH_2COD), 31.9 ($\text{C}(\text{CH}_3)_3$), 29.8 (CH_2COD), 15.6 (NCH_2CH_3).

Electrospray MS (20 V, m/z): 1184.3 $[M-Cl+CH_3CN]^+$. Calcd. for $C_{50}H_{66}Cl_2N_4Ir_2$ (1178.43): C, 50.96; H, 5.65; N, 4.76. Found: C, 50.60; H, 5.90; N, 4.80.

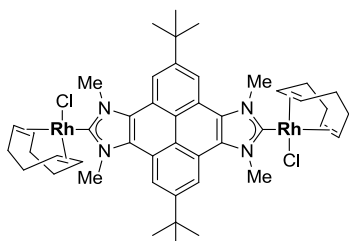
Synthesis of 1F-*n*Pr



The reaction was carried out using bis-imidazolium salt $[FH_2-nPr](BF_4)_2$ (62 mg, 0.08 mmol), $[IrCl(COD)]_2$ (56.4 mg, 0.08 mmol) and $KOtBu$ (20 mg, 0.17 mmol). In this case, broad signals were observed in the NMR spectra, suggesting the presence of the two atropisomers. Yield: 31.6 mg, 32 %. 1H NMR (300 MHz, $CDCl_3$): δ 8.67 (s, CH_{pyr}), 5.72-5.65

(m, 4H, $NCH_2CH_2CH_3$), 5.25-5.19 (m, 4H, $NCH_2CH_2CH_3$), 4.82 (br s, 4H, CH_{COD}), 3.11 (br s, 4H, CH_{COD}), 2.36-2.34 (m, 8H, $NCH_2CH_2CH_3$), 2.12-2.06 (m, 8H, CH_2_{COD}), 1.88-1.86 (m, 4H, CH_2_{COD}), 1.77-1.75 (m, 4H, CH_2_{COD}), 1.65 (s, 18H, $C(CH_3)_3$), 1.28 (t, $^3J_{H-H} = 6$ Hz, 12H, $NCH_2CH_2CH_3$). ^{13}C NMR (300 MHz, $CDCl_3$): δ 188.6 (Ir- $C_{carbene}$), 148.9 (C_q pyr), 129.0 (C_q pyr), 121.5 (C_q pyr), 118.8 (C_q pyr), 115.9 (CH_{pyr}), 85.4 (CH_{COD}), 53.9 ($NCH_2CH_2CH_3$), 52.9 (CH_{COD}), 35.8 ($C(CH_3)_3$), 33.8 (CH_2_{COD}), 31.9 ($C(CH_3)_3$), 29.8 (CH_2_{COD}), 23.6 ($NCH_2CH_2CH_3$), 11.6 ($NCH_2CH_2CH_3$). Electrospray (20 V, m/z): 1240.4 $[M-Cl+CH_3CN]^+$. Calcd. for $C_{54}H_{74}Cl_2N_4Ir_2$ (1234.53): C, 52.53; H, 6.04; N, 4.54. Found: C, 52.60; H, 6.00; N, 4.60.

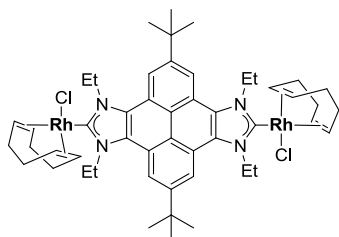
Synthesis of 2F-Me



The reaction was carried out using bis-imidazolium salt $[FH_2-Me](BF_4)_2$ (127 mg, 0.2 mmol), $[RhCl(COD)]_2$ (100 mg, 0.2 mmol) and $KOtBu$ (49.4 mg, 0.44 mmol). The reaction yielded a mixture of two atropisomers in a 1:1 ratio, which could not be separated. Yield: 95.4 mg, 50 %. 1H NMR (75 MHz, CD_2Cl_2): δ 8.92 (s, 2H, CH_{pyr}), 8.92 (s, 2H, CH_{pyr}), 5.13 (s, 12H, NCH_3), 5.52 (br s, 4H, CH_{COD}), 3.52 (br s, 4H, CH_{COD}), 2.58-2.52 (m, 8H, CH_2_{COD}), 2.09-2.05 (m, 8H, CH_2_{COD}), 1.66 (s, 18H, $C(CH_3)_3$). ^{13}C NMR (75 MHz, CD_2Cl_2): δ 193.0 (d, $^1J_{Rh-C} = 51.9$ Hz, Rh- $C_{carbene}$), 149.5 (C_q pyr), 129.8 (C_q pyr), 122.2 (C_q pyr), 118.8 (C_q pyr), 116.1 (CH_{pyr}), 99.7 (d, $^1J_{Rh-C} = 6.7$ Hz, Rh- CH_{COD}), 69.3 (d, $^1J_{Rh-C} = 14.5$ Hz, Rh- CH_{COD}), 69.2 (d, $^1J_{Rh-C} = 14.2$ Hz, Rh- CH_{COD}), 40.8 (NCH_3), 36.0 ($C(CH_3)_3$), 33.4 (CH_2_{cod}), 31.9 ($C(CH_3)_3$), 28.4 (CH_2_{COD}). Electrospray MS (20V, m/z): 948.0 $[M-Cl+CH_3CN]^+$.

Anal. Calcd. for $C_{46}H_{58}Cl_2N_4Rh_2$ (943.70): C, 58.54; H, 6.20; N, 5.94. Found: C, 58.40; H, 6.20; N, 5.60.

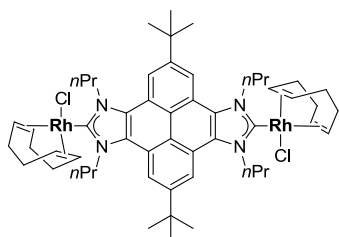
Synthesis of 2F-Et



The reaction was carried out using bis-imidazolium salt $[FH_2-Et](BF_4)_2$ (69 mg, 0.10 mmol), $[RhCl(COD)]_2$ (50 mg, 0.10 mmol) and $KOtBu$ (26 mg, 0.22 mmol). The reaction yielded a mixture of two atropisomers in a 1:1 ratio, which could not be separated. Yield: 72.7 mg, 74 %. 1H NMR (500 MHz, $CDCl_3$): δ 8.75 (s, 4H, CH_{pyr}), 6.12-6.07 (m, 4H, NCH_2CH_3), 5.55-5.43 (m, 4H, NCH_2CH_3), 5.23 (br s, 4H, CH_{COD}), 3.53 (br s, 2H, CH_{COD}), 3.49 (br s, 2H, CH_{COD}), 2.56-2.54 (m, 8H, CH_2_{COD}), 2.08-2.07 (m, 8H, CH_2_{COD}), 1.86 (t, $^3J_{H-H} = 6.9$ Hz, 12H, NCH_2CH_3), 1.66 (s, 18H, $C(CH_3)_3$). ^{13}C NMR (75 MHz, $CDCl_3$): δ 192.7 (d, $^1J_{Rh-C} = 51.4$ Hz, Rh- $C_{carbene}$), 192.5 (d, $^1J_{Rh-C} = 51.6$ Hz, Rh- $C_{carbene}$), 148.99 (C_q pyr), 148.95 (C_q pyr), 129.0 (C_q pyr), 121.4 (C_q pyr), 121.3 (C_q pyr), 118.7 (C_q pyr), 118.6 (C_q pyr), 116.1 (CH_{pyr}), 99.4 (d, $^1J_{Rh-C} = 6.7$ Hz, Rh- CH_{COD}), 69.3 (d, $^1J_{Rh-C} = 14.4$ Hz, Rh- CH_{COD}), 69.2 (d, $^1J_{Rh-C} = 14.2$ Hz, Rh- CH_{COD}), 47.42 (NCH_2CH_3), 47.36 (NCH_2CH_3), 35.9 ($C(CH_3)_3$), 33.1 (CH_2_{COD}), 31.9 ($C(CH_3)_3$), 29.1 (CH_2_{COD}), 15.6 (NCH_2CH_3).

Electrospray MS (20V, m/z): 1004.1 $[M-Cl+CH_3CN]^+$. Anal. Calcd. for $C_{50}H_{66}Cl_2N_4Rh_2$ (999.80): C, 60.06; H, 6.65; N, 5.61. Found: C, 59.70; H, 6.94; N, 5.70.

Synthesis of 2F-nPr

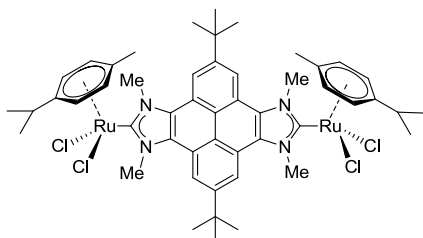


The reaction was carried out using bis-imidazolium salt $[FH_2-nPr](BF_4)_2$ (100 mg, 0.14 mmol), $[RhCl(COD)]_2$ (69 mg, 0.14 mmol) and $KOtBu$ (35 mg, 0.27 mmol). In this case, broad signals were observed in the NMR spectra, suggesting the presence of the two atropisomers.. Yield: 47 mg, 32 %. 1H NMR

(300 MHz, $CDCl_3$): δ 8.66 (s, 4H, CH_{pyr}), 5.89-5.79 (m, 4H, $NCH_2CH_2CH_3$), 5.46-5.36 (m, 4H, $NCH_2CH_2CH_3$), 5.22 (br s, 4H, CH_{COD}), 3.54 (br s, 4H, CH_{COD}), 2.59-2.42 (m, 16H; 8H, $NCH_2CH_2CH_3$, 8H, CH_2_{COD}), 2.10-2.06 (m, 8H, CH_2_{COD}), 1.65 (s, 18H, $C(CH_3)_3$), 1.34 (t, $^3J_{H-H} = 7.3$ Hz, 12H, $NCH_2CH_2CH_3$). ^{13}C NMR (300 MHz, $CDCl_3$): δ 192.6 (d, $^1J_{Rh-C} = 51$ Hz, Rh- $C_{carbene}$), 148.9 (C_q pyr), 129.1 (C_q pyr), 121.4 (C_q

pyr), 118.6 ($C_{\text{q pyr}}$), 115.9 (CH_{pyr}), 99.2 (d, $^1J_{\text{Rh-C}} = 6.8$ Hz, Rh- CH_{COD}), 69.2 (d, $^1J_{\text{Rh-C}} = 14.3$ Hz, Rh- CH_{COD}), 54.3 ($\text{NCH}_2\text{CH}_2\text{CH}_3$), 35.8 ($\text{C}(\text{CH}_3)_3$), 33.2 (CH_2_{COD}), 32.0 ($\text{C}(\text{CH}_3)_3$), 29.2 (CH_2_{COD}), 23.6 ($\text{NCH}_2\text{CH}_2\text{CH}_3$), 11.8 ($\text{NCH}_2\text{CH}_2\text{CH}_3$). Electrospray MS (20 V, m/z): 1060.4 [$\text{M-Cl}+\text{CH}_3\text{CN}$] $^+$. Calcd. for $\text{C}_{54}\text{H}_{74}\text{Cl}_2\text{N}_4\text{Rh}_2$ (1055.91): C, 61.42; H, 7.06; N, 5.31. Found: C, 61.40; H, 6.70; N, 5.50.

Synthesis of 3F-Me



KHMDS (0.5 M in toluene, 1.3 mL, 0.65 mmol, 2 equiv.) was added dropwise to a suspension of $[\text{FH}_2\text{-Me}](\text{BF}_4)_2$ (204.4 mg, 0.325 mmol) in THF (20 mL) at 0°C . After stirring at 0°C for 10 minutes, this solution was added *via* oven dried cannula to a mixture of

$[\text{RuCl}_2(p\text{-cymene})]_2$ (200 mg, 0.325 mmol) in CH_2Cl_2 . The resulting suspension was stirred at 45°C for 1 h, and after that was refluxed for 20 min. The mixture was filtered through a pad of Celite and the solid residue eluted with CH_2Cl_2 . The solvent was removed on a rotatory evaporator. The solid residue was dissolved in acetone and precipitated with diethyl ether to afford compound **3F-Me** as a brownish solid. Only one atropisomer was observed by NMR. Yield: 261.3 mg (75 %). ^1H NMR (300 MHz, CDCl_3): δ 8.99 (s, 4H, CH_{pyr}), 5.60 (d, $^3J_{\text{H-H}} = 5.2$ Hz, 4H, $\text{CH}_{p\text{-cym}}$), 5.33 (d, $^3J_{\text{H-H}} = 4.8$ Hz, 4H, $\text{CH}_{p\text{-cym}}$), 4.92 (s, 12H, NCH_3), 3.11 (m, 2H, $\text{CH}_{\text{isop } p\text{-cym}}$), 2.19 (s, 6H, $\text{CH}_3_{p\text{-cym}}$), 1.61 (s, 18H, $\text{C}(\text{CH}_3)_3$), 1.32 (d, $^3J_{\text{H-H}} = 6.0$ Hz, 12H, $\text{CH}_3_{\text{isop } p\text{-cym}}$). ^{13}C NMR (75 MHz, CDCl_3): δ 186.7 (Ru- $\text{C}_{\text{carbene}}$), 149.1 ($\text{C}_{\text{q pyr}}$), 130.5 ($\text{C}_{\text{q pyr}}$), 121.7 ($\text{C}_{\text{q pyr}}$), 119.6 ($\text{C}_{\text{q pyr}}$), 116.8 (CH_{pyr}), 110.6 ($\text{C}_{\text{q } p\text{-cym}}$), 99.8 ($\text{C}_{\text{q } p\text{-cym}}$), 85.7 ($\text{CH}_{p\text{-cym}}$), 83.7 ($\text{CH}_{p\text{-cym}}$), 43.2 (NCH_3), 35.8 ($\text{C}(\text{CH}_3)_3$), 31.8 ($\text{C}(\text{CH}_3)_3$), 31.1 ($\text{CH}_{\text{isop } p\text{-cym}}$), 22.7 ($\text{CH}_3_{\text{isop } p\text{-cym}}$), 19.1 ($\text{CH}_3_{p\text{-cym}}$). Electrospray MS (20V, m/z): 496.3 [M-2Cl] $^{2+}$. Anal. Calcd. for $\text{C}_{50}\text{H}_{62}\text{N}_4\text{Ru}_2\text{Cl}_4(\text{CH}_2\text{Cl}_2)_2$ (1230.09): C, 50.66; H, 5.40; N, 4.55. Found: C, 50.63; H, 5.63; N, 4.78.

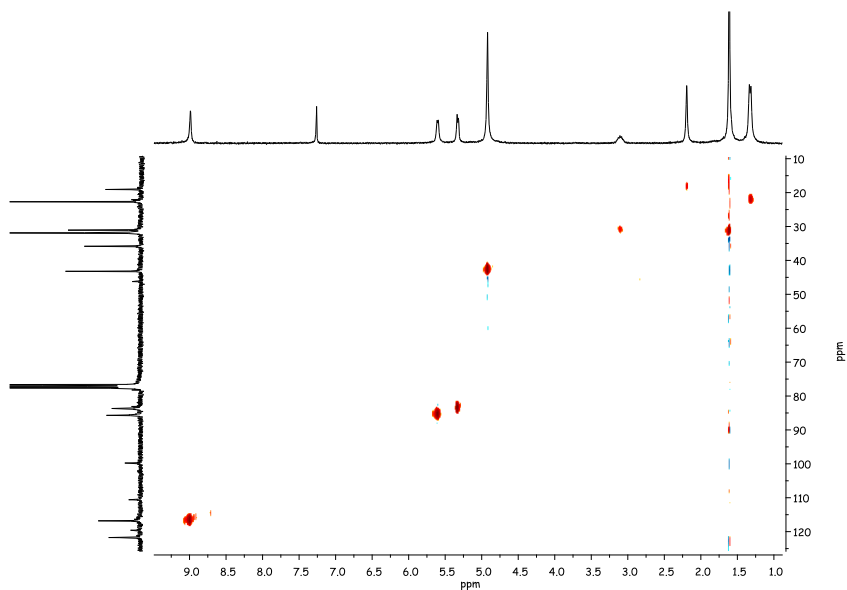


Figure 5.15 HSQC spectrum of **3F-Me** in CDCl_3 ($^1J_{\text{H-C}} = 145 \text{ Hz}$)

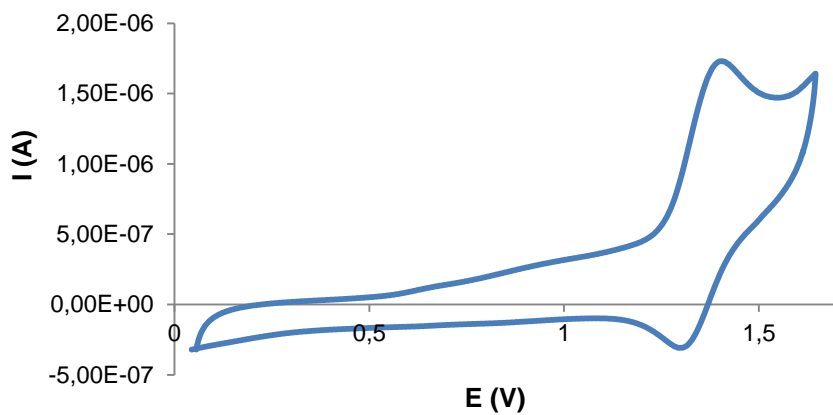


Figure 5.16 Cyclic voltammetry diagram of complex **3F-Me**

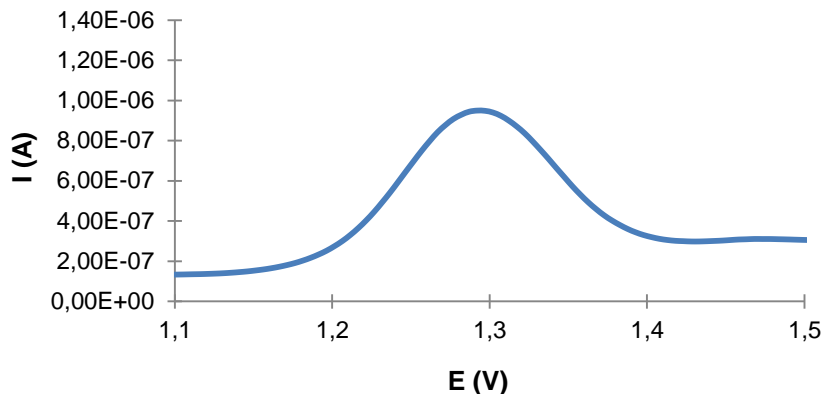


Figure 5.17 Relevant section of the differential pulse voltammetry analysis of complex **3F-Me**

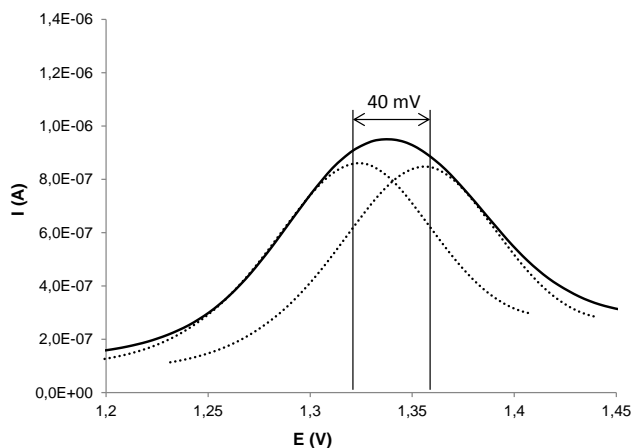
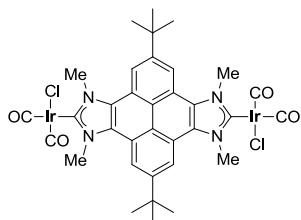


Figure 5.18 Deconvolution of the DPV signal of **3F-Me** (black line) obtained from adding two potential-shifted and weighted signals of monometallic complex **1I** (gray dotted lines)

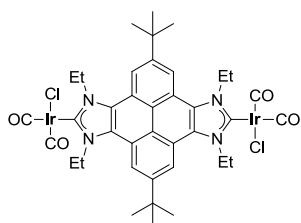
General procedure for the synthesis of complexes 4F-Me and 4F-Et: CO gas was passed through a solution of complexes **1F-Me** and **1F-Et** (30 mg) in dichloromethane (10 mL) for 20 minutes at 0°C. After this time, the solution was concentrated under reduced pressure. After the addition of hexanes, the corresponding carbonyl derivative precipitated as a pale yellow solid.

Synthesis of 4F-Me



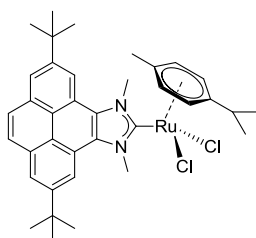
The reaction yielded only one atropisomer. ^1H NMR (300 MHz, CDCl_3): δ 8.95 (s, 4H, CH_{pyr}), 4.89 (s, 12H, NCH_3), 1.65 (m, 18H, $\text{C}(\text{CH}_3)_3$). ^{13}C NMR (75 MHz, CDCl_3): δ 181.0 (Ir- $\text{C}_{\text{carbene}}$), 167.8 (Ir-CO), 167.8 (Ir-CO), 149.9 (C_{q} pyr), 129.4 (C_{q} pyr), 122.1 (C_{q} pyr), 120.0 (C_{q} pyr), 116.7 (CH_{pyr}), 41.2 (NCH_3), 35.9 ($\text{C}(\text{CH}_3)_3$), 31.9 ($\text{C}(\text{CH}_3)_3$). IR (CH_2Cl_2): 2069 ($\nu_{\text{C=O}}$), 1988 ($\nu_{\text{C=O}}$) cm^{-1} . Electrospray MS (20 V, m/z): 1024.2 [$\text{M}-\text{Cl}+\text{MeCN}$] $^+$. HRMS ESI-TOF-MS (positive mode): [$\text{M}-\text{Cl}+\text{MeCN}$] $^+$ monoisotopic peak 1024.1786, calcd 1024.1782, $\epsilon_r = 0.39$ ppm. Slow decomposition of the compound prevented a correct elemental analysis.

Synthesis of 4F-Et



The reaction yielded a mixture of two atropisomers in a 1:1 ratio, which could not be separated. ^1H NMR (500 MHz, CDCl_3): δ 8.83 (s, 4H, CH_{pyr}), 5.54-5.41 (m, 8H, NCH_2CH_3), 1.85 (t, $^3J_{\text{H-H}} = 6.8$ Hz, 12H, NCH_2CH_3), 1.66 (s, 18H, $\text{C}(\text{CH}_3)_3$). ^{13}C NMR (75 MHz, CDCl_3): δ 181.0 (Ir- $\text{C}_{\text{carbene}}$), 180.4 (Ir- $\text{C}_{\text{carbene}}$), 168.3 (Ir-CO), 168.2 (Ir-CO), 149.9 (C_{q} pyr), 128.8 (C_{q} pyr), 121.5 (C_{q} pyr), 119.9 (C_{q} pyr), 116.9 (CH_{pyr}), 47.8 (NCH_2CH_3), 36.0 ($\text{C}(\text{CH}_3)_3$), 28.2 ($\text{C}(\text{CH}_3)_3$), 15.0 (NCH_2CH_3). IR (CH_2Cl_2): 2069 ($\nu_{\text{C=O}}$), 1987 ($\nu_{\text{C=O}}$) cm^{-1} . Electrospray MS (20 V, m/z): 791.2 [$\text{M}-\text{IrCl}(\text{CO})_2+\text{H}$] $^+$. HRMS ESI-TOF-MS (positive mode): [$\text{M}-\text{Cl}+\text{MeCN}$] $^+$ monoisotopic peak 1080.2406, calcd 1080.2410, $\epsilon_r = 0.37$ ppm. Slow decomposition of the compound prevented a correct elemental analysis.

Synthesis of 1I



A suspension of compound **[IH](I)** (166.3 mg, 0.32 mmol) and Ag_2O (37.5 mg, 0.16 mmol) in CH_2Cl_2 (15 mL) was stirred at room temperature for 2 h under the exclusion of light. Then, $[\text{RuCl}_2(p\text{-cymene})]_2$ (100 mg, 0.16 mmol) was added and the resulting mixture was stirred at room temperature for 2 h. The suspension was filtered through a pad of Celite and the solvent removed under vacuum. Precipitation with a mixture

$\text{CH}_2\text{Cl}_2/\text{hexane}$ afforded compound **11** as a brownish solid. Yield: 163.2 mg, 73 %. ^1H NMR (500 MHz, CDCl_3): δ 8.91 (s, 2H, CH_{pyr}), 8.21 (s, 2H, CH_{pyr}), 8.06 (s, 2H, CH_{pyr}), 5.57 (d, $^3J_{\text{H-H}} = 5.7$ Hz, 2H, $\text{CH}_{p\text{-cym}}$), 5.30 (d, $^3J_{\text{H-H}} = 5.7$ Hz, 2H, $\text{CH}_{p\text{-cym}}$), 4.90 (s, 6H, NCH_3), 3.09 (m, 1H, $\text{CH}_{\text{isop } p\text{-cym}}$), 2.16 (s, 3H, $\text{CH}_3_{p\text{-cym}}$), 1.59 (s, 18H, $\text{C}(\text{CH}_3)_3$), 1.29 (d, $^3J_{\text{H-H}} = 6.9$ Hz, 6H, $\text{CH}_3_{\text{isop } p\text{-cym}}$). ^{13}C NMR (126 MHz, CDCl_3): δ 184.2 (Ru-C_{carbene}), 148.9 (C_q_{pyr}), 131.8 (C_q_{pyr}), 130.5 (C_q_{pyr}), 128.3 (CH_{pyr}), 122.6 (CH_{pyr}), 121.4 (C_q_{pyr}), 121.1 (C_q_{pyr}), 117.0 (CH_{pyr}), 110.4 ($\text{C}_q_{p\text{-cym}}$), 99.8 ($\text{C}_q_{p\text{-cym}}$), 85.5 ($\text{CH}_{p\text{-cym}}$), 83.6 ($\text{CH}_{p\text{-cym}}$), 42.9 (NCH_3), 35.6 ($\text{C}(\text{CH}_3)_3$), 32.0 ($\text{C}(\text{CH}_3)_3$), 31.0 ($\text{CH}_{\text{isop } p\text{-cym}}$), 22.7 ($\text{CH}_3_{\text{isop } p\text{-cym}}$), 19.0 ($\text{CH}_3_{p\text{-cym}}$). Electrospray MS (20V, m/z): 653.0 $[\text{M}-\text{Cl}]^+$. Anal. Calcd. for $\text{C}_{37}\text{H}_{44}\text{N}_2\text{RuCl}_2(\text{H}_2\text{O})$ (706.20): C, 62.88; H, 6.56; N, 3.96. Found: C, 63.14; H, 6.17; N, 3.86.

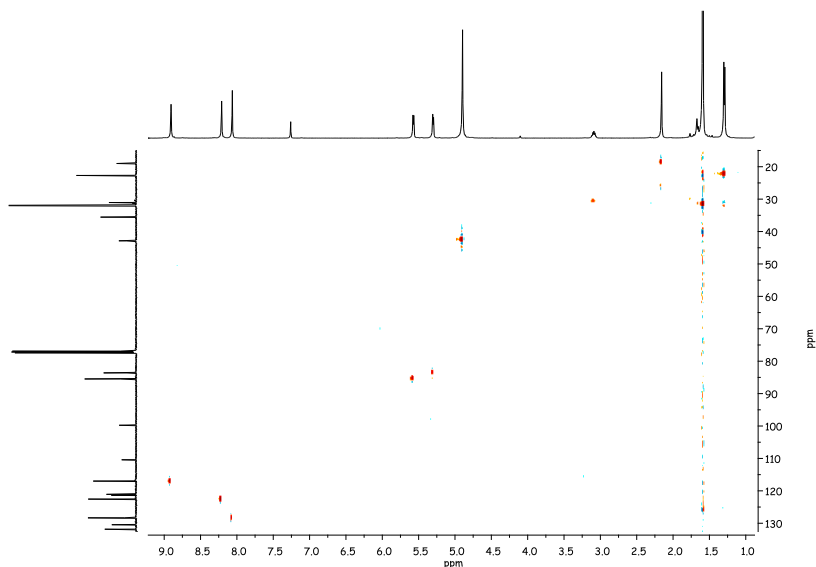


Figure 5.19 HSQC spectrum of **11** in CDCl_3 ($^1J_{\text{H-C}} = 145$ Hz)

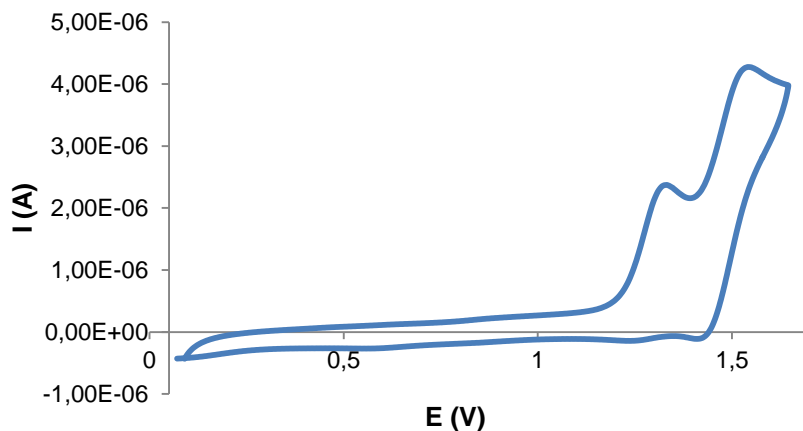


Figure 5.20 Cyclic voltammety diagram of complex **11**

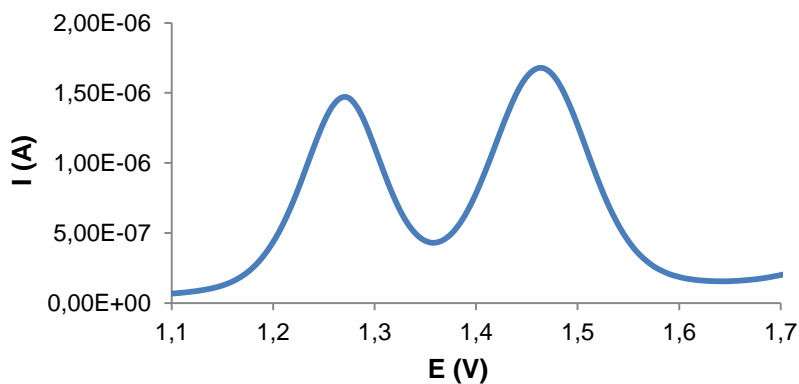
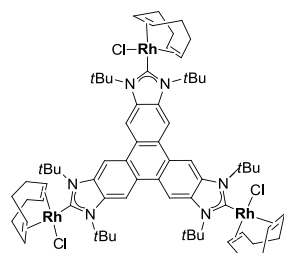


Figure 5.21 Relevant section of the differential pulse voltammety analysis of complex **11**

5.2.4 Synthesis and characterization of complexes of Chapter 4

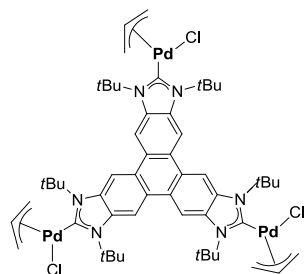
Synthesis of 1K



KHMDS (0.5 M in toluene, 0.85 mL, 0.425 mmol, 3.15 equiv.) was added dropwise to a suspension of $[\text{KH}_3](\text{BF}_4)_3$ (128.2 mg, 0.135 mmol) in THF (10 mL) at 0°C. After stirring at that temperature for 10 minutes, a solution of $[\text{RhCl}(\text{COD})]_2$ (100 mg, 0.203 mmol) in THF (5 mL) was added *via* oven dried cannula. The resulting mixture was stirred for 10 minutes at 0°C and for 2 hours at 50°C. After this time, the volatile

components were removed under vacuum. The crude solid was dissolved in CH_2Cl_2 and purified by column chromatography. Flash chromatography using mixtures of CH_2Cl_2 /acetone (from 95:5 to 7:3) afforded the separation of a yellow band that contained compound **1K**. Compound **1K** was obtained as a yellow solid after precipitation in a mixture of dichloromethane/hexanes. Yield: 81.4 mg (42 %). ^1H NMR (300 MHz, CDCl_3): δ 8.74 (s, 6H, CH_{arom}), 5.10 (br s, 6H, CH_{COD}), 3.08 (brs, 6H, CH_{COD}), 2.58 (s, 54H, $\text{C}(\text{CH}_3)_3$), 2.50 (brs, 12H, CH_2_{COD}), 1.78-1.86 (m, 12H, CH_2_{COD}). ^{13}C NMR (75 MHz, CDCl_3): δ 200.9 (d, $^1J_{\text{Rh-C}} = 49.1$ Hz, Rh-C_{carbene}), 135.5 ($\text{C}_{\text{q arom}}$), 124.0 ($\text{C}_{\text{q arom}}$), 107.8 (CH_{arom}), 94.4 (d, $^1J_{\text{Rh-C}} = 15.8$ Hz, Rh- CH_{COD}), 67.9 (d, $^1J_{\text{Rh-C}} = 15.8$ Hz, Rh- CH_{COD}), 60.9 ($\text{C}(\text{CH}_3)_3$), 32.6 ($\text{C}(\text{CH}_3)_3$), 32.4 (CH_2_{COD}), 28.8 (CH_2_{COD}). Electrospray MS (20 V, m/z): 676.5 $[\text{M}-2\text{Cl}]^{2+}$. HRMS ESI-TOF-MS (positive mode): $[\text{M}-\text{Cl}]^+$ monoisotopic peak 1387.4236, calcd 1387.4238, $\epsilon_r = 0.14$ ppm. Anal. Calcd. for $\text{C}_{69}\text{H}_{96}\text{Cl}_3\text{N}_6\text{Rh}_3$ (1424.60): C, 58.17; H, 6.79; N, 5.90. Found: C, 58.26; H, 7.05; N, 5.58.

Synthesis of **2K**

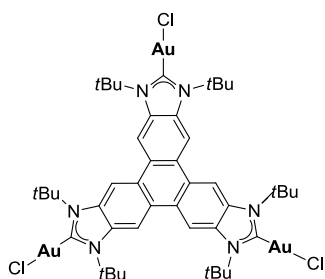


KHMDS (0.5 M in toluene, 1.2 mL, 0.6 mmol, 3.3 equiv.) was added dropwise to a suspension of $[\text{KH}_3](\text{BF}_4)_3$ (172.4 mg, 0.18 mmol) in THF (10 mL) at 0°C . After stirring at 0°C for 10 minutes, a solution of $[\text{PdCl}(\eta^3\text{-allyl})_2]$ (100 mg, 0.27 mmol) in THF (5 mL) was added *via* oven dried cannula. The resulting mixture was stirred for 10 min at 0°C and for 2 h at room temperature. After

this time, the volatile components were removed under vacuum. The crude solid was dissolved in CH_2Cl_2 and purified by column chromatography. Flash chromatography using mixtures of CH_2Cl_2 /acetone (from 8:2 to 1:1) afforded the separation of a yellow band that contained compound **2K**. Compound **2K** was obtained as a pale yellow solid after precipitation in a mixture of dichloromethane/hexanes. Yield: 89.3 mg (40 %). ^1H NMR (300 MHz, CDCl_3): δ 8.85 (m, 6H, CH_{arom}), 5.34 (m, 3H, CH_{allyl}), 4.25 (m, 3H, $\text{CH}_2_{\text{allyl}}$), 3.46 (m, 6H, $\text{CH}_2_{\text{allyl}}$), 2.38 (d, $^4J_{\text{H-H}} = 3.1$ Hz, 27H, $\text{C}(\text{CH}_3)_3$), 2.28 (m, 3H, $\text{CH}_2_{\text{allyl}}$), 2.20 (d, $^4J_{\text{H-H}} = 3.1$ Hz, 27H, $\text{C}(\text{CH}_3)_3$). ^{13}C NMR (300 MHz, CDCl_3): δ 193.9 (Pd-C_{carbene}), 135.5 ($\text{C}_{\text{q arom}}$), 124.5 ($\text{C}_{\text{q arom}}$), 112.9 (CH_{allyl}), 108.6 (CH_{arom}), 69.0 ($\text{CH}_2_{\text{allyl}}$), 60.3 ($\text{C}(\text{CH}_3)_3$), 51.8 ($\text{CH}_2_{\text{allyl}}$), 32.0 ($\text{C}(\text{CH}_3)_3$), 31.9 ($\text{C}(\text{CH}_3)_3$). Electrospray MS (20 V, m/z): 1198.1 $[\text{M}-\text{Cl}]^+$. Anal. Calcd. for

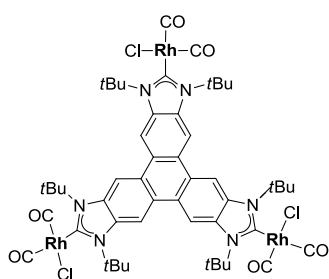
$C_{54}H_{75}Cl_3N_6Pd_3$ (1230.22): C, 52.57; H, 6.13; N, 6.81. Found: C, 52.82; H, 6.43; N, 6.86.

Synthesis of 3K



KHMDS (0.5 M in toluene, 0.74 mL, 0.37 mmol, 3.3 equiv.) was added dropwise to a suspension of $[KH_3](BF_4)_3$ (106.5 mg, 0.112 mmol) in THF (10 mL) at 0°C. After stirring at that temperature for 10 minutes, the resulting solution was transferred *via* oven dried cannula to a stirred THF suspension (5 mL) of $[AuCl(SMe_2)]$ (100 mg, 0.337 mmol). The resulting solution was kept in the dark and stirred at room temperature for 2 h. Under air, a spatula of charcoal was added and the mixture was stirred for 30 minutes. The suspension was then filtered through oven dried Celite, washed with CH_2Cl_2 and the solvent was removed under vacuum. The solid was dissolved in the minimum amount of CH_2Cl_2 and precipitated with pentane to afford the desired gold(I) compound as a yellow solid. Yield 96 mg (62 %). 1H NMR (300 MHz, $CDCl_3$): δ 9.02 (s, 6H, CH_{arom}), 2.39 (s, 54H, $C(CH_3)_3$). ^{13}C NMR (75 MHz, $CDCl_3$): δ 182.5 ($Au-C_{carbene}$), 134.4 (C_q arom), 125.6 (C_q arom), 109.6 (CH_{arom}), 62.9 ($C(CH_3)_3$), 33.3 ($C(CH_3)_3$). HRMS ESI-TOF-MS (positive mode): $[M-AuCl+H]^+$ monoisotopic peak 1149.3689, calcd 1149.3666, $\epsilon_r=2$ ppm. Anal. Calc. for $Au_3Cl_3N_6C_{45}H_{60}$ (1380.29): C, 39.10; H, 4.38; N, 6.08. Found: C, 39.32; H, 4.53; N, 6.18.

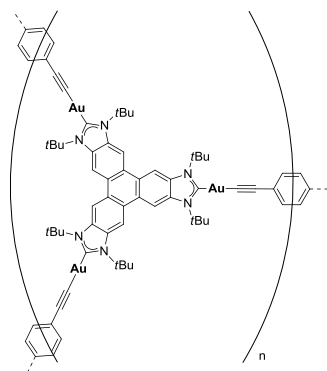
Synthesis of 4K



KHMDS (0.5 M in toluene, 0.54 mL, 0.27 mmol, 3.15 equiv.) was added dropwise to a suspension of $[KH_3](BF_4)_3$ (81.5 mg, 0.086 mmol) in THF (10 mL) at 0°C. After stirring at that temperature for 10 minutes, a solution of $[RhCl(CO)_2]_2$ (50 mg, 0.13 mmol) in THF (5 mL) was added *via* oven dried cannula. The resulting mixture was stirred for 10 minutes at 0°C and for 2 hours at 50°C. After this time, the volatile components were removed under vacuum. The crude solid was dissolved in CH_2Cl_2 and filtered through a pad of Celite. Precipitation with a mixture CH_2Cl_2 /hexane afforded compound **5** as a yellow solid. Yield: 27 mg (26 %). 1H NMR (500 MHz, $CDCl_3$): δ 8.94 (s, 6H, CH_{arom}), 2.58 (s,

54H, C(CH₃)₃). ¹³C NMR (126 MHz, CDCl₃): δ 187.5 (d, ¹J_{Rh-C} = 42.4 Hz, Rh-C_{carbene}), 185.8 (d, ¹J_{Rh-C} = 57.2 Hz, Rh-CO), 182.7 (d, ¹J_{Rh-C} = 75.7, Rh-CO), 135.5 (C_q arom), 125.0 (C_q arom), 109.4 (CH_{arom}), 61.3 (C(CH₃)₃), 32.9 (C(CH₃)₃). IR (CH₂Cl₂) = 2078 (ν_{C=O}), 1999 (ν_{C=O}) cm⁻¹. Electrospray MS (20 V, *m/z*): 1073.2 [M-(Rh(CO)₂Cl)+H]⁺, 1216.1 [M-2CO-Cl+MeCN]⁺, 1285.2 [M-2CO-Cl+2MeCN]⁺. HRMS ESI-TOF-MS (positive mode): [M-Cl-2CO+MeCN]⁺ monoisotopic peak 1216.1488, calcd 1216.1483, ε_r = 0.4 ppm. Slow decomposition of the compound prevented a correct elemental analysis.

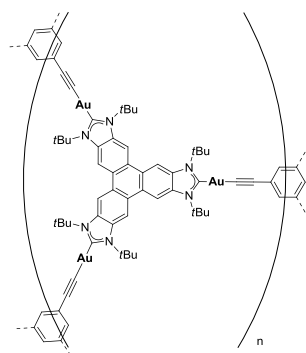
Synthesis of 5K



Under aerobic conditions, NaOH (40.6 mg, 0.51 mmol) and 1,4-diethynylbenzene (7.13 mg, 0.054 mmol) were dissolved in methanol (20 mL) in a round bottom flask. This mixture was refluxed for 15 min and then compound **3K** (50 mg, 0.036 mmol) was added as a solid. The resulting suspension was refluxed for 4 hours. After this time, a brown solid was formed. It was collected by filtration and subsequently washed with water, methanol, acetonitrile, dichloromethane, toluene,

hexane and diethyl ether. Yield: 35 mg (68 %). IR(ATR) = 2102 (ν_{C=C}) cm⁻¹. Anal. Calcd. for (C₆₀H₆₆N₆Au₃)_n: C, 49.29; H, 4.55; N, 5.75. Found: C, 48.95; H, 4.60; N, 5.39.

Synthesis of 6K



Under aerobic conditions, NaOH (31.7 mg, 0.76 mmol) and 1,3,5-triethynylbenzene (5.43 mg, 0.036 mmol) were dissolved methanol (20 mL) in a round bottom flask. This mixture was refluxed for 15 min and then compound **3K** (50 mg, 0.036 mmol) was added as a solid. The resulting suspension was refluxed for 4 hours. After this time, a yellow solid was formed. It was collected by filtration and subsequently washed with water, methanol, acetonitrile, dichloromethane, toluene, hexane and diethyl ether.

Yield: 46.6 mg (90 %). IR(ATR) = 2103 ($\nu_{C\equiv C}$) cm^{-1} . Anal. Calcd. for $(\text{C}_{57}\text{H}_{63}\text{N}_6\text{Au}_3)_n$: C, 48.11; H, 4.46; N, 5.91. Found: C, 47.75; H, 4.56; N, 5.56.

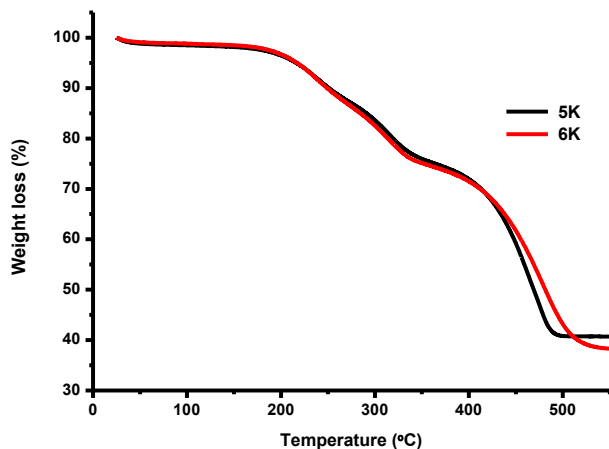


Figure 5.22 TGA plots of compounds **5K** and **6K** under air conditions

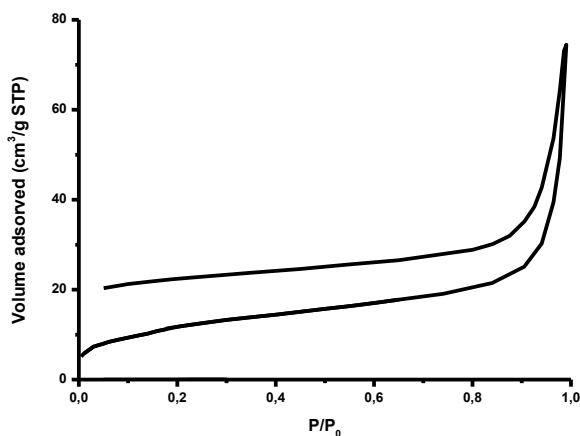


Figure 5.23 N₂ sorption isotherm of compound **5K** at 77K

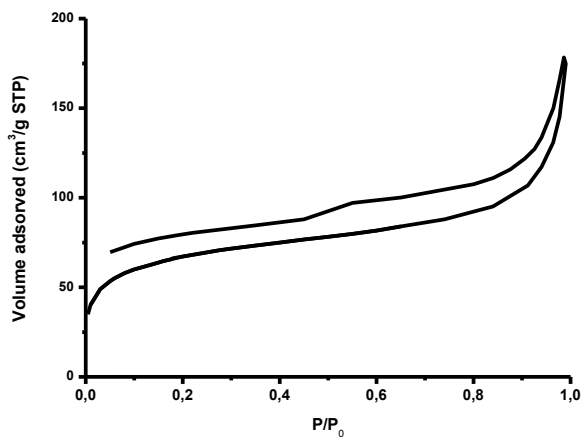


Figure 5.24 N₂ sorption isotherm of compound **6K** at 77K

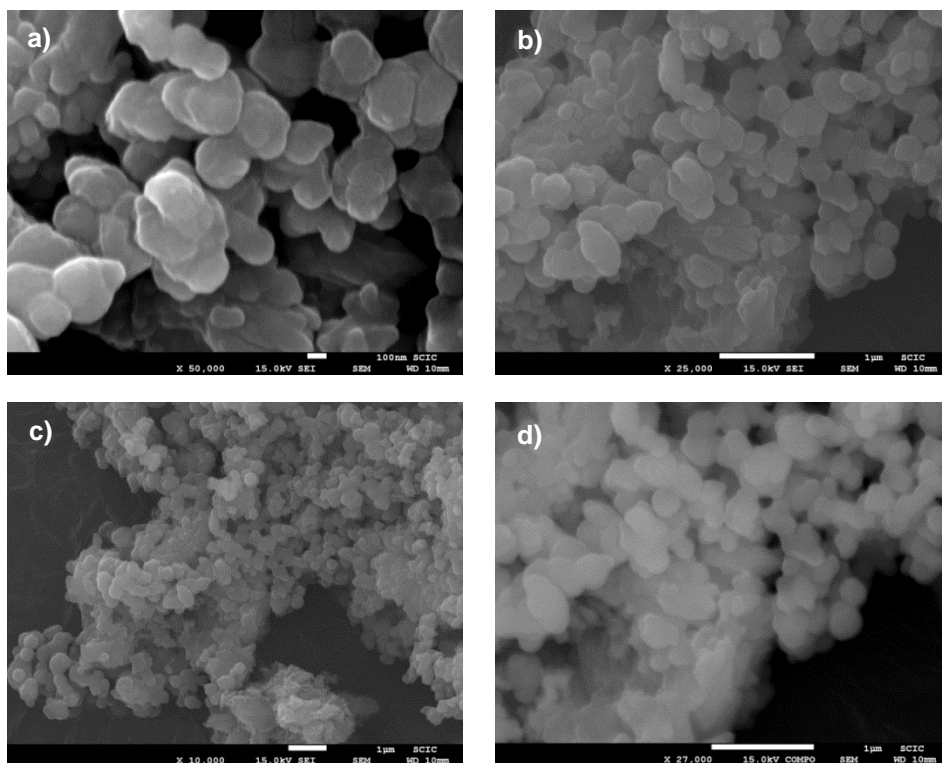


Figure 5.25 SEM micrographs at different magnifications (50.000x, 25.000x, 10.000x and 27.000x) of **5K**. Images a), b) and c) were taken using the secondary electrons (SE) signal of the SEM. Image d) was taken using the back-scattered electrons (BSE) signal of the SEM. Scale bar: 100 nm (S4.1) and 1 μ m (S4.2-4).

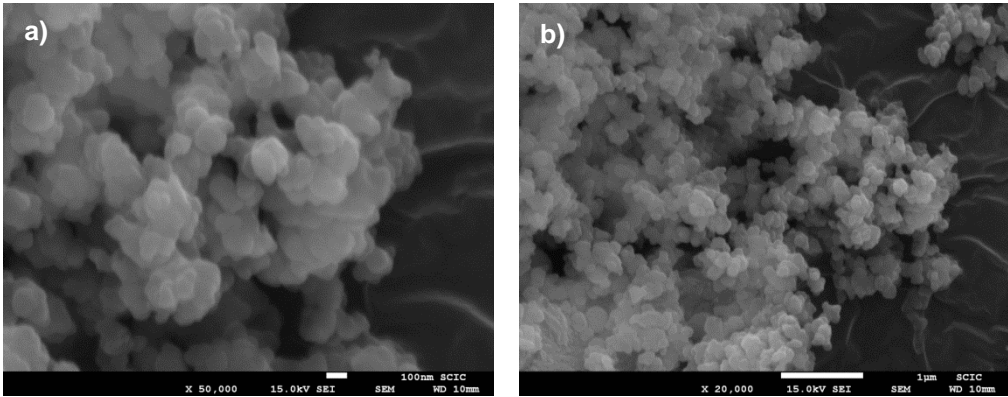


Figure 5.26 SEM micrographs at different magnifications (50.000x and 20.000x) of **6K**. Images were taken using the secondary electrons (SE) signal of the SEM. Scale bar: 100 nm a) and 1 μm b).

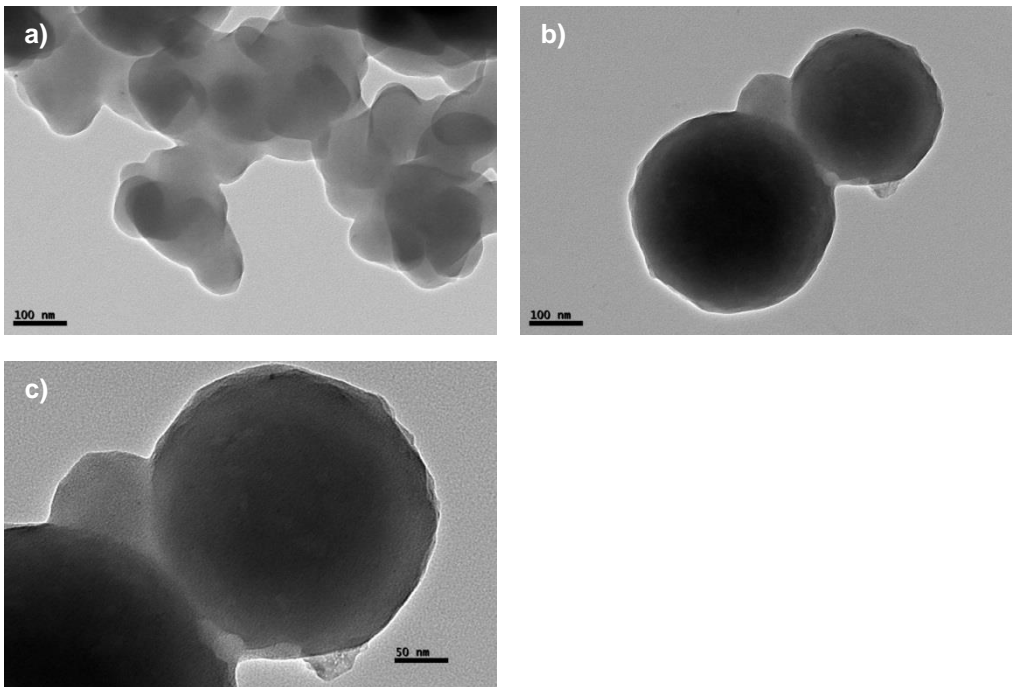


Figure 5.27 TEM images of **5K** at different magnifications (50.000x and 25.000x). Scale bar: 100 nm (a) and b)) and 50 nm (c)).

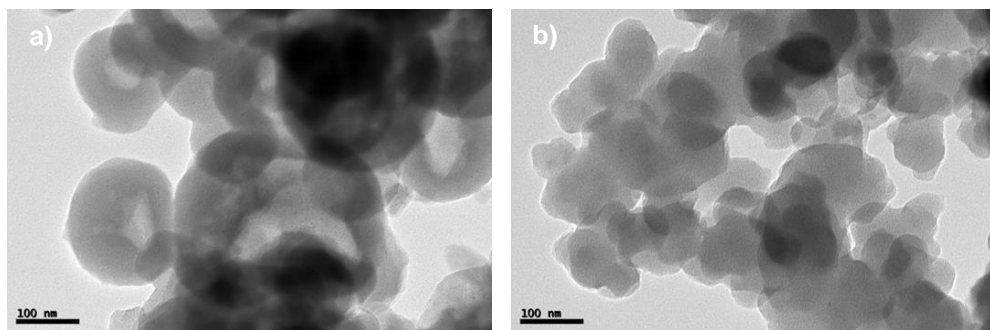
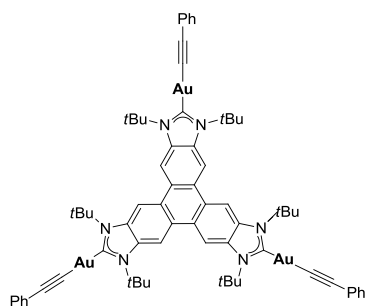


Figure 5.28 TEM images of **6K** at a magnifications of 30.000x. Scale bar: 100 nm.

Synthesis of **7K**



Under aerobic conditions, in a round bottom flask, NaOH (31.7 mg, 0.76 mmol) and phenylacetylene (17.6 μ L, 0.108 mmol) were dissolved in methanol (20 mL). This mixture was refluxed for 15 min and then compound **3K** (50 mg, 0.036 mmol) was added as a solid. The resulting suspension was refluxed for 4 hours. After this time, a white solid was formed.

The volatiles were evaporated. The resulting solid was dissolved in dichloromethane, filtered through a pad of Celite and the solvent was removed under vacuum. Precipitation with a mixture of CH_2Cl_2 /hexane gave the desired product as a white solid. Yield: 77 mg (91 %). ^1H NMR (500 MHz, CDCl_3): δ 9.01 (s, 6H, CH_{arom}), 7.52 (d, $^3J_{\text{H-H}} = 8.3$ Hz, 6H, CH_{arom}), 7.23 (t, $^3J_{\text{H-H}} = 7.4$ Hz, 6H, CH_{arom}), 7.17 (d, $^3J_{\text{H-H}} = 7.4$ Hz, 3H, CH_{arom}), 2.39 (s, 54H, $\text{C}(\text{CH}_3)_3$). ^{13}C NMR (126 MHz, CDCl_3): δ 199.6 (Au- $\text{C}_{\text{carbene}}$), 134.7 (C_{q} arom), 132.4 (CH_{arom} acetylide), 127.9 (CH_{arom} acetylide), 126.4 (CH_{arom} acetylide), 126.0 (C_{q} acetylide), 125.5 (C_{q} arom), 121.8 (C_{q} acetylide), 109.3 (CH_{arom}), 106.7 (C_{q} acetylide), 62.6 ($\text{C}(\text{CH}_3)_3$), 33.5 ($\text{C}(\text{CH}_3)_3$). Electrospray MS (20 V, m/z): 1281.6 [$\text{M-Au-C}_8\text{H}_5+\text{H}$] $^+$, 492.5 [$\text{M-2Au-2C}_8\text{H}_5+2\text{H}$] $^{2+}$. Anal. Calcd. for $\text{C}_{69}\text{H}_{75}\text{N}_6\text{Au}_3(\text{H}_2\text{O})_2$: C, 51.3; H, 4.93; N, 5.2. Found: C, 51.4; H, 5.25; N, 5.05.

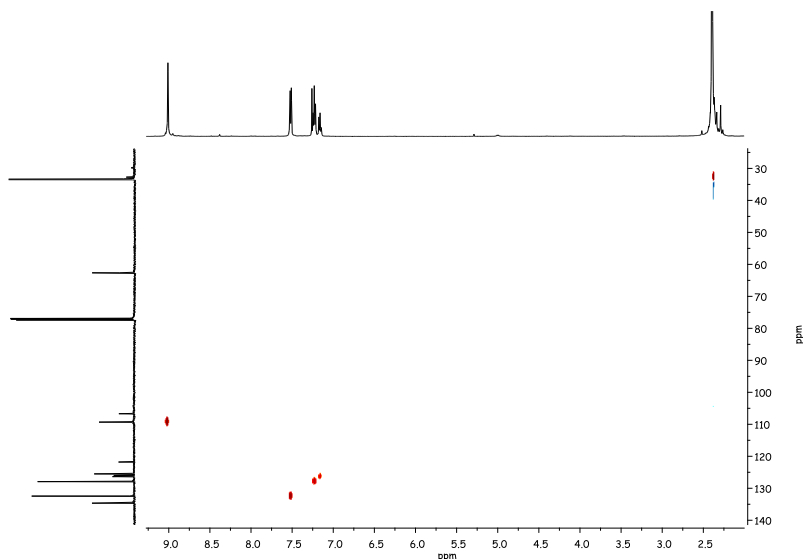
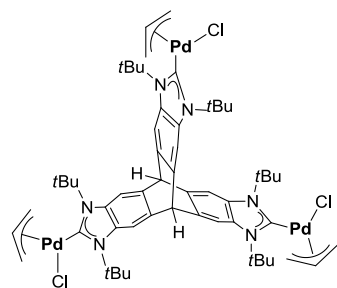


Figure 5.29 HSQC spectrum of **7K** in CDCl_3 ($^1J_{\text{H-C}} = 145 \text{ Hz}$)

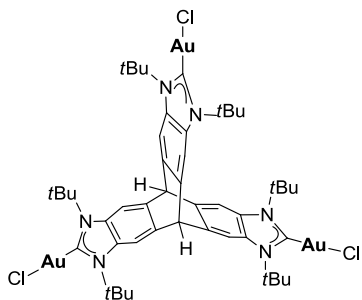
Synthesis of **2M**



Compound **2M** was synthesized in a similar manner as that for **2K**, using tris(azolium) salt $[\text{MH}_3](\text{BF}_4)_3$ (177.43 mg, 0.18 mmol), KHMDS (0.5 M in toluene, 1.2 mL, 0.6 mmol, 3.3 equiv.) and $[\text{PdCl}(\eta^3\text{-allyl})_2]$ (100 mg, 0.27 mmol). The reaction crude was purified by column chromatography. Elution with $\text{CH}_2\text{Cl}_2/\text{acetone}$ (8:2) afforded the separation of a pale yellow band that contained **2M**. Compound **2M** was obtained as a pale yellow solid after precipitation in a mixture of dichloromethane/hexanes. Yield: 70 mg (31 %).

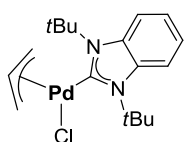
^1H NMR (300 MHz, CDCl_3): δ 7.87 (m, 6H, CH_{arom}), 5.66 (m, 1H, $\text{CH}_{\text{tritycene}}$), 5.61 (m, 1H, $\text{CH}_{\text{tritycene}}$), 5.21 (m, 3H, CH_{allyl}), 4.10 (m, 3H, $\text{CH}_2_{\text{allyl}}$), 3.28 (m, 6H, $\text{CH}_2_{\text{allyl}}$), 2.20 (m, 3H, $\text{CH}_2_{\text{allyl}}$), 2.15 (s, 27 H, $\text{C}(\text{CH}_3)_3$), 1.97 (s, 27 H, $\text{C}(\text{CH}_3)_3$). ^{13}C NMR (125 MHz, CDCl_3): δ 188.4 (Pd-C_{carbene}), 138.4 (C_{q} arom), 138.3 (C_{q} arom), 133.4 (C_{q} arom), 133.3 (C_{q} arom), 112.5 (CH_{arom}), 111.0 (CH_{allyl}), 68.3 ($\text{CH}_2_{\text{allyl}}$), 59.8 ($\text{C}(\text{CH}_3)_3$), 59.7 ($\text{C}(\text{CH}_3)_3$), 54.2 ($\text{CH}_{\text{tritycene}}$), 54.1 ($\text{CH}_{\text{tritycene}}$), 51.8 ($\text{CH}_2_{\text{allyl}}$), 31.8 ($\text{C}(\text{CH}_3)_3$), 31.7 ($\text{C}(\text{CH}_3)_3$). Electrospray MS (20 V, m/z): 1264.2 $[\text{M}-\text{Cl}+\text{MeCN}]^+$. Anal. Calcd. for $\text{C}_{56}\text{H}_{77}\text{Cl}_3\text{N}_6\text{Pd}_3$ (1256.24): C, 53.39; H, 6.16; N, 6.67. Found: C, 53.04; H, 6.35; N, 6.48.

Synthesis of 3M



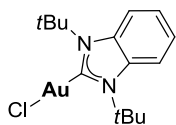
Compound **3M** was prepared following the same synthetic procedure of compound **3K**, using tris(azolium) salt $[\text{MH}_3](\text{BF}_4)_3$ (109 mg, 0.112 mmol), KHMDS (0.5 M in toluene, 0.74 mL, 0.37 mmol, 3.3 equiv.) and $[\text{AuCl}(\text{SMe}_2)]$ (100 mg, 0.337 mmol). Compound **3M** was obtained as a white solid. Yield 85 mg (54 %). ^1H NMR (500 MHz, CDCl_3): δ 8.05 (s, 6H, CH_{arom}), 5.73 (s, 2H, $\text{CH}_{\text{tritycene}}$), 2.13 (s, 54H, $\text{C}(\text{CH}_3)_3$). ^{13}C NMR (75 MHz, CD_2Cl_2): δ 178.1 ($\text{Au-C}_{\text{carbene}}$), 139.7 ($\text{C}_{\text{q arom}}$), 132.2 ($\text{C}_{\text{q arom}}$), 112.2 (CH_{arom}), 62.0 ($\text{C}(\text{CH}_3)_3$), 53.3 ($\text{CH}_{\text{tritycene}}$), 33.07 ($\text{C}(\text{CH}_3)_3$). HRMS ESI-TOF-MS (positive mode): $[\text{M}+\text{Na}]^+$ monoisotopic peak 1429.2994, calcd 1429.2996, $\epsilon_r=0.1$ ppm. Anal. Calc. for $\text{Au}_3\text{Cl}_3\text{N}_6\text{C}_{47}\text{H}_{62}$ (1408.31): C, 40.08; H, 4.44; N, 5.97. Found: C, 40.21; H, 4.63; N, 6.08.

Synthesis of 2N



Compound **2N** was synthesized in a similar manner as that for **2K**, using 1,3-bis(*tert*-butyl)benzimidazolium chloride (170.3 mg, 0.55 mmol), KHMDS (0.5 M in toluene, 1.2 mL, 0.6 mmol, 1.1 equiv.) and $[\text{PdCl}(\eta^3\text{-allyl})]_2$ (100 mg, 0.27 mmol). The reaction crude was purified by column chromatography. Elution with CH_2Cl_2 /acetone (95:5) afforded the separation of a pale yellow band that contained **2N**. Compound **2N** was obtained as a pale yellow solid after precipitation in a mixture of dichloromethane/hexanes. Yield: 78.5 mg (35 %). ^1H NMR (300 MHz, CDCl_3): δ 7.75 (m, 2H, CH_{arom}), 7.20 (m, 2H, CH_{arom}), 5.26 (m, 1H, CH_{allyl}), 4.14 (dd, $^3J_{\text{H-H}} = 7.5$ Hz, $^4J_{\text{H-H}} = 3$ Hz, 1H, CH_2 allyl), 3.31 (d, $^3J_{\text{H-H}} = 12$ Hz, 1H, CH_2 allyl), 3.31 (m, 1H, CH_2 allyl), 2.23 (d, $^3J_{\text{H-H}} = 12$ Hz, 1H, CH_2 allyl), 2.18 (s, 9H, $\text{C}(\text{CH}_3)_3$), 1.99 (s, 9H, $\text{C}(\text{CH}_3)_3$). ^{13}C NMR (300 MHz, CDCl_3): δ 187.7 ($\text{Pd-C}_{\text{carbene}}$), 135.4 ($\text{C}_{\text{q arom}}$), 135.3 ($\text{C}_{\text{q arom}}$), 121.4 (CH_{arom}), 121.3 (CH_{arom}), 115.3 (CH_{arom}), 112.5 (CH_{allyl}), 68.5 (CH_2 allyl), 59.9 ($\text{C}(\text{CH}_3)_3$), 59.8 ($\text{C}(\text{CH}_3)_3$), 50.8 (CH_2 allyl), 31.7 ($\text{C}(\text{CH}_3)_3$), 31.6 ($\text{C}(\text{CH}_3)_3$). Electrospray MS (20 V, m/z): 418.3 $[\text{M}-\text{Cl}+\text{MeCN}]^+$, 377.3 $[\text{M}-\text{Cl}]^+$. Anal. Calcd. for $\text{C}_{18}\text{H}_{27}\text{ClN}_2\text{Pd}$ (412.09): C, 52.31; H, 6.59; N, 6.78. Found: C, 51.98; H, 6.73; N, 6.51.

Synthesis of 3N



Compound **3N** was prepared following the same synthetic procedure of compound **3K**, using 1,3-bis(*tert*-butyl)benzimidazolium chloride (89.9 mg, 0.337 mmol), KHMDS (0.5 M in toluene, 0.74 mL, 0.37 mmol, 1.1 equiv) and [AuCl(SMe₂)] (100 mg, 0.337 mmol).

Compound **3N** was obtained as a white solid. Yield 83 mg (53 %). ¹H NMR (500 MHz, CDCl₃): δ 7.81 (m, 2H, CH_{arom}), 7.21 (m, 2H, CH_{arom}), 2.07 (s, 18H, C(CH₃)₃). ¹³C NMR (126 MHz, CDCl₃): δ 177.0 (Au-C_{carbene}), 134.0 (C_q arom), 123.0 (CH_{arom}), 116.2 (CH_{arom}), 61.7 (C(CH₃)₃), 32.9 (C(CH₃)₃). Electrospray MS (20 V, *m/z*): 485.1 [M+Na]⁺. Anal. Calc. for AuClN₂C₁₅H₂₂ (462.11): C, 38.93; H, 4.79; N, 6.05. Found: C, 38.75; H, 5.16; N, 5.71.

5.3 Catalytic experiments

5.3.1 Catalytic experiments described in Chapter 2

Hydroarylation of acetylenes

The arene (2.65 mmol) and the palladium catalyst (0.00265 mmol or 0.00132 mmol) were placed together in a thick-walled Schlenk tube fitted with a Teflon cap. The tube was then evacuated and filled with nitrogen three times. Diethyl phthalate (2.65 mmol), trifluoroacetic acid (4 mL) and 1,2-dichloroethane (1 mL) were added and the resulting mixture stirred at room temperature for 5 minutes. After this time, the acetylene (2.65 mmol) was added and the reaction mixture was stirred at the desired temperature (80°C or room temperature). Aliquots were taken at the desired times and analysed by ¹H NMR spectroscopy. The products were identified by comparison to previously reported spectroscopic data.¹⁷

Tandem dehalogenation/transfer hydrogenation

Under aerobic conditions, a capped vessel containing a stirring bar was charged with 4-bromoacetophenone (0.36 mmol), Cs₂CO₃ (0.43 mmol), anisole as internal reference (0.36 mmol), catalyst (2% or 1% mmol), and 2 mL of 2-propanol. The reaction mixture was heated at 100°C for the appropriate time. Reaction monitoring, yields, and conversions were determined by GC. The products were identified by comparison to previously reported spectroscopic data.^{18–20}

Tandem Suzuki-Miyaura coupling/transfer hydrogenation

Under aerobic conditions, a capped vessel containing a stirring bar was charged with 4-bromoacetophenone (0.36 mmol), phenylboronic acid (0.55 mmol), Cs₂CO₃ (1.08 mmol), anisole as internal reference (0.36 mmol), catalyst (2% mmol), 2 mL of 2-propanol and 2 mL of THF. The reaction mixture was heated at 100°C for the appropriate time. Reaction monitoring, yields, and conversions were determined by GC. The products were identified by comparison to previously reported spectroscopic data.^{18–20}

5.3.2 Catalytic experiments and products described in Chapter 3

Arylation of arylpyridines

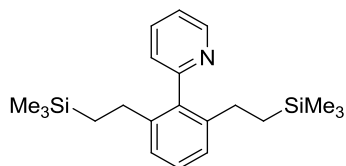
KOAc (0.05 mmol) and the ruthenium catalyst (5 % based on metal) were placed together in a thick-walled Schlenk tube fitted with a Teflon cap. The tube was then evacuated and filled with nitrogen three times. Afterward, 2 mL of NMP were added, and the mixture was stirred at room temperature for 1h. After this time, K_2CO_3 (1.25 mmol), the corresponding substrate (0.5 mmol), aryl halide (1.25 mmol) and anisole (0.5 mmol) as internal reference were subsequently added. The resulting mixture was stirred at 120°C for the appropriate time. H_2O and EtOAc were added to the cold reaction mixture. The organic phase was separated, dried with $MgSO_4$ and concentrated under vacuum. The remaining residue was purified by column chromatography on silica gel (Merck Silica 60 (0.063–0.200 mm)) with mixtures of hexanes/AcOEt to yield the corresponding *ortho*-arylated products. The evolution of the reactions and yields were determined by GC analysis. The products were identified by comparison to previously reported spectroscopic data, 2-(2-phenyl)phenylpyridine²¹ and 2-(2,6-diphenyl)phenylpyridine,²¹ 2-(2,6-di-*p*-methoxyphenyl)phenylpyridine,²² 2-(2,6-di-*p*-nbutylphenyl)phenylpyridine,²³ 2-(2,6-di-*p*-methylphenyl)phenylpyridine,²¹ 2-(2,6-diphenyl)phenylpyrazole,²⁴ and 10-phenylbenzo[*h*]quinoline.²¹

Hydroarylation of terminal alkenes

KOAc or KO_2CMes (0.15 mmol) and the ruthenium catalyst (5 % based on metal) were placed together in a thick-walled Schlenk tube fitted with a Teflon cap. The tube was then evacuated and filled with nitrogen three times. Afterward, 2 mL of toluene, 2-phenylpyridine (0.5 mmol), the corresponding alkene (1.5 mmol) and anisole (0.5 mmol) as internal reference were subsequently added. The resulting mixture was stirred at 120°C for 20 h. The mixture was filtered through a pad of Celite, eluted with CH_2Cl_2 and the solvent was removed under vacuum. The remaining residue was purified by column chromatography on silica gel (Merck Silica 60 (0.063–0.200

mm)) with a mixture of hexanes/AcOEt 20:1 to yield the corresponding *ortho*-alkylated arylpyridines. The evolution of the reactions and yields were determined by GC analysis. The products were identified by comparison to previously reported spectroscopic data, 2-(*n*-decyl)phenylpyridine,²⁵ 2-(*n*-octyl)phenylpyridine,²⁵ 2-(*n*-hexyl)phenylpyridine,²⁵ and 2-(2-(2-(trimethylsilyl)ethyl)phenyl)pyridine.²⁵

2-(2,6-Di-(2-trimethylsilyl)ethyl)-phenylpyridine



¹H NMR (300 MHz, CDCl₃): δ 8.73 (ddd, *J* = 4.9, 1.7, 0.8 Hz, 1H), 7.75 (td, *J* = 7.7, 1.7 Hz, 1H), 7.29-7.24 (m, 3H), 7.13 (d, *J* = 7.6 Hz, 2H), 2.31 (dd, *J* = 10.0, 7.8 Hz, 4H), 0.76-0.70 (m, 2H), 0.65-0.61 (m, 2H), -0.18 (s, 18H). ¹³C NMR (126 MHz, CDCl₃): δ 159.8 (C_q), 149.4 (CH), 143.6 (C_q), 138.9 (C_q), 135.8 (CH), 128.4 (CH), 125.9 (CH), 125.2 (CH), 121.7 (CH), 27.9 (CH₂), 19.3 (CH₂), -2.0 (CH₃). Electrospray MS (20 V, *m/z*): 356.2 [M+H]⁺. HRMS ESI-TOF-MS (positive mode): [M+H]⁺ monoisotopic peak 356.2233, calcd 356.2230, ε_r = 0.8 ppm.

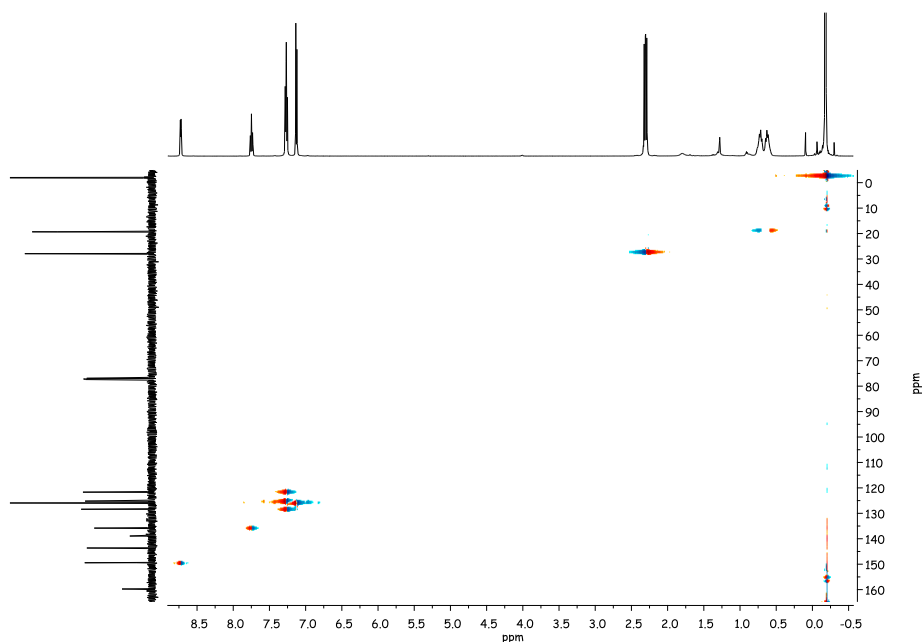
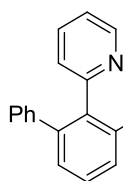


Figure 5.30 HSQC spectrum of 2-(2,6-di-(2-trimethylsilyl)ethyl)-phenylpyridine in CDCl₃ (¹*J*_{H-C} = 146 Hz)

Sequential hydroarylation of alkenes-arylation of arylpyridines

KO₂CMes (0.15 mmol) and the catalyst (5 % based on metal) were placed together in a thick-walled Schlenk tube fitted with a Teflon cap. The tube was then evacuated and filled with nitrogen three times. Afterward, 2 mL of toluene, 2-phenylpyridine (0.5 mmol), the corresponding alkene (1.5 mmol) and anisole (0.5 mmol) as internal reference were subsequently added. The resulting mixture was stirred at 120°C for 20 h. Then K₂CO₃ (1 mmol) and the corresponding aryl halide (1 mmol) were added. The resulting mixture was stirred at 120°C for the appropriate time. The mixture was filtered through a pad of Celite, eluted with CH₂Cl₂ and the solvent was removed under vacuum. The remaining residue was purified by column chromatography on silica gel (ZEOCHEM Silicagel ZEOprep 60 (40-63 μm)) with a mixture of toluene/AcOEt 20:1 to yield the corresponding *ortho*-alkylated/arylated arylpyridines. The evolution of the reactions and yields were determined by GC analysis.

2-(2-*n*-Decyl-6-phenyl)-phenylpyridine



¹H NMR (500 MHz, CDCl₃): δ 8.61 (ddd, *J* = 4.8, 1.6, 0.8 Hz, 1H), 7.42 (td, *J* = 7.7, 1.7 Hz, 1H), 7.38 (t, *J* = 7.6 Hz, 1H), 7.31 (dd, *J* = 7.6, 1.0 Hz, 1H), 7.27 (dd, *J* = 7.4, 1.3 Hz, 1H), 7.14-7.05 (m, 6H), 6.89 (dt, *J* = 7.8, 1.0 Hz, 1H), 2.53-2.47 (m, 2H), 1.46-1.37 (m, 2H), 1.31-1.08 (m, 14H), 0.87 (t, *J* = 7.1 Hz, 3H). ¹³C NMR (75 MHz, CDCl₃): δ 159.8 (C_q), 148.8 (CH), 142.1 (C_q), 141.7 (C_q), 141.6 (C_q), 139.4 (C_q), 135.4 (CH), 129.9 (CH), 128.6 (CH), 128.1 (CH), 127.7 (CH), 127.6 (CH), 126.3 (CH), 126.2 (CH), 121.3 (CH), 33.7 (CH₂), 32.1 (CH₂), 31.2 (CH₂), 29.7 (CH₂), 29.7 (CH₂), 29.6 (CH₂), 29.4 (CH₂), 29.4 (CH₂), 22.8 (CH₂), 14.2 (CH₃). Electrospray MS (20 V, *m/z*): 372.3 [M+H]⁺. HRMS ESI-TOF-MS (positive mode): [M+H]⁺ monoisotopic peak 372.2689, calcd 372.2691, ε_r = 0.5 ppm.

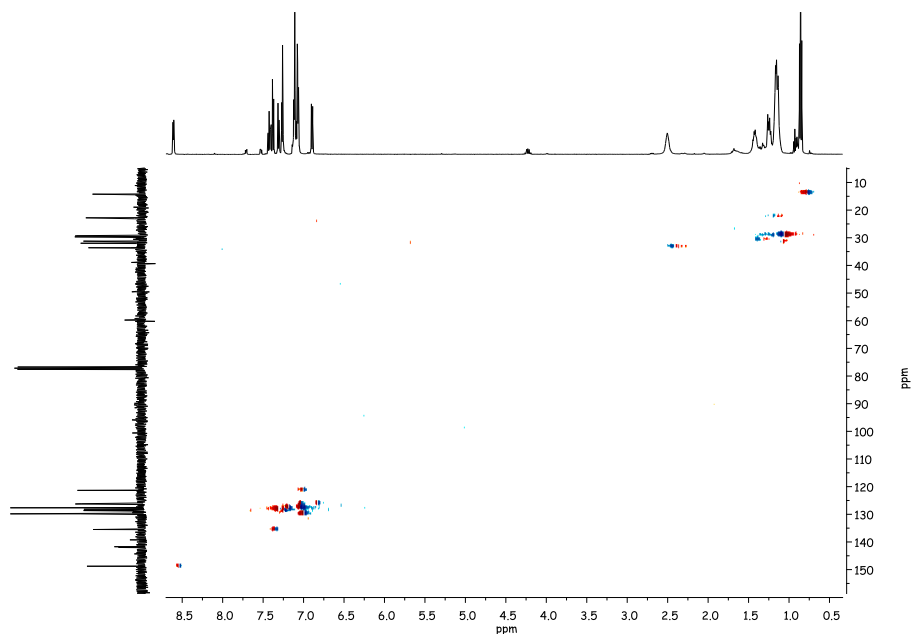
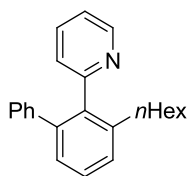


Figure 5.32 HSQC spectrum of **2-(2-*n*-octyl-6-phenyl)-phenylpyridine** in CDCl_3 ($^1J_{\text{H-C}} = 146$ Hz)

2-(2-*n*-Hexyl-6-phenyl)-phenylpyridine



^1H NMR (500 MHz, CDCl_3): δ 8.60 (ddd, $J = 4.9, 1.7, 0.9$ Hz, 1H), 7.41 (td, $J = 7.7, 1.0$ Hz, 1H), 7.37 (t, $J = 7.9$ Hz, 1H), 7.30 (d, $J = 7.6$ Hz, 1H), 7.25 (d, $J = 7.2$ Hz, 1H), 7.13-7.05 (m, 6H), 6.89 (dt, $J = 7.8, 0.9$ Hz, 1H), 2.57-2.43 (m, 2H), 1.49-1.36 (m, 2H), 1.24-1.10 (m, 6H), 0.80 (t, $J = 7.1$ Hz, 3H). ^{13}C NMR (126 MHz, CDCl_3): δ 159.6 (C_q), 148.8 (CH), 142.0 (C_q), 141.7 (C_q), 141.5 (C_q), 139.2 (C_q), 135.5 (CH), 129.8 (CH), 128.6 (CH), 128.2 (CH), 127.7 (CH), 127.6 (CH), 126.3 (CH), 126.2 (CH), 121.3 (CH), 33.6 (CH_2), 31.6 (CH_2), 31.2 (CH_2), 29.3 (CH_2), 22.6 (CH_2), 14.2 (CH_3). Electrospray MS (20 V, m/z): 316.2 $[\text{M}+\text{H}]^+$. HRMS ESI-TOF-MS (positive mode): $[\text{M}+\text{H}]^+$ monoisotopic peak 316.2061, calcd 316.2065, $\epsilon_r = 1.3$ ppm.

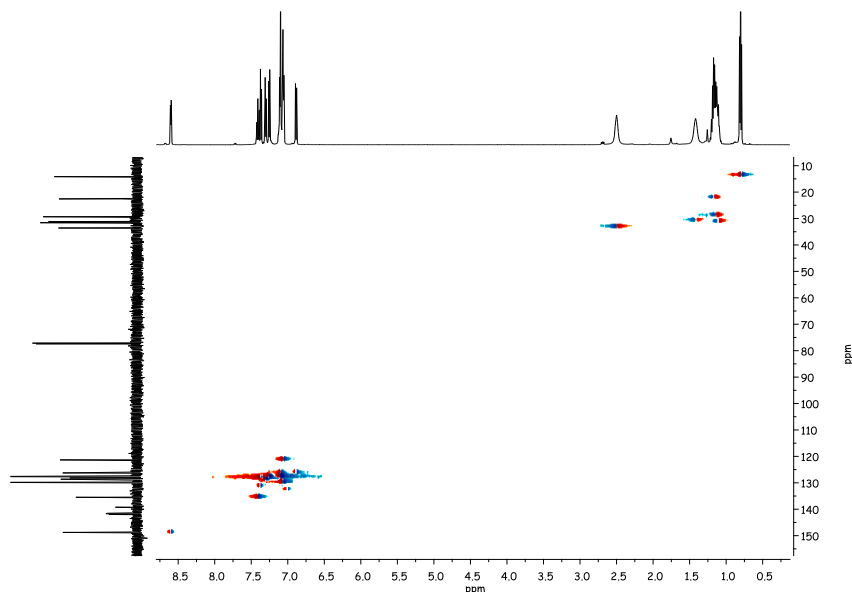


Figure 5.33 HSQC spectrum of **2-(2-*n*-hexyl-6-phenyl)-phenylpyridine** in CDCl_3 ($^1J_{\text{H-C}} = 146 \text{ Hz}$)

5.3.3 Catalytic experiments described in Chapter 4

α -Arylation of ketones

Palladium catalyst (1 mol % based on metal) and NaOtBu (0.65 mmol) were placed together in a thick-walled Schlenk tube fitted with a Teflon cap. The tube was then evacuated and filled with nitrogen three times. Afterward, 2 mL of toluene were added and the mixture was stirred at room temperature for 5 minutes. After this time, the corresponding arylbromide (0.55 mmol), propiophenone (0.5 mmol) and anisole as internal reference (0.5 mmol) were subsequently added. The resulting mixture was stirred at 120°C for 1 hour. The evolution of the reactions and yields were determined by GC analysis. The products were identified by comparison to previously reported spectroscopic data.^{26,27}

Suzuki-Miyaura cross-coupling reaction

The corresponding aryl boronic acid (0.6 mmol), Cs_2CO_3 (1 mmol) and the palladium catalyst (2 mol % based on the metal) were placed together in a thick-walled Schlenk tube fitted with a Teflon cap. The tube was then evacuated and filled with nitrogen three times. 1,4-Dioxane (2 mL), the corresponding arylbromide (0.5 mmol) and

anisole as internal standard (0.5 mmol) were subsequently added, and the resulting mixture heated at 80°C for the desired time. Yields were determined by GC analysis. The products were identified by comparison to commercially available samples and previously reported spectroscopic data.²⁸

Hydroamination of alkynes

Typical procedure for catalytic hydroamination of alkynes: gold catalysts (1 mol % based on metal) and AgBF₄ (2 mol %, 0.01 mmol) were placed together in a thick-walled Schlenk tube fitted with a Teflon cap. The tube was then evacuated and filled with nitrogen three times. Afterward, 1 mL of MeCN was added and the mixture was stirred at room temperature for 5 minutes. After this time, the corresponding arylamine (0.55 mmol), phenylacetylene (0.5 mmol) and anisole as internal reference (0.5 mmol) were subsequently added. The resulting mixture was stirred at 90°C for the appropriate time. The evolution of the reactions and yields were determined by GC analysis. The products were identified by comparison to commercially available samples and previously reported spectroscopic data.^{29–31}

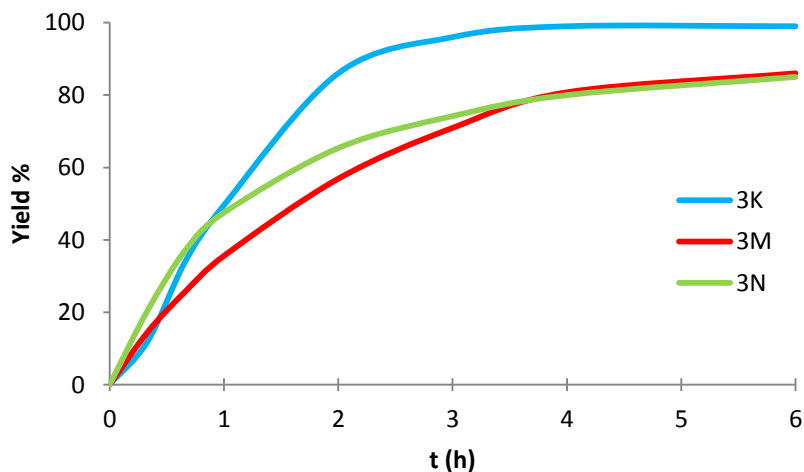


Figure 5.34 Time-course for the hydroamination of *o*-methylaniline and phenylacetylene using catalysts **3K**, **3M** and **3N**

Reduction of nitroarenes in aqueous medium

The corresponding nitroarene (1.078 mmol) and sodium borohydride (50 mmol) were placed together in a Schlenk tube. The tube was evacuated and filled with nitrogen three times. The solids were stirred in 10 mL of a 1:1 mixture of Mili-Q water and MeOH under a nitrogen steam for 15 minutes. Then, 2.5 mg of solids **5K** or **6K** (containing 5.1×10^{-3} mmol of gold, 0.5 mmol %) were added. The resulting mixture was stirred at room temperature for 5h. The solid residue was separated by filtration and subsequently washed with distilled water and acetone. The filtrate containing the reaction mixture was extracted with ethyl acetate (3 x 10 mL), and dried over MgSO_4 . The solvent was evaporated under vacuum. Yields were determined by ^1H NMR spectroscopy using 1,3,5-trimethoxybenzene (1.078 mmol) as internal standard. The products were identified by comparison to commercially available samples and previously reported spectroscopic data.³²

Three-component Strecker reaction

Under aerobic conditions, a capped vessel containing a stirrer was charged with the corresponding ketone (0.5 mmol), aniline (0.55 mmol), TMSCN (1 mmol), anisole as internal reference (0.5 mmol), the catalyst (0.02 mmol Au) and 2 mL of dichloromethane. The resulting mixture was stirred for 12 hours at room temperature. For recycling tests, the catalyst was recovered by centrifugation and washed with dichloromethane. The evolution of the reactions and yields were determined by GC analysis. The products were identified by comparison to commercially available samples and previously reported spectroscopic data.³³

5.3.3.1 Post-catalytic experiments

Physical properties of compounds **5K** and **5K** after the Strecker reaction

Compound **5K**

IR(ATR) = 2142 ($\nu_{\text{C}=\text{C}}$) cm^{-1} (before catalysis $\nu_{\text{C}=\text{C}}$ = 2102 cm^{-1})

Anal. Calcd. for $(\text{C}_{60}\text{H}_{66}\text{N}_6\text{Au}_3)_n$: C, 48.11; H, 4.46; N, 5.91. Found: C, 40.95; H, 4.7; N, 10.35.

BET surface area: 18 m^2/g (BET surface area before catalysis: 43 m^2/g)

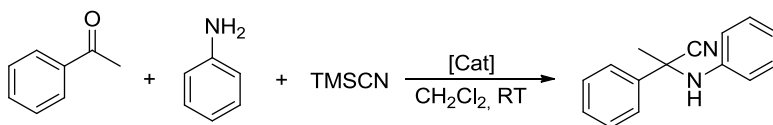
Compound 6K

IR(ATR) = 2138 ($\nu_{C=C}$) cm^{-1} (before catalysis $\nu_{C=C}$ = 2103 cm^{-1})

Anal. Calcd. for $(\text{C}_{57}\text{H}_{63}\text{N}_6\text{Au}_3)_n$: C, 48.11; H, 4.46; N, 5.91. Found: C, 45.00; H, 4.75; N, 9.00.

BET surface area: 26 m^2/g (BET surface area before catalysis: 222 m^2/g)

Table 5.1 Strecker reaction using recovered catalysts from reduction of nitroarenes^a



Entry	Recovered Catalyst	Yield(%) ^b
1	5K	12
2	6K	6

^aReaction conditions: 0.5 mmol acetophenone, 0.55 mmol aniline, 1 mmol TMSCN, 6 mg of recovered catalyst from the reduction of nitroarenes, 2 mL of CH_2Cl_2 , 12 h at room temperature. ^bYields determined by GC using anisole (0.5 mmol) as internal standard.

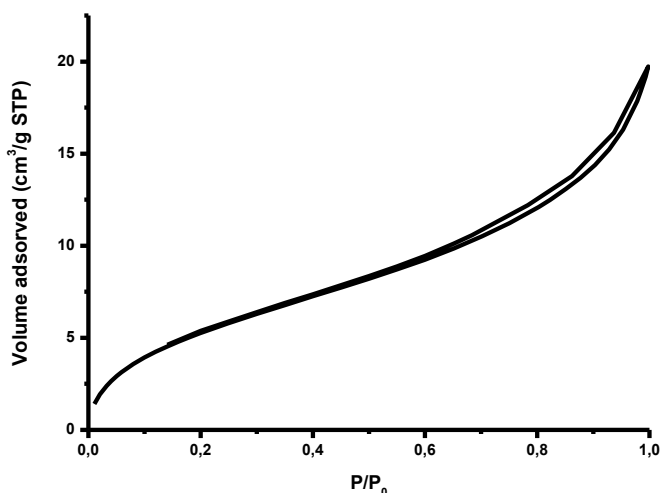


Figure 5.35 N_2 sorption isotherm of compound 5K after the Strecker reaction at 77K

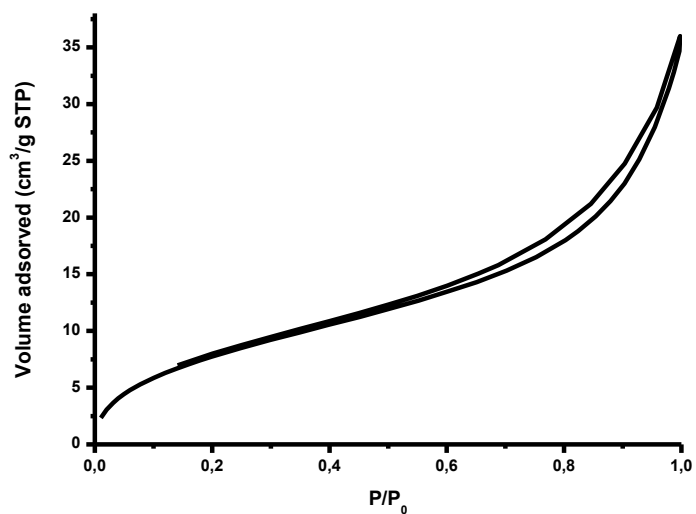


Figure 5.36 N₂ sorption isotherm of compound **6K** after the Strecker reaction at 77K

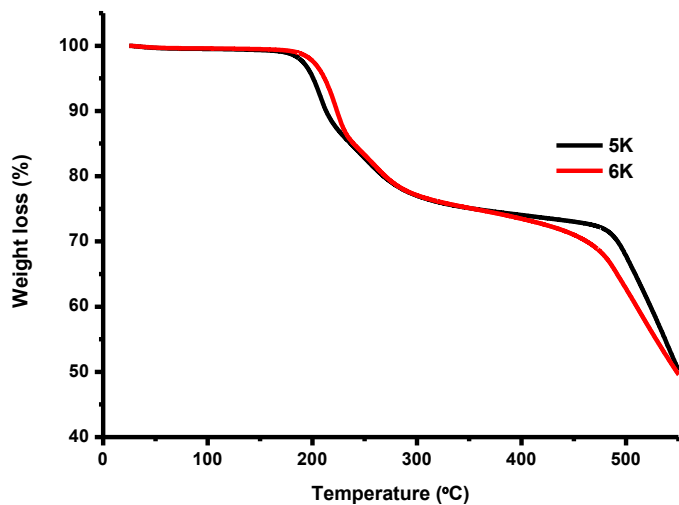


Figure 5.37 TGA plots of compounds **5K** and **6K** after the Strecker reaction under air conditions

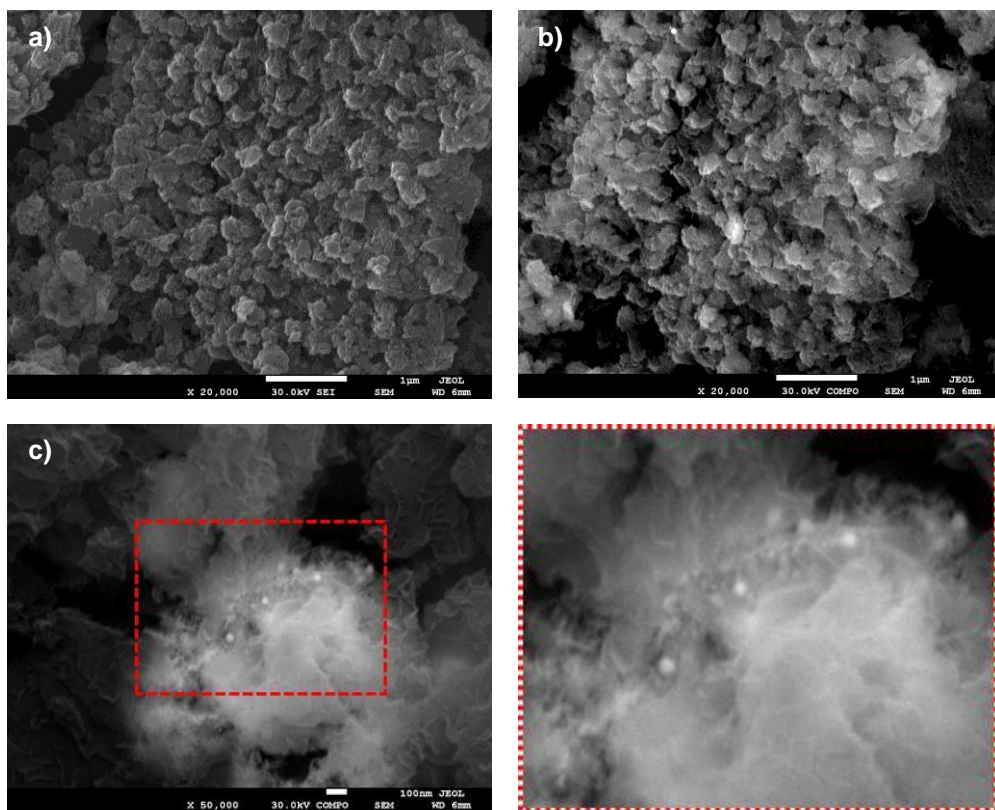


Figure 5.38 SEM micrographs of **5K** after three runs of the Strecker reaction (a) and b)) and the reduction of nitroarenes (c). Image a) was taken using the secondary electrons (SE) signal of the SEM. Images b) and c) were taken using the back-scattered electrons (BSE) signal of the SEM. Scale bar: 1 μm (a) and b) and 100 nm (c)).

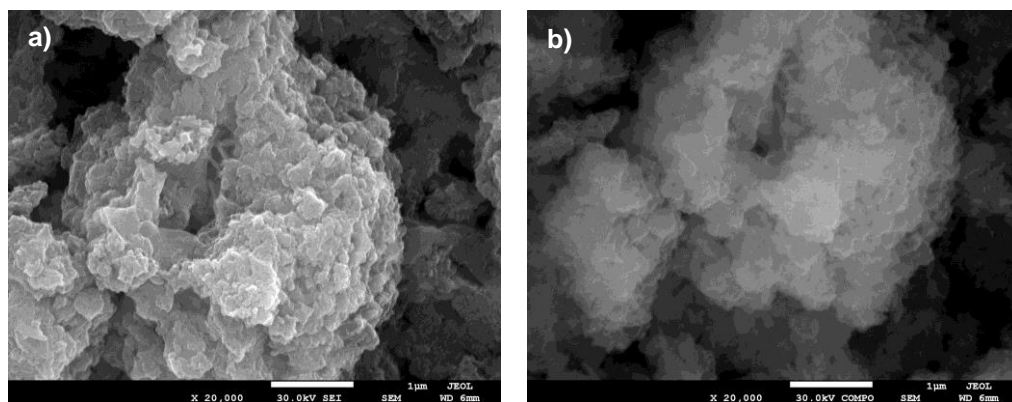


Figure 5.39 SEM micrographs of **6K** after three runs of the Strecker reaction. Image a) was taken using the secondary electrons (SE) signal of the SEM. Image b) was taken using the back-scattered electrons (BSE) signal of the SEM. Scale bar: 1 μm .

5.4 X-Ray Diffraction

Single crystals suitable for X-Ray Diffraction were mainly obtained by slow diffusion of hexane or Et₂O into a concentrated solution of the compound in different solvents or slow evaporation of a concentrated solution of the compound in the appropriated solvent. Diffraction data were collected on an Agilent SuperNova diffractometer equipped with an Atlas CCD detector. Single crystals were mounted on a MicroMount® polymer tip (MiteGen) in a random orientation. Absorption corrections based on the multiscan method were applied.³⁴ The structure was solved by direct methods in SHELXS-97 and refined by the full-matrix method based on F² with the program SHELXL-97 using the OLEX software package.^{35,36}

Key details of the crystal and structure refinement data are summarized in the following tables.

Table 5.2 Structural parameters, register conditions and refinement of **1DH** and **2D**

	1DH	2D
Empirical formula	C ₁₃ H ₁₇ BF ₄ I ₂ N ₆ Pd	C ₄₀ H ₅₂ I ₈ N ₁₄ Pd ₄
Formula weight	704.34	2185.76
Temperature/K	293(2)	293(2)
Crystal system	Monoclinic	Orthorhombic
Space group	<i>P</i> 2 ₁ / <i>c</i>	<i>Pccn</i>
a/Å	9.4486(2)	15.4313(4)
b/Å	23.6206(6)	20.7211(7)
c/Å	9.3608(2)	19.7639(5)
α/°	90.00	90.00
β/°	90.187(2)	90.00
γ/°	90.00	90.00
Volume/Å ³	2089.15(8)	6319.6(3)
Z	4	4
ρ _{calc} /cm ³	2.239	2.297
μ/mm ⁻¹	3.889	5.069
F(000)	1320.0	4024.0
Crystal size/mm ³	0.17 × 0.15 × 0.10	0.18 × 0.16 × 0.11
Radiation	MoKα (λ = 0.71073)	MoKα (λ = 0.71073)
2θ range for data collection/°	5.52 to 55	6.28 to 55
Index ranges	-12 ≤ h ≤ 11, -23 ≤ k ≤ 30, -12 ≤ l ≤ 12	-18 ≤ h ≤ 19, -25 ≤ k ≤ 26, -25 ≤ l ≤ 23
Reflections collected	12023	30510
Independent reflections	4461 [R _{int} = 0.0376, R _{sigma} = N/A]	6908 [R _{int} = 0.0408, R _{sigma} = N/A]
Data/restraints/parameters	4461/0/268	6908/5/307
Goodness-of-fit on F ²	1.051	1.052
Final R indexes [I >= 2σ (I)]	R ₁ = 0.0324, wR ₂ = 0.0624	R ₁ = 0.0428, wR ₂ = 0.1104
Final R indexes [all data]	R ₁ = 0.0490, wR ₂ = 0.0712	R ₁ = 0.0638, wR ₂ = 0.1279
Largest diff. peak/hole / e Å ⁻³	0.79/-0.89	2.87/-1.55

Table 5.3 Structural parameters, register conditions and refinement of **3D** and **6D**

	3D	6D
Empirical formula	C ₂₃ H ₃₀ I ₃ IrN ₇ Pd	C ₂₃ H ₃₁ I ₃ N ₆ O ₂ Rh ₂
Formula weight	1083.84	1010.06
Temperature/K	199.95(10)	200.00(10)
Crystal system	Monoclinic	Monoclinic
Space group	P2 ₁	P2 ₁ /m
a/Å	13.2740(5)	10.4283(3)
b/Å	16.7105(4)	12.2666(3)
c/Å	14.4848(5)	11.9217(3)
α/°	90.00	90.00
β/°	108.107(4)	96.174(2)
γ/°	90.00	90.00
Volume/Å ³	3053.83(17)	1516.17(6)
Z	4	2
ρ _{calc} /g/cm ³	2.357	2.212
μ/mm ⁻¹	7.999	4.173
F(000)	1996.0	952.0
Crystal size/mm ³	0.1 × 0.09 × 0.08	0.13 × 0.11 × 0.1
Radiation	Mo Kα (λ = 0.7107)	Mo Kα (λ = 0.7107)
2θ range for data collection/°	5.58 to 59	5.94 to 61.78
Index ranges	-17 ≤ h ≤ 17, -22 ≤ k ≤ 22, -19 ≤ l ≤ 19	-15 ≤ h ≤ 14, -17 ≤ k ≤ 17, -16 ≤ l ≤ 16
Reflections collected	35772	21203
Independent reflections	14702 [R _{int} = 0.0476, R _{sigma} = 0.0743]	4649 [R _{int} = 0.0492, R _{sigma} = 0.0394]
Data/restraints/parameters	14702/19/641	4649/12/178
Goodness-of-fit on F ²	1.026	1.065
Final R indexes [I ≥ 2σ(I)]	R ₁ = 0.0430, wR ₂ = 0.0525	R ₁ = 0.0356, wR ₂ = 0.0823
Final R indexes [all data]	R ₁ = 0.0630, wR ₂ = 0.0582	R ₁ = 0.0541, wR ₂ = 0.0936
Largest diff. peak/hole / e Å ⁻³	1.21/-0.90	1.29/-1.10

Table 5.4 Structural parameters, register conditions and refinement of **4,5-di-*tert*-butylamine-9,10-diamine-2,7-di-*tert*-butylpyrene (TBP)** and **[FH₂-Me](BF₄)₂**

	TBP	[FH₂-Me](BF₄)₂
Empirical formula	C ₃₂ H ₄₆ N ₄	C ₃₂ H ₃₉ B ₂ F ₈ N ₅
Formula weight	486.73	667.30
Temperature/K	1995.95(10)	200.00(14)
Crystal system	Triclinic	Monoclinic
Space group	P-1	P2 ₁ /n
a/Å	9.24620(17)	11.65560(17)
b/Å	11.16699(18)	12.00334(17)
c/Å	14.5542(2)	23.8016(4)
α/°	105.3304(13)	90.00
β/°	97.0444(14)	91.2040(14)
γ/°	96.8875(14)	90.00
Volume/Å ³	1420.00(4)	3329.26(9)
Z	2	4
ρ _{calc} /g/cm ³	1.138	1.331
μ/mm ⁻¹	0.507	0.941
F(000)	532.0	1392.0
Crystal size/mm ³	0.4666 × 0.2495 × 0.0597	0.3664 × 0.1882 × 0.1619
Radiation	CuKα (λ = 1.54184)	Cu Kα (λ = 1.5418)
2θ range for data collection/°	6.38 to 144.4	8.26 to 145.22
Index ranges	-11 ≤ h ≤ 10, -13 ≤ k ≤ 13, -17 ≤ l ≤ 17	-14 ≤ h ≤ 14, -14 ≤ k ≤ 14, -25 ≤ l ≤ 29
Reflections collected	26056	25660
Independent reflections	5506 [R _{int} = 0.0226, R _{sigma} = 0.0158]	6529 [R _{int} = 0.0248, R _{sigma} = 0.0193]
Data/restraints/parameters	5506/0/337	6529/0/475
Goodness-of-fit on F ²	1.051	1.037
Final R indexes [I >= 2σ (I)]	R ₁ = 0.0646, wR ₂ = 0.1835	R ₁ = 0.0668, wR ₂ = 0.1986
Final R indexes [all data]	R ₁ = 0.0735, wR ₂ = 0.1933	R ₁ = 0.0812, wR ₂ = 0.2168
Largest diff. peak/hole / e Å ⁻³	0.40/-0.68	1.16/-0.33

Table 5.5 Structural parameters, register conditions and refinement of **1F-Et** and **3F-Me**

	1F-Et	3F-Me
Empirical formula	C ₅₀ H ₆₆ Cl ₂ Ir ₂ N ₄	C ₅₆ H ₇₀ Cl ₁₀ N ₄ Ru ₂
Formula weight	1178.37	1355.80
Temperature/K	164(20)	293(2)
Crystal system	Triclinic	Monoclinic
Space group	P-1	C2/c
a/Å	12.8705(4)	23.4392(7)
b/Å	12.9226(3)	12.8809(3)
c/Å	14.1663(5)	20.9819(6)
α/°	93.668(2)	90.00
β/°	90.542(3)	108.654(3)
γ/°	103.248(3)	90.00
Volume/Å ³	2288.03(12)	6002.0(3)
Z	2	4
ρ _{calc} /cm ³	1.710	1.500
μ/mm ⁻¹	5.966	8.475
F(000)	1164.0	2768.0
Crystal size/mm ³	0.2682 × 0.0647 × 0.0336	0.278 × 0.1182 × 0.0397
Radiation	MoKα (λ = 0.71073)	CuKα (λ = 1.54184)
2θ range for data collection/°	6 to 53.9	7.94 to 146.3
Index ranges	-15 ≤ h ≤ 16, -16 ≤ k ≤ 15, -15 ≤ l ≤ 17	-28 ≤ h ≤ 25, -15 ≤ k ≤ 15, -25 ≤ l ≤ 25
Reflections collected	28715	16589
Independent reflections	8522 [R _{int} = 0.0427, R _{sigma} = 0.0436]	5862 [R _{int} = 0.0441, R _{sigma} = 0.0414]
Data/restraints/parameters	8522/0/533	5862/15/351
Goodness-of-fit on F ²	1.130	1.069
Final R indexes [I ≥ 2σ (I)]	R ₁ = 0.0379, wR ₂ = 0.0732	R ₁ = 0.0635, wR ₂ = 0.1794
Final R indexes [all data]	R ₁ = 0.0652, wR ₂ = 0.0875	R ₁ = 0.0808, wR ₂ = 0.1913
Largest diff. peak/hole / e Å ⁻³	3.25/-1.53	1.47/-1.11

Table 5.6 Structural parameters, register conditions and refinement of **1K** and **3K**

	1K	3K
Empirical formula	$C_{73}H_{102}Cl_3N_8Rh_3$	$C_{45}H_{60}Au_3Cl_3N_6$
Formula weight	1506.71	1382.24
Temperature/K	199.95(10)	100(2)
Crystal system	Monoclinic	Triclinic
Space group	C2/m	P-1
a/Å	16.9664(10)	12.7389(11)
b/Å	20.9747(7)	13.0922(10)
c/Å	21.9872(9)	16.2843(13)
$\alpha/^\circ$	90.00	97.940(4)
$\beta/^\circ$	107.965(6)	96.143(4)
$\gamma/^\circ$	90.00	100.019(5)
Volume/Å ³	7443.0(6)	2624.8(4)
Z	4	2
$\rho_{\text{calc}}/\text{cm}^3$	1.345	1.749
μ/mm^{-1}	6.644	8.55
F(000)	3128.0	1320.0
Crystal size/mm ³	0.13 × 0.11 × 0.09	0.26 × 0.1 × 0.06
Radiation	CuK α ($\lambda = 1.54180$)	MoK α ($\lambda = 0.71073$)
2 θ range for data collection/ $^\circ$	6.92 to 146.44	2.548 to 50.052
Index ranges	-20 ≤ h ≤ 20, -25 ≤ k ≤ 21, -27 ≤ l ≤ 26	-15 ≤ h ≤ 15, -15 ≤ k ≤ 15, -19 ≤ l ≤ 19
Reflections collected	34869	60032
Independent reflections	7563 [$R_{\text{int}} = 0.0517$, $R_{\text{sigma}} = 0.0411$]	9233 [$R_{\text{int}} = 0.0579$, $R_{\text{sigma}} = \text{N/A}$]
Data/restraints/parameters	7563/20/416	9233/3061/939
Goodness-of-fit on F ²	1.079	1.066
Final R indexes [$I \geq 2\sigma(I)$]	$R_1 = 0.0711$, $wR_2 = 0.2116$	$R_1 = 0.0658$, $wR_2 = 0.1437$
Final R indexes [all data]	$R_1 = 0.0948$, $wR_2 = 0.2281$	$R_1 = 0.1028$, $wR_2 = 0.1652$
Largest diff. peak/hole / e Å ⁻³	1.89/-0.60	2.13/-1.30

Table 5.7 Structural parameters, register conditions and refinement of **3M** and **3N**

	3M	3N
Empirical formula	C ₉₈ H ₁₃₄ Au ₆ Cl ₆ N ₁₂ O	C ₁₅ H ₂₂ AuClN ₂
Formula weight	2890.67	462.76
Temperature/K	200.00(10)	200(2)
Crystal system	Orthorhombic	Monoclinic
Space group	C222 ₁	P2 ₁ /n
a/Å	18.1243(5)	10.2926(3)
b/Å	28.6993(15)	9.65460(18)
c/Å	17.9079(5)	16.1601(3)
α/°	90.00	90.00
β/°	90.00	95.8698(19)
γ/°	90.00	90.00
Volume/Å ³	9314.9(6)	1597.42(6)
Z	2	4
ρ _{calc} /g/cm ³	1.031	1.924
μ/mm ⁻¹	9.664	9.366
F(000)	2780.0	888.0
Crystal size/mm ³	0.234 × 0.106 × 0.04	0.1912 × 0.1327 × 0.0469
Radiation	Cu Kα (λ = 1.5418)	Mo Kα (λ = 0.7107)
2θ range for data collection/°	7.6 to 133.96	5.8 to 58.64
Index ranges	-21 ≤ h ≤ 18, -34 ≤ k ≤ 34, -21 ≤ l ≤ 21	-13 ≤ h ≤ 14, -13 ≤ k ≤ 12, -22 ≤ l ≤ 22
Reflections collected	21749	18356
Independent reflections	8120 [R _{int} = 0.0430, R _{sigma} = 0.0561]	3993 [R _{int} = 0.0360, R _{sigma} = 0.0301]
Data/restraints/parameters	8120/38/281	3993/0/178
Goodness-of-fit on F ²	1.184	1.062
Final R indexes [I >= 2σ (I)]	R ₁ = 0.0811, wR ₂ = 0.2886	R ₁ = 0.0228, wR ₂ = 0.0428
Final R indexes [all data]	R ₁ = 0.1292, wR ₂ = 0.3186	R ₁ = 0.0305, wR ₂ = 0.0459
Largest diff. peak/hole / e Å ⁻³	1.48/-0.54	0.93/-0.81

5.5 References

- (1) Dawson, W. R.; Windsor, M. W. *J. Phys. Chem.* **1968**, *72*, 3251.
- (2) Komiyama, S. *Synthesis of Organometallic Compounds. A Practical Guide*; Wiley, 1997.
- (3) Giordano, G.; Crabtree, R. *Inorg. Synth.* **1990**, *28*, 88.
- (4) Malbosc, F.; Chauby, V.; Serra-Le Berre, C.; Etienne, M.; Daran, J.; Kalck, P. *Eur. J. Inorg. Chem.* **2001**, 2689.
- (5) Uson, R.; Laguna, A.; Laguna, M.; Briggs, D.; Murray, H.; Fackler, J. *Inorg. Synth.* **1989**, *26*, 85.
- (6) Bennett, M. A.; Smith, A. K. *J. Chem. Soc. Dalton Trans.* **1974**, 233.
- (7) Arduengo, A. J.; Krafczyk, R.; Schmutzler, R.; Craig, H. A.; Goerlich, J. R.; Marshall, W. J.; Unverzagt, M. *Tetrahedron* **1999**, *55*, 14523.
- (8) Hu, J.; Era, M.; Elsegood, M. R. J.; Yamato, T. *Eur. J. Org. Chem.* **2010**, 72.
- (9) Er, J. A. V.; Tennyson, A. G.; Kamplain, J. W.; Lynch, V. M.; Bielawski, C. W. *Eur. J. Inorg. Chem.* **2009**, 1729.
- (10) Hu, J.; Zhang, D.; Harris, F. W. *J. Org. Chem.* **2005**, *70*, 707.
- (11) Yatabe, T.; Harbison, M. A.; Brand, J. D.; Wagner, M.; Müllen, K.; Samorí, P.; Rabe, J. P. *J. Mater. Chem.* **2000**, *10*, 1519.
- (12) Hilton, C. L.; Jamison, C. R.; Zane, H. K.; King, B. T. *J. Org. Chem.* **2009**, *74*, 405.
- (13) Dickstein, J. S.; Curto, J. M.; Gutierrez, O.; Mulrooney, C. A.; Kozlowski, M. C. *J. Org. Chem.* **2013**, *78*, 4744.
- (14) Khramov, D. M.; Bielawski, C. W. *J. Org. Chem.* **2007**, *72*, 9407.
- (15) Boydston, A. J.; Vu, P. D.; Dykhno, O. L.; Chang, V.; Wyatt, A. R.; Stockett, A. S.; Ritschdorff, E. T.; Shear, J. B.; Bielawski, C. W. *J. Am. Chem. Soc.* **2008**, *130*, 3143.
- (16) Williams, K. A.; Bielawski, C. W. *Chem. Commun.* **2010**, *46*, 5166.
- (17) Jia, C.; Lu, W.; Oyamada, J.; Kitamura, T.; Matsuda, K.; Irie, M.; Fujiwara, Y. *J. Am. Chem. Soc.* **2000**, *122*, 7252.
- (18) Long, L. M.; Henze, H. R. *J. Am. Chem. Soc.* **1941**, *63*, 1939.
- (19) Henze, H. R.; Long, L. M. *J. Am. Chem. Soc.* **1941**, *63*, 1941.

- (20) Mohrbacher, R. J.; Cromwell, N. H. *J. Am. Chem. Soc.* **1957**, *79*, 401.
- (21) Oi, S.; Fukita, S.; Hirata, N.; Watanuki, N.; Miyano, S.; Inoue, Y. *Org. Lett.* **2001**, *3*, 2579.
- (22) Ackermann, L. *Org. Lett.* **2005**, *7*, 3123.
- (23) Prades, A.; Poyatos, M.; Peris, E. *Adv. Synth. Catal.* **2010**, 352, 1155.
- (24) Kim, M.; Kwak, J.; Chang, S. *Angew. Chem. Int. Ed.* **2009**, *48*, 8935.
- (25) Schinkel, M.; Marek, I.; Ackermann, L. *Angew. Chem. Int. Ed.* **2013**, *52*, 3977.
- (26) Landers, B.; Berini, C.; Wang, C.; Navarro, O. *J. Org. Chem.* **2011**, *76*, 1390.
- (27) Nicolaou, K. C.; Montagnon, T.; Baran, P. S.; Zhong, Y.-L. *J. Am. Chem. Soc.* **2002**, *124*, 2245.
- (28) Cano, R.; Ramón, D. J.; Yus, M. *Tetrahedron* **2011**, *67*, 5432.
- (29) Samec, J.; Backvall, J. *Chem. Eur. J.* **2002**, *8*, 2955.
- (30) Samec, J. S. M.; Ell, A. H.; Bäckvall, J.-E. *Chem. Eur. J.* **2005**, *11*, 2327.
- (31) Li, W.; Hou, G.; Chang, M.; Zhang, X. *Adv. Synth. Catal.* **2009**, *351*, 3123.
- (32) Layek, K.; Kantam, M. L.; Shirai, M.; Nishio-Hamane, D.; Sasaki, T.; Maheswaran, H. *Green Chem.* **2012**, *14*, 3164.
- (33) Jarusiewicz, J.; Choe, Y.; Yoo, K. S.; Park, C. P.; Jung, K. W. *J. Org. Chem.* **2009**, *74*, 2873.
- (34) Clark, R. C.; Reid, J. S. *Acta Crystallogr. Sect. A Found. Crystallogr.* **1995**, *51*, 887.
- (35) Sheldrick, G. M. *Acta Crystallogr. A.* **2008**, *64*, 112.
- (36) Dolomanov, O. V.; Bourhis, L. J.; Gildea, R. J.; Howard, J. A. K.; Puschmann, H. *J. Appl. Crystallogr.* **2009**, *42*, 339.

Chapter 6

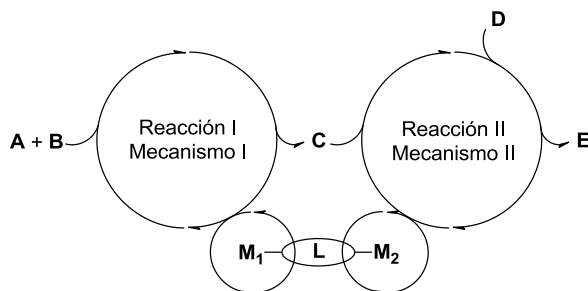
Diseño de ligandos politópicos para la preparación de catalizadores multifuncionales

En aplicación de la normativa de estudios de doctorado sobre la elaboración de Tesis Doctorales según el programa RD 99/2011, por la que se establece que: *la Tesis Doctoral escrita en una lengua diferente del valenciano o del castellano, en el momento de ser depositada, debe contener un apartado suficientemente amplio en una de estas dos lenguas, y debe formar parte de la encuadernación de la tesis*; el siguiente capítulo contiene un resumen en castellano del trabajo recogido en la presente Tesis Doctoral.

6.1 Introducción

En el contexto actual en el que son necesarios procesos más respetuosos con el medio ambiente y menos contaminantes, los procesos catalíticos son de vital importancia, dado que se puede reducir tiempo, energía y subproductos mediante la utilización de catalizadores selectivos y eficientes.¹ En este sentido, si además se pueden realizar varias reacciones catalíticas en un mismo reactor las ventajas son claras, ya que no es necesario emplear energía ni esfuerzo en procesos de purificación de productos intermedios.

En los últimos años se han utilizado uno o varios catalizadores para desarrollar procesos en los que más de una reacción catalítica ocurre en un solo reactor.²⁻⁸ De estos procesos, los más atractivos son aquellos en los que dos catalizadores metálicos diferentes promueven simultáneamente dos reacciones, dada la elevada versatilidad y complejidad de procesos que se puede conseguir (Esquema 6.1).



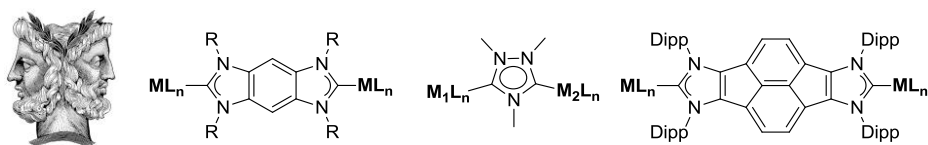
Esquema 6.1

La eficiencia de estos procesos puede aumentarse de forma considerable si los dos centros metálicos están unidos mediante un ligando apropiado (**L** en el Esquema 6.1), de forma que puedan producirse efectos cooperativos entre los dos centros metálicos.

Para que esto suceda la distancia que el ligando establece entre los metales debe ser corta (3.5-6 Å), de manera que estos catalizadores bimetalicos pueden promover la reacción de forma más eficiente que sus análogos monometálicos.

Uno de los factores claves para obtener catalizadores bimetalicos eficientes, y que de hecho constituye un reto en la actualidad, es el diseño de los ligandos que unen ambos metales. Los ligandos deben proporcionar las propiedades estereoelectrónicas apropiadas, de la misma manera que deben facilitar una distancia y disposición geométrica óptima entre ellos. Multitud de ligandos politópicos basados en diferentes átomos dadores han sido sintetizados para obtener catalizadores multimetalicos con propiedades catalíticas mejoradas.^{9,10}

Los carbenos N-heterocíclicos (NHCs en sus siglas en inglés)^{11,12} son un tipo de ligandos que en los últimos años se ha utilizado ampliamente para la preparación de compuestos multimetalicos debido a su alta versatilidad coordinativa,¹³ a la estabilidad que muestran los complejos derivados de ellos y a que sus precursores (normalmente sales de azolio) son relativamente fáciles de obtener¹⁴ y permiten el acceso a un gran número de geometrías. Esta última característica ha permitido sintetizar NHCs rígidos y politópicos cuyas arquitecturas no se pueden obtener utilizando otro tipo de ligandos.¹⁰ En este sentido, son muy interesantes los ligandos que permiten la coordinación facialmente opuesta de los dos fragmentos metalicos (Esquema 6.2), también conocidos como ligando de tipo *Janus*, en referencia a su similitud con el dios romano de dos caras, Jano.¹⁵⁻¹⁷

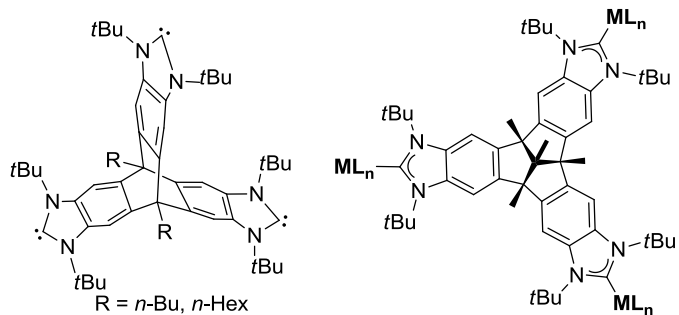


Esquema 6.2 Dios romano Jano (izquierda) y complejos bimetalicos basados en ligandos bis-NHCs de tipo *Janus* (derecha)

Estos ligandos se han utilizado para obtener compuestos homo-¹⁸⁻²¹ o heterobimetalicos¹⁰ con aplicaciones en numerosos campos además de la catálisis tándem, como en la obtención de polímeros organometálicos^{15,22} o la obtención de nuevos compuestos luminiscentes.²³

Durante el transcurso de esta tesis, se han descrito nuevos ligandos tris-NHC con simetría C_3 (Esquema 6.3). El primero, basado en un esqueleto tripticénico (Esquema 6.3, izquierda), fue descrito por Bielawski y colaboradores y no fue coordinado a ningún fragmento metalico. Otro ejemplo interesante es el tribenzotriquinaceno-tris-

imidazolilideno, que fue descrito en nuestro grupo de investigación y con el que se obtuvieron compuestos homo-trimetálicos de rodio (Esquema 6.3, derecha).



Esquema 6.3 Tris-NHCs rígidos con simetría C_3 , (M = RhCl(COD))

6.2 Objetivos

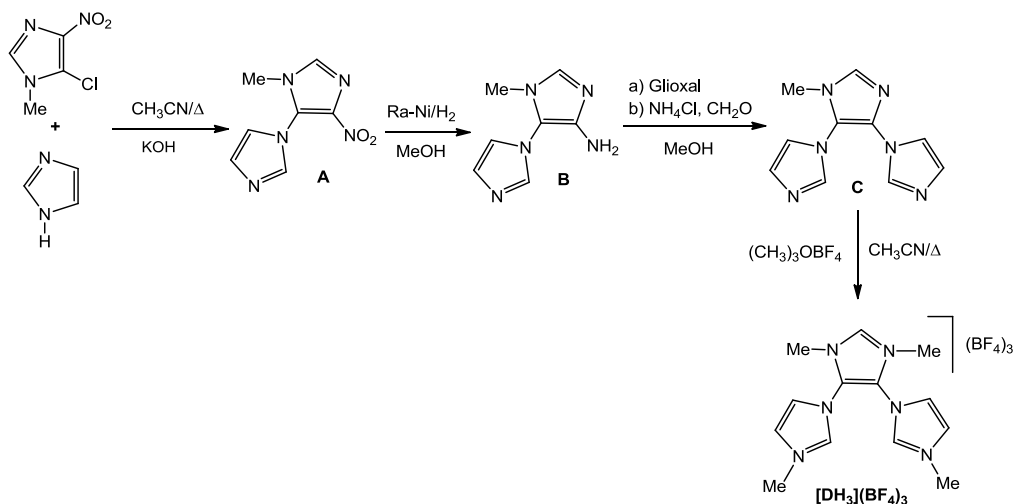
Durante los últimos años nuestro grupo de investigación ha desarrollado nuevos complejos basados en NHCs. En particular, nos hemos interesado en sistemas catalíticos más activos y selectivos, a la vez que más versátiles. Teniendo esto en cuenta, el objetivo general de esta Tesis Doctoral es obtener nuevos complejos multimetálicos para el desarrollo de procesos catalíticos mejorados. Este objetivo general se puede dividir en los siguientes objetivos específicos:

- Síntesis de nuevas sales de poli-azolio con *cores* poliaromáticos, para la generación de ligandos poli-NHC rígidos geoméricamente aislados.
- Coordinación de estos NHCs a diferentes metales, para obtener complejos multimetálicos con distancias fijas entre los metales.
- Estudio de las propiedades físico-químicas de los nuevos compuestos obtenidos (electroquímica, luminiscencia, etc).
- Estudio de la propiedades catalíticas de los nuevo complejos, prestando especial atención a la existencia de efectos cooperativos entre ellos.
- Síntesis de nuevos polímeros organometálicos basados en los nuevos poli-NHCs sintetizados, y estudio de sus propiedades catalíticas.

6.3 Discusión de resultados

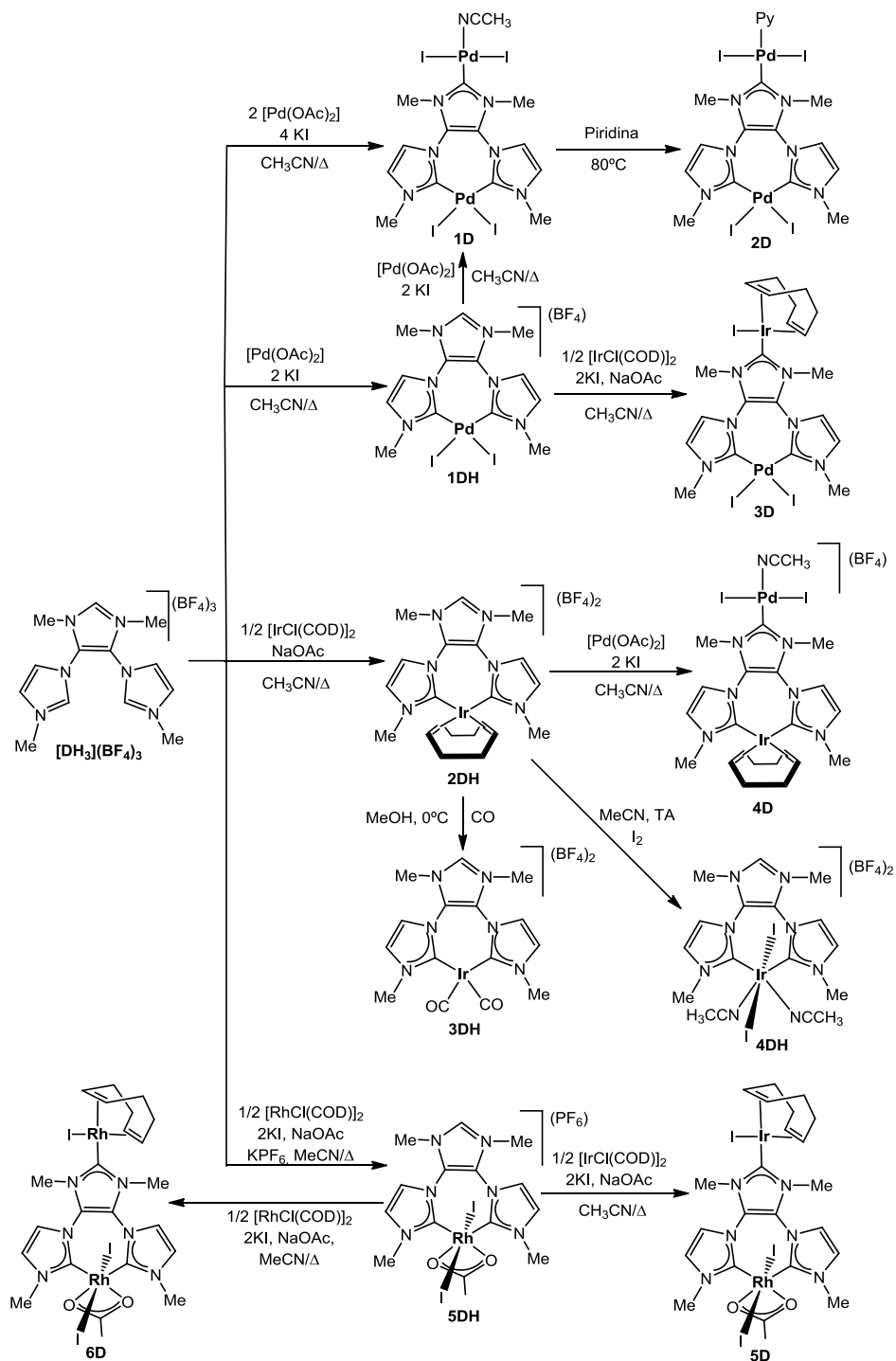
6.3.1 Complejos metálicos basados en un ligando tris-NHC en forma de Y

El Esquema 6.4 muestra la síntesis de la sal de tris-imidazolio $[\text{DH}_3](\text{BF}_4)_3$ que fue utilizada como precursora de un ligando tris-NHC. La síntesis consta de cuatro pasos. En primer lugar se obtuvo el compuesto **A** mediante una sustitución nucleofílica aromática del imidazol desprotonado a 5-cloro-1-metil-4-nitroimidazol. El segundo paso consiste en la reducción del grupo nitro del compuesto **A** para dar lugar a la correspondiente amina **B**, que fue ciclada mediante su reacción con glioxal, cloruro amónico y formaldehído,²⁴ para obtener el tris-imidazol **C**. Finalmente, este compuesto fue alquilado en presencia de un exceso de $(\text{CH}_3)_3\text{OBF}_4$ (sal de Meerwein), para dar lugar a la sal de tris-imidazolio $[\text{DH}_3](\text{BF}_4)_3$.



Esquema 6.4 Síntesis de $[\text{DH}_3](\text{BF}_4)_3$

Esta sal es precursora de un ligando tris-NHC que puede coordinarse simultáneamente en forma quelato a un metal y de forma monodentada a otro. El Esquema 6.5 muestra la versatilidad coordinativa del ligando derivado de $[\text{DH}_3](\text{BF}_4)_3$. Se obtuvieron cinco compuestos monometálicos (**1DH** a **5DH**), tres homo-bimetálicos (**1D**, **2D** y **6D**) y tres hetero-bimetálicos (**3D**, **4D** y **5D**) basados en paladio, iridio y rodio.



Esquema 6.5 Síntesis de los complejos 1DH a 5DH y 1D a 6D

En general se utilizaron similares condiciones de reacción para obtener todos los complejos mostrados del Esquema 6.5, es decir, se hizo reaccionar $[\text{DH}_3](\text{BF}_4)_3$ con acetato sódico en presencia del precursor metálico deseado, a reflujo de acetonitrilo. Este hecho es muy interesante, dado que facilita enormemente la síntesis de compuestos hetero-bimetalicos muy sofisticados. De hecho, se puede sintetizar el compuesto monometálico y añadir al mismo crudo de reacción los reactivos necesarios para que tenga lugar la segunda metalación, sin necesidad de aislar y purificar el intermedio monometálico. Además, la primera coordinación siempre tiene lugar selectivamente de manera que se forma complejo coordinado en forma quelato, debido a que este proceso está favorecido respecto a la coordinación en forma monodentada por motivos entrópicos (efecto quelato).²⁵

La sal de tris-imidazolio $[\text{DH}_3](\text{BF}_4)_3$, los compuestos intermedios necesarios para su obtención (**A**, **B** y **C** en el Esquema 6.4) y todos los complejos mostrados en el Esquema 6.5 (**1DH** a **5DH** y **1D** a **6D**) son compuestos nuevos que se han sintetizado por primera vez a lo largo del trabajo de investigación que se presenta. Dichos compuestos se han caracterizado mediante espectroscopia de RMN, espectrometría de masas y análisis elemental. Las estructuras moleculares de los complejos **1DH**, **2D**, **3D** y **6D** fueron confirmadas mediante Difracción de Rayos X (DRX) de monocristal.

6.3.2 Propiedades catalíticas de los complejos basados en un ligando tris-NHC en forma de Y

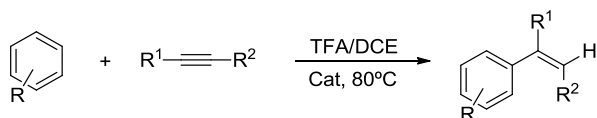
La actividad catalítica de los compuestos basados en paladio (**1DH**, **1D** y **2D**) y en iridio/paladio (**3D** y **4D**) mostrados en el apartado anterior fue evaluada en diferentes reacciones catalíticas.

Esta sección se divide en dos apartados que recogen los resultados catalíticos obtenidos en la reacción de hidroarilación de alquinos (catalizadores **1DH**, **1D** y **2D**) y en dos reacciones tándem: dehalogenación/transferencia de hidrógeno de *p*-bromoacetofenona y acoplamiento C-C de Suzuki-Miyaura/transferencia de hidrógeno de *p*-bromoacetofenona (catalizadores **3D** y **4D**).

6.3.2.1 Hidroarilación de alquinos catalizada por **1DH**, **1D** y **2D**

La reacción de hidroarilación de alquinos (también conocida como la reacción de Fujiwara)^{26,27} consiste en la adición de un arilo rico en electrones y un átomo de hidrógeno a un enlace C-C acetilénico, produciendo un areno vinílico (Esquema 6.6).

Diferentes compuestos basados en Pd(II)-mono-NHC^{28,29} y Pd(II)-bis-NHC³⁰⁻³⁴ han mostrado elevada actividad catalítica en esta reacción, por lo que pensamos que los compuestos **1D** y **2D** podrían ser unos buenos candidatos. Las reacciones se llevaron a cabo utilizando dos tipos de arenos (pentametilbenceno y 1,3,5-trimetilbenceno) y cinco alquinos (etil propiolato, etil fenilpropiolato, fenilacetileno, difenilacetileno y 1-fenil-1-propino) en una mezcla de ácido trifluoroacético/dicloroetano (4:1) a 80°C durante 5 horas utilizando un 0.1 % mol de los catalizadores **1DH**, **1D** o **2D**.



Esquema 6.6 Hidroarilación de alquinos

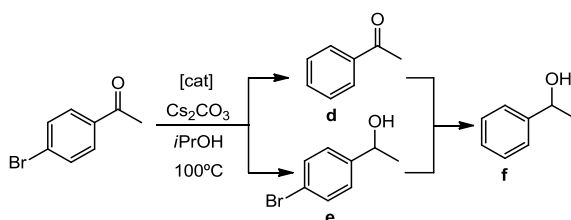
Los resultados obtenidos permitieron concluir que el catalizador **1D** es el más activo para este tipo de reacciones. En general, los arenos vinílicos se obtuvieron con rendimientos moderados, lo que es remarcable dado la baja carga de catalizador empleada (0.1 % mol). Incluso se pudieron realizar reacciones a temperatura ambiente en presencia de AgOAc, que actúa como activador del catalizador.

6.3.2.2 Procesos tándem catalizados por **3D** y **4D**

Recientemente, nuestro grupo de investigación ha descrito toda una serie de compuestos hetero-bimetálicos basados en Pd/Ir.³⁵ Su actividad catalítica fue estudiada en diferentes reacciones tándem. Todas ellas tienen en común el uso de 4-halo-acetofenonas como sustratos adecuados para combinar ciclos catalíticos promovidos por paladio e iridio. El enlace C-haluro es típicamente activado por el primero, mientras que el enlace C=O es susceptible de entrar en ciclos catalíticos asociados a iridio. Por lo tanto, decidimos comparar la actividad catalítica de los catalizadores ya descritos con la proporcionada por los nuevos compuestos hetero-bimetálicos de Pd/Ir (**3D** y **4D**). La comparación de la actividad catalítica entre estos dos nuevos complejos es muy interesante, debido a que contienen los mismos metales en los mismos estados de oxidación, pero con diferente entorno de coordinación. Es decir, el compuesto **3D** contiene paladio quelato/iridio mono-coordinado mientras que **4D** contiene iridio quelato/paladio mono-coordinado.

Dehalogenación/transferencia de hidrógeno de p-bromoacetofenona

En primer lugar se estudió la actividad catalítica de los complejos **3D** y **4D** en la reacción tándem de dehalogenación/transferencia de hidrógeno de *p*-bromoacetofenona (Esquema 6.7).

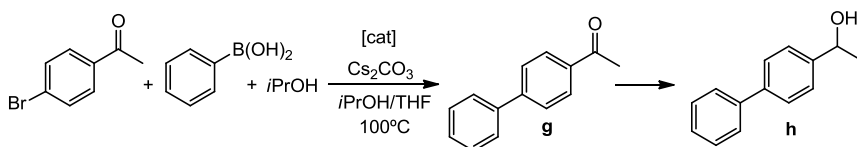


Esquema 6.7 Dehalogenación/transferencia de hidrógeno de *p*-bromoacetofenona

Las reacciones se llevaron a cabo en isopropanol a 100°C en presencia de Cs_2CO_3 y 2 % mol de catalizador. El catalizador **4D** mostró una mayor actividad catalítica comparada con la de **3D** y proporcionó selectivamente 1-feniletanol (**f** en el Esquema 6.7) tras 20 horas de reacción. Este resultado es comparable al obtenido anteriormente en nuestro grupo de investigación con otros catalizadores basados en Pd/Ir y es mejor que el obtenido mediante la combinación de compuestos homo-bimetálicos de paladio e iridio.³⁵ En cambio, el catalizador **3D** proporcionó mayoritariamente acetofenona (**d**), incluso después de periodos largos de reacción.

Suzuki-Miyaura/transferencia de hidrógeno de p-bromoacetofenona

Teniendo en cuenta los resultados obtenidos en la reacción anterior, decidimos estudiar la actividad catalítica de **4D** en la reacción tándem de acoplamiento cruzado C-C de Suzuki-Miyaura/transferencia de hidrógeno de *p*-bromoacetofenona (Esquema 6.8).



Esquema 6.8 Suzuki-Miyaura/transferencia de hidrogeno de *p*-bromoacetofenona

La reacción se llevó a cabo en una mezcla de isopropanol/THF (1:1) en presencia de Cs_2CO_3 y 2 % mol de catalizador. El compuesto **h** se obtuvo con buen rendimiento después de 24 horas de reacción. Aunque esta actividad catalítica es menor que la

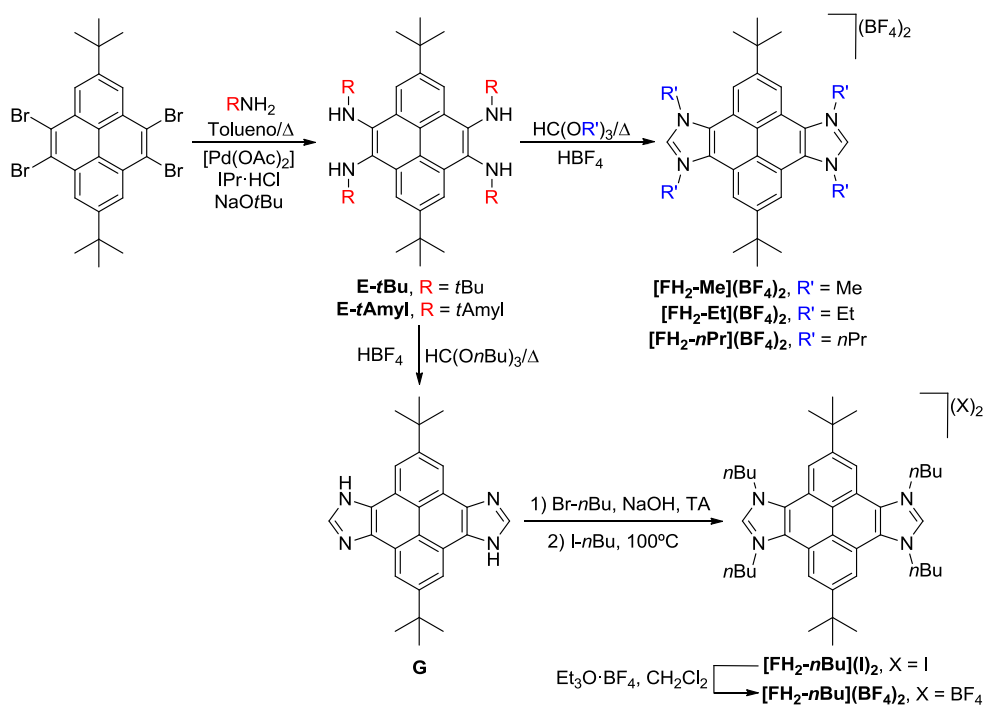
proporcionada por compuestos hetero-bimetálicos de Pd/Ir previamente sintetizados en nuestro grupo de investigación, es superior a la mostrada por la combinación de catalizadores homo-bimetálicos de paladio e iridio.³⁵

6.3.3 Complejos bimetálicos basados en ligandos pireno-bis-imidazolilideno

En la bibliografía podemos encontrar pocos ejemplos de ligandos bis-NHC que se puedan coordinar a dos metales diferentes, de manera que su disposición sea facialmente opuesta (ligandos de tipo *Janus*).^{16,20,36,37} En este contexto, decidimos aumentar la librería de este tipo de ligandos obteniendo un nuevo ligando bis-NHC basado en pireno.

6.3.3.1 Síntesis de sales de imidazolio basadas en pireno

El Esquema 6.9 muestra la ruta sintética utilizada para obtener las diferentes sales de bis-imidazolio basadas en pireno. La primera reacción consiste en la aminación de 4,5,9,10-tetrabromo-2,7-di-*terc*-butilpireno³⁸ en presencia de un catalizador de paladio para dar lugar al correspondiente compuesto tetra-aminado (**E-*t*Bu** o **E-*t*Am**).^{39,40} El segundo paso implica una ciclación formilativa de las aminas obtenidas en presencia de ácido tetrafluorobórico y un trisalquil ortoformiato. Sorprendentemente, en lugar de obtener las sales de bis-imidazolio con los grupos voluminosos *terc*-butilo o *terc*-amilo como N-sustituyentes (*wingtips*), las nuevas sales contienen grupos metilo, etilo o *n*-propilo (**[FH₂-Me](BF₄)₂**, **[FH₂-Et](BF₄)₂** y **[FH₂-*n*Pr](BF₄)₂**, respectivamente en el Esquema 6.9) dependiendo del trisalquil-ortoformiato utilizado en la ciclación. Formalmente, los grupos *terc*-butilo (o *terc*-amilo) de los compuestos **E-*t*Bu** (o **E-*t*Amyl**) han sido reemplazados por los sustituyentes que contiene el agente de ciclación (HC(OR')₃). Cuando la ciclación se llevó a cabo empleando tris-*n*-butil ortoformiato se obtuvo el bis-imidazol **G**. La alquilación de **G** mediante metodologías descritas anteriormente,⁴¹ proporciona la sal de bis-imidazolio que posee grupos *n*-butilos como *wingtips* (**[FH₂-*n*Bu](I)₂**), a partir de la cual se puede obtener mediante metátesis de aniones la sal **[FH₂-*n*Bu](BF₄)₂**.

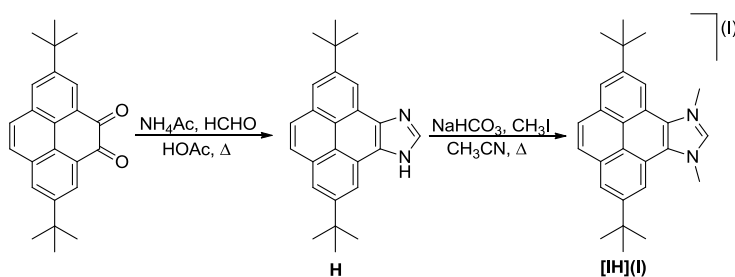


Esquema 6.9 Síntesis de sales de bis-azolio basadas en pireno

La reactividad observada es inesperada y no tiene precedentes en la literatura. Además, constituye una transformación de un gran valor sintético, dado que la reacción de aminación de compuestos bromados catalizada por paladio suele estar restringida a aminas sin protones en la posición beta (normalmente *tert*-butil aminas o anilinas), para evitar posibles procesos de β -eliminación. Con esta metodología, pueden ser introducidos sustituyentes alquílicos lineales en las sales de imidazolio utilizando los trisalquil ortoformiatos apropiados, evitando así el uso de agentes alquilantes fuertes, comúnmente utilizados en este tipo de reacciones.⁴²⁻⁴⁴

La formación de **G** sugiere que los grupos voluminosos, *tert*-butilo (o *tert*-amilo) se pierden durante la reacción, probablemente como consecuencia del gran impedimento estérico impuesto durante el proceso de rehibridación de sp^3 a sp^2 del átomo de nitrógeno.

Con objetivos comparativos, se sintetizó la sal **[IH](I)**, que se muestra en el Esquema 6.10. La reacción de 2,7-di-*tert*-butilpireno-4,5-diona⁴⁵ con formaldehído, acetato amónico en ácido acético a reflujo, produjo el imidazol **H** que fue alquilado en presencia de bicarbonato sódico y yoduro de metilo, para proporcionar la sal **[IH](I)**.

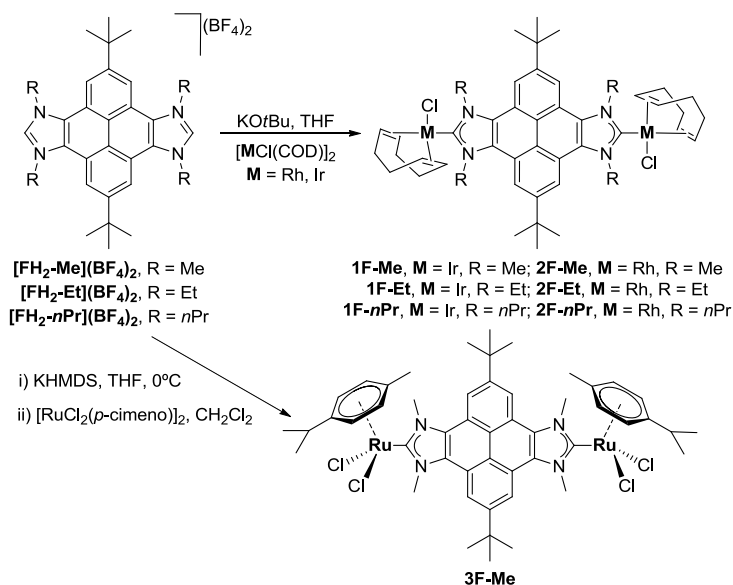


Esquema 6.10 Síntesis de la sal de pireno mono-azolio **[IH](I)**

Todos los compuestos mostrados en este apartado son nuevos y se han sintetizado por primera vez a lo largo del trabajo de investigación que se presenta. Estos compuestos fueron caracterizados mediante espectroscopia de RMN, espectrometría de masas y análisis elemental. Además, las sales de imidazolio demostraron ser fluorescentes, emitiendo entre 370 y 420 nm, y con rendimientos cuánticos de 0.29 a 0.41. Las estructuras moleculares de **[FH₂-Me](BF₄)₂** y de un intermedio en la reacción de ciclación formilativa (4,5-di-*terc*-butilamina-9,10-diamina-2,7-di-*terc*-butilpireno) fueron confirmadas mediante Difracción de Rayos X (DRX) de monocristal.

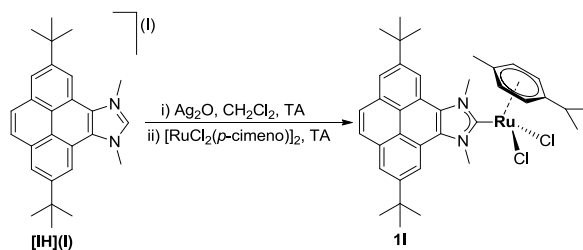
6.3.3.2 Síntesis de complejos basados en ligandos pireno-imidazolilideno

El Esquema 6.11 muestra la estrategia sintética utilizada para activar las sales de pireno-bis-imidazolio y coordinar el ligando bis-NHC generado a $[\text{MCl}(\text{COD})]_2$ ($\text{M} = \text{Ir}$ o Rh) y $[\text{RuCl}_2(p\text{-cimeno})]_2$. En el primer caso, las sales de bis-imidazolio se hicieron reaccionar con NaOtBu y $[\text{MCl}(\text{COD})]_2$ ($\text{M} = \text{Ir}$ o Rh) en THF a temperatura ambiente, obteniéndose los correspondientes complejos basados en iridio (**1F**) y rodio (**2F**), que fueron purificados mediante cromatografía en columna. En cuanto al compuesto basado en rutenio (**3F-Me**), **[FH₂-Me](BF₄)₂** se trató con bis(trimetilsilil)amida de potasio (KHMDS) a 0°C en THF, para generar el carbeno libre, que se hizo reaccionar con el dímero de $[\text{RuCl}_2(p\text{-cimeno})]_2$.



Esquema 6.11 Síntesis de complejos bimetalicos basados en ligandos pireno-bis-imidazolilideno

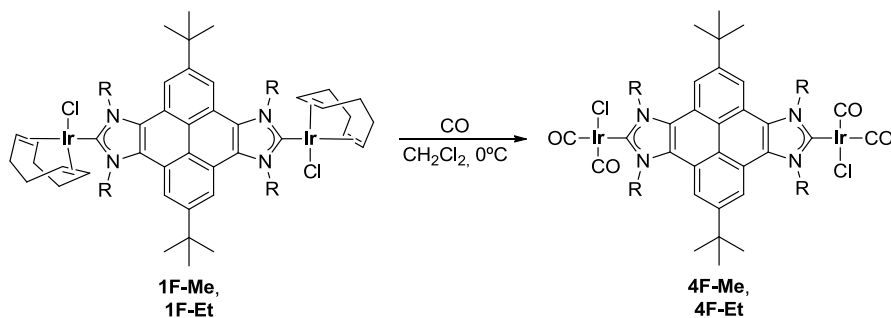
La síntesis del complejo de mono-rutenio basado en pireno **1I**, se llevó a cabo mediante transmetalación (Esquema 6.12).⁴⁶ La sal **[IH](I)** se trató con Ag_2O en diclorometano durante dos horas en ausencia de luz, para generar el carbeno de plata, que no fue aislado. Después, se añadió $[\text{RuCl}_2(p\text{-cimeno})]_2$ y la reacción se agitó a temperatura ambiente durante dos horas, para dar lugar al compuesto **1I**.



Esquema 6.12 Síntesis de **1I**

La propiedades electroquímicas de los complejos **1F-Et**, **3F-Me** y **1I** fueron estudiadas mediante voltametría cíclica (CV) y voltametría de pulso diferencial (DPV). Empleando ambas técnicas, se pudo concluir que los dos centros metálicos de estos compuestos bimetalicos están esencialmente desacoplados.

Para estimar la capacidad dadora del nuevo ligando bis-NHC basado en pireno se sintetizaron los compuestos de iridio carbonilo (**4F**) mediante el borboteo de CO a través de una disolución del correspondiente compuesto de iridio (**1F**) en diclorometano (Esquema 6.13).



Esquema 6.13 Síntesis de **4F-Me** y **4F-Et**

Mediante los espectros de IR de los complejos **4F-Me** y **4F-Et** y el uso de correlaciones conocidas,⁴⁷⁻⁴⁹ se estimó que la capacidad dadora de estos ligandos es similar a la proporcionada por el ligando 1,3-dietilbencimidazolilideno.

Todos los complejos mostrados en este apartado (**1F**, **2F**, **3F-Me**, **4F** y **1I**) se han sintetizado por primera vez a lo largo del trabajo de investigación que se presenta. Dichos compuestos fueron caracterizados mediante espectroscopia de RMN, espectrometría de masas y análisis elemental. Las estructuras moleculares de **1F-Et** y **3F-Me** fueron confirmadas mediante Difracción de Rayos X (DRX) de monocristal.

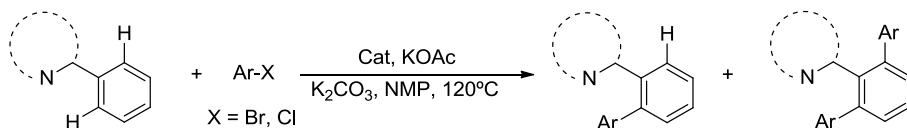
6.3.4 Propiedades catalíticas de complejos de rutenio basados en ligandos pireno-imidazolilideno

Las reacciones de funcionalización selectiva mediante la utilización de grupos directores han recibido mucha atención en los últimos años, dado que normalmente implican la activación de un enlace C-H y la formación de un nuevo enlace C-C, por lo que constituyen reacciones con una elevada economía atómica.⁵⁰ Desde el pionero trabajo de Murai y colaboradores,⁵¹ en el que por primera vez se utilizaron heteroátomos como agentes directores, el número de publicaciones relacionadas con este tema ha crecido exponencialmente.⁵²⁻⁵⁴ Los catalizadores basados en Ru(II) son los más ampliamente utilizados en este tipo de reacciones, por ello decidimos estudiar la actividad catalítica de **3F-Me** y **1I** en las reacciones de arilación de arilpiridinas e

hidroarilación de alquenos terminales, así como en la combinación de ambas reacciones en un proceso secuencial.

6.3.4.1 Arilación de arilpiridinas

Oi y colaboradores describieron los primeros ejemplos de reacciones de arilación de arilpiridinas con haluros de arilo catalizadas por rutenio.⁵⁵ Esta reacción consiste en la arilación selectiva de arilpiridinas en la posición *orto* del anillo de arilo. Así pues, se pueden producir los compuestos mono- y bis-arilado (Esquema 6.14). Para llevar a cabo esta reacción, **3F-Me** y **1I** (5 % mol basado en metal) se trataron inicialmente con KOAc en NMP y después se añadieron los sustratos y K₂CO₃. La mezcla de reacción se calentó a 120°C durante el tiempo deseado. Se utilizaron tres sustratos (2-fenilpiridina, benzo[*h*]quinolina y N-fenilpirazol) con diferentes agentes arilantes.

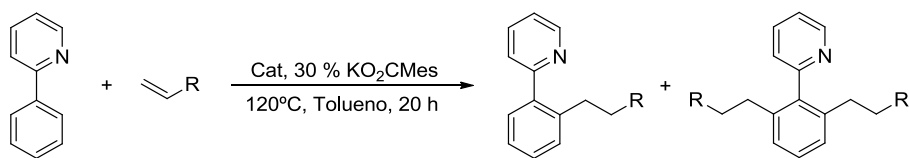


Esquema 6.14 Arilación de arilpiridinas

Ambos catalizadores mostraron una excelente actividad catalítica, y una elevada selectividad hacia los productos bis-arilados. Los resultados obtenidos mostraron ser mejores que los previamente observados empleando otros catalizadores de tipo RuCl₂(*p*-cymene)(NHC).⁴⁴ No se observaron diferencias sustanciales entre la actividad catalítica mostrada por **3F-Me** y su análogo mono-metálico, **1I**.

6.3.4.2 Hidroarilación de alquenos terminales

Animados por los resultados obtenidos en la reacción de arilación, decidimos estudiar la actividad catalítica de nuestros catalizadores en la hidroarilación de alquenos terminales (Esquema 6.15). Esta reacción se conoce desde hace más de dos décadas⁵¹ y se puede considerar como una alquilación de anillos aromáticos utilizando alquenos. Una de las limitaciones de este proceso es que normalmente requería el uso de alquenos activados como estirenos y vinilsilanos. Sin embargo, este problema ha sido solucionado recientemente por Ackermann y colaboradores utilizando catalizadores de rutenio asistidos por carboxilatos, que permitieron la utilización de alquenos terminales desactivados.^{56,57}

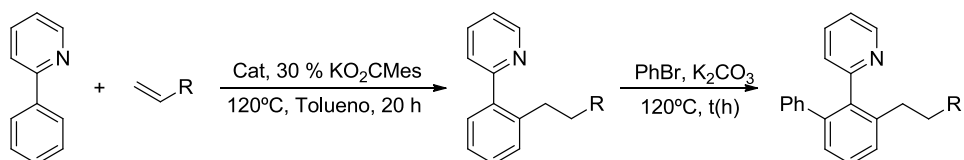


Esquema 6.15 Hidroarilación de alquenos terminales

Las reacciones se llevaron a cabo utilizando los catalizadores **3F-Me** y **II** (5 % mol basado en metal), KO₂Mes como aditivo en tolueno a 120°C durante 20 horas. En cuanto a los sustratos, se decidió utilizar 2-fenilpiridina y cuatro tipos de alquenos (1-hexeno, 1-octeno, 1-deceno y trimetilvinilsilano). Ambos complejos mostraron ser excelentes catalizadores para esta reacción. Cuando se utilizaron los alquenos no activados (1-hexeno, 1-octeno, 1-deceno) se obtuvo selectivamente el producto de mono-alquilación, mientras que cuando se utilizó trimetilvinilsilano (alqueno activado) se observó la formación del compuesto bis-alquilado en una cantidad no despreciable. En esta reacción tampoco se observaron diferencias en las actividades catalíticas de **3F-Me** y **II**. Los resultados obtenidos son comparables a los recientemente obtenidos por Ackermann y colaboradores.⁵⁶

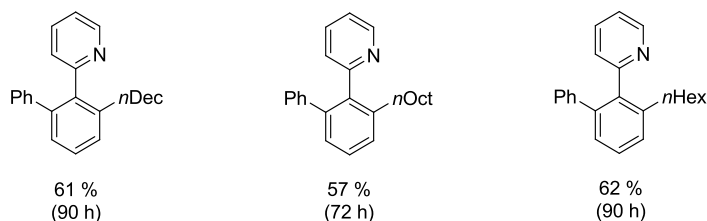
6.3.4.3 Hidroarilación de alquenos terminales y arilación de arilpiridinas secuencial

Dado que nuestros catalizadores de rutenio mostraron buena actividad en las dos reacciones tratadas en los apartados anteriores, decidimos estudiar la viabilidad de combinar ambos procesos de forma secuencial con el fin de producir arilpiridinas asimétricamente sustituidas. Como la hidroarilación de alquenos no activados produce selectivamente los productos mono-alquilados, decidimos diseñar la secuencia de reacción llevando a cabo en primer lugar la alquilación y después la arilación del enlace C-H en posición *orto* que todavía queda en el anillo de fenilo. Como se puede observar en el Esquema 6.16, las reacciones se realizaron tratando 2-fenilpiridina con el alqueno terminal correspondiente (1-hexeno, 1-octeno, 1-deceno), en tolueno, en presencia de KO₂CMes y 5 % mol de catalizador (basado en metal), a 120°C durante 20 horas. Transcurrido este tiempo, se añadieron bromobenceno y K₂CO₃ y la reacción resultante se calentó a 120°C.



Esquema 6.16 Hidroarilación de alquenos/arilación de arilpiridinas secuencial

Se obtuvieron buenos rendimientos para las arilpiridinas asimétricamente sustituidas (Esquema 6.19). En este caso se observó que la actividad del catalizador de bis-Ru (**3F-Me**) fue mayor que la proporcionada por su análogo de mono-Ru (**1I**). Es importante destacar que esta es la primera vez que se utiliza una estrategia secuencial combinando alquilación/arilación para obtener este tipo de arilpiridinas asimétricamente sustituidas. Además, estos productos son nuevos y se han obtenido y caracterizado por primera vez a lo largo del trabajo de investigación que se presenta.



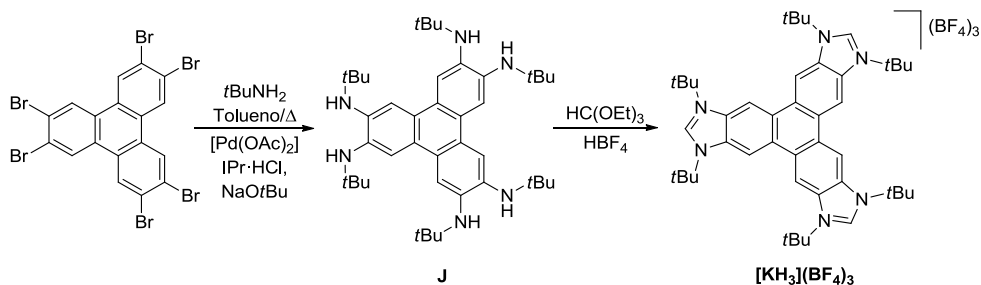
Esquema 6.17 Rendimiento aislado máximo en la obtención de arilpiridinas asimétricamente sustituidas utilizando **3F-Me**

6.3.5 Síntesis de compuestos trimetálicos basados en ligandos tris-NHC

Cuando empezó el proyecto que se describe en esta sección, en la literatura sólo había un ejemplo de un ligando tris-NHC con un *core* de naturaleza rígida con simetría D_{3h} . Bielawski y colaboradores describieron este ejemplo basado en tripticeno (**Error! No s'ha trobat l'origen de la referència.**, izquierda),⁴⁰ aunque únicamente describieron la generación del tris-NHC libre y no el estudio de su versatilidad coordinativa. Además, en este ejemplo las tres unidades carbénicas se encuentran electrónicamente desacopladas debido a la presencia del *core* tripticénico. Teniendo todo esto en cuenta, decidimos sintetizar un nuevo ligando tris-NHC que contuviera un *core* poliaromático como el trifenileno.

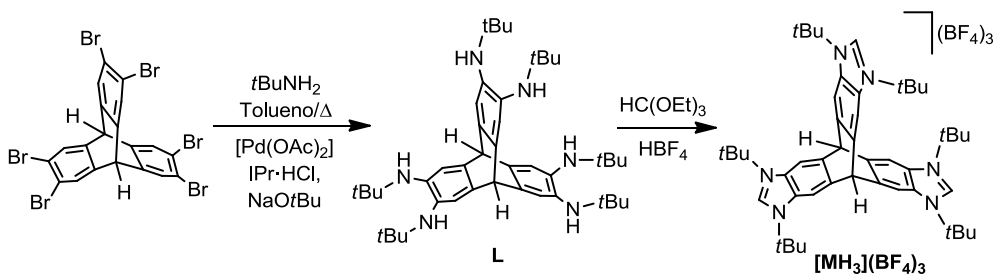
El Esquema 6.18 muestra los dos pasos necesarios para la obtención de la sal de trisimidazolio $[\text{KH}_3](\text{BF}_4)_3$. El primer paso consiste en la aminación catalizada por

paladio de 2,3,6,7,10,11-hexabromotrifeníleno,⁵⁸ para obtener la hexa-amina **J**. El segundo paso consiste en la ciclación formilativa de **J** en presencia de ácido tetrafluorobórico y trietil ortoformiato, obteniéndose de esta forma la sal de tris-imidazolio basada en trifeníleno $[\text{KH}_3](\text{BF}_4)_3$.



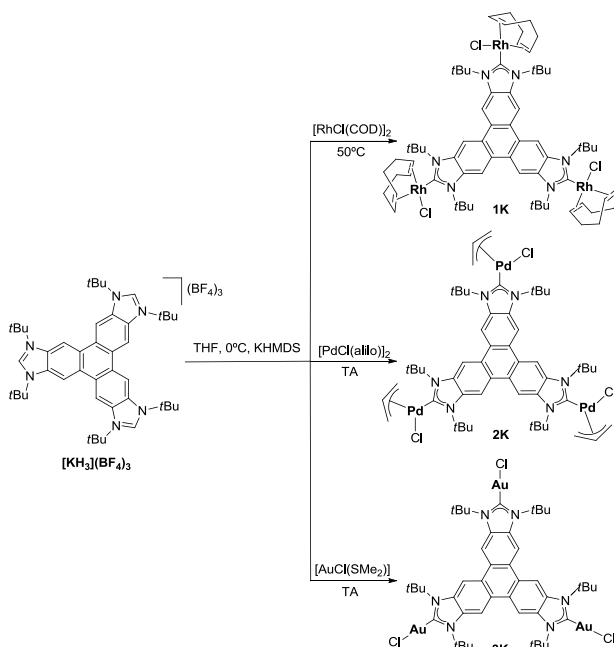
Esquema 6.18 Síntesis de $[\text{KH}_3](\text{BF}_4)_3$

A efectos comparativos también se sintetizó una nueva sal de tris-imidazolio basada en triptíceno ($[\text{MH}_3](\text{BF}_4)_3$ en el Esquema 6.19). La ruta sintética para la obtención de $[\text{MH}_3](\text{BF}_4)_3$ a partir de 2,3,6,7,12,13-hexabromotriptíceno,⁵⁹ es idéntica a la descrita para la obtención de $[\text{KH}_3](\text{BF}_4)_3$.



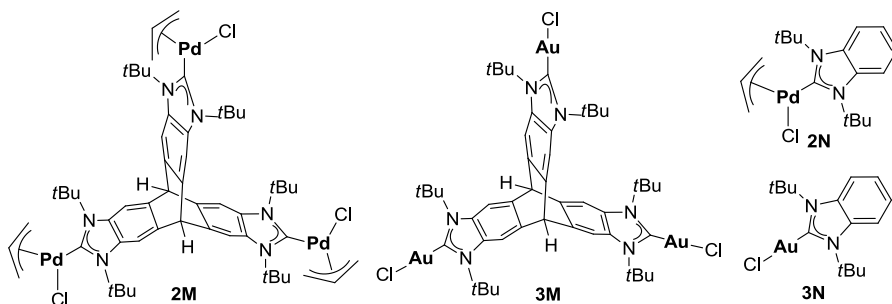
Esquema 6.19 Síntesis de $[\text{MH}_3](\text{BF}_4)_3$

El Esquema 6.20 muestra la metodología utilizada para la obtención de complejos trimetálicos de rodio (**1K**), paladio (**2K**) y oro (**3K**) basados en un ligando trifeníleno-tris-imidazolilideno. En todos los casos se trató la sal $[\text{KH}_3](\text{BF}_4)_3$ con KHMDS a 0°C en THF, para generar el carbeno libre, que se hizo reaccionar *in situ* con el correspondiente precursor metálico.



Esquema 6.20 S3ntesis de **1K** a **3K**

Con objetivos comparativos se sintetizaron los complejos trimet3licos **2M** y **3M** (Esquema 6.21) a partir de $[MH_3](BF_4)_3$ utilizando las mismas condiciones de reacci3n mostradas en el Esquema 6.20. Desafortunadamente, el compuesto de tris-RhCl(COD) basado en el ligando tripticen-tris-imidazolilideno no pudo sintetizarse. A partir de cloruro de 1,3-di(*terc*-butil)bencimidazolio⁶⁰ y empleando las mismas condiciones de reacci3n utilizadas para la s3ntesis de los otros complejos mostrados en este apartado, se obtuvieron los compuestos mono-met3licos **2N** y **3N** (Esquema 6.21).



Esquema 6.21

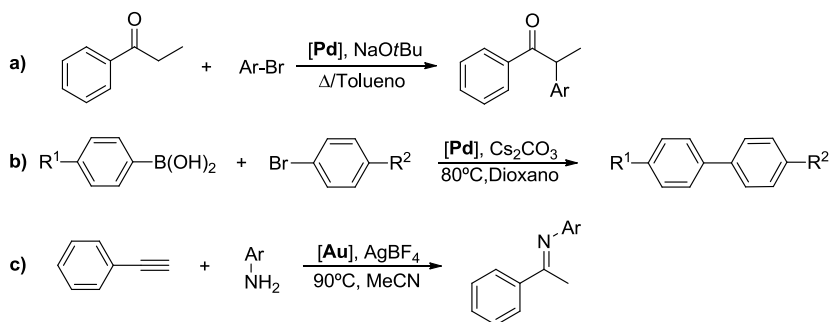
Como puede apreciarse en el Esquema 6.24, los complejos mono-metálicos (**2N** y **3N**) se pueden considerar como exactamente la tercera parte de los complejos trimetálicos (**2K** y **3K**, respectivamente).

Las propiedades estereoelectrónicas de los tres ligandos utilizados en este apartado se estudiaron mediante la estimación del porcentaje de volumen encapsulado ($\% V_{\text{Bur}}$)⁶¹ y mediante la síntesis del derivado carbonilado de **1K** (**4K**), y posterior estimación del TEP empleando correlaciones conocidas⁴⁷⁻⁴⁹ o mediante cálculos DFT. Se concluyó que las propiedades estereoelectrónicas de los tres ligandos son muy similares. Mediante estudios electroquímicos (CV y DPV) del compuesto **1K** se concluyó que la comunicación electrónica entre los tres metales unidos por el ligando trifenilen-tris-imidazolilideno es muy débil.

Todos los compuestos mostrados en este apartado se han sintetizado por primera vez a lo largo del trabajo de investigación que se presenta. Dichos compuestos fueron caracterizados mediante espectroscopia de RMN, espectrometría de masas y análisis elemental. Las estructuras moleculares de **1K**, **3K**, **3M** y **3N** fueron confirmadas mediante Difracción de Rayos X (DRX) de monocristal.

6.3.6 Propiedades catalíticas de complejos trimetálicos basados en ligandos tris-NHC

Las propiedades catalíticas de los complejos de paladio (**2K**, **2M** y **2N**) y de oro (**3K**, **3M** y **3N**) fueron estudiadas en reacciones típicamente promovidas por estos metales. En cuanto a los complejos de paladio, las reacciones estudiadas fueron la α -arilación de propiofenona [Esquema 6.22, reacción a)] y el acoplamiento C-C cruzado de Suzuki-Miyaura [Esquema 6.22, reacción b)], mientras que para los complejos de oro se estudió la hidroaminación de alquinos [Esquema 6.22, reacción c)].



Esquema 6.22

En general se observó que la actividad catalítica de los complejos basados en el ligando trifenilen-tris-imidazolilideno (**2K** y **3K**) era mayor que las proporcionadas por los otros catalizadores, tanto trimetálicos (**2M** y **3M**) como monometálicos (**2N** y **3N**).

Teniendo en cuenta que los tres ligandos utilizados tienen propiedades estereoelectrónicas similares y después de realizar diferentes experimentos, concluimos que la naturaleza trimetálica de los complejos **2K** y **3K** puede producir un efecto beneficioso en las reacciones catalíticas, debido a la alta nano-concentración local de sitios catalíticamente activos que proporcionan. Además, la presencia de un *core* poliaromático en estos compuestos parece ser clave, ya que probablemente la interacción de los sustratos con los centros metálicos esté siendo facilitada mediante interacciones de tipo π -stacking a través del *core* trifenilénico del ligando.

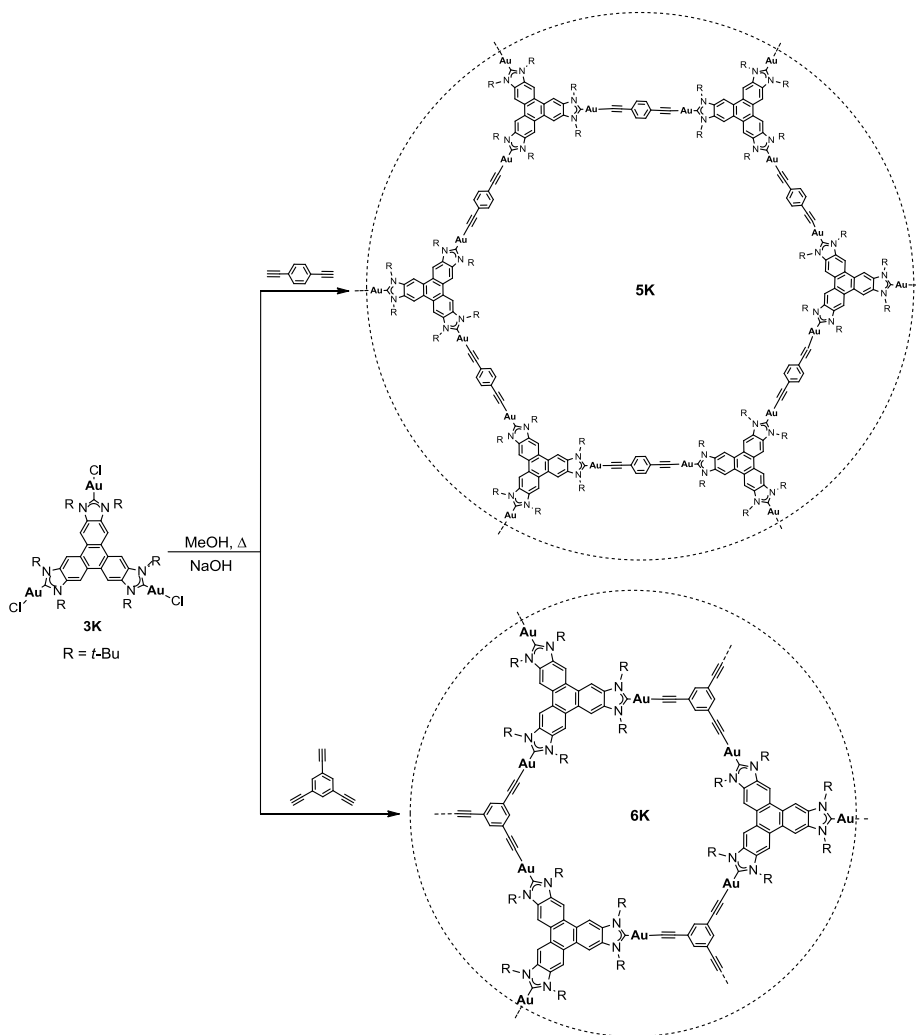
6.3.7 Polímeros organometálicos microporosos basados en especies trifenileno-tris-NHC de oro

6.3.7.1 Síntesis y caracterización

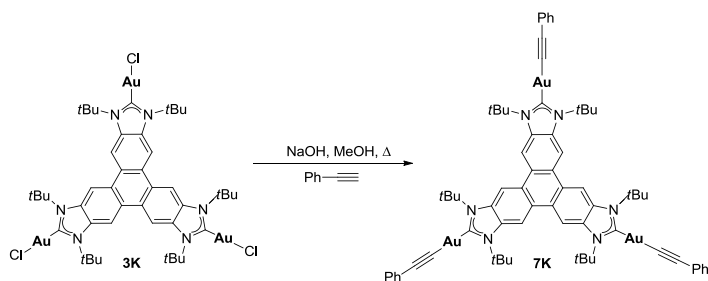
La particular geometría del ligando trifenilen-tris-imidazolilideno nos permitió la obtención de redes organometálicas bi- o tri-dimensionales. Para ello decidimos hacer uso de la gran afinidad que los ligandos acetiluro presentan por los centros de oro.⁶²⁻⁶⁷ Como muestra el Esquema 6.23, hicimos reaccionar el complejo trimetálico de oro **3K** con 1,4-dietinilbenceno o 1,3,5-trietinilbenceno, en condiciones básicas a reflujo de metanol para obtener los nuevos polímeros organometálicos **5K** y **6K**, respectivamente. Estos materiales fueron caracterizados mediante espectroscopia de

^{13}C CP/MAS NMR y FT-IR, SEM, TEM, TGA, análisis elemental, experimentos de adsorción-desorción de N_2 y difracción de rayos X en polvo.

Con objetivos comparativos se sintetizó el análogo molecular de estos materiales (**7K**) mediante la reacción de **3K** con fenilacetileno en presencia de hidróxido sódico a reflujo de metanol (Esquema 6.24). Este compuesto fue caracterizado mediante espectroscopia de RMN, espectrometría de masas y análisis elemental.



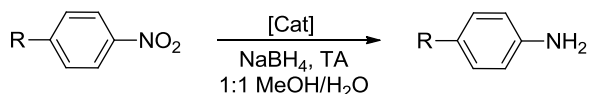
Esquema 6.23 Síntesis de **5K** y **6K**

Esquema 6.24 Síntesis de **7K**

6.3.7.2 Actividad catalítica

Dada la naturaleza altamente insoluble de los polímeros **5K** y **6K** decidimos estudiar sus propiedades en reacciones catalizadas heterogéneamente.

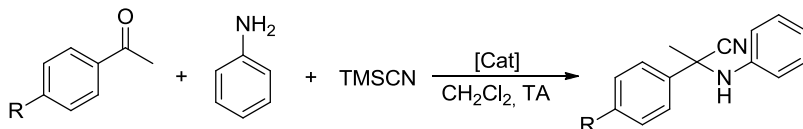
La primera reacción que se estudió fue la reducción de nitroarenos a anilinas (Esquema 6.25), ya que las anilinas funcionalizadas son compuestos importantes en la industria farmacéutica⁶⁸⁻⁷¹ y numerosos catalizadores basados en oro han mostrado buenas actividades catalíticas en esta reacción.⁷²⁻⁷⁵ Se utilizaron tres nitroarenos (4-metoxinitrobenzoceno, 4-metilnitrobenzoceno y 4-bromonitrobenzoceno) que se hicieron reaccionar en una mezcla MeOH/H₂O (1:1), en presencia de NaBH₄ y de los polímeros organometálicos **5K** ó **6K** (0.5 % mol basado en oro) a temperatura ambiente (Esquema 6.25). Se observó una actividad catalítica de buena a excelente en función del sustrato utilizado. Sin embargo, mediante SEM se observó la descomposición del catalizador y la generación de nanopartículas de oro, que probablemente sean las verdaderas responsables de la actividad catalítica observada.



Esquema 6.25 Reducción de nitroarenos

La otra reacción que se estudió fue la reacción de tres componentes de Strecker. Esta reacción fue descrita por primera vez en 1850,⁷⁶ pero aún hoy en día suscita un gran interés, sobre todo en su versión asimétrica.⁷⁷ Con esta reacción se pueden obtener α -aminonitrilos a partir de reactivos muy baratos: cetonas o aldehídos, aminas y una fuente de cianuro (normalmente ácido cianhídrico o cianuro de trimetilsililo (TMSCN)) (Esquema 6.26). Los α -aminonitrilos obtenidos de esta manera se pueden

transformar fácilmente mediante hidrólisis a los correspondientes α -aminoácidos, que son compuestos de gran valor en campos como la biología.



Esquema 6.26 Reacción de tres componentes de Strecker

Las reacciones se llevaron a cabo utilizando cuatro tipos de cetonas (acetofenona, 4-bromoacetofenona, 4-metoxiacetofenona y 4-nitroacetofenona), anilina y TMSCN, en presencia de **5K** ó **6K** (4 % mol basado en oro) en diclorometano a temperatura ambiente durante 12 horas. En primer lugar se realizaron ensayos de reciclado utilizando acetofenona como sustrato. Se observó que en el primer ciclo ambos catalizadores proporcionaron rendimientos superiores al 95 %. Sin embargo, se produjo una disminución en la actividad catalítica de los dos materiales en los sucesivos ciclos de reutilización, siendo ésta más acusada para **5K**. Se caracterizaron los catalizadores recuperados y se observó que los materiales habían sufrido cambios morfológicos y que apenas habían cambiado composicionalmente. Por lo tanto, probablemente la disminución en la actividad catalítica esté relacionada con estos cambios morfológicos. Además, debe tenerse en cuenta que la masa de catalizador utilizada para estos ensayos de reciclado está entorno a los 10 mg, una cantidad mucho menor de la que se suele utilizar en sistemas heterogéneos. Probablemente, durante el proceso de reciclado se esté produciendo pérdida de catalizador que también influye en la disminución de su actividad catalítica.

En cuanto a los otros sustratos utilizados, ambos catalizadores proporcionaron excelentes rendimientos hacia los correspondientes α -aminonitrilos. Se observó una mayor actividad de **6K** respecto a **5K**, probablemente debido a la mayor área superficial del primero.

6.4 Conclusiones

En esta Tesis Doctoral se han sintetizado tres nuevos ligandos politópicos basados en ligandos NHC con arquitecturas muy sofisticadas, mediante diferentes rutas sintéticas.

En primer lugar se obtuvo un ligando tris-NHCs con forma de Y que permitió obtener compuestos mono-metálicos en los que el ligando actúa en forma quelato. También se obtuvieron compuestos homo- y hetero-bimetálicos basados en este ligando. En ellos el ligando está actuando como puente entre dos metales, coordinándose a uno en forma quelato y al otro en forma monodentada. Las actividades catalíticas de estos complejos fueron estudiadas en la reacción de hidroarilación de alquinos y en dos procesos tándem.

En segundo lugar se sintetizó una serie de ligandos mono- y bis-imidazolilideno basados en pireno, de manera que se incrementó el número de ligandos de tipo *Janus* basados en bis-NHCs. En la ruta sintética para obtener las sales precursoras de estos ligandos se observó un comportamiento inédito en la reacción de ciclación formilativa. Se obtuvieron diferentes tipos de compuestos homo-bimetálicos y monometálicos basados en estos ligandos. La actividad catalítica de los compuestos de rutenio se estudió en arilación de arilpiridinas, hidroarilación de alquenos y un proceso secuencial en el que se combinan estas dos reacciones.

Finalmente, se sintetizó un nuevo ligando tris-imidazolilideno basado en trifenileno con el que se pudieron obtener compuestos homo-trimetálicos que contienen un *core* rígido poliaromático. Con objetivos comparativos, se obtuvieron compuestos mono- y trimetálicos basados en 1,3-di(*tert*-butil)imidazolilideno y un ligando tripticen-tris-imidazolilideno, respectivamente. Se estudió la actividad catalítica de estos compuestos en α -arilación de cetonas, acoplamiento cruzado C-C de Suzuki-Miyaura e hidroaminación de alquinos. Se observó que los catalizadores basados en el ligando trifenilen-tris-imidazolilideno (**2K** y **3K**) proporcionan mejores actividades catalíticas que los demás. Este hecho se atribuyó a la naturaleza trimetálica de estos compuestos y a las interacciones de tipo π -stacking entre los catalizadores y los sustratos. Por último, se sintetizaron polímeros organometálicos microporosos basados en especies trifenileno-tris-NHC de oro, cuya actividad catalítica fue estudiada en la reducción de nitroarenos y en la reacción de tres componentes de Strecker.

Mediante la utilización de los nuevos ligandos sintetizados en esta Tesis Doctoral se abre la puerta para obtener nuevos compuestos hetero-bimetálicos o hetero-trimetálicos. Utilizando estos complejos con dos o tres metales diferentes unidos por un único ligando, potencialmente se podrán diseñar ciclos catalíticos multimetálicos mejorados y muy sofisticados, aprovechando los nano-volúmenes de reacción bien definidos y las posibles interacciones de tipo π -stacking entre los sustratos y los ligandos.

6.5 Referencias

- (1) Beller, M.; Renken, A.; van Santen, R. A. *Catalysis. From Principles to Applications*; Wiley-VCH, 2012.
- (2) Van den Beuken, E. K.; Feringa, B. L. *Tetrahedron* **1998**, *54*, 12985.
- (3) Fogg, D. E.; dos Santos, E. N. *Coord. Chem. Rev.* **2004**, *248*, 2365.
- (4) Lee, J. M.; Na, Y.; Han, H.; Chang, S. *Chem. Soc. Rev.* **2004**, *33*, 302.
- (5) Wasilke, J.-C.; Obrey, S. J.; Baker, R. T.; Bazan, G. C. *Chem. Rev.* **2005**, *105*, 1001.
- (6) Shindoh, N.; Takemoto, Y.; Takasu, K. *Chem. Eur. J.* **2009**, *15*, 12168.
- (7) Allen, A. E.; Macmillan, D. W. C. *Chem. Sci.* **2012**, 633.
- (8) Park, J.; Hong, S. *Chem. Soc. Rev.* **2012**, *41*, 6931.
- (9) Bratko, I.; Gómez, M. *Dalton Trans.* **2013**, *42*, 10664.
- (10) Mata, J. A.; Hahn, F. E.; Peris, E. *Chem. Sci.* **2014**, *5*, 1723.
- (11) Herrmann, W. A.; Köcher, C. *Angew. Chemie Int. Ed.* **1997**, *36*, 2162.
- (12) Bourissou, D.; Guerret, O.; Gabbaï, F. P.; Bertrand, G. *Chem. Rev.* **2000**, *100*, 39.
- (13) Díez-González, S.; Marion, N.; Nolan, S. P. *Chem. Rev.* **2009**, *109*, 3612.
- (14) Benhamou, L.; Chardon, E.; Lavigne, G.; Bellemin-Laponnaz, S.; César, V. *Chem. Rev.* **2011**, *111*, 2705.
- (15) Boydston, A. J.; Williams, K. A.; Bielawski, C. W. *J. Am. Chem. Soc.* **2005**, *127*, 12496.
- (16) Khramov, D. M.; Boydston, A. J.; Bielawski, C. W. *Angew. Chem. Int. Ed.* **2006**, *45*, 6186.
- (17) Boydston, A. J.; Bielawski, C. W. *Dalton Trans.* **2006**, 4073.
- (18) Viciano, M.; Sanaú, M.; Peris, E. *Organometallics* **2007**, *26*, 6050.
- (19) Zanardi, A.; Mata, J. A.; Peris, E. *Organometallics* **2009**, *28*, 4335.
- (20) Prades, A.; Peris, E.; Alcarazo, M. *Organometallics* **2012**, *31*, 4623.
- (21) Guisado-Barrios, G.; Hiller, J.; Peris, E. *Chem. Eur. J.* **2013**, *19*, 10405.
- (22) Guerret, O.; Solé, S.; Gornitzka, H.; Teichert, M.; Trinquier, G.; Bertrand, G. *J. Am. Chem. Soc.* **1997**, *119*, 6668.

- (23) Tennyson, A. G.; Rosen, E. L.; Collins, M. S.; Lynch, V. M.; Bielawski, C. W. *Inorg. Chem.* **2009**, *48*, 6924.
- (24) Ahrens, S.; Herdtweck, E.; Goutal, S.; Strassner, T. *Eur. J. Inorg. Chem.* **2006**, 1268.
- (25) Ribas Gispert, J. *Coordination Chemistry*; Wiley-VCH Verlag, 2008.
- (26) Jia, C.; Piao, D.; Oyamada, J.; Lu, W.; Kitamura, T.; Fujiwara, Y. *Science* **2000**, 287, 1992.
- (27) Jia, C.; Lu, W.; Oyamada, J.; Kitamura, T.; Matsuda, K.; Irie, M.; Fujiwara, Y. *J. Am. Chem. Soc.* **2000**, *122*, 7252.
- (28) Viciu, M. S.; Stevens, E. D.; Petersen, J. L.; Nolan, S. P. *Organometallics* **2004**, *23*, 3752.
- (29) Saravanakumar, R.; Ramkumar, V.; Sankararaman, S. *Organometallics* **2011**, *30*, 1689.
- (30) Biffis, A.; Tubaro, C.; Buscemi, G.; Basato, M. *Adv. Synth. Catal.* **2008**, *350*, 189.
- (31) Buscemi, G.; Biffis, A.; Tubaro, C.; Basato, M. *Catal. Today* **2009**, *140*, 84.
- (32) Biffis, A.; Gazzola, L.; Gobbo, P.; Buscemi, G.; Tubaro, C.; Basato, M. *Eur. J. Org. Chem.* **2009**, 3189.
- (33) Buscemi, G.; Biffis, A.; Tubaro, C.; Basato, M.; Graiff, C.; Tiripicchio, A. *Appl. Organomet. Chem.* **2009**, *24*, 285.
- (34) Gazzola, L.; Tubaro, C.; Biffis, A.; Basato, M. *New J. Chem.* **2010**, *34*, 482.
- (35) Zanardi, A.; Mata, J. A.; Peris, E. *J. Am. Chem. Soc.* **2009**, *131*, 14531.
- (36) Mas-Marzá, E.; Mata, J. A.; Peris, E. *Angew. Chem. Int. Ed.* **2007**, *46*, 3729.
- (37) Prades, A.; Poyatos, M.; Mata, J. A.; Peris, E. *Angew. Chem. Int. Ed.* **2011**, *50*, 7666.
- (38) Hu, J.; Era, M.; Elsegood, M. R. J.; Yamato, T. *Eur. J. Org. Chem.* **2010**, 72.
- (39) Khramov, D. M.; Boydston, A. J.; Bielawski, C. W. *Org. Lett.* **2006**, *8*, 1831.
- (40) Williams, K. A.; Bielawski, C. W. *Chem. Commun.* **2010**, *46*, 5166.
- (41) Tapu, D.; Owens, C.; VanDerveer, D.; Gwaltney, K. *Organometallics* **2009**, *28*, 270.
- (42) Corberán, R.; Sanaú, M.; Peris, E. *J. Am. Chem. Soc.* **2006**, *128*, 3974.
- (43) Viciano, M.; Mas-Marzá, E.; Sanaú, M.; Peris, E. *Organometallics* **2006**, *25*, 3063.
- (44) Prades, A.; Poyatos, M.; Peris, E. *Adv. Synth. Catal.* **2010**, *352*, 1155.

- (45) Hu, J.; Zhang, D.; Harris, F. W. *J. Org. Chem.* **2005**, *70*, 707.
- (46) Wang, H. M. J.; Lin, I. J. B. *Organometallics* **1998**, *17*, 972.
- (47) Chianese, A. R.; Li, X.; Janzen, M. C.; Faller, J. W.; Crabtree, R. H. *Organometallics* **2003**, *22*, 1663.
- (48) Kelly III, R. A.; Clavier, H.; Giudice, S.; Scott, N. M.; Stevens, E. D.; Bordner, J.; Samardjiev, I.; Hoff, C. D.; Cavallo, L.; Nolan, S. P. *Organometallics* **2008**, *27*, 202.
- (49) Nelson, D. J.; Nolan, S. P. *Chem. Soc. Rev.* **2013**, *42*, 6723.
- (50) Arockiam, P. B.; Bruneau, C.; Dixneuf, P. H. *Chem. Rev.* **2012**, *112*, 5879.
- (51) Murai, S.; Kakiuchi, F.; Sekine, S.; Tanaka, Y.; Kamatani, A.; Sonoda, M.; Chatani, N. *Nature* **1993**, *366*, 529.
- (52) Kakiuchi, F.; Murai, S. *Acc. Chem. Res.* **2002**, *35*, 826.
- (53) Ackermann, L.; Vicente, R.; Kapdi, A. R. *Angew. Chem. Int. Ed.* **2009**, *48*, 9792.
- (54) Ackermann, L. *Chem. Commun.* **2010**, *46*, 4866.
- (55) Oi, S.; Fukita, S.; Hirata, N.; Watanuki, N.; Miyano, S.; Inoue, Y. *Org. Lett.* **2001**, *3*, 2579.
- (56) Schinkel, M.; Marek, I.; Ackermann, L. *Angew. Chem. Int. Ed.* **2013**, *52*, 3977.
- (57) Schinkel, M.; Wallbaum, J.; Kozhushkov, S. I.; Marek, I.; Ackermann, L. *Org. Lett.* **2013**, *15*, 4482.
- (58) Yatabe, T.; Harbison, M. A.; Brand, J. D.; Wagner, M.; Müllen, K.; Samorí, P.; Rabe, J. P. *J. Mater. Chem.* **2000**, *10*, 1519.
- (59) Hilton, C. L.; Jamison, C. R.; Zane, H. K.; King, B. T. *J. Org. Chem.* **2009**, *74*, 405.
- (60) Khramov, D. M.; Bielawski, C. W. *J. Org. Chem.* **2007**, *72*, 9407.
- (61) Clavier, H.; Nolan, S. P. *Chem. Commun.* **2010**, *46*, 841.
- (62) Wang, H. M. J.; Chen, C. Y. L.; Lin, I. J. B. *Organometallics* **1999**, *18*, 1216.
- (63) Gao, L.; Partyka, D. V.; Updegraff, J. B.; Deligonul, N.; Gray, T. G. *Eur. J. Inorg. Chem.* **2009**, 2711.
- (64) Fortman, G. C.; Poater, A.; Levell, J. W.; Gaillard, S.; Slawin, A. M. Z.; Samuel, I. D. W.; Cavallo, L.; Nolan, S. P. *Dalton Trans.* **2010**, *39*, 10382.
- (65) Konkolewicz, D.; Gaillard, S.; West, A. G.; Cheng, Y. Y.; Gray-Weale, A.; Schmidt, T. W.; Nolan, S. P.; Perrier, S. *Organometallics* **2011**, *30*, 1315.

- (66) Garg, J. A.; Blacque, O.; Heier, J.; Venkatesan, K. *Eur. J. Inorg. Chem.* **2012**, 1750.
- (67) Zhou, Y.-P.; Liu, E.-B.; Wang, J.; Chao, H.-Y. *Inorg. Chem.* **2013**, 52, 8629.
- (68) Wienhöfer, G.; Sorribes, I.; Boddien, A.; Westerhaus, F.; Junge, K.; Junge, H.; Llusar, R.; Beller, M. *J. Am. Chem. Soc.* **2011**, 133, 12875.
- (69) Sorribes, I.; Wienhöfer, G.; Vicent, C.; Junge, K.; Llusar, R.; Beller, M. *Angew. Chem. Int. Ed.* **2012**, 51, 7794.
- (70) Verma, P. K.; Bala, M.; Thakur, K.; Sharma, U.; Kumar, N.; Singh, B. *Catal. Letters* **2014**, 144, 1258.
- (71) Feng, Y.-S.; Ma, J.-J.; Kang, Y.-M.; Xu, H.-J. *Tetrahedron* **2014**, 70, 6100.
- (72) Corma, A.; Serna, P. *Science* **2006**, 313, 332.
- (73) Lou, X.-B.; He, L.; Qian, Y.; Liu, Y.-M.; Cao, Y.; Fan, K.-N. *Adv. Synth. Catal.* **2011**, 353, 281.
- (74) Choi, Y.; Bae, H. S.; Seo, E.; Jang, S.; Park, K. H.; Kim, B.-S. *J. Mater. Chem.* **2011**, 21, 15431.
- (75) Layek, K.; Kantam, M. L.; Shirai, M.; Nishio-Hamane, D.; Sasaki, T.; Maheswaran, H. *Green Chem.* **2012**, 14, 3164.
- (76) Strecker, A. *Ann. Chem. Pharm* **1850**, 75.
- (77) Gröger, H. *Chem. Rev.* **2003**, 103, 2795.